UNIVERSITY OF SOUTHAMPTON

Characterisation and optimisation of energy storage installations for low voltage networks and EV chargers

by

George Hilton

A thesis submitted for the degree of
Doctor of Philosophy

in the
Faculty of Engineering and the Environment
Engineering Sciences

February 2019

UNIVERSITY OF SOUTHAMPTON

ABSTRACT

FACULTY OF ENGINEERING AND THE ENVIRONMENT
ENGINEERING SCIENCES

PhD Thesis Title

CHARACTERISATION AND OPTIMISATION OF ENERGY STORAGE INSTALLATIONS FOR LOW VOLTAGE NETWORKS AND EV CHARGERS

by George Hilton

Energy storage has been widely suggested as an enabling technology to aid society's transition to zero carbon emissions. This thesis focuses on two of the locations in which energy storage can be installed to aid this transition.

Energy storage installations in high rate electric vehicle chargers are also examined in this thesis. To inform this work, a model for predicting the power demand at high rate chargers was produced. This model is based on open source, freely available data and can be used for any location on the strategic road network in the UK.

Using this model paired with solar energy generation patterns, it was found that energy storage is able to balance the load and supply in the day scale for a high rate charger powered by renewable energy. However, for longer durations, a grid connection is necessary due to the seasonal changes inherent in solar power generation.

A model of a high rate electric vehicle charger is also presented in this thesis. This was used to examine the different potential use cases for a high rate EV charger with an associated off-vehicle energy store and solar PV generation. Additionally, the optimal design of such a system is presented in this thesis for various future scenarios. This shows that the inclusion of energy storage at high rate EV chargers is both technically and financially sensible when the price of the grid connection is high and the EV fleet grows at a high rate.

The efficacy of batteries installed on the low voltage feeder network are then compared to domestic batteries. It was seen that feeder connected batteries are better able to respond to changes in the feeder load patterns, leading to more desirable outcomes.

Contents

List of Figures

List of Tables

Acronyms

CAES	Compressed Air Energy Storage
CCCV	Constant Current Constant Voltage
CDT	Centre for Doctoral Training
DNO	Distribution Network Operator
EFR	Enhanced Frequency Response
EHV	Extra High Voltage
EV	Electric Vehicle
FFR	Firm Frequency Response
HV	High Voltage
HREVC	High Rate Electric Vehicle Charger
ICE	Internal Combustion Engine
NPV	Net Present Value
NREL	National Renewable Energy Laboratory
O&M	Operation and Maintanance
OVES	Off-Vehicle Energy Store
PHS	Pumped Hydro Storage
PV	Photo- Voltaic
SOC	State of Charge
SRN	Strategic Road Network

Declaration of Authorship

I, George Hilton, declare that this thesis entitled Characterisation and optimisation of energy storage installations for low voltage networks and EV chargers and the work presented in it are my own and has been generated by me as the result of my own original research.

I confirm that:

1. This work was done wholly or mainly while in candidature for a research degree at this University;
2. Where any part of this thesis has previously been submitted for a degree or any other qualification at this University or any other institution, this has been clearly stated;
3. Where I have consulted the published work of others, this is always clearly attributed;
4. Where I have quoted from the work of others, the source is always given. With the exception of such quotations, this thesis is entirely my own work;
5. I have acknowledged all main sources of help;
6. Where the thesis is based on work done by myself jointly with others, I have made clear exactly what was done by others and what I have contributed myself;
7. Parts of this work have been published as:
    - Hilton, G., Cruden, A., Kent, J. (2017). Comparative analysis of domestic and feeder connected batteries for low voltage networks with high photovoltaic penetration. *Journal of Energy Storage*, 13, 334-343.
    - Hilton, G., Kiaee, M., Bryden, T., Dimitrov, B., Cruden, A., Mortimer, A. (2018). A Stochastic Method for Prediction of the Power Demand at High Rate EV Chargers. *IEEE Transactions on Transportation Electrification.*.
    - Hilton, G., Bryden, T. S., de Leon, C. P., Cruden, A. J. (2018) Dynamic charging algorithm for energy storage devices at high rate EV chargers for integration of solar energy. *3rd Annual Conference in Energy Storage and Its Applications,*
    - Hilton, G., Kiaee, M., Bryden, T., Cruden, A., Mortimer, A. (2019). The case for energy storage installations at high rate EV chargers to enable solar energy

integration in the UK. An optimised approach. *Journal of Energy Storage*, 21, 435-444.

Signed:

Date:

Acknowledgements

Firstly I would like to thank my supervisor **Prof. Andy Cruden**. Always truthful and robust with his comments, his guidance has kept me working hard and improving.

Dr. Mahdi Kiaee was a strong, calming and positive influence when improvements needed to be made. His straight talking, no-nonsense approach did a great deal to teach me how to research.

The support and teaching I recieved from the CDT Energy Storage and its Applications provided an excellent basis for me to begin my research. **Sharon Brown** was a pivotal part of this, and her hard work and determination to do the best for all the students is truly admirable.

I must acknowledge **Alan Mortimer** at SgurrEnergy / Wood. His support, through offering me two placements, allowed me to gain perspective and guidance outside the university setting.

A crucial part of the journey for me was in making the strong friendships I found with **Tom Bryden** and **Alex Holland**. The help I found from their laughs when times were tough, and questions when times were good, cannot be measured.

And finally, **Jess**, you have been an inspiration to me throughout this process, I have been incredibly lucky to have your unwavering support. Thank you for believing in me when I didn't believe in myself.

Thank you all, I could not have done it alone.

Chapter 1

Introduction

Climate change is a critical issue leading to the need to reduce greenhouse gas emissions caused by our society. The two largest sources of emissions in the UK are power generation and transportation [1]. Alternative methods of power generation exist, such as wind and solar power. These do not release greenhouse gases but are not yet used in sufficient quantities to significantly mitigate climate change. Additionally, emission-free surface transportation can be enabled by electric vehicles (EVs) when they are powered by renewable sources. Therefore, it is important to facilitate and promote rapid uptake of these technologies in order to effectively combat climate change.

The UK Government has taken action against fossil fuel powered cars with a ban on petrol and diesel cars expected to come into force in 2040 [2]. In addition, and at a closer timescale to this, clean air zones will be implemented in the centre of many UK cities, limiting the use of conventionally fuelled vehicles well before 2040. With this in mind, the importance of developing an alternative, widely available option for road transport is clear.

Without the proliferation of enabling technologies, power distribution issues will limit the penetration of low carbon technologies as renewable energy sources are, by their nature, intermittent. A mechanism must be adopted to reduce mismatch between the demand and supply of electrical energy. Energy storage has been proposed as one method of achieving this [3], where energy is stored when supply peaks and released

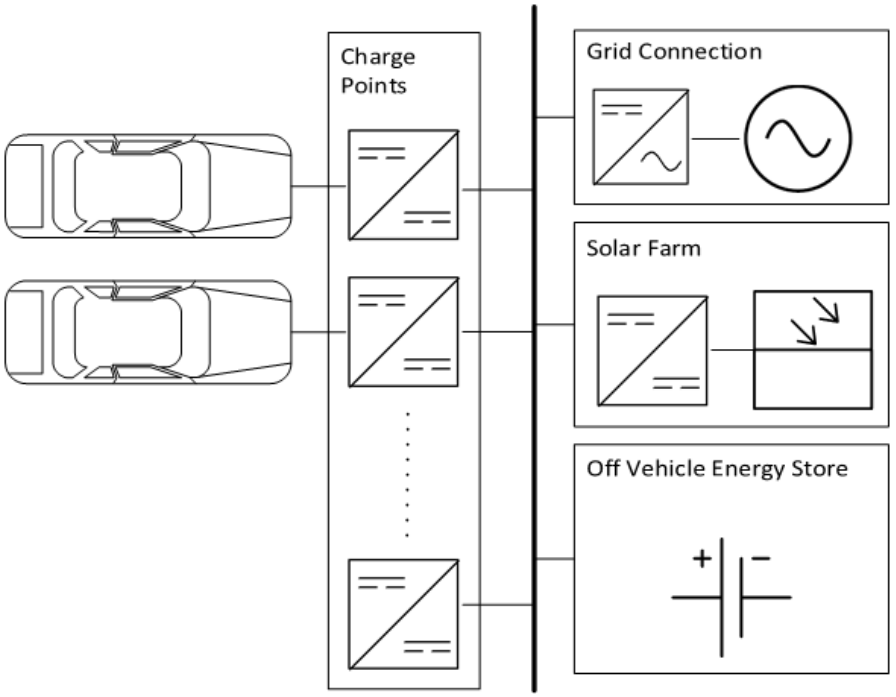

FIGURE 1.1: Schematic of HREVC with integrated Solar PV and energy storage.

when demand peaks. Additionally, capacity issues within the electrical distribution network cause limitations on the deployment of renewable energy sources. This is a significant effect as, due to the nature of the resource, solar energy must be harvested over a wide geographical area. This leads to a paradigm shift in the generation and distribution of electrical energy; instead of easily controlled centralised generators with a hierarchical distribution network based on uni-directional power flow from high voltage to low voltage, distributed energy sources can cause unpredictable and reverse power flows [4]. Local energy storage co-located with the renewable resource can prevent these reverse power flows and as such, reduce the constraints in the distribution network to unlock higher penetration levels.

With ever tightening constraints for renewable energy installations on the distribution network, it is important to assess not just the algorithms for controlling energy storage to best effect, but the locations at which they are most effective. For this, high value, specialist locations should be found. A particular location of interest is when energy storage is co-located with other technologies, this enables it to enhance the usability of these technologies by reducing power/energy constrains. The case which was selected for further study in this thesis is the pairing energy storage with EVs and renewable energy.

One particular enabling technology which, if implemented, will ease the transition from conventional vehicles to wide-scale use of EVs is high rate electric vehicle chargers (HREVCs). This has the potential for the charging of an EV to be equivalent in time to that of a fuel stop for conventional vehicles. Such high power flow levels can require reinforcement of the distribution network [5]. However, co-locating the HREVC with the renewable generators enables this grid impact to be minimised by preferentially charging the EVs with the renewable energy generated on-site. Indeed, by utilising the energy storage within the charger, a reduction in the grid impact of the solar array could also be achieved. Thereby allowing installation of further PV farms within constrained networks and encouraging wider EV take-up. Such a charging system can be seen schematically in Figure 1.1. The off-vehicle energy store charges from the solar PV whenever excess power is available. An EV can then rapidly charge without such a high power level being drawn from the grid by discharging the off-vehicle energy store. This thesis, therefore, addresses the suitability of using energy storage in this way.

The location of an energy storage installation has a significant effect on its efficacy. Each location of installation comes with a set of constraints which govern the use of that energy store. For example energy stored in a home must be done so for the maximum benefit of the home owner, as it is invariably they who have invested in it. Equally, energy storage on the grid must not overload the local network, or cause voltage violations. It is to further understand the implications of these effects that the locational aspect of energy storage is studied in Chapter 6 of this thesis.

1.1 Claims for Novelty

The author makes the following claims for novel contributions resulting from the work in this thesis:

Novel Contributions	**Associated Publication**

1. Direct comparison between domestic and feeder connected batteries, operating within the same system and responding to the same load patterns. Presented in Section 6.1. 2. Conclusions showing the lower levels of grid stability improvement available from domestic batteries when compared to feeder connected batteries. (a) Domestic batteries exhibit lower peak load export reduction, particularly in periods of high solar irradiance. Shown in both the specific case in Figure 6.8 compared to Figure 6.12, and the general case with Figures 6.17 and 6.18. (b) Domestic batteries lead to higher energy exports from feeder systems. Figure 6.16.	Hilton, G., Cruden, A., Kent, J. (2017). Comparative analysis of domestic and feeder connected batteries for low voltage networks with high photovoltaic penetration. *Journal of Energy Storage*, 13, 334-343.
3. A novel method is proposed for predicting future EV battery capacity distributions in a future scenario when the EV market has become balanced i.e. it reflects the use and purchase patterns currently seen with conventional vehicles. This is discussed in detail in Section 3.2.4. 4. A novel method for predicting HREVC power demand patterns in a locationally dependent way at any location on the SRN in the UK. (a) This method uses new data which has not previously been used for a similar study, mined from the Open street map [6]. This is discussed in Section 3.1.1. (b) Discreet probability distributions for journey distance for each hour of the day are generated. These can be used to temporally predict demand at HREVCs. This is highlighted in Section 3.2.2. (c) This shows a potentially earlier peak in high rate EV demand when compared to other prediction methods.	Hilton, G., Kiaee, M., Bryden, T., Dimitrov, B., Cruden, A., Mortimer, A. (2018). A Stochastic Method for Prediction of the Power Demand at High Rate EV Chargers. *IEEE Transactions on Transportation Electrification*.

5. A unique HREVC model has been produced. This is detailed in Section 4.3.

   (a) This integrates EV queuing and limited charge points as discussed in Section 4.3.3.1.

   (b) A novel OVES charging methodology is presented in Section 4.3.6 where the charge rate responds to seasonal changes in solar farm production resulting in greater utilisation of the energy store.

6. Analysis of two potential use cases for an HREVC:

   (a) Solar farm with HREVC - Section 4.4.1

   (b) HREVC with small solar - Section 4.4.2

7. A methodology to optimise the author's models from Chapters 4 and 5 to:

   (a) Optimise for maximum profit. Results shown in Section 5.4.1 supported by the financial model presented in Section 5.2. These results indicate higher profitability for the energy storage installation when compared with other business cases for energy storage in the UK.

   (b) Optimise for minimum use of grid connection. Results shown in Section 5.4.2.

1. Hilton, G., Bryden, T. S., de Leon, C. P., Cruden, A. J. (2018) Dynamic charging algorithm for energy storage devices at high rate EV chargers for integration of solar energy. *3rd Annual Conference in Energy Storage and Its Applications*
2. Hilton, G., Kiaee, M., Bryden, T., Cruden, A., Mortimer, A. (2018). The case for energy storage installations at high rate EV chargers to enable solar energy integration in the UK - an optimised approach. *Journal of Energy Storage.* SUBMITTED 24/09/2018 - Under Review ref EST 2018 572.

1.2 Publications

A number of publications have also resulted from the work in this thesis. They are listed here, with the corresponding claims for novelty to which they contribute.

1.2.0.1 Journal Papers

1. Hilton, G., Cruden, A., Kent, J. (2017). Comparative analysis of domestic and feeder connected batteries for low voltage networks with high photovoltaic penetration. *Journal of Energy Storage*, 13, 334-343.

2. Hilton, G., Kiaee, M., Bryden, T., Dimitrov, B., Cruden, A., Mortimer, A. (2018). A Stochastic Method for Prediction of the Power Demand at High Rate EV Chargers. *IEEE Transactions on Transportation Electrification*.

3. Hilton, G., Kiaee, M., Bryden, T., Cruden, A., Mortimer, A. (2019). The case for energy storage installations at high rate EV chargers to enable solar energy integration in the UK. An optimised approach. *Journal of Energy Storage*, 21, 435-444.

Second Author Journal Papers

1. Bryden, T. S., Hilton, G., Cruden, A., Holton, T. (2018). Electric vehicle fast charging station usage and power requirements. *Energy*, 152, 322-332.

2. Bryden, T. S., Dimitrov, B., Hilton, G., de Leon, C. P., Bugryniec, P., Brown, S., Cruden, A. (2018). Methodology to determine the heat capacity of lithium-ion cells. *Journal of Power Sources*, 395, 369-378.

3. Dimitrov, B., Cruden, A., Sharkh, S., Ponce De Leon Albarran, C., Bryden, T., Hilton, G. (2017). Design process for a parallel LLC resonant converter for powered electric vehicle charging systems. *International Journal of Health Sciences and Research (IJHSR)*.

1.2.0.2 Conference Papers

1. Hilton, G., Bryden, T. S., de Leon, C. P., Cruden, A. J. (2018) Dynamic charging algorithm for energy storage devices at high rate EV chargers for integration of solar energy. *3rd Annual Conference in Energy Storage and Its Applications*

Second Author Conference Papers

1. Bryden, T. S., Cruden, A. J., Hilton, G., Dimitrov, B. H., de Leon, C. P., Mortimer, A. (2016). Off-vehicle energy store selection for high rate EV charging station. *6th Hybrid and Electric Vehicles Conference (HEVC 2016)*

2. Bryden, T. S., Holland, A., Cruden, A. J., Hilton, G., Dimitrov, B. H., de Leon, C. P. (2018). Lithium-ion degradation at varying discharge rates. *3rd Annual Conference in Energy Storage and Its Applications*

Chapter 2

Background

In this chapter background information is given for each of the key components addressed in the modelling approaches used in this thesis: energy storage, EV charging and renewable energy as well as information relating to the methods used in this thesis: grid modelling techniques, optimisation techniques and sensitivity analysis techniques.

A key aspect of the work in Chapters 3, 5 and 6 is regarding the rating, implementation and control of energy storage, as such a discussion of energy storage technologies and current use cases is included first in Section 2.1. Then, as an understanding of high rate EV charging is critical for Chapters 4, 5 and 6 a detailed review of current installations and issues associated with them is covered in Section 2.2.

The motivation for the work in Chapter 2 is covered in Section 2.3 where difficulties arising from the integration of renewable energy resources with the electrical network are addressed. Subsequently, the literature providing motivation for the system studied in Chapters 4, 5 and 6 is discussed in Section 2.4 where the potential for overcoming the difficulties highlighted in Section 2.3 by pairing with EV charging is presented. As Chapter 4 discusses the field of transportation modelling, which differs from the rest of the thesis, a discussion of modelling techniques used for simulating EV mobility is included in Section 2.5.

Finally, background relating to the modelling techniques used in this thesis, particularly in Chapter 6, is included in Sections 2.7 and 2.8 and also background relating to the grid modelling tools used in Chapter 3 is included in Section 2.6.

2.1 Energy storage

Energy storage has widely been recognised as a key enabling technology for the development of an electrical grid largely powered by renewable energy [7]. The development of energy storage technologies and their effective use in the grid is therefore key to the future low carbon agenda.

There are three main emerging use cases for energy storage:

1. **Frequency response** - High power, short duration (<30 mins) grid connected interventions to aid stabilisation of grid frequency at 50Hz.
2. **Energy arbitrage** - Bulk energy storage, store energy at low prices and release at high prices.
3. **Behind the meter** - Energy storage used to reduce costs of a customer by, for example: attempting to reduce grid connection costs through usage alteration (for example triad avoidance), reducing peak loads and time shifting load to avoid associated grid costs.

2.1.1 Frequency Response

Frequency response forms part of the ancillary services procured by National Grid [8]. It involves providing additional power in low frequency situations and absorbing power in high frequency situations. A schematic view of this is shown in Figure 2.1. There are two specific services pertaining to frequency response; Enhanced frequency response (EFR) and firm frequency response (FFR).

EFR is a relatively new product, announced in 2016 [9]. It requires participants to commit to providing or absorbing power in relation to the grid frequency at that time and rapidly responding to changes in frequency (under 1 second). There are two specifications - wide and narrow - relating to the width of the “deadband” around 50Hz where no response is required. These are $\pm$0.05Hz and $\pm$0.015Hz respectively. Beyond this “deadband” the energy store must respond to maintain frequency stability. The EFR contracts stipulate that projects must deliver at least 1MW response. This maximum power must be available for at least 15 minutes, equating to a 2C (power level which

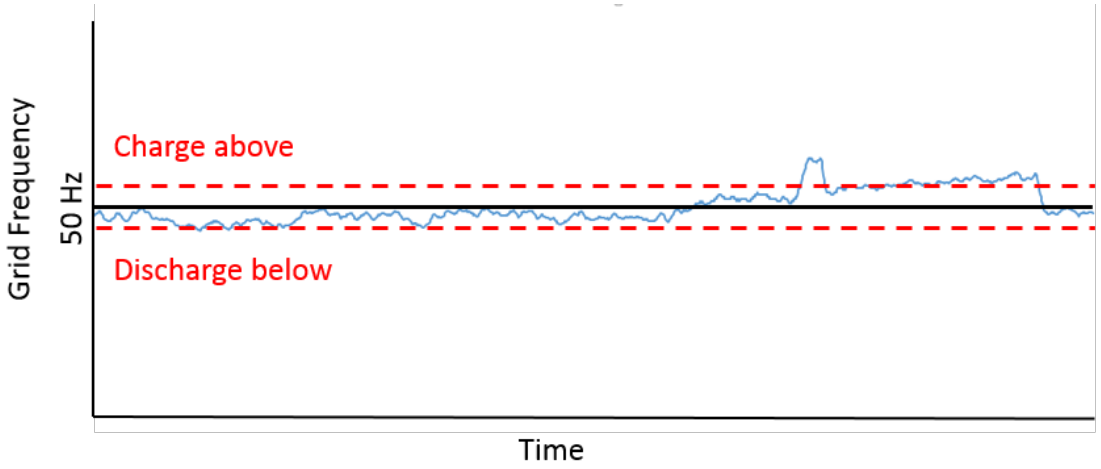

FIGURE 2.1: Schematic view of the principle of using energy storage to control grid frequency.

would charge/discharge the battery in 30 mins) charge or discharge (since the battery is typically held at 50% State of Charge (SOC) by default).

In 2016 National Grid released a tender for 200MW of EFR. This was wholly taken by energy storage projects and now forms the bulk of energy storage projects in the UK. The tender price for these projects varied between 7 £/MW/h to 12 £/MW/h. This equates to 61 320 £/MW/year to 105 120 £/MW/year discharge to meet contractual minimum power provision times of 30 minutes, these figures can be doubled to give £/MWh/year)[9].

FFR differs from EFR by having a longer response time. This is within 10 seconds, maintained for 20 seconds for primary response or within 30 seconds, maintained for 30 minutes for secondary response. This means that it is popular with traditional power generating assets such as gas turbines. However, a small number of energy storage facilities participate in FFR [9].

2.1.2 Energy arbitrage

Energy arbitrage is the act of charging the energy store when the electricity price is cheap and discharging when it is expensive, as shown in Figure 2.2. In this way, a profit can be made by taking advantages of the varying price of energy over time.

It is thought that the increasing inclusion of renewables onto the grid will lead to wider fluctuations in energy price and therefore a greater scope for energy arbitrage. In particular it was found that whilst solar power substantially reduced the price of energy in

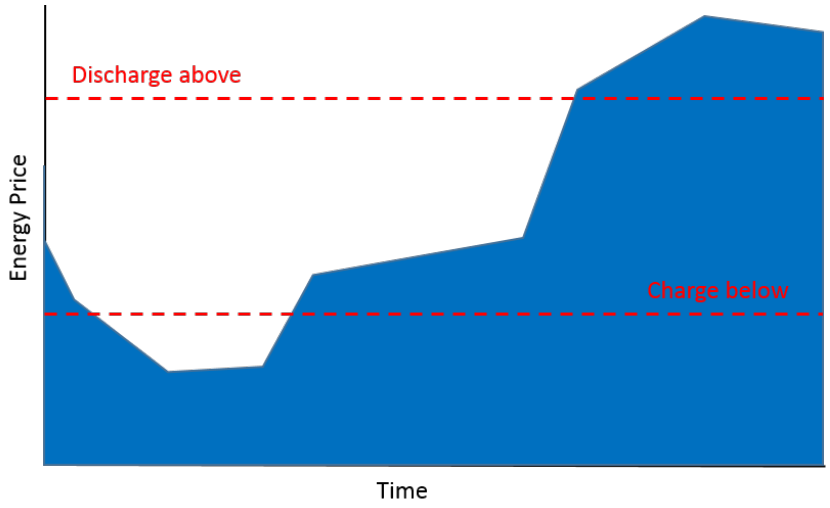

FIGURE 2.2: Schematic view of the principle of using energy storage for energy arbitrage.

the day time, that is paired with an increase in electricity price on the shoulders of this price reduction in the USA [10] . These findings were echoed in other work where the authors found an overall reduction in average electricity price and an increase in price volatility following the introduction of variable renewable energy [11].

It has been suggested by the UK consultancy company Aurora Energy Research that it is possible for an energy store to be profitable by conducting energy arbitrage in the UK. However, a key variable in this is the cost arising from degradation of the battery. Additionally, it is highlighted that arbitrage is ultimately the bigger market (than frequency response) for energy storage [12].

Energy arbitrage also provides a key system requirement from energy storage by automatically valley filling and peak shaving. Thereby working to match the supply and demand in the system. This can be done at either the day scale, i.e. responding to shifts in price throughout the day, or the season scale, whereby inter-seasonal differences in energy supply due to solar penetration are accounted for.

Revenue for arbitrage has been estimated by Aurora Energy Research [13]. In their analysis two scenarios were envisaged, optimal battery penetration which would give arbitrage revenues of £/MWh/year of 68 000 and an over-build case where too much storage has been installed leading to revenue cannibalisation of 20% (55 000 £/MWh/year). Additionally, in the US market in New Jersey, revenue was presented to be 50 000 - 100 000 $/MWh/year dependent on the duration of the store (revenue per MWh diminished for

storage durations over 4 hours). Therefore, dependent on exchange rates, this is similar to the revenue for EFR in the UK. However, the same paper highlighted the difficulty in achieving the higher end of these revenues due to shifting locations where arbitrage is most profitable (although this would not be the case in the UK).

2.1.3 Behind the meter

Behind the meter energy storage refers to energy storage installations which are co-located with another installation with which it shares a grid connection. This can be done for a number of reasons, not limited to:

1. Domestic energy storage - store domestic solar energy to enable greater self sufficiency [14] .
2. Reduce energy cost arising from a variable tariff by shifting load patterns [15].
3. Reduce necessary grid connection capacity for a given project (renewable, EV charging, large but intermittent energy user etc) by providing or absorbing energy at peak demand or generation times [16].
4. Reduce variability of energy supplied to the grid in the case of co-location with intermittent renewables by providing a back up power supply [17].

In the case of behind the meter energy storage, the key beneficiary of that installation is the system with which the energy store is combined. Therefore, behind the meter energy storage does not primarily lead to positive grid impact. However, in the case of responding to variable tariffs or other policies, the greater flexibility enabled through the inclusion of the energy store does lead to grid stability improvements.

It is difficult to assess the revenue available for behind the meter installations in the UK as it depends heavily on the specific use case in question. In particular, the other technologies the energy store is paired with, the location of the installation and the control algorithms would each play a key role in generating a business case.

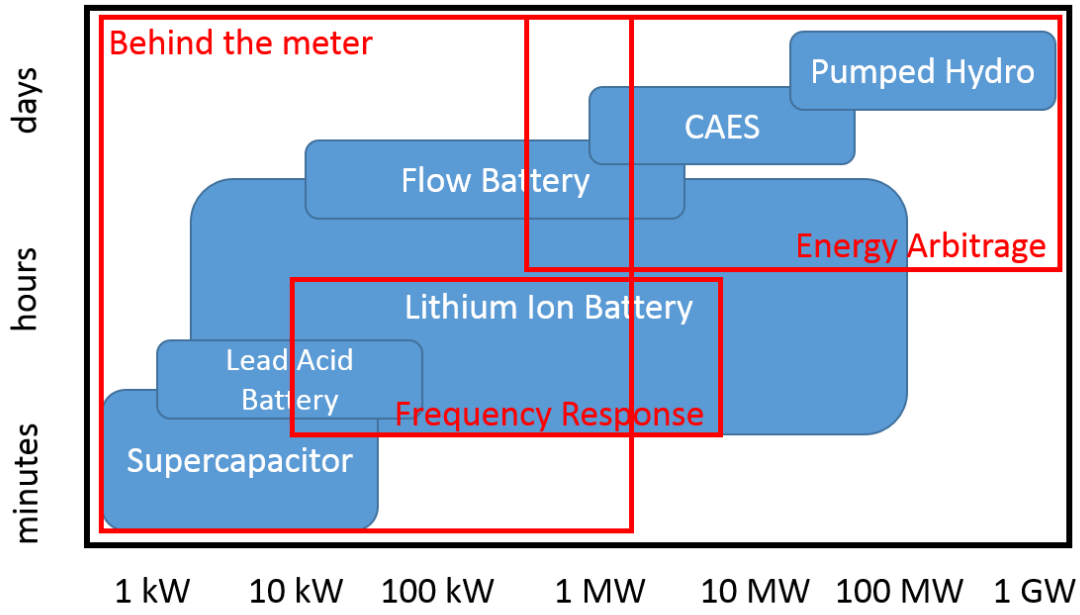

FIGURE 2.3: Ragone plot of different energy storage technologies.

2.1.4 Energy storage technologies

Many different energy storage technologies exist, each with key differences in their operation and capability. This leads to some technologies being more suited for particular applications.

Energy storage technologies can be categorised as follows [18]:

- **Electrochemical** - such as batteries, supercapacitors and flow batteries
- **Kinetic** - such as flywheels
- **Thermodynamic** - such as pumped heat or superconducting magnetic energy storage
- **Potential** - such as compressed air or pumped hydro.

A typical way of visualising which technology is suited to a given application is the ragone plot shown in Figure 2.3. This is intended to show comparison between the technologies, and is not a presentation of simulation results, therefore it is not specific in nature. It is based on published data [18] [19] [20].

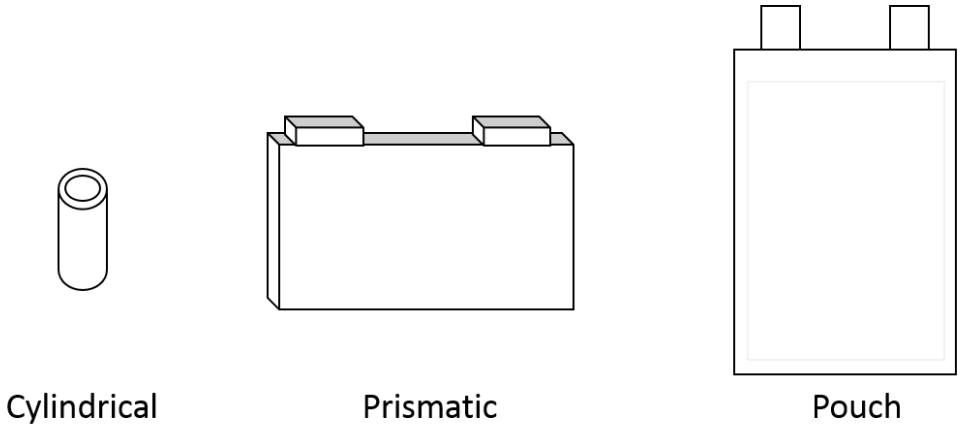

FIGURE 2.4: Schematic representation of cylindrical, prismatic and pouch cells.

2.1.4.1 Lithium ion batteries

The key technology which is currently the most popular for each of the use cases of energy storage is the lithium ion battery. This consists of two intercalation electrodes which exchange lithium ions to enable charge and discharge of the battery. The positive electrode is generally a metal oxide (such as iron phosphate (LFP), or lithium nickel cobalt aluminium oxide (NCA), amongst others) whilst the negative electrode is generally graphite, although titanate is also used for some applications [21].

The lithium ion battery is popular due to its high energy density (200Wh/kg), long cycle life (2000+ cycles)[22] and relatively low cost. There is however, a requirement for lithium ion batteries to remain within temperature (25°C - 55°C) [23] and voltage limits. This is achieved through complex and costly battery management equipment.

There are three common cell geometries for lithium-ion batteries, cylindrical, prismatic and pouch [24]. These are shown schematically in Figure 2.4. For the cylindrical cell the electrodes are rolled and inserted into a small cylinder. Each end of the cylinder is then enclosed and used as an electrode [25]. Cylindrical cells are common due to low costs and high reliability, however their packing density is lower than other methods [26]. In the prismatic geometry, the electrodes are also rolled, however, into a much flatter shape such that they can be inserted into a rectangular container. The connection electrodes are generally on the top of the enclosure. Pouch cells on the other hand, are simple and easy to manufacture as they do not require electrode rolling; the electrodes are layered and then enclosed in a bag. These offer the highest packing density, however, due to the low stiffness of the enclosure material are liable to swelling and puncture [27].

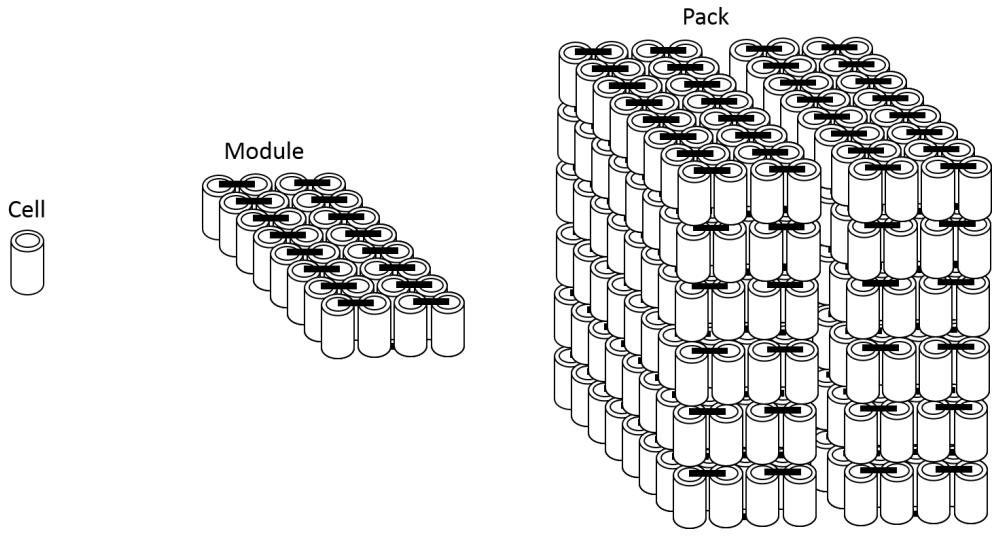

FIGURE 2.5: Schematic representation of cell, module and packs for lithium ion battery applications.

Large, grid scale (such as those constructed for the National Grid EFR tender which are typically >1MWh) lithium ion batteries are manufactured by combining many thousands of cells. This requires the addition of many components to maintain the batteries at serviceable temperatures and voltages [28]. The cells are organised into modules, by combining them in series (to achieve the desired voltage) and parallel (to achieve the desired capacity). Multiple modules are then combined to achieve the desired voltage and capacity of the entire storage installation, as shown schematically in Figure 2.5. Battery management systems (BMS) are used to monitor and control cell voltages and temperatures, these are generally controlled by cell balancing and air/liquid cooling systems respectively [29].

Overcharging of the lithium-ion cell, or heating above 100°C can result in break-down of the charged positive electrodes, this can cause thermal runaway, leading to the cell degassing [30]. In the case of a large battery pack, this may lead to a chain reaction as the adjacent cell is taken out of safety limits by the runaway of the first cell. As such, great care is needed when charging the cells, a constant voltage charging regime is used for the final part of charging to prevent overcharging. However, cell imbalances in large battery packs can lead to overcharging of a cell if not properly managed [31]. Indeed, in a large scale battery application even modest overcharging causes corrosion, reduced cell life and an increased risk of safety incidents [29].

Specific figures for the cost of lithium ion batteries are difficult to find due to commercial sensitivity. However, it is clear that their costs are falling rapidly [32]. Bloomberg New Energy Finance suggest that the average cell cost had fallen to $208/kWh as of 2017 [33]. The cost of the cell does not however, account for the full cost of a battery installation. For this, the *turnkey* battery installation company Tesla has widely been reported to supply and install a grid connected lithium ion battery for $400/kWh [34].

2.1.4.2 Other battery technologies

The lead-acid battery has been the most popular battery technology for over 100 years, no other battery technology has been able to compete with lead-acid on cost grounds and the technology is very effectively recycled with over 90% recovery of material.

Lead-acid batteries often exhibit a relatively low cycle life of $<$1000 due to physical changes in the positive active material specifically when the battery is subject to regular deep discharge [35]. This foreshortening effect is due to the expansion and contraction of the active mass, as it changes form it progressively dislodges from the positive electrode [36] and is one of the major drawbacks of the lead-acid battery. Other disadvantages of the lead-acid battery are the low power to weight ratio due to the intrinsically high mass of lead.

Flow batteries differ from conventional batteries in that the stored energy is held separately to the reactor cell. This is achieved through the use of large electrolyte storage tanks and pumping of the electrolyte through the reactor. An image of a demonstration flow battery is shown in Figure 2.6. Thus, the maximum amount of energy stored depends solely on the size of these tanks. Peak current is controlled by the surface area of the cell electrodes, and the voltage by the number and connectivity of the cells. Thus, the power and voltage can be specifically designed for an application independently of energy capacity [37]. When the battery is in discharge mode the electrolyte flows through the reaction chamber and reacts at the anode to produce electrons, a reduction reaction occurs at the cathode of equal rate to absorb the resulting electron flow. A key attribute of the flow battery is that (for the majority of chemistries) the reactants are soluble in the electrolyte, as such there is no deposition of compounds onto, or physical changes of the electrodes. This allows greater simplification of the electrode design

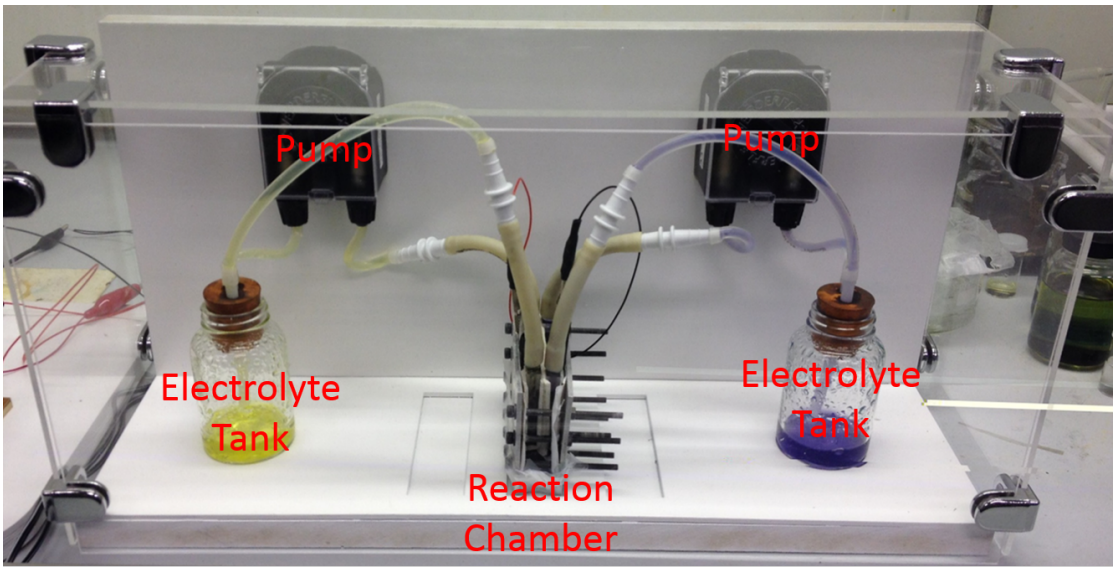

FIGURE 2.6: A demonstration flow battery built by cohort 1 of the Centre for Doctoral Training in Energy Storage and its Applications

and electrode life is significantly increased. A change in the concentration of reduced and oxidised compounds in each tank is an indicator of the level of charge [38].

The cell usually consists of porous electrodes to provide a large surface area for reactions to occur and an ion exchange membrane, which forces the electrons to flow through the external circuit. This arrangement is held in a chamber through which the electrolytes are pumped. Generally, each cell is connected to the next in series to create a bipolar stack. Since the tank size is the only factor affecting energy storage quantity, increasing the energy capacity is a very easy and economical way of storing large amounts of chemical potential, even into the MWh range [39].

2.1.4.3 Other storage technologies

Pumped hydro storage (PHS) is the oldest form of energy storage, dating back to the 1920s. It works by transferring water between two lakes at different altitudes. When the water is pumped to the higher lake, energy is stored, and when it is released through turbines to the lower lake energy is released. Clearly, PHS must be installed where there is readily available water, and a significant change in height, this limits potential locations significantly. This is by far the most popular form of energy storage in the world to date and accounts for 87% of global energy storage capacity [40].

Compressed air energy storage (CAES) is a technique for storing large quantities of electrical energy in the form of compressed air [41]. It is thought that CAES has scope for use for long duration storage needs, such as those posed by energy arbitrage (intra-day to intra-season). It is achieved by compressing air using electrical energy, storing this air in large containers, and then recombining this compressed air with natural gas in a combustion process [42].

CAES, does not have the same locational restriction as PHS. However, for large scale storage it has been suggested that underground caverns (vacant due to the extraction of oil) could be used to store compressed gas [43]. This would clearly reduce the scope for suitable locations, however a reduction in cost would be seen for the project.

2.2 High Rate EV Charging

2.2.1 Charging Standards and Systems

There is no commonly accepted power level which defines the transition to "High Rate" EV chargers (HREVCs). However, current charging methods can be split into four regimes [44].

1. **Level 1 (3kW)** - 13 amp, single phase AC connection, commonly in a domestic setting. Most units have a standard 3-pin connection to the mains.
2. **Level 2 (7-22kW)** - 32 amp, single or three phase AC connection. Commercial and public charging stations are often of this type.
3. **Level 3 (43kW)** - 63 amp, three phase AC connection. Not commonly available as there are few vehicles capable of charging in this mode.
4. **Level 4 (Up to 400kW)** - DC connection through off-vehicle AC/DC converter. Power levels vary with manufacturer and grid connection.

High rate charging is generally considered to be either Level 3 or 4. A schematic representation of standard HREVC topologies are shown in Figures 2.7 and 2.8. Level 4 chargers are more common and offer higher power level capabilities. It is this charging

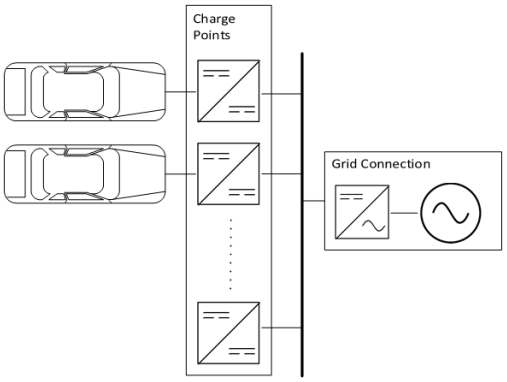

FIGURE 2.7: Schematic representation of a high rate EV charger with single main converter.

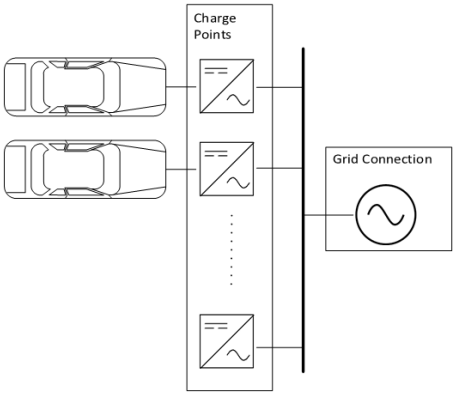

FIGURE 2.8: Schematic representation of a typical high rate EV charger, with converters at each charge point.

level which is discussed further. There are currently 4 DC HREVCs connection standards available:

1. **CHAdeMO [45]** - The DC HREVC supported by Japanese vehicle manufacturers [46]. This is currently the most common charging regime with 20 EV models able to use this charger. CHAdeMO is recognised by the IEC61851-23:2014 standard [47]. The maximum power available through a CHAdeMO charger is 62.5kW, however most currently installed are only capable of 50kW. Typically these charging stations have a converter at each charge point (as shown in Figure 2.8).

2. **Combined Charging System (CCS)** - The DC HREVC supported by European and American vehicle manufacturers. It allows for Levels 2 and 4 charging with a single plug. CCS is recognised by the IEC61851-23:2014 standard [47]. The maximum power available from CCS chargers is currently 350kW. However, most charging installations are not capable of this and are limited to 80kW. Typically these charging stations have a converter at each charge point (as shown in Figure 2.8).

3. **Tesla Supercharger** - The DC HREVC supported by Tesla Motors Inc. [48]. It is currently the HREVC with the highest power capability (145kW) [48]. As the Tesla Supercharger is a proprietary charging system, very little information regarding it is available to the public and it is the only HREVC not to be recognised by the IEC61851-23:2014 standard [47]. Typically these charging stations have one central converter with multiple charge points connected in DC (as shown in Figure 2.7).

TABLE 2.1: Cost of charging at HREVCs.

Provider	Cost	Citation
Ecotricity	15-30p/kWh	[55]
Engenie	36p/kWh	[56]
Genie Point	30p/kWh + £1 - 1.80	[57]
INSTAVOLT	35p/kWh	[58]
Polar	9p/kWh + £7.85/month	[59]
Shell Recharge	49p/kWh	[60]

4. **GB/T** - The DC HREVC standard supported in China and by Chinese vehicle manufacturers [49]. Chargers based on this standard have a range of maximum power levels from 50-80kW [50] [51].

The most widely used charging profile for Lithium-Ion batteries is the constant-current-constant-voltage (CCCV) protocol [52]. In this strategy a constant current is applied to charge the battery up to a nominal value, this voltage is then maintained, thus, the current reduces until a set shut-off point where the charge is terminated. This strategy is popular as it prevents overcharging of the battery by limiting the voltage to a set value. This means lithium plating on the anode and can be effectively prevented in many cases [53]. However, due to the prolonged constant current section of the charge, the charging rate is reduced significantly. If it is accepted that the battery does not need a full charge then the charging time can be shortened.

Attempts to achieve a short charge duration for lithium-ion batteries always result in reduced cycle life of the battery [54]. When the current selected for the constant current period of the CCCV charge protocol is increased, the SOC the battery achieves when the nominal voltage is reached is reduced. This is due to increased ohmic losses and a higher over-potential. Thus, when the CCCV charge method is used at high initial currents, in order to achieve faster charging, the efficiency drops and cycle life is reduced. Although the charge time is reduced, the energy delivered to the battery and the eventual SOC is also reduced.

HREVCs tend to charge a higher price for the electricity (30 - 50 p/kWh) than a standard domestic tariff (12 - 16 p/kWh). This is shown in Table 2.1. There are many providers of HREVCs with many different charging regimes and memberships etc.

2.2.2 Charging rate limits

There are three main factors which impose limits on the maximum power a HREVC charger can transmit.

1. **Cost** - The cost of a DC high rate charger is significantly higher than level 1 and 2 chargers due to the greater complexity and higher power rating of the charger [61].
2. **Grid connection maximum power** - Locational constraints apply for low cost, high power installations. If the charger is to be located where available grid capacity is low the charger power will be limited to the available capacity or the charger owner will be required to pay for additional network reinforcement to achieve a greater capacity.
3. **Vehicle capability** - Only 12 EVs and 1 PHEV models are currently able to accept DC fast charge (shown in Table 2.3). These EVs do not all have the same charge capability.

2.2.2.1 Cost

The cost of a Level 4 charger is an order of magnitude more expensive than a Level 2 charger [62] [61] and is generally quoted as being in the region of £50,000. Due to the higher usage rate of level 4 chargers, this higher cost can be justified, especially since there is some scope for the electricity to be sold at a higher price per kWh. However, as rated power increases the cost of the installation increases. Chargers of higher power levels are likely to use higher component ratings. This places limits on the maximum achievable charger power for a certain cost.

2.2.2.2 Grid connection maximum power

High power loads on the grid (such as high rate EV charging) can cause many negative effects if not properly managed. These include power system instability, voltage violations, thermal overload of distribution network components and increasing losses [63].

Requesting a high power connection from the distribution network operator (DNO) may require network enhancements in order to protect against these issues. Conditions where additional work is necessary are described in *Engineering Recommendation G81* [64]. The costs of these upgrades, and the cost of additional work is met by the organisation requesting the high power connection. Where large works must be completed to provide the required power, these costs can be prohibitively expensive. However, in locations where there are already strong network connections (such as close to a 33kV/11kV transformer), additional work and upgrades can be limited, as such the cost of connection can be low. This geographically limits HREVC installations if a large network reinforcement cost is to be avoided. Since the requester of a connection must pay for grid reinforcements at the voltage level of the connection and reinforcements at one voltage level higher (for their share of usage), there is a great incentive to connect at lower voltage levels. As such, HREVC power can be limited by the network conditions at the location it is to be sited. However, reducing peak power drawn by the HREVC can mitigate these constrains by reducing the need for reinforcement and by allowing connections at lower voltages.

2.2.2.3 Vehicle charging capability

In the UK there are currently 12 EV models capable of fast charging. These are detailed in Table 2.3. This number is anticipated to grow with many new EVs coming to the market. There are also many other EVs available in the UK at the moment which are not capable of high rate charge, as such the charging rate when charging these EVs is limited by the EV itself.

Many EVs which are currently in development are going to be capable of higher driving ranges and charge powers. The Audi Q6 e-tron Quattro has recently been announced. This EV will have a range of 248 miles and a fast charge capability of 150kW [65]. The Porsche Mission E is currently under development and will feature a higher battery voltage of 800V and be capable of charging at 300kW [66]. It has been announced that this EV will be in production by 2020. The battery capacity with which both these EVs will be equipped has not been disclosed, however it is anticipated that this will be greater than 100kWh due to the expected range.

The trend of the EVs shown in Table 2.3 and those not yet in production is towards bigger batteries and higher power charging. EVs are emerging as a luxury product and as such, purchasers of these EVs expect fast and easy charging, this is a leading driver of higher power charging infrastructure.

Currently, the capability of the EV to accept a high charge rate is a limiting factor due to the relatively small capacity of the batteries on the EVs. However, it is anticipated that with the emergence of new EVs capable of much higher charging powers than current models, this will change and the capability of charging infrastructure will become the limiting factor. Indeed, if the Porsche Mission E is the first of a new standard EV operating with a battery voltage in the region of 800V, the capability gap between the EVs and the charging infrastructure will be especially large.

EV	Reference	Release Year	EV/PHEV	Charger Type	Battery Capacity (kWh)	All electric range (km)	Battery Type	Charge time to 80% (mins)	Maximum current (A)	Battery Voltage (V)	Motor Power (kW)
BMW i3	[67]	2013	EV	CCS	18.8	190	Li-Ion	30	125		125
Kia Soul EV	[68]	2014	EV	CHAdeMO	27	212	Li-Ion	33	125	360	81.4
Citroen C-Zero Mitshubishi i-Miev Peugeot iON	[69] [70] [71]	2012	EV	CHAdeMO	16	160	Li-Ion	30	125	330	49
Jaguar I-Pace	[72]	2018	EV	CCS	90	479	Li-Ion				294
Mitshubishi Outlander	[73]	2014	PHEV	CHAdeMO	12	52	Li-Ion	30	125	300	60
Nissan Leaf	[74]	2013	EV	CHAdeMO	24-60	200	Li-Ion	30	125		80
Nissan e-NV200	[75]	2014	EV	CHAdeMO	24	171	Li-Ion	30	125		80
Tesla Model S	[76]	2014	EV	Tesla	60-100	443-563	Li-Ion	40		400	193/375
Tesla Model X	[77]	2015	EV	Tesla	90-100	414	Li-Ion				193/375
VW E-Up	[78]	2014	EV	CCS	18.7	150	Li-Ion	30	125	374	82
VW E-Golf	[79]	2014	EV	CCS	24.2	190	Li-Ion	35	125	323	115

TABLE 2.3: EVs and PHEVs currently available in the UK capable of fast charging.

2.2.3 High rate charging motivation

Ubiquitous high rate charging infrastructure has been stated to be necessary for large scale EV up-take [80]. This is linked to the three main disadvantages of EVs, which are limited range, slow recharging time [81] and availability of charging infrastructure [82]. High rate charging has the potential to mitigate each of these issues, leading to greater uptake of EVs. The increased rate of charge leads to users remaining with their vehicles for the duration of the charge, thus, the charging procedure becomes very similar to that of refilling a petrol vehicle.

Limited range is a major concern for prospective EV owners. However, fast charging has the potential to alleviate this concern. When fast chargers are used such that a charging instance has a small enough duration and gives enough additional range to act as a range extender. In this way the vehicle can cover much further distances in a single trip than could with only level 1 and 2 chargers. This is only enabled when there are widespread level 4 chargers such that, on any given journey, there will be a suitable charger. This was shown by the review of psychological factors affecting EV ownership conducted by Anable et al. [83] where the importance of public charging infrastructure was highlighted. Additionally, the Element Energy report *Pathways to high penetration of electric vehicles* [82] discusses charging infrastructure effects on overall EV uptake rates. It has been reported that EV owners would use their vehicles more if increased public charging infrastructure were present and non-EV owners are more reluctant to purchase an EV due to the lack of available charging infrastructure and due to the range extending ability of the HREVC. Both studies, directly linking fast charging and public charging infrastructure to increased uptake of EVs.

Reliability is a key issue for vehicle owners. HREVCs lend the EV greater reliability when longer trips are planned. With the range of EVs currently being lower than that expected for a conventional vehicle, consumers are justified in feeling "range anxiety" [84]. As the overall length of a trip is not always known, HREVCS give an assurance that a trip can remain timely even if the SOC of the battery runs low. Some trips have a very high importance to consumers, such as those in emergency situations [85]. The nature of EVs prevents the EV being used for the time when the SOC of the battery is low. Fast charging, though provides the possibility that prospective EV owners would not have to give

up this capability since charging would become more akin to fuel filling for conventional vehicles.

In an EV usage pattern trial, measured data also highlighted the role of high rate charging in growing public charging infrastructure [86]. When level 2 chargers are common EV users tend to use the chargers as parking spaces. Thus, the charging infrastructure becomes under-utilised. It was suggested that level 4 chargers be installed in preference to level 2 to enable higher utilisation of the charging network. Morrissey et al. [87] conducted a study of public charging infrastructure in Ireland. It was seen that the HREVCs recorded the highest usage frequencies, indeed, although the number of standard chargers is far greater than fast chargers, the usage of fast chargers is higher than the usage of standard chargers.

As well as increasing the effective range and reliability of an EV HREVCs are essential for those who occupy a property without off-road parking and therefore have no ability to charge an EV at home. As of 2010, 32% of dwellings rely on on-street parking and 2% of homes have no parking provision at all [88]. If the occupants of these dwellings purchase an EV, they will be reliant on public infrastructure for charging. It is important that the owners of these EVs do not use public charging infrastructure for long term parking, therefore (as shown in [86]) level 4 chargers are preferable to prevent this. The company Fastned [89] has cited this reason for their progressive deployment of fast charge infrastructure in the Netherlands since 75% of all Dutch households do not have their own driveway or parking space.

Thus, it can be seen that increased public infrastructure should lead to a greater uptake of EVs and this public infrastructure should include fast charging to be most effective and have the highest utilisation rate.

2.2.4 Grid effects of high rate charging

The topic of the impact of EVs on the distribution network and wider electrical grid has received much attention in recent years. Most research has been based on domestic and low power charging as these are the preferred charge procedure for most EV owners [87] [90]. These studies have demonstrated the need for smart charging protocols [91],[92], Vehicle-to-Grid (V2G) technologies [93] and variable tariff structures. However,

the field of the impact of fast charging is far less explored despite the load pattern being more intermittent and at a higher power level.

High rate charging at low voltage is limited by the rating of the network infrastructure at this level. Masoum et al [94] performed a comparative study on the effects of charging rates on the distribution grid. All charging points were specified in a domestic setting, as such high rate charging was limited to 11.4kW. It was noted that the higher rate of charging lead to the highest level of voltage deviation and power losses in the distribution system. If a higher charge rate is desired the charger would need to be connected at a higher voltage level within the distribution network for this simulation.

A main issue of having very high power charging capability is that this limits availability of connections to the grid. A study was conducted by Yunus et al [95] based on 250kW chargers responding to 500 charge instances per day with a stochastic distribution of charge demand. These chargers were simulated on the 11kV network. It was shown that voltages in the distribution network dropped below 0.95pu and voltage flicker increased by 2%. These results are both beyond allowable limits and suggest that this simulated high rate charge demand is not suitable for the 11kV network. Thus, a more expensive, higher power grid connection is required. This study has a high power and usage case for the high rate charger, therefore the deleterious effects of high rate charging are exaggerated. But, the same effects will be seen at lower power levels, although to a lower extent.

As such, the connection to the grid must always be rated correctly due to the high capacity needed for HREVCs. However, higher power grid connections are geographically limited without substantial additional cost implications. So providing high power with lower grid impact through the use of energy storage is of clear value.

2.2.4.1 Power quality

As well as capacity issues, HREVCs can have an adverse effect on power quality.

One effect caused by many electrical devices connected to the distribution network is harmonics. Harmonics are defined as:

Nonlinear devices are a common cause of distortion, i.e. the current is not proportional to the voltage of the device. This leads to periodic disturbances in the voltage or current waveform. Harmonics cause power losses in the distribution system and can introduce inefficiencies in network connected devices. Power electronic devices can commonly cause harmonic distortion due to intermittent nature of power flows in common power electronic topologies [96].

IEEE 519-1995 is the standard which describes allowable harmonic distortion levels on an electrical network [97]. It is required that any individual distortion should be less than 3% of the fundamental frequency, and the total harmonic distortion of voltage (THD_V) should be less than 5% with harmonic distortion of currents being less.

Electric vehicle chargers were highlighted as a source of harmonic distortion in reference [98]. In this work the effect of many geographically clustered EV chargers on power quality was studied. It was shown that 25kW chargers can cause 3rd order harmonic currents of up to 3.5A, however, total harmonic distortion is less than the sum of all harmonic distortions. This study shows the motivation for low harmonic charging solutions. Additionally, the harmonic content of the GB/T fast charge protocol used in China was studied in reference [99], it was found that a peak harmonic distortion of 2.9% was seen in the 3rd order and the total harmonic content was 3.58%. The authors also predicted that increasing numbers of EV chargers does not lead to a proportional increase in the harmonic distortion, rather a saturation occurs due to the counteraction of harmonic currents.

Whilst harmonic content was not seen to be excessively high in these studies, they were conducted at a low charge rate. Power drawn from HREVCs may have substantially more harmonic content, causing issues on the distribution network, however, no studies were found looking at higher rate charging.

Due to the rapidly fluctuating power demand causing voltage drop, fast charging is particularly deleterious to the local network and requires to be connected at a higher voltage per capacity than most other loads.

2.2.4.2 Network connection considerations

If capacity or power quality issues are deemed to be too severe, network reinforcement works will be required.

Regulations for connecting to the distribution network are described in *The Distribution Connection and Use of System Agreement* (DCUSA) [100].

Since the circumstances of each connection is different, the cost of new connections to the distribution network is calculated on a case by case basis. It is dependent on the work which needs to be carried out to maintain grid stability. Extension assets are all infrastructure which needs to be installed in addition to the existing network in order to provide a connection for a new customer. Costs of extension assets are payed by the requester of the connection. Thus, if distance of the requested connection from the existing network is large, this cost will be higher due to the length of cabling required. Similarly, if the voltage of the connection is different to that of the local network and a substation is required, this will add to the cost of connection. Thus, geographical and voltage limitations exist for designers and installers of HREVCs if the cost of connection is to be minimised.

The cost of reinforcement of the existing infrastructure is payed by both the DNO and the requester of the connection. The cost apportionment factor (CAF) for reinforcement is calculated by using one of two formulas 2.1, 2.2.

$$\text{Security CAF} = \frac{\text{Required Capacity}}{\text{New Network Capacity}} \times 100 \tag{2.1}$$

$$\text{Fault Level CAF} = 3 \times \frac{\text{Fault Level Contribution from Connection}}{\text{New Fault Level Capacity}} \times 100 \tag{2.2}$$

When the main cost of reinforcement is driven by thermal capacity or voltage stability the Security CAF equation 2.1 is used. Equally, when the main cost of reinforcement is due to fault level restrictions, the Fault Level CAF equation 2.2 is used. Thus, for a new connection the cost to both the DNO and the requester of the connection can be significantly reduced through lowering the fault level and the required capacity of the connected device.

The fault level is defined in Equation 2.3.

$$\text{Fault Level} = \text{Open Circuit Voltage} \times \text{Short Circuit Current} \tag{2.3}$$

Since a HREVC is neither a generator or a spinning load with inertia, it will not significantly increase the open circuit voltage of the network and as such will not have a substantial effect on the fault level. As such, the reinforcement which will be caused by the HREVC will be due to capacity issues caused by the large power demand.

Faults on the distribution network are generally classified as either a short circuit between 2 phases, or 1 phase to ground. These faults cause a large spike in the current which, if no action is taken, can cause substantial damage to the network infrastructure. Circuit breakers are placed on the network in order to interrupt fault currents. When the fault current is interrupted, an arc occurs between the contacts, the ability of the circuit breaker to clear this arc is dependent on its rating. As such, the rating of a circuit breaker must always be above the fault level of the circuit it needs to break [101]. Thus, increasing the fault level on the grid can be very dangerous unless the rating of local circuit breakers is also increased.

2.3 Renewable power integration into electrical networks

The need to provide low carbon electricity has motivated the proliferation of many distributed renewable generators. Solar power is particularly popular due to the predictability of its power generation profile, the high energy density and minimal geographical constraint of the resource. Southern parts of the UK have seen a substantial growth of large scale solar farms due to the relatively high solar irradiance levels. Current solar farms operating in the area surrounding Southampton are shown in Figure 2.11.

Since PV arrays produce DC power, solar farms need power conversion equipment. This is achieved through power electronic inverters. There are many configurations of inverters which can be used to connect the PV arrays to the grid, these are shown in Figure 2.9.

One approach is to use string inverters (Fig 2.9 b) whereby large numbers of low rating inverters are placed at a string of PV arrays and convert the power from that string.

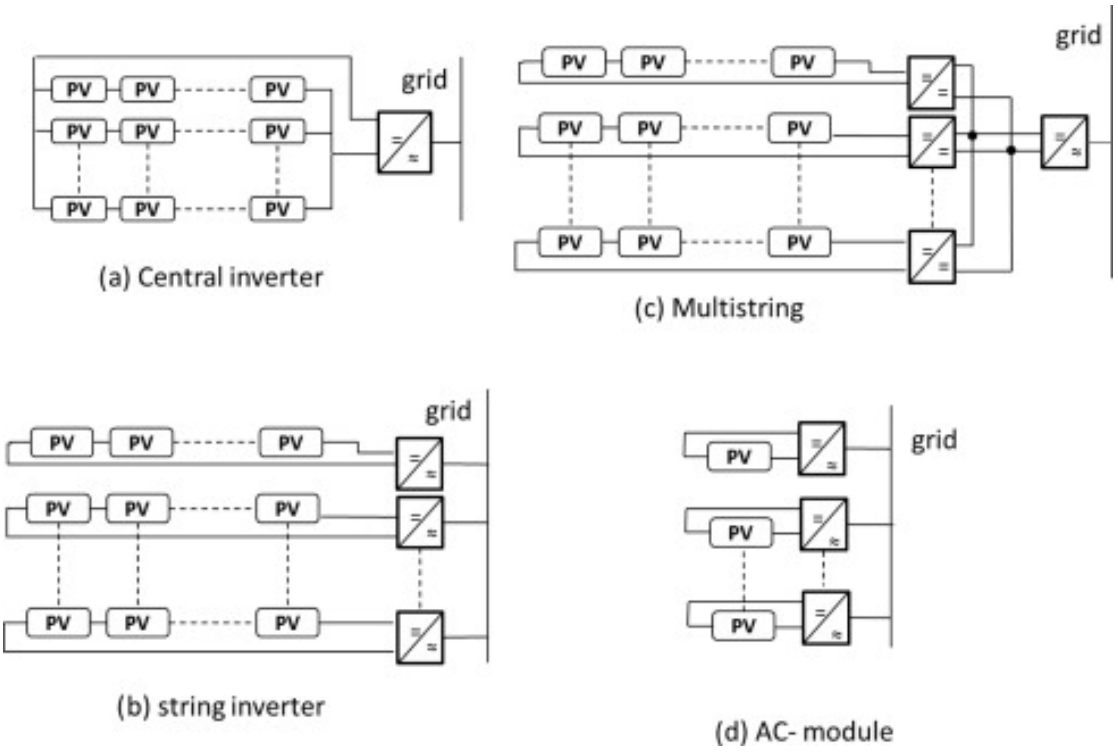

FIGURE 2.9: System configuration for a grid-connected large scale PV farms [102].

This allows maximum power point tracking (MPPT) control for each string individually, improving overall efficiency of the solar farm [102]. Alternatively a single large central inverter can be used (Fig 2.9 a) . This simplifies the installation and results in low cost, however the same MPPT control must be used for the whole farm. This results in losses when partial shading occurs [103]. A multi-string system (Fig 2.9 c) provides MPPT at a string level with cheaper DC-DC converters whilst using a larger AC-DC inverter, serving the entire farm. This allows a reduction in cost over the string inverter system without sacrificing string level MPPT control, although the extra level of conversion results in an efficiency loss [102]. AC module systems are also available (Fig 2.9 d), where an inverter is placed within each PV module such that it produces AC power automatically. These are more popular in small scale installations since a greater level of complexity is introduced and lifetime of the module is reduced [104]. As such, there is a wide variety of connection methods, however, further discussion in this work is not connection specific and refers instead to generic effects of large scale solar.

Lines and substations in the distribution network become constrained due to the voltage and thermal issues arising from grid connected renewable resources. The extent of this is shown in Figure 2.10. It can be seen that, for the area near Southampton, the pattern

of constrained substations suggests that the rural network is more constrained. This is due to longer feeders leading to a greater likelihood of voltage violations and a higher density of renewable generation. There are three issues which cause constraint of the distribution network. These are:

1. **Voltage Violations -** Power quality issues such as harmonic distortion and voltage rise cause substations to become constrained through voltage. This effect is where the voltage and power quality in the network supplied by the substation does not conform with regulation.
2. **Thermal Overload -** Reverse power flows in the network caused by renewable generators can excessively load the distribution network causing heating of components. Cables and transformers have a thermal rating and as such networks can become thermally constrained when apparent power flows become to high.
3. **Fault Level -** Protective instruments on the distribution network such as circuit breakers must be able to interrupt current flow in the event of a fault. If the fault level is close to that of the protection equipment rating the network becomes constrained.

2.3.1 Power quality

In order to achieve the stated Quality of Service Guaranteed Standards [105] the voltage on the system must not go above or below set limits of 1.1pu and 0.94pu [106]. These regulations are in place in order to prevent damage to network connected infrastructure. In the case of renewable generators the rise can be very large and unpredictable due to the nature of the generation profile.

Voltage rise at the connection point of a distributed generator is caused by power injection. For a radial feeder layout it can be expressed by Equation 2.4 [107].

$$\Delta V \approx \frac{(P_G - P_L)R + (Q_G - Q_L)X}{V} \tag{2.4}$$

Where P_G and Q_G are the real (kW) and reactive (kVA) powers of the distributed generator and P_L and Q_L are same for the line load. R and X are the line resistance and

reactance between the distributed generator and the substation and V is the line voltage at the connection point. As such it can be seen that the problem of voltage rise is exacerbated by low load power on the feeder and high line resistance and reactance or line length.

Voltage rise is a major issue with domestic solar installations since the PV arrays can be connected to long feeders with low load. Large solar farms, however, are necessarily connected to HV or EHV cables. The voltage on these lines is more stable to to inherently high loads, however high penetration of large PV farms can see voltage rise. In addition to being more critical due to having wider ranging effects, issues at this higher voltage level require more substantial reinforcement works and as such, are more serious.

As discussed, harmonic distortion is caused by non-linear loads and is a power quality issue. Solar PV installations cause harmonic distortions on the network dependent on the inverter technology, the control strategy used and the presence of a coupling transformer [108]. A study showed the THD_I emitted by the PV array, peaking in the morning and the evening, when the PV array is producing only a small amount of power. This is due to an inverse relationship between generated power and TDH_I [108]. This result was confirmed by measurement in reference [109].

Voltage unbalance is caused by non-equal loads on each of the phases in the distribution system. Imbalance is one of the biggest problems facing LV networks [110]. It is recommended in Engineering Recommendation P29 [111] that voltage unbalance be kept to within 3% for the entire network. This recommendation is in place to prevent damage to 3-phase equipment which can be caused by voltage unbalance [112]. Large scale solar power necessarily has a 3-phase connection and therefore voltage unbalance is mitigated.

2.3.2 Thermal overload

Thermal overload threatens the components of the distribution system through heating caused by the actual power exceeding equipment rated power levels.

Power transformers are the most expensive and important components in the electrical distribution network [113] and a power overload of this component can lead to multiple

failure mechanisms [114]. Heating of the top oil in a power transformer, is often a precursor to failure.

The maximum current which overhead lines are permitted to carry is dependent on the overall heat transfer to the cable and the resistance as described in Equation 2.5 [115].

$$I_{OL} = \sqrt{\frac{\Delta H}{R}} \tag{2.5}$$

Where I_{OL} is the current in the overhead line (A), R is the resistance (Ω) of those lines and ΔH is the heat transfer from the cable to the surrounding environment. Thus, it can be seen that, for increasing overload currents, reducing the resistance has a diminishing positive effect, and reducing the current has a squared effect on power loss and overload compared to resistance.

Exceeding the rated thermal capacity of components leads to a need for upgrade to a higher rating. Therefore, large scale solar which exports high levels of power into the surrounding network necessitates high ratings of components on the surrounding distribution network. However, if the peak energy export can be reduced, this will reduce the necessary rating level of the surrounding infrastructure and thus, lower the cost of installation.

2.3.3 Fault level

A third potential effect of large scale solar power which leads to a need for network reinforcement is increases to the fault level. Most literature in the field of fault level contributions looks at synchronous machines since the fault contribution of these is substantial. However, large scale solar PV farms cause an increase in the current which will flow in the event of a short circuit through increased power flows. The standard fault current from a PV system is in the region of twice the inverter rated current and varies based on the inverter specification [116]. Thus, for a large solar farm, this can be significant and require upgrades to the fault tolerance of the local network. This cost must be covered by the solar installer.

2.3.4 South of England case study

Constraints within a real network are complex and can arise from multiple sources. The issues of fault level, thermal overload and voltage violations have caused limitations to be placed on further renewable generator connection in the south of England. Figure 2.10 shows constrained substations in the area surrounding Southampton. The red substations are constrained (As defined by Scottish and Southern Electricity Networks [117]) and as such substantial reinforcement work must be carried out in order to connect further renewable generators in the area these substations serve. in 2016 there was a strong geographical preference towards connections of renewable generators in the cities of Southampton, Bournemouth and Portsmouth since the substations in these areas were, mostly, unconstrained. The rural substations, serving long feeder lines, with low load levels are more likely to become constrained. However, now even the cities have become constrained. This can be seen in Figure 2.10. Since PV farms are suited to rural area installation, the cost and complexity of their installation increases and measures must be taken to allow their safe connection.

More detailed analysis is available for the constraints affecting the distribution network in the South West. Western Power Distribution published data [119] show that the majority of the 33kV lines are constrained through voltage violations with small parts thermally constrained. Indeed, every substation in Exeter and the surrounding area is constrained through fault level.

In addition to that Western Power Distribution released a statement regarding the constraints on the 132kV lines in this area [120]. This states that the South West area has 1.95GW connected generation, whilst the minimum summer demand is only 0.98GW. Therefore, it is likely that generation will be exceeding demand for the South West area during summer months. Since the "*F route*" 132kV line is the main electrical connector to other areas, it has become constrained thermally due to this effect. In order to deal with this, Western Power Distribution, in conjunction with National Grid Electricity Transmission, are in the process of reinforcing the transmission system in this area. A delay of 3-6 years for future distributed generator connections in now in place in the South West Area.

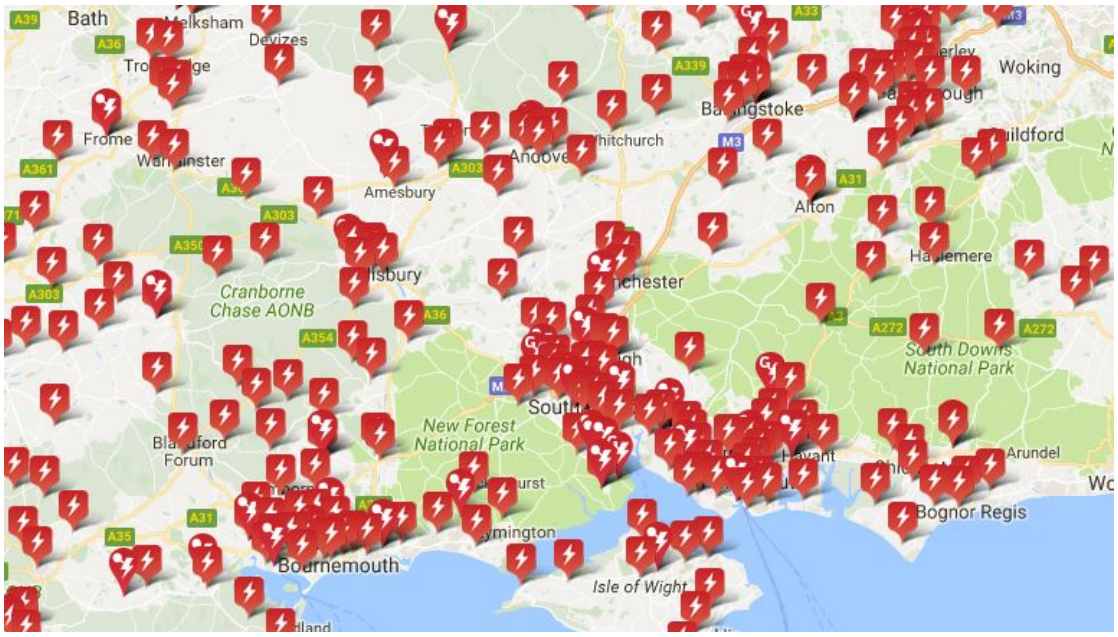

FIGURE 2.10: Map of constrained (red) and un-constrained (green) sub-stations in the area surrounding Southampton UK [117].

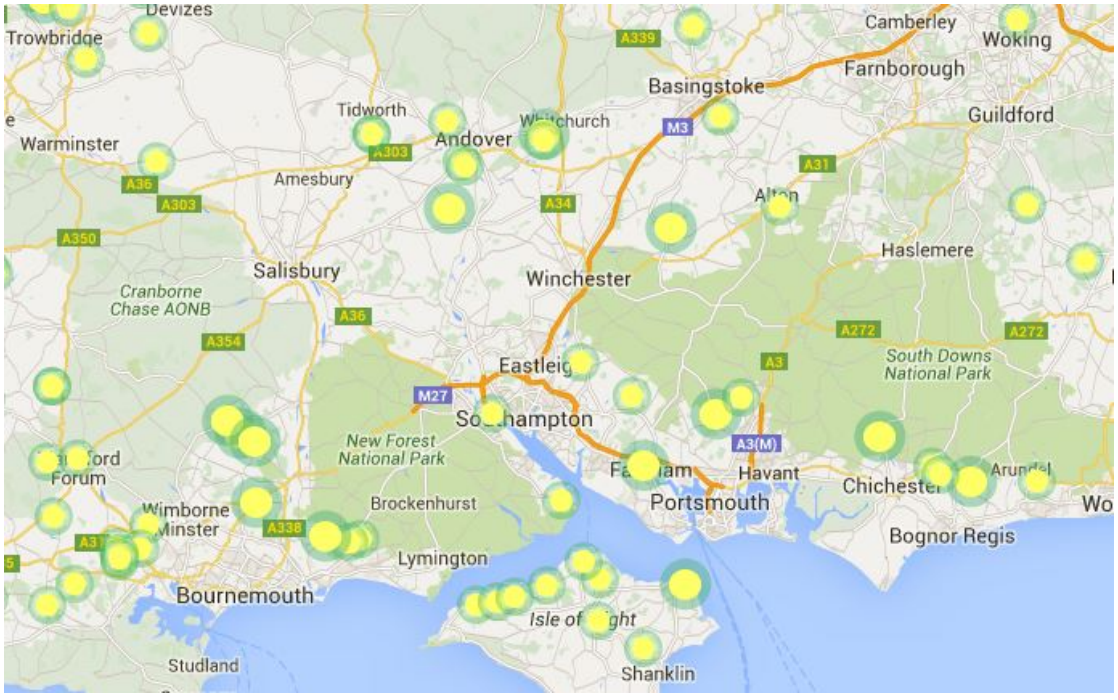

FIGURE 2.11: Map of grid connected PV farms in the area surrounding Southampton UK [118].

Clearly, due to the substantial delay, this is not a suitable solution when the importance of renewable generation is considered. Additionally, transmission level reinforcement is only available when surrounding areas are not experiencing similar capacity issues. It also places a substantial restriction on the further installation of renewable energy. Therefore, a solution which allows further installation of renewable energy into constrained networks, such as those in the south of England, without increasing the required capacity from the transmission and distribution networks is highly desirable.

2.4 Pairing of renewables and EV charging

It is widely agreed that further development of renewable generators is a necessary step for reducing the carbon footprint of electricity generation. As previously discussed though, there are network associated difficulties with high penetrations of renewable generators. This has led to constraints in the network, in places, preventing further installations of renewable generators.

On the other hand, efforts to de-carbonise transport have led to ever increasing numbers of EVs in use, however, the charging of EVs will dramatically increase demand on the distribution networks. One aspect of EV charging with substantial grid impact is fast charging [94] [95], although such wide scale high rate electric vehicle chargers (HREVCs) are seen as critical for EV uptake [80] as their use alleviates many concerns of the potential EV owner such as range anxiety [83], and give a greater sense of reliability [82]. As such they are a popular choice for consumers [86], [87]. Attempts to mitigate their negative effects i.e. capacity demands, on the distribution network must be made in order for effective charger installations.

There is potential for EV charge demand and renewable generation supply to be paired in order to reduce the negative effects of both of them. This would allow further renewable integration within constrained networks whilst promoting EV uptake by providing fast charge stations. A schematic of a system which could achieve this is shown in Figure 2.12.

Much of the work in the area of pairing EV demand with renewables has focused on slow charging of EVs to absorb PV power. For example an older study investigated a

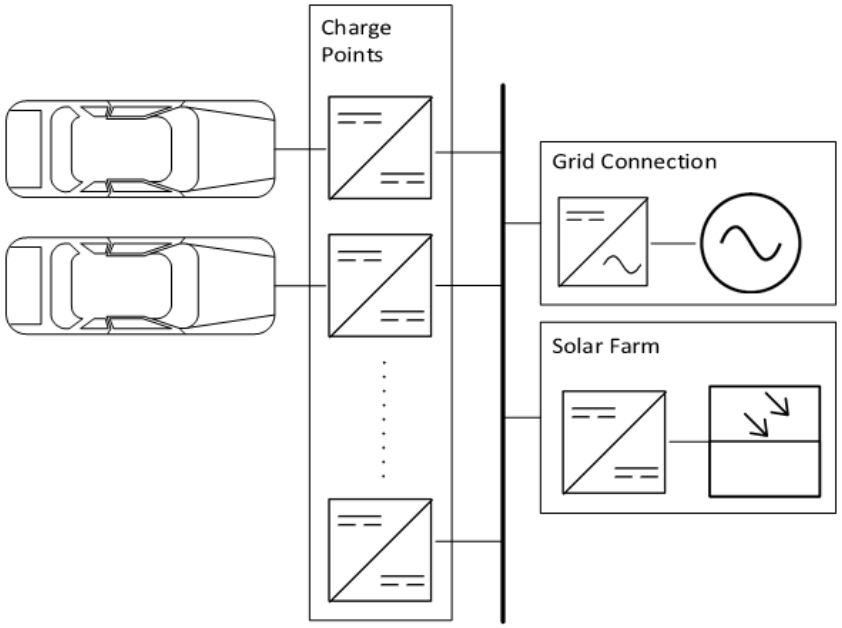

FIGURE 2.12: Schematic of an EV charger with integrated Solar PV.

solar powered EV charging system in the work place, suggesting, in 2009, that this was the ideal scenario for "commuters of the future" [121]. This idea was further developed when it was discovered that solar carports could provide 15-40% of the energy demand of road passenger transport in Switzerland [122]. Additionally, this idea was shown to be economically feasible for the installer (employer, university etc), with an additional parking charge entitling users to a free share of the renewable energy generated [123]. Slow EV charging such as this, has the benefit of power demand over a longer timescale which can more easily be matched to the PV generation profile. Indeed, there is the suggestion that charging rates for workplace installations could follow the generation patterns of the renewable energy resource and as such, the entire system would need no grid connection.

Smart charging can be used at a system scale to match the supply of the PV power with the demand of the EV charging. In this solution there is no need for an intermediary energy store due to the large number of EVs charging. The authors in [124] [125] take a system wide modelling approach to analyse the energy demand of Portugal. It was suggested that for scenarios of high PV penetration EV charging should take place during the day in order to minimise excess PV energy. Looking more closely at the distribution network topology and limiting EV charging to domestic settings, in a study on the combined effect of EV charging and PV penetration in residential distribution systems. It was concluded that, due to the time difference between EV charge demand and PV

generation, energy storage devices are needed if network reinforcement is to be avoided [126]. In contrast, other work concluded that if smart charging and time of day tariffs are implemented effectively EVs could be used to increase demand and reduce exportation related capacity issues in the constrained network of Nova Scotia [127]. When looking at a similar, system wide approach, it was concluded that the smart charging of EVs provided benefit to the system, but the authors stopped short of saying that it would eliminate the need for energy storage [128]. It is not clear then, that EV charging can be proved to be flexible enough to wholly prevent network issues at a system scale without the inclusion of energy storage for high renewable energy penetration levels. In any case, it stands to reason that a good correlation between EV charging and renewable generation is only able to alleviate local grid constraints when close geographical proximity occurs.

More specifically, since the charging location of the EVs will generally be either at home or in the workplace and the main location of network constraints arising due to distributed generation is in rural feeder networks there is little scope to alleviate these with smart EV charging. The location of the EV charge demand is important since adverse grid impacts are mostly at a local level. Matching workplace demand to rural PV generation is only effective when there are no constraints on the grid in between the two. However, as can be seen through the case study of the South of England, this is not the case.

The demand for high rate charging is different though. Since charging of this nature is done during a long journey, rural charging stations are beneficial. If it is assumed that there will be similar demand for charging as their is for fuel, a comparison can be drawn between charge point types and fuel station uses. Currently there are two uses for fuel stations:

1. **Local Serving Stations** are located close to residential centers. They provide fuel for local travel on an ad hoc basis, when the vehicles tank becomes empty.
2. **Through Traffic Stations** are located along major roads. They provide fuel demand for vehicles on longer journey travelling through areas.

It is anticipated that local serving stations will be replaced with smart home charging and workplace charging, since these methods are preferred by the consumer [87] [90].

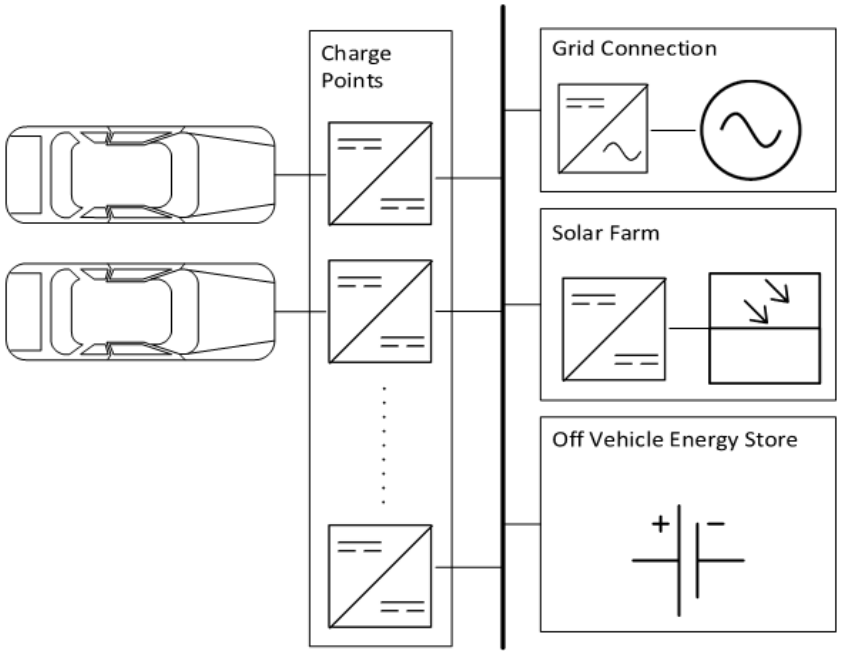

FIGURE 2.13: Schematic of HREVC with integrated Solar PV and energy storage.

However, through traffic stations will correspond to a HREVC, these fuels stations are generally located on or near main roads. Thus, HREVC demand is likely to be in rural areas, where the network is more constrained and there is a higher penetration of solar farms. Comparing this to the map in Figure 2.11 it can be seen that there is good geographical correlation between the potential HREVC demand and current solar farms.

2.4.1 EV chargers with renewable energy and energy storage

It is clear from very simple analysis that high rate charging of EVs cannot be supplied solely from renewable energy in a stand alone system. This particular topic has therefore received very little academic attention. However, if this system includes an energy store, then there is a potential for viability. The conceptual framework for this system was first proposed in the academic community in 2013 [129]. A schematic of this type of charger is shown in Figure 2.13.

The potential implementation topologies for this system have been presented by Sujitha et al [61], showing that there are a number of ways to design the power electronics of such a system. In each of these topologies, a DC bus is included to which a DC charger is connected to enable EV charging. Various energy storage and renewable energy generation devices can then be connected to this DC bus in order to design the

system. The wide variety of possible designs for this system show that it is an ideal candidate for designing through modelling as it is likely that proposed optimal solutions are feasible.

The only HREVC with integrated energy storage demonstrator found in the literature has been implemented at the Italian National Agency for New Technologies [130]. A 16kWh lithium-polymer battery is integrated into a CHAdeMO DC fast charger capable of 50kW. The battery is set to provide 35kW for the first 320s of EV charging, then 15kW for the remaining charge duration. Despite this crude energy store control strategy the grid power for a 50kW charge of the EV was limited to 20kW. This system does not have paired renewable power, however it is a proof of concept on which further work can build.

Capasso and Veneri [131] [132] have designed a HREVC system based on a common DC bus. The possibility of renewable energy integration within such a system is highlighted since additional connections onto the DC bus are simple. A laboratory scale prototype was developed with the ability to integrate Lead acid, $LiFePO_4$ and Li[NiCoMn]O_2 batteries of varying capacities. Again a reduction in the grid power was seen through the use of energy stores, however the focus was on presenting the architecture of the charger and as such repeated analysis including vehicle usage patterns was not included.

Limited work exists which focuses on integrating renewable energy into HREVCs. A system based on a central DC bus, similar to that in [131] [132], the voltage of this bus was used to control the charge and discharge of the energy store [133]. Different control states were imposed, leading to charge and discharge of the energy store when DC bus voltage fluctuated above and below reference voltage. Simulations shows a reduction of 50% in grid power, however transience at switching caused a large spike (50kW) in the power drawn from the grid for 20ms. This was an entirely modelled simulation and no real-life data was used. No work has been found which experimentally looks at integration of HREVCs and renewable energy.

These papers focus on the technical aspect of the HREVC system involving renewable energy, as such, exploration of the control, functionality and optimisation of these systems is under-developed. This is an area of particular importance due to the potential of providing additional renewable energy within constrained networks whilst simultaneously facilitating wider EV uptake.

Other work looked into the optimal design (minimisation of system cost) of a "completely green charging system" [134] i.e. one that is powered by solar panels and uses an energy store. This work attempted to find optimal values of EV charger design variables. It concluded that the capacity of the solar farm and energy store depend mostly on the desired queue length and the number of charging stations. Equally, if the solar farm and energy store capacities were reduced, then longer queues would accumulate. This work has two main flaws; firstly not all the design variables are included in the optimisation process. The number of charging stations is pre-determined, therefore the optimisation does not accurately respond to the expected EV demand. Secondly, the EV demand itself is artificially generated with set and constant interval times, this clearly does not reflect the real scenario. Additionally, whilst not necessarily a flaw, this work does not include a grid connection and therefore does not represent real-world implementations of this system.

Further work has also looked into this area with work on the optimum power flow for each timestep of a simulation [135]. This aims to minimise costs arising from battery degradation whilst responding to a variable grid tariff by finding an optimal schedule for charging and discharging the battery.

Despite this relative lack of academic work in the area, many companies are proceeding with installations of this nature. For example Fastned [89], the Danish company are including energy storage and solar panels with some of their high rate chargers and Tesla [48] have also publicly stated an indention to do so. With this in mind, it is of clear importance to establish the potential impact on grid stability that these installations will have and also inform their design such that these systems are rolled out in an optimal way.

2.5 HREVC demand - transportation modelling

Transportation modelling is a broad section of computational modelling concerned with analysing the movement of various entities within transport systems [136]. It can be classified into two broad areas:

1. **Micro Models** These are concerned with transportation interactions at small scale. Examples might be interactions between pedestrians and pelican crossings or vehicles at roundabouts.

2. **Macro Models** These are concerned with bulk movement within a wide area. For example, assessing traffic flow within a city.

In this thesis, the area of interest is in bulk movement of vehicles over long distances on main roads. As such, methods of predicting HREVC demand through macro transportation modelling are investigated.

2.5.1 Demand pattern time distribution

The expected time distribution of low rate EV charging has been extensively examined, as well as smart techniques which can be used to reduce grid stress [137] [138] [139]. A common method of analysis is using a probability distribution of EV use, such that charging can be predicted for when it is not in use [140]. This is an effective technique for low rate (7kW) “level 2” charging is likely to occur when an EV is parked and the owner is conducting another activity.

The use case of HREVCs differs from that of level 2 chargers since they are designed to be used when the range of the EV is not high enough for the distance of the journey being undertaken. In order to determine a probable time of use a study conducted by The Department for Transport of trip distance for private vehicles in the UK [141] was consulted. 80% of all trips are less than 10 miles in distance. However, these trips only represent 26% percent of the distance covered. Contrasting this to the use of the SRN, which accounts for all the high demand roads in the UK, such as motorways and large A-roads, it is clear that the distances covered using these roads are substantially higher per trip. Unfortunately, details given in [141] regarding long distance journeys are inadequate for this study as journey distances and the type of road used are needed. Since HREVC use will predominantly be during a long trip, it follows that HREVCs should be located on large roads such as those in the SRN. Therefore, in this thesis, the assessment of traffic patterns and journey distances is calculated for journeys which use the SRN.

The literature addressing the problem of predicting EV demand at HREVCs is quite limited. Many studies assume demand will be proportional to traffic flow measurements [142], [143] or "mobility" measurements for urban areas [144]. This gives a characteristic *two peak* EV demand profile, with EVs more likely to visit an HREVC in the morning or evening, aligning with the high use times for the road network. This has the clear flaw of not taking into account the distance of the journey which the EV is undertaking, which is an important predictive factor for HREVC use.

Another method for predicting EV is to liken the HREVC demand to ICE demand for fuel [145]. This gives a demand shape similar to the studies assuming charge demand proportional to traffic flow, with a slight increase through the middle of the day. Whilst this is more enlightening than assuming proportionality with traffic flow, the use of an HREVC will be different to that of a fuel station. The main difference is that there is no option to refill an ICE vehicle whilst it is parked overnight, whereas this is commonplace amongst EVs and therefore will change the charge demand. Due to this, and the extended range of ICE vehicles, their users must use refuelling stations on a more ad-hoc basis, as and when the car is in use and the fuel tank becomes empty.

In addition to these methods vehicle usage data has been previously used to predict HREVC demand. A number of vehicle GPS data studies suitable for this have been found through the National Renewable Energy Laboratory's (NREL) Secure Transportation Data Project [146]. In particular a study with real-world driving times, speeds, and distances collected from the Puget Sound Regional Councils 2008 Traffic Choices Study was used in [147], [148] and [149]. This study comprised of installing GPS devices on 400 vehicles between April and June 2005, resulting in measured 149,000 trips. [148] and [149] were concerned mainly with calculating the necessary battery size for EVs to enable the mobility levels seen in the dataset. However, reference [147] uses this data to predict HREVC demand. This study assigns EVs to the usage patterns of vehicles in the study and initiates an HREVC session whenever the range of that EV is depleted through driving. As this study is based on real world data it can be assumed to be the most accurate in the literature. However, each EV is given either 16kWh or 40kWh of battery capacity which does not reflect the EVs currently on the road and is a major simplification. Additionally, in the real world HREVC locations are set and as such, a HREVC use only when the range is depleted is not reflective of real-world driving conditions.

The demand pattern generated in this study is different to the other two, it shows a demand peak in the evening, with a relatively small demand in the morning. Thus, a move away from a *two peak* demand pattern is seen when journey distance and overnight EV charging are taken into account.

2.5.2 Future EV range prediction

EV range prediction is clearly critical to enable an accurate prediction of the demand at an HREVC as HREVCs are used when the range is lower than the journey distance. The EV battery capacity is closely linked to the EV range. Very little research has been conducted in the literature on the subject of predicting future EV battery capacities. On a broader sense, many reports have stated an expectation for EV battery capacities to increase and costs of battery packs to reduce [32], [150] and [151] however quantitative analysis is often lacking. It is therefore desirable to develop a method to predict future EV battery capacities.

Research on the topic of EV battery prediction tends to focus on the cost of the EV battery pack per kWh with extensive reviews and highly respected work [32] [152] [153]. However, little thought has been given to the likely distribution of kWhs needed for each EV. Clearly this is influential for predictions of the battery cost and needed to inform global supply chains. The work which has been completed in this area uses simple assumptions of compound growth rates applied to current EV fleet [154] [155] and indeed, work looking purely at the techno-economic perspective suggests a capacity in a small range around 15kWh is ideal, independent of the vehicle class [156]. As the EV market is in its infancy and evolving rapidly these methods and predictions quickly become outdated.

2.6 Grid modelling

Grid modelling and simulation is important for quantifying the effects of renewable generation and electric vehicles on the stability of the grid.

The problem of grid modelling, including transient effects, harmonic distortions, voltage drop etc, acting on ever more complex electrical grids is non-trivial and as such many

tools have been developed which researchers can use. These models can be ordered into three categories [157]:

1. **Transient state simulation tools** - these are generally used to evaluate impacts of effects that cause a transient state such as lightening strikes or short circuit. This means these models must be valid over a large frequency range.

2. **Real time software applications** - these are mainly to simulate the effect of additional equipment installation onto the grid. These are designed to be used in real time, with a data feed from the grid and as such concessions are often made in terms of simulation accuracy.

3. **Frequency based load flow tools** - these are designed for load flow calculations and are mainly focused on the steady state condition. As such, the user can enter any network design parameters they wish to. Then the software calculates the voltage and phase at each node, and therefore the power flows can be generated. This is particularly useful for checking for overloaded lines or voltage levels outside of specification.

Frequency based models are those of interest in this thesis as they offer the best value to a researcher interested in an hypothetical case. Many commercial software packages offer this such as: Eaton CYME power engineering software [158], ETAP PS [159] or Siemens PSS/E [160]. However, due to the expense involved with using these software packages, an open source or already available solution was sought.

2.6.1 Open source tools

2.6.1.1 GridLAB-D

GridLAB-D is a grid simulation tool developed by the Pacific Northwest National Laboratory [161]. It was initially designed for simulation of domestic loads and as such includes models for consumer appliances. Additional integration for distributed generation and energy storage is also included. This includes load flow calculations and electricity market integration.

GridLAB-D is capable of linking to Matlab [162] through second party plug-ins providing streamlined model development.

2.6.1.2 OpenDSS

OpenDSS is an open source grid modelling tool developed by the Electric Power Research Institute. It was designed to support the analysis of distributed generation connections to the utility distribution system. It also supports energy efficiency calculations and harmonic current flow [163].

The OpenDSS interface is a command line tool, however graphing functions have been included within the program to facilitate the presentation of results. The IEEE have produced a number of test case feeders within the OpenDSS framework which are designed to be representative of various areas of the electricity network. Additionally, OpenDSS can be used with Python and Matlab through a COM interface and can therefore be included within wider research models.

2.6.2 Simscape power systems

Within the Matlab Simulink environment is the Simscape power systems package [164]. It is therefore not open source as Matlab and Simulink must be purchased under a license. The university does subscribe to this license though, and as such this tool can be considered for use in this thesis. The integration into Simulink allows users to generate models through the use of the graphical user interface.

Component libraries are included with the package which enable the inclusion of many different pre-made models, such as three-phase machines, electric drives and renewable energy components. These allow the user to design a circuit to analyse. Harmonic analysis and load flow are automated.

2.7 Optimisation techniques

Finding optimal solutions to problems is of clear importance in many different areas of engineering, science and finance. In a simple sense optimisation is the process of finding the minimum or maximum value of a function, subject to given constraints.

There are many different techniques for finding an optimal solution to a given problem. The researcher must find and use a technique which is suitable for the aims in question. For example, a simple and highly accurate technique would be to calculate all feasible solutions at certain (suitably small) intervals of the input variables and choose the optimal solution from the set of results. For all but the most simple and highly constrained of problems though, this would be a vast waste of resources. For this reason, much work has been completed to develop more efficient techniques, designed for ever more complex problems. Popular techniques are discussed in greater detail in the following sections.

Optimisation problems are typically defined using two concepts:

1. **Objective function** - the mathematical representation of the goal in question. Calculation of this function gives the output which is to be maximised or minimised.
2. **Constraints** - the bounds of the problem, these can be defined in terms of the input variables, or calculated separately.

2.7.1 Linear programming

Linear programming is a method where a linear objective function can be defined and subjected to linear constraints in the form of inequalities. A solution space can then be formulated which contains the set of feasible solutions and is bounded by these inequalities. As this solution space is bounded by linear edges, and as the objective function can be expressed as a linear equation an optimal solution will then be found at one of the vertices of the solution space or along one of the edges.

Clearly this method is only suitable for problems of a linear nature. However, it has been used in a wide range of research in the transportation and renewable energy fields [165] [166] [167] [168].

2.7.2 Gradient methods

For problems where either the objective function or the constraints cannot be expressed in a linear way, gradient methods are popular. This method is iterative and follows a path in the solution space by following the direction of greatest gradient at each step. The algorithm thereby eventually converges on a local minimum. In these methods, the gradient is either measured or calculated analytically at each iteration. The values of the input variables are then adjusted by the gradient multiplied by a *learning rate* (γ). This *learning rate* controls the speed of convergence. A low value will lead to slow convergence, however, a high value will lead to overshooting. An optimal solution is then found when the derivative is equal to zero.

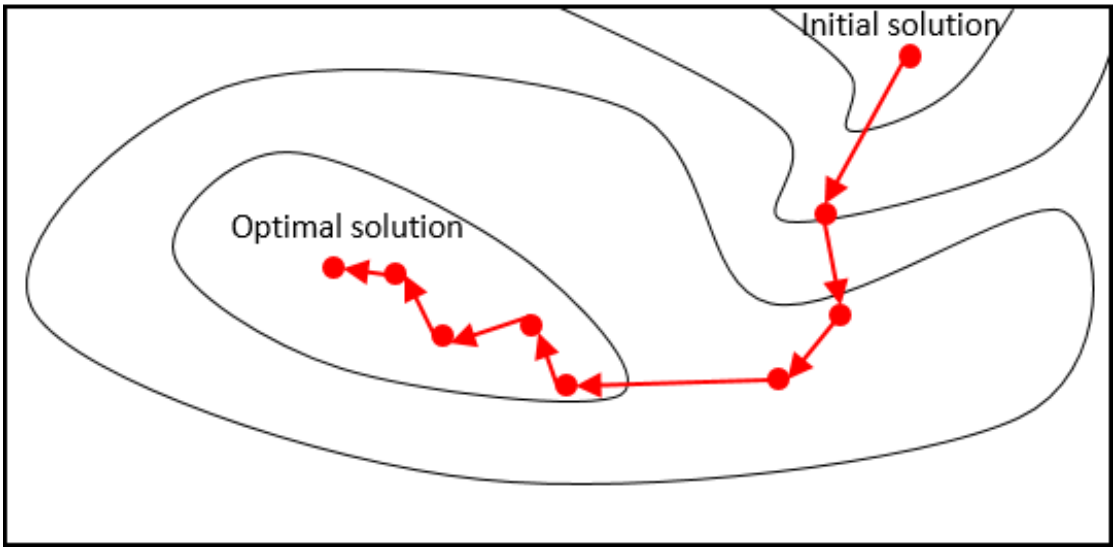

FIGURE 2.14: Schematic representation of convergence for a gradient method optimisation algorithm.

Gradient methods do have some limitations. Firstly, functions which have areas of high gradients and areas of low gradients lead to difficulty in selecting an appropriate *learning rate* as a low value is needed to prevent overshoot and excessive zig-zagging in the high gradient areas, but then a higher value is needed to achieve rapid convergence in the low gradient areas.

Secondly, and most importantly, gradient based methods can easily converge at local minima. To ensure a global minimum is found, a number of paths must be walked by the algorithm from starting points around the solution space. This significantly increases computational time.

Thirdly, the calculation of the gradient at each point becomes very costly when dealing with problems with many variables and an objective function where the derivative cannot be analytically calculated. The objective function must then be calculated for a small perturbation in each variable in order to calculate the gradient in that direction.

And fourthly, for stochastic models where the output space is granular and non-smooth a gradient based model will be ineffective as the local gradient is not dependent on the overall direction of solution improvement.

2.7.3 Heuristic methods

Gradient methods are effective at finding a local minimum, i.e. the algorithm may start in the vicinity of an optimal solution and then will effectively find the closest minimum. However, when there may be more than one minimum in a given solution space, or the solution space is not smooth (as a result of a stochastic problem) this method becomes ineffective Heuristic methods were developed to solve these problems [169]. The aim of heuristic methods is not to find a guaranteed minimum, but rather seek a good solution which satisfies the algorithm stop criteria. Most heuristic methods find their inspiration from aspects of nature (i.e. genetic algorithm, based on genetics and evolution; particle swarm, based on swarming birds/fish; neural networks, based on the human brain etc).

2.7.3.1 Genetic algorithm

A genetic algorithm was first introduced in 1975 [170], it is an optimisation method based on evolution and adaptation in nature. Each species adapts to the environment and makes incremental changes each generation with the aim of survival. Individuals interact to form new generations, with positive characteristics being carried through between generations by the process of natural selection. Other improvements or otherwise of individuals can be caused caused by mutation, where changes are induced in an individual which are not inherited from its parents.

This process is represented mathematically by a population of feasible solutions (chromosomes) being acted upon by three operators - selection, crossover and mutation. Selection allows for the process of natural selection to be expressed. The chromosomes

providing the best output to the fitness function are selected to reproduce in pairs (or higher numbers of parents can also be used [171]). A schematic representation of the genetic algorithm is shown in Figure 2.15.

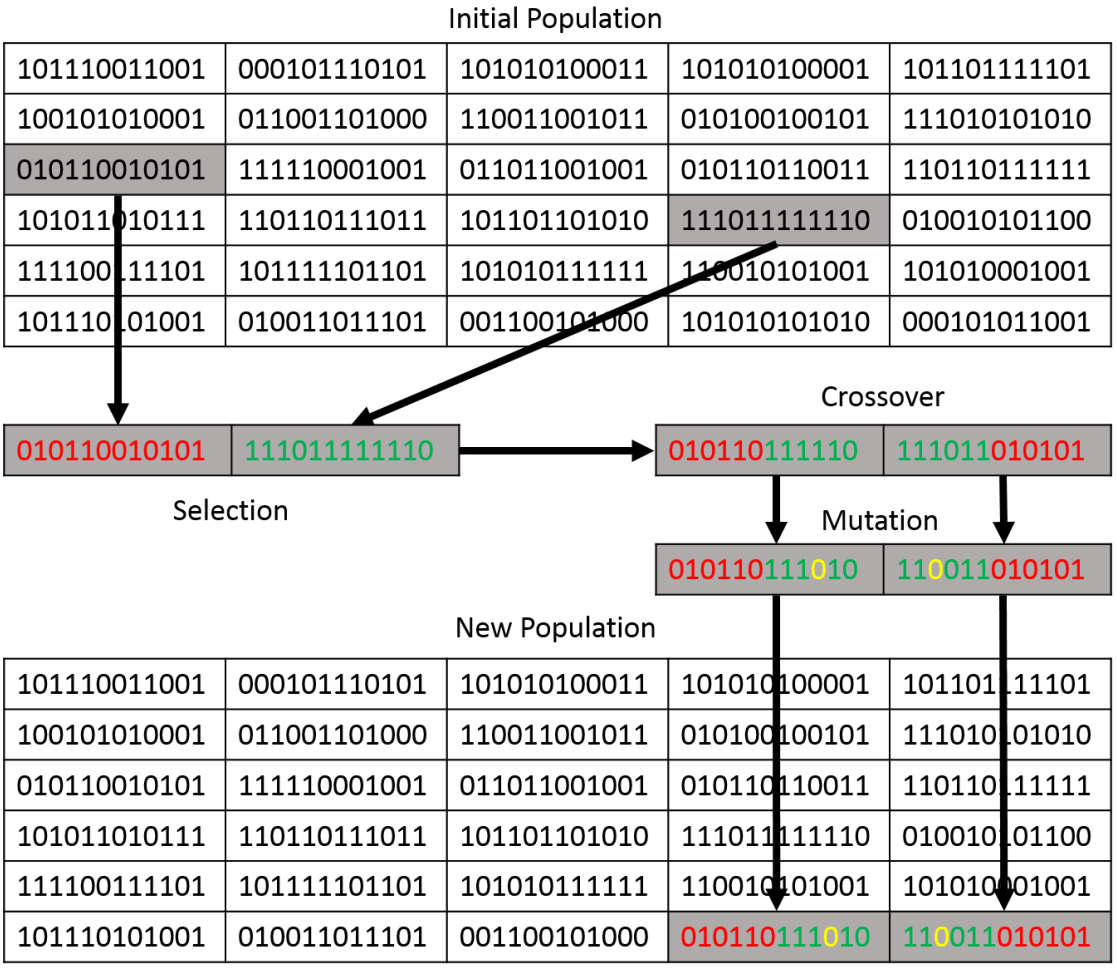

FIGURE 2.15: Schematic representation of the key processes in the genetic algorithm

The crossover operator then acts on these chromosomes to produce offspring. In this procedure parts of the two (or more) parent chromosomes are combined to make the children chromosomes. The combination method is not specific and changes between implementations of the algorithm [172]. For example, a segmented or uniform crossover may take place, where segments or individual elements of the chromosomes are swapped to form the children. Alternatively, a weighted average of parental elements may be calculated for each child element.

Mutations are then needed to enable input variables that are not included in the initial population. This is implemented by randomly changing input variables to a random

value. The rate at which this occurs in general is 1 in every 1000 variables addressed by the algorithm, but this is subject to design and fitting for best performance.

The result of these steps is an algorithm which allows for quick convergence at a global minimum making incremental changes to input variables. There is also the less clear, but important, benefit of enabling the optimisation of problems with discrete variable inputs.

2.7.3.2 Particle swarm

The particle swarm algorithm is a more recent invention. It was proposed by Kennedy et al in 1995 [173]. It is similar to a genetic algorithm in that it uses a set number of feasible solutions (particles) and iteratively changes/moves them through the solution space to converge on the optimal solution.

The method and rationale behind particle movement lies in their analogy to a swarm of fish or birds. In a swarm the particles can communicate with their neighbours and through these communications can move together to reach a common goal [174]. The aim of this algorithm is for all particles to congregate around the global optimum, as shown in Figure 2.16.

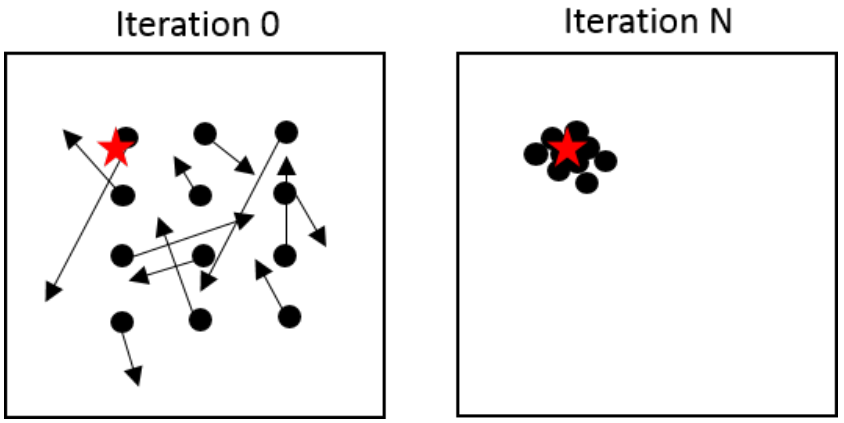

FIGURE 2.16: Schematic representation of the convergence of particles in the particle swarm algorithm.

Initialisation of particle positions is generally uniform across the solution space and each particle is assigned a velocity. This velocity describes the rate at which the input variables change each iteration. After the first iteration the velocity becomes dependent on a number of factors [175]:

- **Physical component** - the particle has inertia and therefore its velocity is dependent on its previous velocity.
- **Cognitive component** - the particle moves towards its best previous position.
- **Social component** - the particle moves towards the best position reached by its neighbours.

Many implementations of this velocity update methodology exist, for example see equation 2.6 [176]:

$$v_i^{t+1} = w^t v_i^t + \phi_1 u_1 (p_i - x_i^t) + \phi_2 u_2 (I_i - x_i^t) \tag{2.6}$$

Where:

- v is the particle velocity.
- w is the particle inertia.
- ϕ is the acceleration coefficient.
- p is the particle's best historic position.
- I is the best historic position of the particle neighbours.
- u is a random number to introduce a chaotic element.

Thereby the first term in Equation 2.6 is the physical component, the second term is the cognitive component and the third term is the social component. This is shown schematically in Figure 2.17.

The algorithm updates the velocity of each particle according to these rules until a stopping criteria is met. These include an iteration limit, or spacial distribution of particle reduction to satisfactory limits or the fitness value of the particles to be deemed satisfactory.

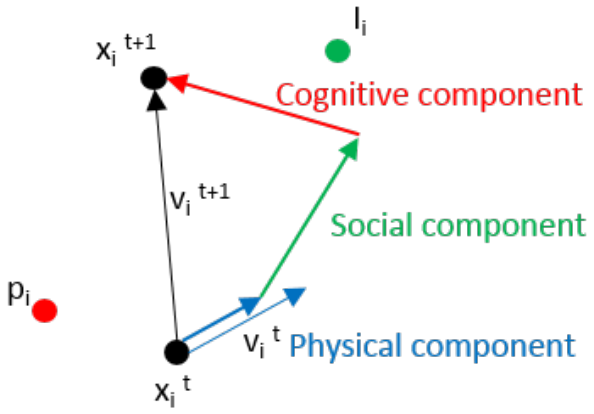

FIGURE 2.17: Schematic representation of particle velocity components in the particle swarm algorithm.

2.8 Sensitivity analysis techniques

Sensitivity analysis is an important and widely used tool for assessing scientific models [177]. The aim of this technique is to apportion the sensitivity of the model in question to each of the designated inputs i.e. find which inputs, when adjusted, have the greatest effect on model outputs.

There are two categories into which sensitivity analysis techniques generally fall:

1. **Local Sensitivity Analysis** - Adjustment of input parameters around a fixed nominal input value. Typically deterministic in approach.
2. **Global Sensitivity Analysis** - Adjustment of input parameters over the global input space.

2.8.1 Local sensitivity analysis

Sensitivity analysis that is carried out around a specific point of interest of the input parameters is called local sensitivity analysis. This is typically carried out in a deterministic framework where no probability distributions are used to select input variable values [178].

One such example of this style of analysis is *one at a time* methods. In this method each variable is adjusted individually. The calculated sensitivity then arises from the relative

change in the output following each input change. Whilst this is a very simple method to implement, there is the clear limitation of the potential for missing interaction effects between separate input variables. First order sensitivity effects can be calculated through *one at a time* methods, as shown in Equation 2.7 (using the notation in reference [178]) also known as trajectories. A nominal and sensitivity case ($\mathbf{x}^0, \mathbf{x}^+$ respectively) are assigned where **x** denotes the set of inputs to the model y.

$$\Delta_i^+ y = g(x_i + \Delta x_i^+, x_{\sim i}^0) - g(x^0) \tag{2.7}$$

Where g is the output of model y. $\Delta_i^+ y$ is then the sensitivity measure for the input variable i. This is classed as the individual sensitivity measure:

$$\phi_i = \Delta_i^+ y \tag{2.8}$$

However, higher order sensitivity measures describe the interaction sensitivity arising from synergistic relationships between input variables. These can be calculated at a penalty of increased model iterations. If the total change in y is defined in Equation 2.9:

$$\Delta y = y(\mathbf{x}^+) - y(\mathbf{x}^0) \tag{2.9}$$

It can be seen that Δy consists of not only of $\sum_i^n \phi_i$ but also the higher order sensitivity measures shown by Equation 2.10.

$$\Delta y = \sum_i^n \phi_i + \sum_{i<j} \phi_{i,j} + \cdots + \phi_{1,2,\ldots,n} \tag{2.10}$$

Where

$$\begin{aligned}
\phi_i &= g(x_i^+, \mathbf{x}_{\sim i}^0) - g(\mathbf{x}^0) \\
\phi_{i,j} &= g(x_i^+, x_j^+, \mathbf{x}_{\sim i,j}^0) - \phi_i - \phi_j - g(\mathbf{x}^0) \\
\phi_{i,j,k} &= g(x_i^+, x_j^+, x_k^+, \mathbf{x}_{\sim i,j,k}^0) - \phi_{i,j} - \phi_{i,k} - \phi_{j,k} - \phi_i - \phi_j - \phi_k - g(\mathbf{x}^0)
\end{aligned} \tag{2.11}$$

From this analysis three indices can be extracted. Firstly the individual sensitivity measure shown in Equation 2.8. Secondly, the total finite change measure is the sum of all measures relating to a given input as shown in Equation 2.12

$$\phi_i^T = \phi_i + \sum_{j=1}^{n} \phi_{i,j} + \sum_{j=1}^{n}\sum_{k=1}^{n} \phi_{i,j,k} + \cdots + \phi_{1,2,\ldots,n} \tag{2.12}$$

Then the interaction measure can be inferred from Equation 2.13.

$$\phi_i^I = \phi_i^T - \phi_i \tag{2.13}$$

Where ϕ_i^T and ϕ_i^I are the total finite change and interaction measures respectively. Together, these metrics can be used to describe individual and interaction based sensitivity of each input variable to a model [179]. Local, deterministic based methods are preferential for when a specific point in the model space is to be addressed for sensitivity, however, many scenarios arise where sensitivity analysis is required over a broader set of input values. For this, global sensitivity analysis is used.

2.8.2 Global sensitivity analysis

2.8.2.1 Morris method

In the Morris method, the gradient of the output space is calculated at each point. The derivative components in the direction of each input variable are known as elementary effects from the original work by Helton [180] and further developed by Morris et al [181] [182].

In this method a uniform input distribution is generally used. This method is generally used for large, computationally expensive models [183]. *One at a time* sampling techniques are used, similar to that described in Section 2.8.1. However r different trajectories are used, sampled randomly across the input space. Therefore, a global estimation for sensitivity is established.

The elementary effect (EE) can then be calculated for each variable at each trajectory as shown in Equation 2.14.

$$EE_i = \frac{Y(x_1, \ldots, x_{i-1}, x_i + \Delta \ldots, x_k) - Y(x_1, \ldots, x_k)}{\Delta_i} \tag{2.14}$$

Where k is the number of model inputs. r EEs are then calculated for each variable. Thus, the mean (μ) of these EEs is the global sensitivity to that variable, as shown in Equation 2.15.

$$\mu_i = \frac{\sum_{t=1}^{r} EE_{i,t}}{r} \tag{2.15}$$

Where t is the index of r. Additionally, the standard deviation (σ) is a measure of the interaction effects with other parameters, as shown in Equation 2.16.

$$\sigma_i = \sqrt{\frac{\sum_{t=1}^{r}(EE_{i,t} - \mu_i)^2}{(r-1)}} \tag{2.16}$$

The number of model evaluations for this sensitivity method then is $r(k+1)$ as $(k+1)$ evaluations are made in each trajectory. Heiselberg et al. [184] suggests a figure between 4-10 for r, with $r = 4$ a minimum for reliable results. It is common practise, however, to use values of r which are much higher ($50 < r < 100$) to accurately estimate the sensitivity across a large input space and achieve stable EE values [185].

2.8.2.2 Sobol method

The Sobol method was first proposed in 1993 [186] and further developed by Satelli in 2002 [187] the Sobol method uses the variance in model output to estimate the sensitivity to input parameters.

Instead of finding the change in the function output arising from small deviations in inputs, the Sobol method measures changes across the entire input solution space. This is achieved by calculating the variance (σ^2) arising from perturbations in each input. The overall variance in function output can be written as shown in Equation 2.17:

$$\sigma_Y^2 = \sum_i \sigma_i^2 + \sum_i \sum_{j>i} \sigma_{i,j}^2 + \sigma_{1,2,\ldots,k}^2 \tag{2.17}$$

The individual and total sensitivities can then be calculated for each variable in the same way as that described in Section 2.8.1.

The Sobol method generates very accurate sensitivity results. However, the number of model evaluations can be very large in some cases. Model evaluations grow linearly with the number of inputs as $N = r(k+2)$ where N is the number of model evaluations Pianosi [188] suggested that r lies in the range 10^2 to 10^4. Therefore, depending on the application a very large number of model evaluations is often needed for conversion of the sensitivity measures. This means it is not suitable for complex models.

2.8.2.3 Fourier amplitude sensitivity test

The Fourier amplitude sensitivity test (FAST) method was developed after the Sobol method by Cuckier et al [189], it used variance as a measure of sensitivity but decomposes the variance results using a Fourier transformation. This creases partial variances for each parameter, which can then be compared to the overall model variance to estimate the sensitivity to that variable.

The use of the Fourier transformation has been found to be computationally less expensive than the Sobol method, however this is at the expense of implementation complexity [190].

The minimum number of model evaluations for FAST is determined by $N = 2Ms\omega_{max} + 1$, where Ms is the maximum harmonic (no less than 4, usually taken to be 4 or 6) and ω_{max} is the maximum frequency [191]. ω_{max} is dependent on the number of input variables, a frequency free of interference to an order of 4 should be selected as discussed in [192]. This is roughly equal to $10k$. It can therefore be seen that whilst the overall number of model evaluations can be lower for FAST than Sobol, it is still a computationally expensive method when compared to Morris.

2.8.2.4 PAWN method

The PAWN (derived from author names) method [188] is designed to be used in conjunction with variance based analysis. In some cases the variance is not an accurate

measure of sensitivity, therefore the PAWN method was developed to examine the entire output distribution. A cumulative probability distribution is generated to describe the output.

This method is particularly useful if the output is especially skewed or multi-modal.

The required number of model evaluations for this method is $N = N_u + k(nN_c)$ where N_u is the number of samples of inputs at nominal values, n is the number of conditioning values, N_c is the number of conditioned samples. This is the case as the method uses a two stage process where N_u samples are used to generate a cumulative density function which is then compared to a conditioned cumulative density function generated from N_c input samples. Typically n is in the order of a few dozens and N_u, N_c are in the order of a few hundreds.

2.8.3 Sensitivity analysis tools

A popular toolbox which includes a number of global sensitivity analysis techniques is the SAFE toolbox which is implemented in Matlab [193] (additional details given in [194]). This is implemented in matlab and therefore can be easily used to assess sensitivity in models implemented on the matlab platform. This toolbox is available for free and the documentation is freely available with open access meaning it is ideally suited to academic work.

Additional commercial software packages exist, such as the Vanguard software package [195] and implementations in R [196]. However, as there is a cost associated with the Vanguard package and R is not used within this PhD these are not considered any further.

2.9 Summary

This chapter has presented the theoretical background which the following work builds upon. This is through analysis of energy storage, electric vehicles and renewable energy. A summary was also presented on the various options for research and computation methods for use in this project, of these, the methods selected are:

- OpenDSS - selected for use of the IEEE test case feeder, and the open source nature of the programme.
- Genetic Algorith - Given the stochastic nature of the optimisation problem considered in this these, heuristic methods must be used. Additionally, the implementation of the genetic algorithm in matlab allows for integer specification of values: important in this work due to the discrete nature of some of the variables (eg. no. of charge points).
- Morris method implemented in the SAFE toolbox - The morris method is car more computationally efficient than the other global sensitivity analysis tools, an important factor given the complexity of the approaches used in this thesis. The SAFE toolbox allows for simple integration into Matlab and some degree of customisation.

Chapter 3

Predicting EV Charge Demand in the UK

This chapter aims to create a method to enable robust, representative generation of EV power demand data. This will be used to inform a wider HREVC model developed in later chapters. The intermittency of the renewable energy resource (which is to be integrated into an HREVC) causes the temporal nature of the EV demand to be of particular interest. If, for instance, the EV demand has a peak at midday, there will be clear synergies with solar power, however, sustained demand through the night will lead to difficulties when attempting this match. Additionally, there is a need for the EV demand throughout the charge cycle to represent realistic charging patterns.

The predicted EV demand can then used used to inform a model of the HREVC which is used to assess the system feasibility and calculate optimum values of design variables. As this will be heavily dependent on the nature of the EV demand there is a clear requirement for the work in this chapter.

The aim of the work set out in this chapter is, therefore, to create a method of predicting the EV power demand at an HREVC throughout a given time period.

3.0.1 Novel contributions

The novel contributions found in this Chapter 3 are highlighted below:

1. A novel method is proposed for predicting future EV battery capacity distributions in a future scenario when the EV market has become balanced and reflects the use and purchase patterns currently seen with conventional vehicles.
    - This is discussed in detail in Section 3.2.4.
2. A novel method for predicting HREVC power demand patterns in a locationally dependent way at any location on the SRN in the UK is explained.
    - This method uses new data which has not previously been used for a similar study, mined from the Open street map. This is discussed in Section 3.1.1.
    - Discreet probability distributions for journey distance for each hour of the day are generated. These can be used to temporally predict demand at HREVCs. This is highlighted in Section 3.2.2.

3.1 Background

To generate the demand pattern at an HREVC requires an understanding of the factors which will lead an EV to use the HREVC. Since EV charging can largely be achieved at home [87], it can be assumed that most journeys begin with a fully charged battery. Therefore, an HREVC will be needed when the journey distance exceeds the range of the EV. To find the demand at an HREVC then, two questions must be answered:

1. What is the range of the EV?
2. What is distance of the journey?

The range of the EV is linked to the battery capacity of that EV. Very little research has been conducted in the literature on the subject of predicting future EV battery capacities. On a broader sense, many reports have stated an expectation for EV battery capacities to increase and costs of battery packs to reduce [32], [150] and [151] however quantitative analysis is often lacking. It is therefore desirable to develop a method to predict future EV battery capacities.

Within this area four main questions must be asked to determine the modelling procedure [197]:

1. How many Trips will there be?
2. Where do the trips go?
3. How will people travel?
4. What route will they take?

This approach can lead to some very complex models which are beyond the scope of this PhD as the main aim of transportation modelling here is to find the distance and time at which EV journeys occur. The particular route is not of concern at this stage and the mode of transportation is predefined as EVs. Nonetheless the principle of the modelling approach should be adhered to by finding reliable data in order to answer the remaining questions.

3.1.1 The Open Street Map

The Open Street Map [6] is an online, open source map which is under an open license, as such, anybody can make changes to it. A screen-shot is shown in Figure 3.1. Crucially for this work, it also has the capability for anyone to upload GPS traces onto it. These GPS traces are available to anonymously download and the overall size of the data is $\approx$ 250GB. This has led to a dataset consisting of 848,062 journeys which are available to download. Whilst these tracks cover all aspects of daily movement of the uploader, a proportion of them are journeys relevant to the HREVC model.

This repository has received little academic interest, however, the information it holds could provide critical insight for many fields of work. It is the aim to use this journey data repository in order to find travel patterns along main roads in the UK to enable a prediction of HREVC demand. Specifically, detailed traffic count data is widely available for many roads in the UK. This is not adequate for predicting HREVC use as the distance of each journey being counted is not known. However, the open street map can be used to find journey distance patterns which can then be added to the existing traffic count data. This enriches the existing data resource and allows for more accurate HREVC use predictions.

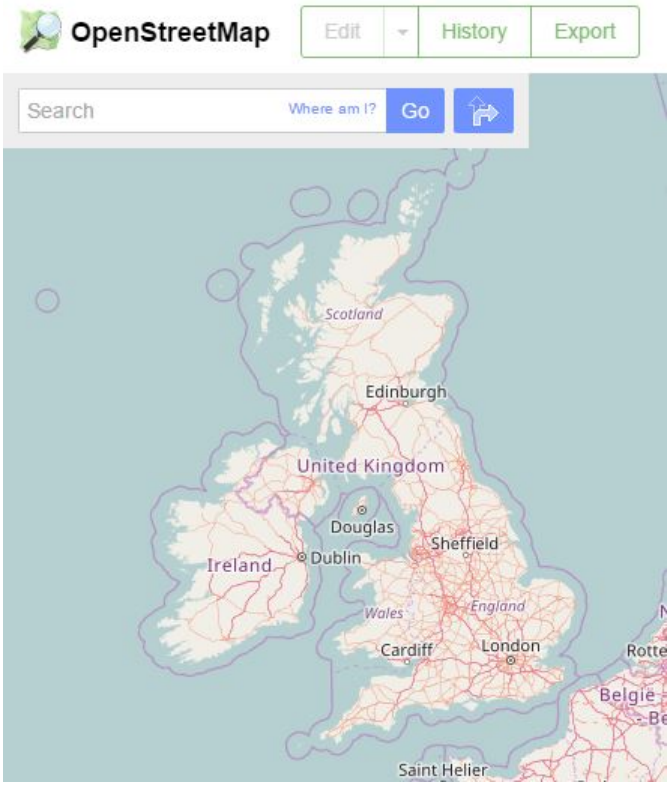

FIGURE 3.1: Screen-shot of the Open Street Map showing the United Kingdom.

3.1.2 Assumptions used in this work

Any modelling approach must be based on assumptions about the system which is to be modelled. In this chapter, there are two on which the work is based.

1. Firstly, it is predicted that EVs will be used in the same manner as conventional vehicles today. This accounts for two specific assumptions, firstly that the proportion of EVs within each segment (i.e. mini cars, small cars etc) is the same as that for conventional vehicles. Secondly, the journeys made by EVs will be the same as those made with conventional vehicles. Ceteris paribus, this assumption is thought to be valid as the motivations for buying and using a vehicle are technology agnostic i.e. a vehicle user needs to go from one location to another at a certain time, this need is not dependent on the type of vehicle which is used to provide this transportation need. This assumption was examined by [198] where EV trials revealed the similar use patterns to conventional vehicles with the exception of long distance journeys. The range of EVs has increased substantially since this work was published, which suggests that similar use patterns will now

extend to journeys of longer distance. This assumption has been used in many works (e.g. [199] [200] [148] [201]) and discussed in greater detail by [202].

2. Secondly, psychological factors which may affect EV use are not considered in this thesis. This assumption is made in order to maintain simplicity in the simulation. There are two likely implications of this. Firstly, it is assumed that there is no link between the type of vehicle being used and the journey it takes. The matching between generated EVs and journey distance is entirely random in this method. Therefore psychological factors such as "*I use my EV for a lot of long distance journeys, so I will buy an EV with a high range*" are not considered. Secondly, it is assumed that the driver will use the last feasible HREVC prior to the EV SOC reaching zero. Therefore, any fear associated with having a low SOC leading to earlier charging is not considered, neither is a charging method designed to save money and time by arriving at the destination at or close to zero SOC. Linked to this, the EVs are each charged to 100% usable SOC when visiting the HREVC, thereby eliminating any preference the driver may have. This assumption greatly improved the simplicity of this study and allows for the use of the Open Street Map dataset. However, there may be some associated limitations with this assumption highlighted in the literature. For example, leading EV charging infrastructure providers suggest that the provision of public charging infrastructure leads to EVs driving further and charging their vehicles more often [203] this correlation could not be possible for ICEs. Equally, reference [204] suggest that EVs will often be used as a second car in a household, leading to shorter journeys and a reduced need for high capacity batteries. These references look at current EV use where there is no consensus on how the future use of an EV (where battery capacities have increased and costs have fallen) compares to that of an ICE. Therefore, this assumption is thought to be the best approach for this work.

3.2 Method

If the assumption that probability of an HREVC charge event during a trip is linearly proportional to the distance of that trip, then it follows that the method needed for HREVC

use prediction is dependent on finding the distance against time of day for trips occurring on the SRN.

There are substantial, freely available data sets, published by the UK government and Highways England regarding traffic flow. These have been collated through counting the number of vehicles passing a certain point for set periods [205].

It is desirable to configure an approach for predicting HREVC demand which uses this data as it is both geographically dependent and has high temporal resolution. It could therefore be used as a tool for predicting HREVC demand dependent on geographical placement. As the number of journeys passing near the HREVC can be assessed by the traffic flow data, an accurate method for predicting the distance of those journeys is needed. Such a method is presented in this work.

In this work, journey data from GPS traces were used to generate probability distributions of the journey travelled for each hour of the day. Thus, dependent on the time of day of the journey, it's distance can be stochastically predicted based on real-world journeys available in open-source GPS tracks downloaded from the Open Street Map [206]. The need for a high-rate charge during this journey can then be calculated if the battery capacity and energy usage per mile of the EV is known. With an average speed then applied to the journey, the time and energy demand of the high rate charge instance can be calculated.

The initial input for this method of HREVC demand prediction is the number of EVs using the SRN each day. For each of these the following calculations are carried out:

1. Calculate battery capacity
2. Calculate departure time
3. Calculate distance of journey
4. Using results from calculations 1-3, calculate whether the range of the EV is sufficient for the journey distance. If it is not, then the EV must utilise the HREVC.

These calculations filter out the EVs which do not need to use the HREVC. Further calculations are then needed to determine the specific use case of the HREVC for each EV. These are:

1. Calculate point along journey at which charging occurs.
2. Calculate time to begin charge.
3. Calculate SOC of EV when arriving at the HREVC.

The results of these calculations, with the battery capacity of the EV, form the outputs from the EV demand prediction model. The method briefly covered here is discussed in detail in the following sections.

The five main steps within the method presented in this thesis are as follows:

1. **Extraction of relevant journeys from Open Street Map GPS Track Dump.** Detailed in Section 3.2.1. Assumed to be those journeys which intersect with the SRN.
2. **Prediction of journey distances for each hour of the day.** This will be achieved through fitting probability distributions to extracted journeys. The aim of this process is to create a probability distribution for each hour of the day which can be used to predict the distance of a given journey which has its mid point (in time) within that hour. This information can be used to find the time of arrival at the HREVC and estimate the EV's State of Charge (SOC) at arrival. This is detailed in Section 3.2.2.
3. **Production of locationally dependent probability distributions of journey distance.** This is achieved through scaling the probability distributions to the traffic flow observed at the chosen site. This is detailed in Section 3.2.3.
4. **Prediction of battery capacities of the EVs which will use the HREVC.** This is required to find the energy demand for a given EV if the initial and final SOCs are known (through use of probability distributions created in steps 2 and 3 above). This is achieved through probability distributions fitted to characteristics in the current conventional vehicle fleet in order to predict a future case where EV ownership is widespread. This is discussed in Section 3.2.4.
5. **Execution of Stochastic Simulation.** In this step, random numbers are generated from the probability distributions. In this way, an EV is given a battery capacity, a journey distance and a departure time. This information is then used to calculate the HREVC demand. This is detailed in Section 3.2.5.

3.2.1 Data Mining Approach

As the dataset is large a data mining approach was utilised to find relevant GPS traces. The aim of this approach was to identify all the traces which overlapped with the SRN. As very little walking or cycling is conducted on the SRN it is assumed that each GPS trace which intersects with it is a vehicle journey.

The strategic road network is managed by Highways England. A shapefile describing the land managed by Highways England is available as an open source download from the data.gov.uk repository [207]. This is shown in Figure 3.2.

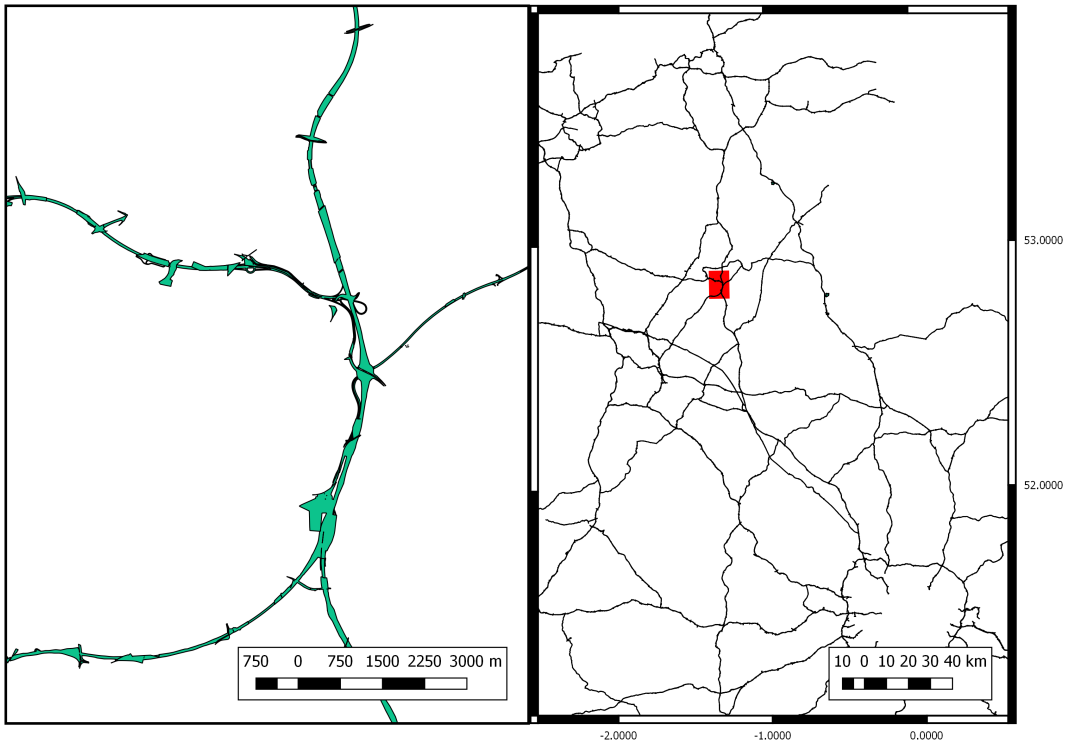

FIGURE 3.2: Highways England Shapefile shown at macro and micro scales. The area in green represents land managed by Highways England.

Examples of some of the GPS traces can be seen in Figure 3.3. Each journey consists of a number of GPS points, with a timestamp. As the timestamps follow in chronological order, these points can be joined to form a trace.

Individually assessing each point on each GPS trace to determine whether it lay within the bounds of the SRN shapefile would have been far too computationally intensive

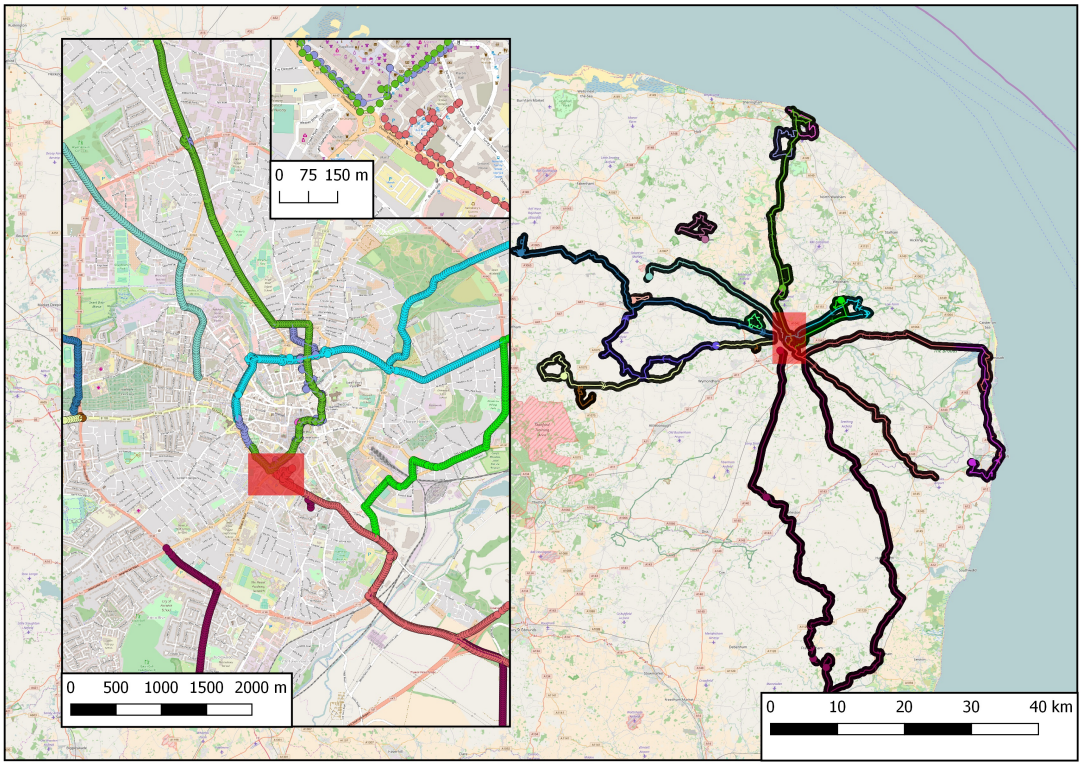

FIGURE 3.3: Example GPS traces from the Open Street Map shown at 3 scales.

(indicated time to compute this was 3 years!). As such, an imaginary box was constructed for each GPS trace, the edges of which lay at the furthest bounds of the journey, this could then be assessed for intersection with the SRN shapefile. This reduced the computational time substantially. A schematic example of this method is shown in Figure 3.4.

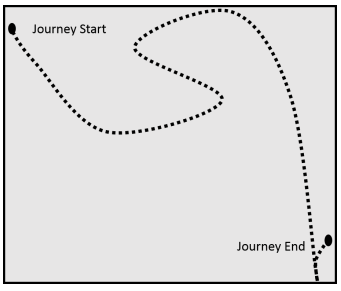

FIGURE 3.4: Representative, schematic journey with grey box showing the area which would be assessed for intersection with the SRN shapefile.

After running this data mining procedure on the dataset, the number of relevant journeys on the SRN was found to be 2287.

3.2.2 Constructing Probability Distributions from Mined Data

The aim of using the Open Street Maps GPS tracks was to create representative probability distributions of journey distance. In order to achieve this, the filtered GPS tracks were split into distinct arrays dependent on the mid point in time for that journey. This gave 24 datasets each corresponding to the previous hour. Journeys with distance of less than 1 mile were removed as they were assumed to be anomalous for journeys on the SRN. The 24 datasets can then be used to generate probability distributions for each hour of the day. The mid point in time for each journey was used to generate the probability distributions since, in the general case, this is the point at which the EV is most likely to be using the SRN and therefore able to use the HREVC.

It was decided that for this task, the log-normal distribution was not suitable as it does not represent the varying shape of the distribution of journey distances exhibited in different hours of the day (in particular journeys beginning early in the morning do not follow a log-normal distribution shape). For this feature either the Weibull or Gamma distributions must be used. The gamma distribution assumes an equal chance of a journey termination in each timestep, however the Weibull distribution allows for either increasing or decreasing chances of journey termination as the journey progresses. This feature of the Weibull distribution was found to enable a better fit to the journey distances found and also to provide distinction between journeys beginning at different times of the day.

The Weibull distribution was therefore selected for fitting to these datasets. It is commonly used in failure and reliability analysis. In this use case, the predicted variable x refers to the lifetime of a component allowing a prediction of the “time-to-failure”, however, in this work it refers to the point at which the EV journey finished or the “distance-to-end”. Therefore, this use of the Weibull distribution can be seen to be appropriate for journey length prediction. This is supported because the Weibull Distribution can have a long tail, which reflects real world journey distance distributions well as high journey distances are relatively common and would not be evident if a gamma or log-normal distribution were chosen.

The three parameter Weibull distribution is shown in Equation 3.1:

$$f(x) = \frac{\gamma}{\alpha}\left(\frac{x-\mu}{\alpha}\right)^{(\gamma-1)} exp\left(\frac{x-\mu}{\alpha}\right)^{\gamma} \tag{3.1}$$

Where:

- γ is the shape parameter.
- α is the scale parameter.
- μ is the location parameter.

μ indicates the beginning value of the distribution and is commonly equal to zero i.e. a journey distance of zero at the start of the journey. In this case the Weibull distribution becomes:

$$f(x) = \frac{\gamma}{\alpha}\left(\frac{x}{\alpha}\right)^{(\gamma-1)} exp\left(\frac{x}{\alpha}\right)^{\gamma} \tag{3.2}$$

An example of the fit of the Weibull distribution to the measured data is shown in Figure 3.5. The distribution returns a higher number of very short journeys than is observed in the GPS traces. However, as the model concerns itself only with the journeys of high distance, accurately predicting probability of high mileage journeys is the key output of the selected distribution.

This fitting procedure was carried out for each array of journey distances (accounting for each hour of the day) as shown in Figures 3.6 and 3.7. However, despite the size of the original dataset, in the hours 02:00-04:00, 05:00-06:00 and 23:00-00:00 there were not enough journeys to generate a probability distribution (<5).

It it not surprising that, for the majority of the hourly distributions γ is less than 1 as drivers are more likely to reach their destination as distance increases. However, for journeys beginning between 22:00 and 23:00 this is not the case. This parameter of the distributions alone does not reveal the propensity for long distance journeys in each hour though, the scale parameter is needed for this.

The scale parameter α is the mean journey distance. This is not constant through the day. In the morning for the hour 04:00-05:00, a distinctly higher mean journey distance

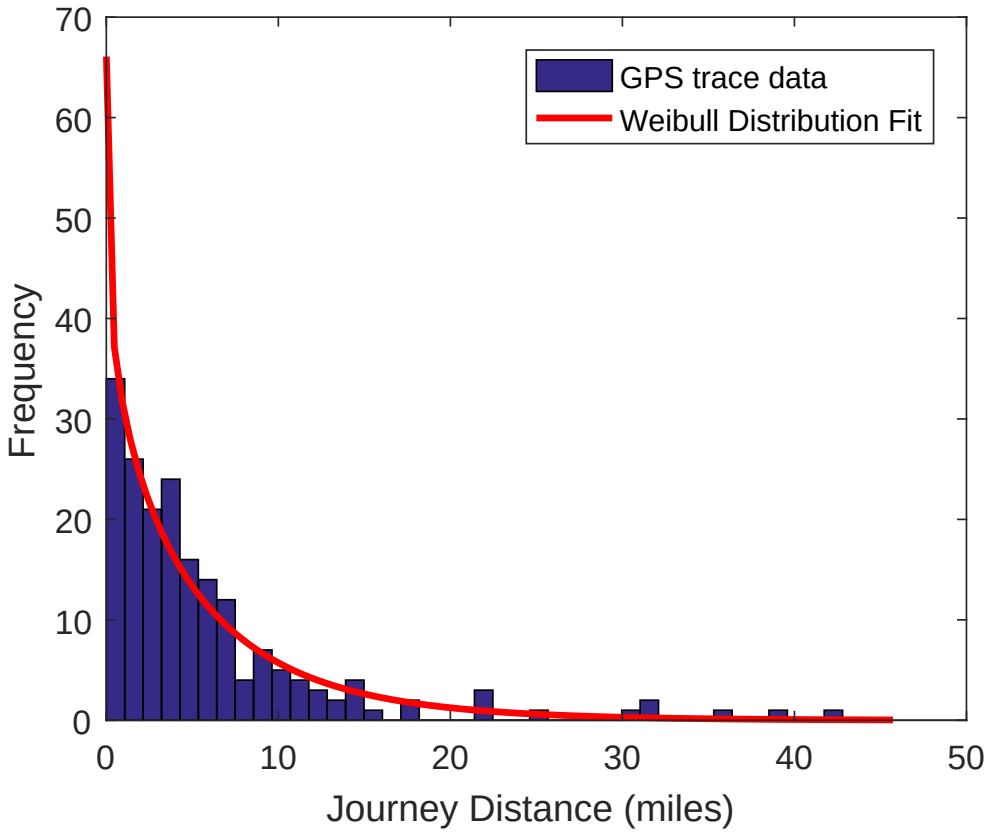

FIGURE 3.5: Histogram of GPS trace journey distance over duration 1400-1500, overlayed with the fitted Weibull Distribution.

is observed (Figure 3.7). This could be caused by a preference for long distance, non-routine, journeys to be started in the morning.

This effect is further seen in Figure 3.8 which shows the probability that a journey will finish by given distances, as calculated from the Weibull Distributions for each hour. For journeys with mid-points between 04:00 and 08:00 a preference for long distance ($>$100 mile) can be seen. The hours with the highest probability of short journeys are between 16:00 and 18:00 with the probability of long journeys beginning in this window becoming small to non-existent. This representation is independent of the frequency with which journeys begin, which is clearly higher during busy periods (see Figure 3.10). To make a prediction of the number of journeys of a given distance being undertaken at a given time, this analysis must be combined with measured traffic flow data.

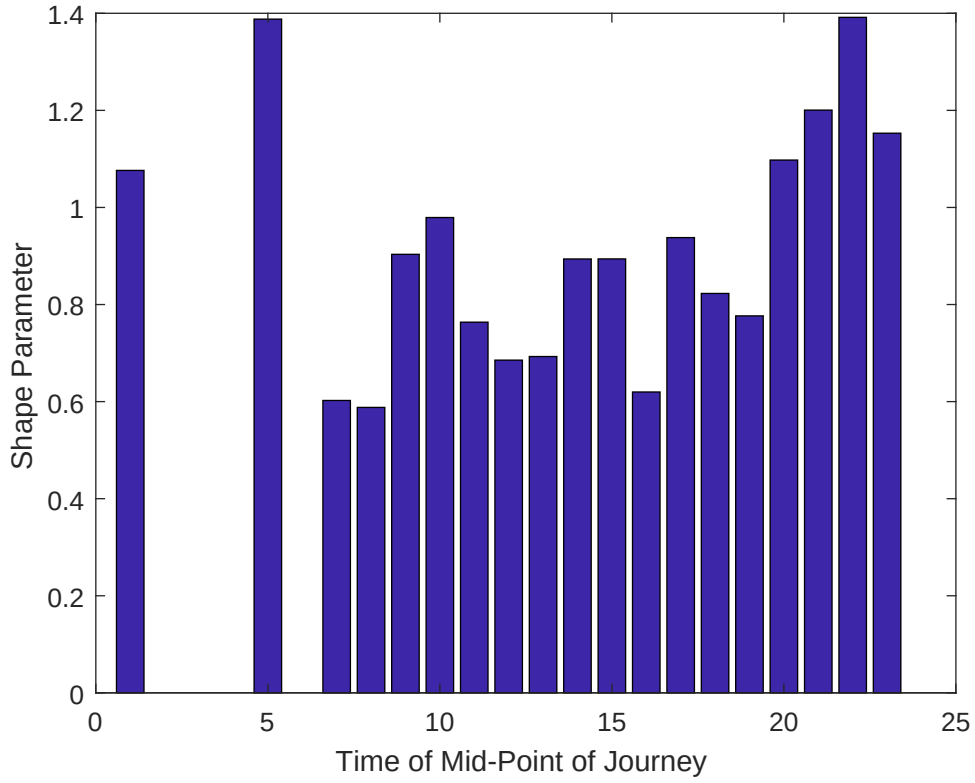

FIGURE 3.6: Weibull Shape parameter for each hour distribution.

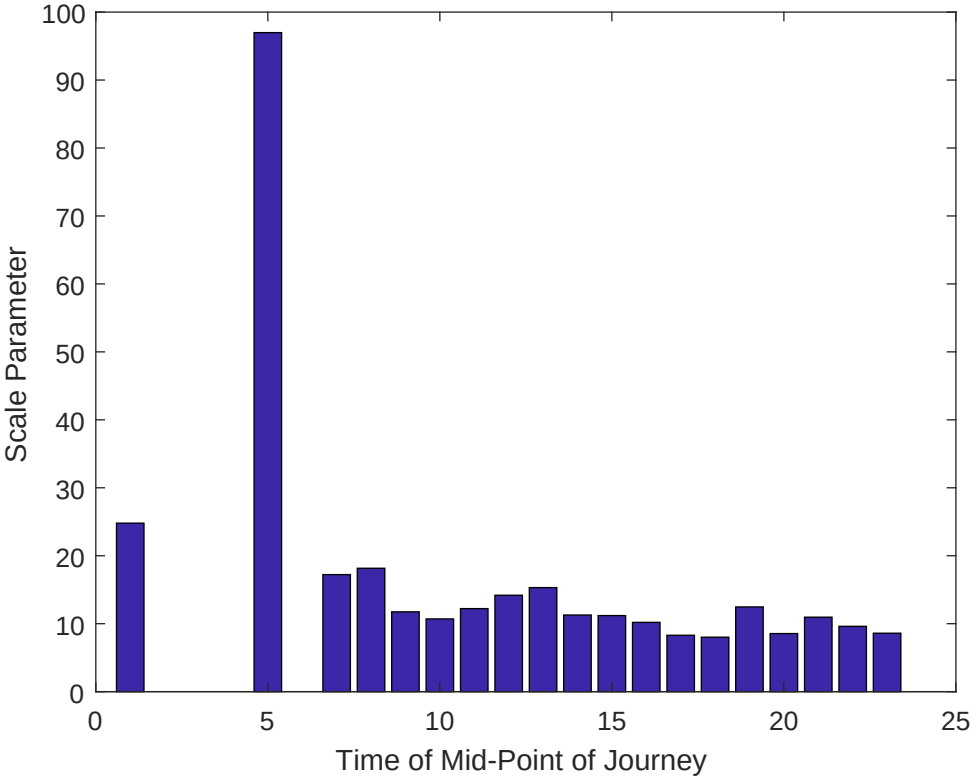

FIGURE 3.7: Mean journey distance against time of day for Weibull Distributions.

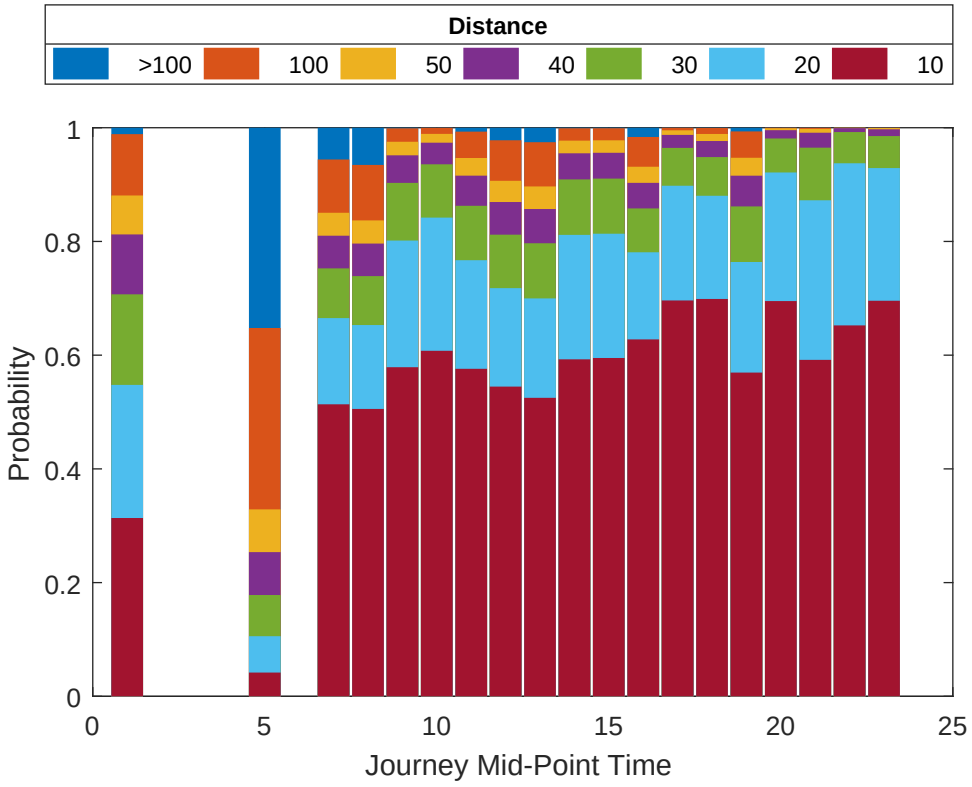

FIGURE 3.8: Cumulative probability of journey distance for each hourly probability distribution.

3.2.3 Including Traffic Flow Data

The Highways England data repository [208] is a rich source for traffic flow data in the UK. 15 minute resolution vehicle count data can be found for all the roads on the SRN. Additionally, it is possible to select the section of road at which the traffic flow count is desired. The database is also kept up to date with monthly updates for each road section.

This data resource is used in this work to provide relevant traffic flow data. Indeed, this method of high rate EV demand prediction was designed to be used as a tool with this dataset such that EV demand can be calculated in any location on the SRN.

For example Figure 3.9 shows the measured traffic flow for a section of the A45 on 01/06/2014.

For this data to be useful in predicting high rate EV demand at this section of the A45, the Weibull distance distributions can be utilised with the number of journey distances

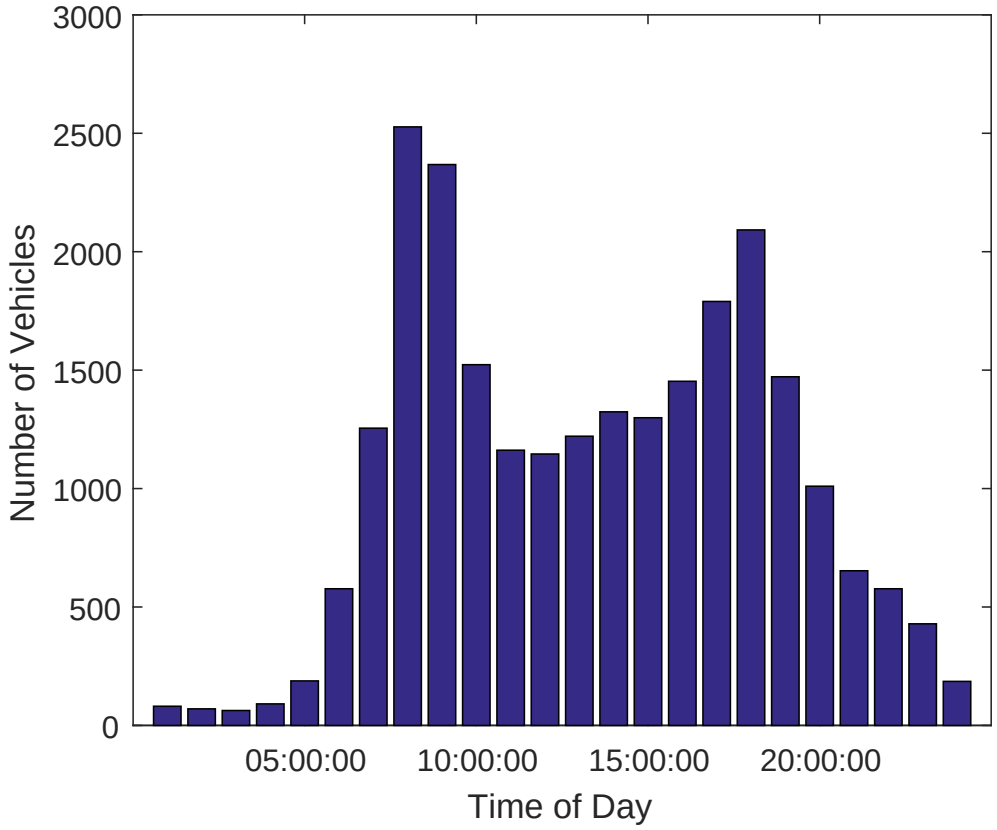

FIGURE 3.9: Measured traffic for the A45 (between A509 and A509) on 01/06/2014.

predicted, using the probability distribution, for each hour, dependent on the measured traffic flow for that hour. This gives a detailed distribution of the number of journeys of certain lengths being undertaken in a given hour. A representation of this analysis is shown in Figure 3.10. Importantly, the figures shown in Figure 3.10 can be recreated for any point on the SRN by using the traffic flow data for that point.

In order to use this analysis to predict the demand for the HREVC the capacity of the EV battery must first be assessed. This will allow a calculation of the EV range and therefore, whether a HREVC must be used en-route in order to complete the journey. The work covering this analysis is discussed in the following section (Section 3.2.4).

3.2.4 EV Battery Capacity Prediction

An estimation of the distribution of future EV battery capacity (E_{cap}) has been formulated from the market share of current vehicle segments. Previously proposed vehicle

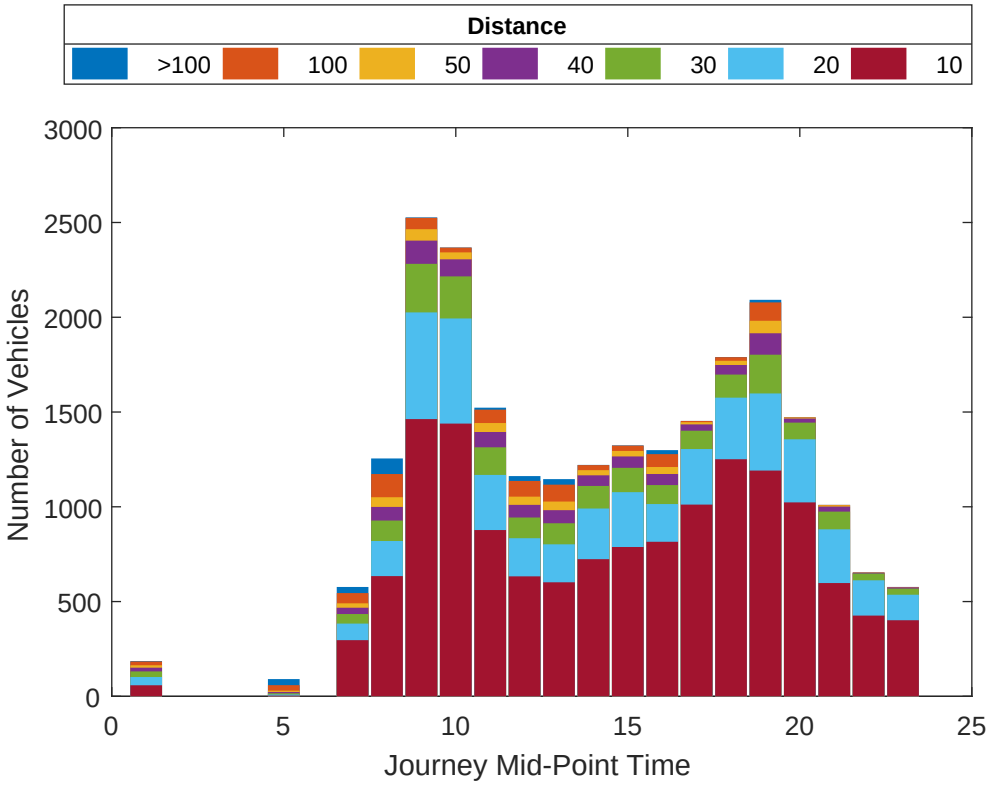

FIGURE 3.10: Predicted journey distances for the A45 (between A509 and A509) on 01/06/2014.

segmentation characteristics is shown in Table 3.1 from [209], this follows the segmentation employed by the European Commission and adopted in the UK. A UK source of this data was sought, however, the inclusion of the mean and standard deviation of engine capacity and mean annual mileage with the market share for each segment led to the selection of this reference for the data source. The market share for each segment of vehicle in the UK is similar to that presented by [210].

Since the conventional vehicle market is mature, it can be assumed that proportions of each segment of vehicle are likely to remain the same after electrification, specifically, the mean annual mileage and the market share of each segment will remain constant. Therefore, with these assumptions, in order to predict the distribution of E_{cap} in a future fleet of EVs a prediction must be made for the mean and standard deviation E_{cap} within each segment. This will differ from the current distribution of EV capacities as the priorities of future EV buyers will be different from the current early adopters [211].

In order to use this assumption to generate EV battery capacity distributions a relationship must be sought between a current attribute of the vehicles and E_{cap}, so an equivalent attribute to E_{cap} in conventional vehicles must be used. Although both the capacity of the fuel tank and E_{cap} are directly proportional to vehicle range, the cost of the fuel tank is very low and adding additional capacity is relatively easy. This is not the case for E_{cap} where additional capacity is very costly. Additionally, for the most part, fuel tank capacity is not a primary driver for purchasing decisions in the same way that battery capacity will be [212]. For this reason, the engine capacity is taken as proportional to equivalent E_{cap}.

Whilst at first impression this may seem illogical, a larger battery pack will lead to a greater available power in the same way as a larger engine capacity. The sales of each segment of vehicle are largely driven by consumer preferences, in this context, the battery capacity is a primary driver for purchasing decisions in the same way as engine capacity. Indeed, EV manufacturers use the E_{cap} value for branding (displayed on the body of the EV) in the same way as conventional vehicle manufacturers. This is likely to be due to customer perception that a higher capacity battery correlates to a more capable and expensive vehicle. This assumption is backed up by Hidrue et al [212] who conducted a study of the willingness to pay for enhanced features of EVs, it was seen that consumers are willing to pay substantially more for higher range and faster charging capabilities.

TABLE 3.1: Market share of vehicle segments in the EU in 2011 [209].

Segment	Segment Name	Examples	Market Share (%)	Engine Capacity (l)		Mean Annual Mileage
				u	σ	
A	Mini Cars	Fiat 500, Smart ForTwo	8.7	1.12	13.4	8600
B	Small Cars	Vauxhall Corsa, Peugeot 207	26.0	1.34	14.5	10800
C	Medium Cars	Volkswagen Golf	23.3	1.63	22.8	13300
D	Large Cars	Ford Mondeo, BMW 3-series	11.0	2.02	36.4	15900
E	Executive Cars	Audi A6, Lexus GS	3.3	2.48	59.5	17500
F	Luxury Cars	Mercedes S-Class	0.3	3.76	97.8	13000
J	Sport Utility Cars	Toyota RAV 4, Hyundai Santa Fe	10.3	2.08	56.2	14000
M	Multi Purpose Cars	Citroen C4 Picasso, Honda F-RV	13.1	1.66	28.2	16800
S	Sport Vehicles	Maxda MX-5, Porsche 911	1.3	2.45	110.3	8700

TABLE 3.2: Classification of current EVs capable of high rate charging

EV Model	E_{cap}	Segment
BMW i3	18.8	B
Kia Soul EV	27	C
Citroen C-Zero		
Mitshubishi i-Miev	16	A
Peugeot iON		
Nissan Leaf	24-30	C
Tesla Model S	70-100	F
Tesla Model X	90	J
VW E-Up	18.7	A
VW E-Golf	24.2	C

In order to find the relationship between engine capacity and E_{cap}, current EVs (Table 2.3) are compared to conventional vehicle counterparts. First, these EVs are classified into the European Commission segments. This is shown in Table 3.2.

The ratio $\frac{E_{cap}}{EngineCapacity}$ is then found for each segment, as shown in Table 3.3. There is some variation here due to the relative immaturity of the EV market and recognising that the Tesla vehicles have proportionally larger batteries. Since the aim is for an indicative ratio this is ignored. The mean of the $\frac{E_{cap}}{EngineCapacity}$ ratios for each vehicle segment is calculated to be 21.8. In this chapter values of $\frac{E_{cap}}{EngineCapacity}$ of 30, 40 and 50 are used as these correspond to a growth in the size of batteries installed in EVs consistent with the future scenario assumed.

The probability distribution for E_{cap} can, therefore, be calculated as the sum of the probability distributions for as shown in Equation 3.3. The probability density function for each vehicle segment is scaled to the proportion of total miles driven by that segment.

TABLE 3.3: Comparison of Engine capacity and E_{cap} for vehicle segments

Segment	Mean E_{cap} (kWh)	Mean Engine Capacity (l)	$\frac{E_{cap}}{EngineCapacity}$
A	17.35	1.12	15.49
B	18.8	1.34	14.03
C	26.06	1.63	15.99
D	-	2.02	-
E	-	2.48	-
F	85	3.76	22.61
J	85	2.08	40.87
M	-	1.66	-
S	-	2.45	-

This is achieved by multiplying each segment by the market share and mean annual mileage for that segment. A log-normal distribution is assumed for each vehicle segment since a normal distribution is assumed, but zero or negative values of E_{cap} do not make sense, and so attenuation of the probability of small values of E_{cap} is useful.

$$PDF_{E_{cap}} = \sum_{A=i}^{S} M_i \cdot Y_i \cdot \frac{1}{\sigma_i \sqrt{2\pi}} e^{\frac{-(E_{cap}-(\mu_i \times 21.8))^2}{2\sigma_i^2}} \tag{3.3}$$

Where:

- M is the market share
- Y is the normalised annual mileage
- i is the vehicle segment
- S is the no. of vehicle segments
- μ is the mean battery capacity
- σ is the standard deviation of battery capacities

The probability density function for each vehicle segment is shown in Figure 3.11. The two vehicle segments which have the largest impact on the overall probability density function are B and C, this is mainly due to the higher market share of these vehicles. Conversely, the S and F segments have very little contribution to the overall probability density function since their market share is low. It should be noted that this is not what is currently seen in the EV market, as it is distorted by an over-sized luxury segment due to the popularity of the Tesla model S. It is expected that this factor will increase in this case and Figure 3.12 shows the effect of this change in the future.

The sum of the probability density functions for each segment is shown in Figure 3.12. The $\frac{E_{cap}}{EngineCapacity}$ figure of 21.8 is derived from EVs currently available. However, as the price of lithium-ion batteries is subject to further reductions, this is likely to change. It is expected that this factor will increase in this case and Figure 3.12 shows the effect of this. As this factor increases, the peaks for each vehicle segment become more distinct and E_{cap} covers a wider range. By varying the value of this factor, a future case can be analysed. In this case the values of 30, 40 and 50 are used.

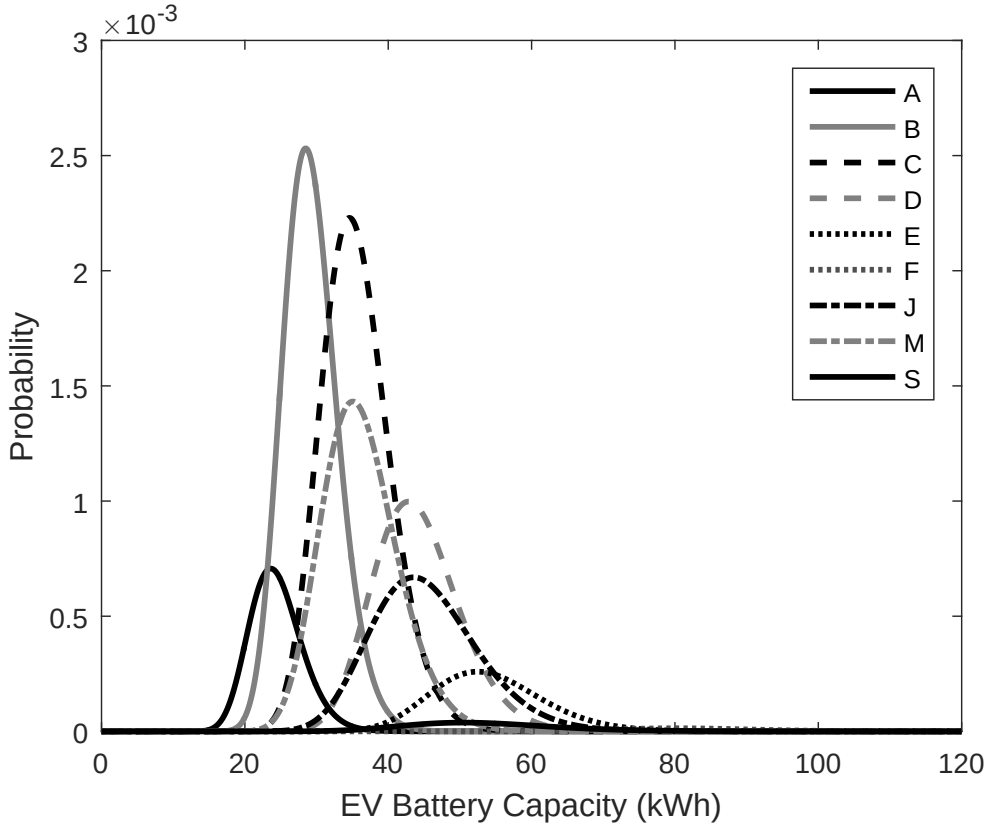

FIGURE 3.11: Probability density functions for E_{cap} for each segment of car.

3.2.5 Running the Stochastic Simulation

The relevant parameters for calculating the charge profile for the EV are described in Section 3.2.5.2 and are the EV battery capacity, the initial SOC and the final SOC. As such, the use of the probability density functions must result in relevant predictions of these parameters. Additionally, the time at which a charge instance begins is also a key output. These parameters are calculated as follows:

By generating random numbers from the distributions discussed in Sections 3.1.1 and 3.2.4 and assigning these numbers to the following variables, we find for each EV:

- D - Journey Distance (miles)
- T_{Start} - Journey Start Time
- E_{cap} - EV battery capacity

The range of the EV is then calculated:

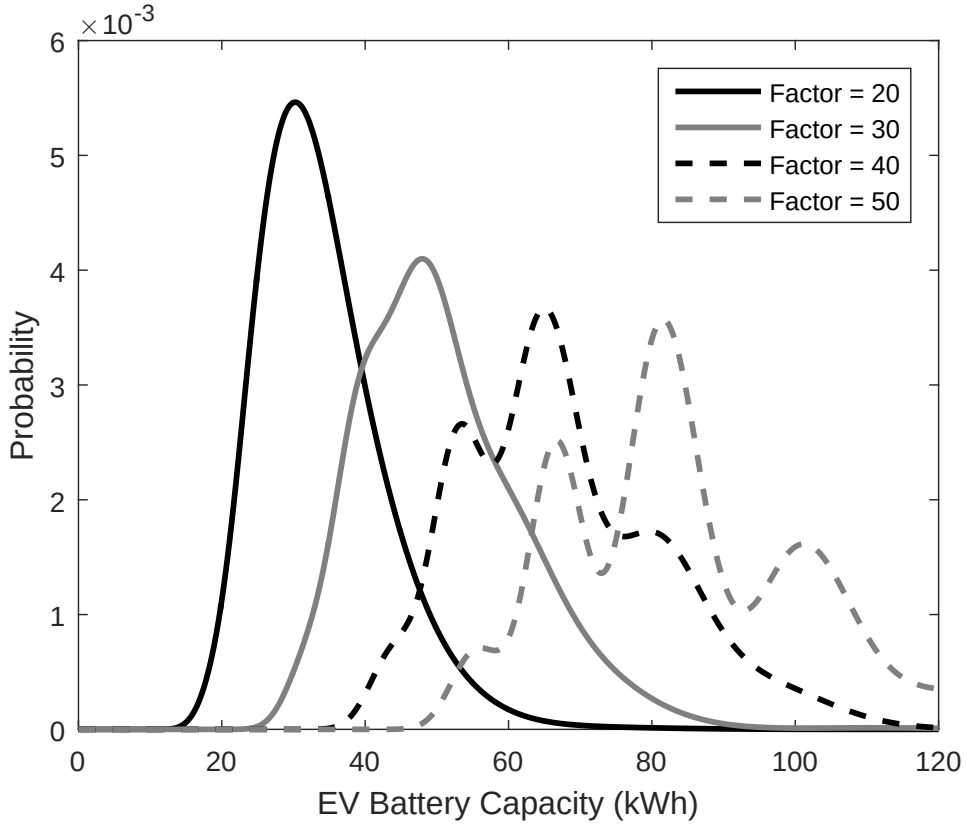

FIGURE 3.12: The effect of varying $\frac{E_{cap}}{EngineCapacity}$ on the probability density function for E_{cap} for the sum of all segments.

$$Range = E_{cap} \times W_{avg} \tag{3.4}$$

Where W_{avg} is the number of miles which can be driven for each kWh or stored energy, this is constant for all vehicle segments. If the Range (R) is less than the journey distance (D) then a HREVC must be used. For EVs where the Range exceeds the journey distance, the HREVC is not needed and therefore no further calculation is needed. For the journeys where a HREVC use is required two pertinent questions now arise. Firstly, at what distance in the journey will the HREVC use be required? And secondly, at what time will this arise?

To find the distance, a mesh of potential HREVC locations is created, each 28 miles (justified in Table 3.4) apart with the first being a random number in the range $0 < X < 28$:

$$\begin{aligned} &if\ D > R \\ &n = floor\left(\frac{R - X}{28}\right) \end{aligned} \tag{3.5}$$

Where:

- n is the HREVC number
- X is a random number in the range $0 < X < 28$

The selected HREVC is then the last feasible station prior to the EVs SOC reaching zero:

$$HREVC_{dist} = X + 28n \tag{3.6}$$

Where $HREVC_{dist}$ is the distance to the selected HREVC from the journey start point. Thus, we have the distance after beginning the journey at which the HREVC use will arise, hence the outstanding variable is now the journey time. For this the distance to the HREVC is divided by the mean speed and that time is then added to the journey start time.

$$T_{charge} = T_{start} + \left(\frac{HREVC_{dist}}{V_{EV}}\right) \tag{3.7}$$

The state of charge at the HREVC can then be found by dividing the energy used to get to the selected HREVC by the energy capacity of the EV.

$$SOC_{ini} = \left(\frac{HREVC_{dist}/W_{avg}}{E_{cap}}\right) \tag{3.8}$$

3.2.5.1 Assumptions

These calculations are based on a number of assumptions included for simplicity. They are detailed in Table 3.4.

Whilst these assumptions are largely representative, the inclusion of them leads to additional error in the model. For example, the P_{avg} is unlikely to be the same for each

TABLE 3.4: Assumptions using in the calculation of the HREVC use parameters.

Variable	Value	Justification
EV SOC at the start of the journey	1	Overnight charging is the main form of EV charging. This leads to an EV beginning each journey with full charge.
Mean Speed	48 mph	Quoted mean speed in *Free Flow Vehicle Speed Statistics: Great Britain 2015* [213].
Distance between HREVCs	28 miles	This is set as a target for spacing of services in Department for *Transport Circular 01/2008* [214].
EV Energy Use (P_{avg})	3 m/kWh	Conservative estimate from [215].

vehicle segment and W_{avg} will not always be 28 miles. However, these assumptions are assumed to be the average across the system within the case considered and as such, at the scale of this model where thousands of cars are simulated, have minimal impact on the accuracy of results.

3.2.5.2 EV charge calculations

The energy demand per charge instance is dependent on the EV battery capacity, the initial SOC and the final SOC. Therefore the energy transferred to an EV utilising the HREVC can be given by Equation 3.9.

$$E_{trans} = E_{cap} \times (SOC_{fin} - SOC_{ini}) \tag{3.9}$$

Where:

- E_{trans} is the energy transferred to the EV (kWh)
- E_{cap} is the battery capacity of the EV (kWh)
- SOC_{ini} and SOC_{fin} are the initial and final SOCs of the EV battery when arriving and leaving the HREVC respectively (0-1).

As such, the three variables; E_{cap}, SOC_{ini} and SOC_{fin} are key to predicting the power demand of the HREVC since they control the overall energy transferred to the EV and the power profile during the charging process.

The temporal change in power demand over the duration of the EV charge has been derived from Tesla Supercharger power data [216]. This is shown in equation 3.10.

The charge demand for each EV can be split into two stages, the first is given by maximum charging power (P_{max}) until SOC is increased to SOC 0.22. The second stage increases the SOC from 0.22 to 1 with diminishing power following the relationship derived from Tesla Supercharger curves [216]. Equation 3.10 shows how the power to the EV changes as a function of SOC.

$$P(t) = \begin{cases} P_{max} & 0 < SOC(t) < 0.22 \\ P_{max} e^{(-k \cdot 0.22))} & 0.22 \leq SOC(t) < 1 \end{cases} \tag{3.10}$$

Where k is the exponential decay constant of Power with respect to SOC. With SOC changing as a function of energy transferred and battery capacity, as shown in Equation 3.11:

$$SOC(t) = \frac{\int_0^t P(t)dt}{E_{cap}} \tag{3.11}$$

Solving Equations 3.10 and 3.11 yields Equation 3.12, where $SOC(t)$ is expressed solely as a function of P_{max} and E_{cap}:

$$SOC(t) = \frac{ln\left(-k\left(C - \frac{P_{max} \cdot t}{E_{cap}}\right)\right)}{k} \tag{3.12}$$

Where C is the integration constant found using initial conditions.

For this simulation a future situation where EV batteries have an increased ability to accept fast charging is used, therefore P_{max} is set to 300kW. It is more difficult to predict a value for k, a smaller value of k would result in a quicker overall charge, however, this may not be achievable within the constraints of a future EV battery. In this simulation, it is assumed that k remains the same as is currently observed using the Tesla Supercharger profiles and is set to 2.0, this value is found through curve fitting.

A sample EV charge demand profile is shown in Figure 3.13.

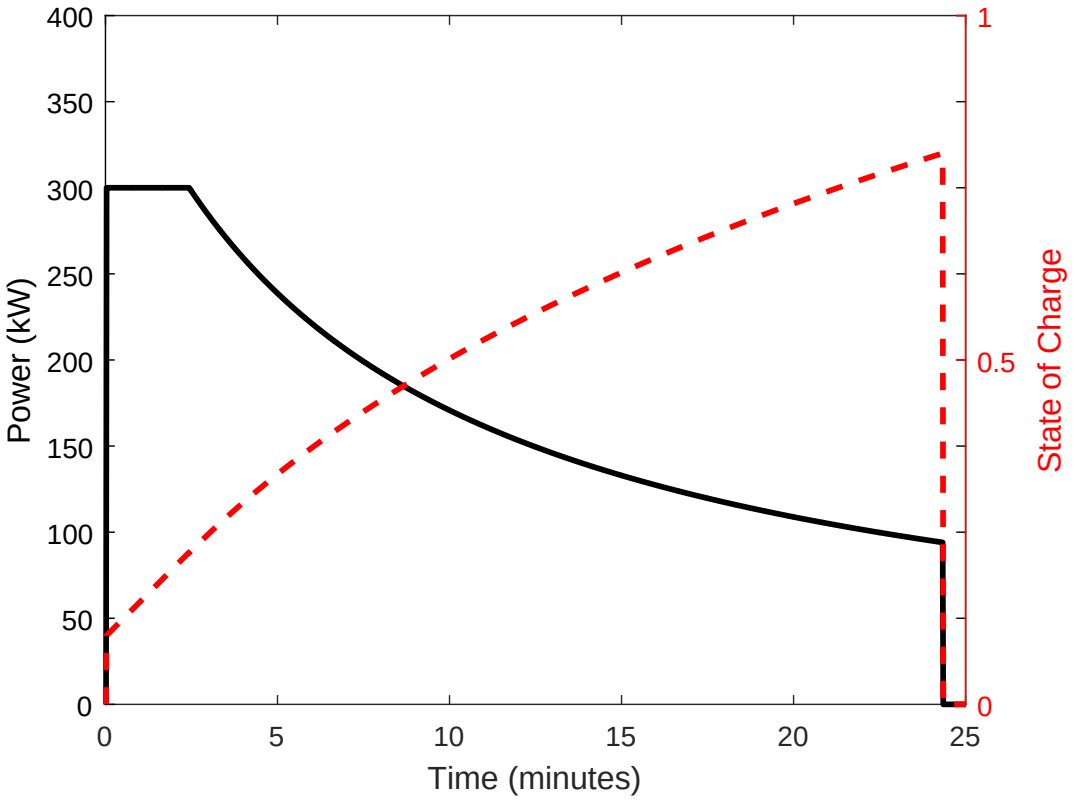

FIGURE 3.13: EV power demand for E_{cap} = 100kWh, P_{max} = 300kW, SOC_{ini} = 0.1, SOC_{ini} = 0.8

3.3 Results

In order to generate these example results, traffic flow data from 3 motorways in the UK were used. These are highly utilised roads and are therefore locations likely to require HREVC installations. The motorways selected are the M25, the main circular motorway around London, the M3 and the M4. The location on these motorways is indicated by the numbers of the junctions the measurement point lies between (i.e. J15-16).

An EV demand for an HREVC can now be generated stochastically for any location on the SRN in the UK. An example is shown in Figure 3.14, showing results for the M25.

3.3.1 Effect of EV Battery Size

The effect of different EV battery size scenarios is shown in Figure 3.15 where the probability of HREVC use for each hour of the day is plotted for 3 EV_{cap} factors (30,40,50).

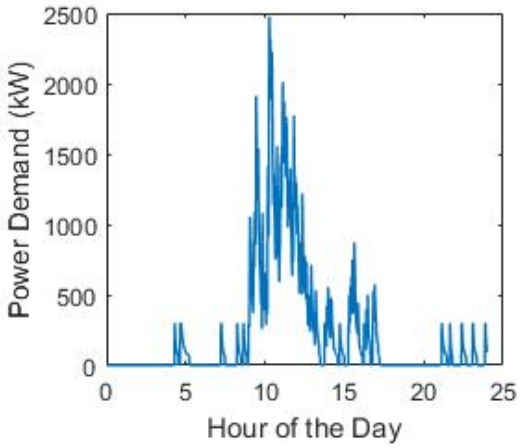

FIGURE 3.14: Example HREVC EV Demand for M25 J15-16.

TABLE 3.5: Effect of EV battery size on HREVC use for 10% EVs at the M25 J15-16.

EV Battery Capacity Factor	Mean No. HREVC Uses / day	Mean Total Energy (MWh)
30	58.8	2.40
40	27.8	1.47
50	13.8	0.89

Due to the tendency for long journeys to start in the morning (as shown in Figure 3.8), a peak in demand is seen in the late morning. This is in contrast to the predictions made in the literature; if the demand is assumed to be proportional to traffic flow, two peaks would be evident, one in the morning and one in the evening. However, as is shown in Figure 3.15, the journeys which are long enough to result in a HREVC use tend to begin in the morning and lead to a high demand for charging in the middle of the day. After this peak, demand diminishes through the rest of the day. This reduction in demand after the initial peak is due to the increasing probability that a given journey will finish as its distance increases, thus additional HREVC use is increasingly unlikely.

Larger EV batteries (higher EV capacity factors) lead to a later HREVC demand due to their increased range leading to longer journey times before needing an HREVC charge. Additionally, the overall number of charges (Table 3.6) is reduced through increasing EV battery capacity factor as the probability of the range of the EV being sufficient to power the entire journey increases. The predicted total energy transferred to EVs also diminishes with higher EV battery capacities due to fewer charging instances.

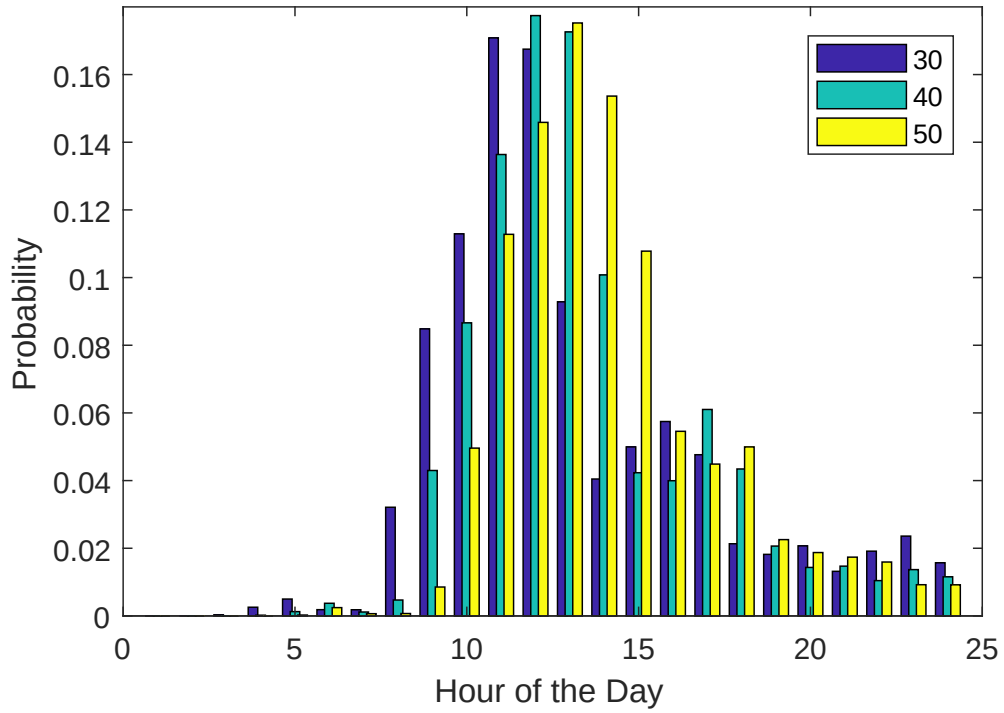

FIGURE 3.15: Probability of HREVC use against time of day for 3 different EV battery capacity factors on the M25 J15-16.

TABLE 3.6: Effect of location on number of uses per day of the HREVC with an EV capacity factor of 30 and an EV penetration of 10%.

Location	Total Traffic Flow	Mean HREVC Uses / day	Percentage Use (EVs)
M25 J15-16	112 675	58.8	0.52
M4 J17-18	45 474	31.4	0.69
M3 J13-14	64 393	43.2	0.67

3.3.2 Effect of HREVC Location

An EV demand pattern for an HREVC can now be generated stochastically for any location on the SRN in the UK. Three locations have been selected for illustration purposes, as shown in Table 3.6, and the traffic flow patterns for these locations are also shown in Figure 3.16. To populate the data in Table 3.6, the simulation was repeated ten times to achieve mean values with an EV penetration value of 10%. Clearly, when there is a higher level of traffic flow over a road, the HREVC is utilised more. Curiously though, the percentage of vehicles using the HREVC is not constant. In the examples studied here, it varies between 0.5-0.7% of EVs.

The cause of this variation lies in the difference in shape of the traffic flow patterns. The

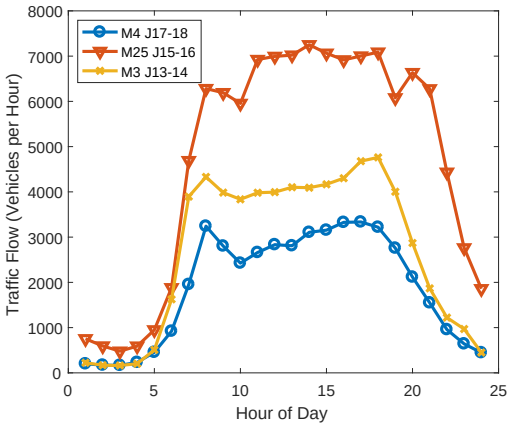

FIGURE 3.16: Traffic flow measurements for 3 motorway locations in the UK.

M3 and M4 motorways have higher percentage of HREVC use due to a higher proportion of the journeys occurring in the morning. Likewise, the M25 has sustained high traffic flow levels throughout the day, thus, a lower proportion of journeys occur in the morning leading to lower overall percentage HREVC use on the M25 as shown in Figure 3.16.

Using traffic flow data for different locations on the SRN, an HREVC demand pattern can be generated for each of them. An example of this is shown in Figure 3.17. For these simulations, the number of EVs was assumed to be 10% of the overall traffic flow, the peak charge power for each EV was 300kW and the EV battery factor was 30. Of these EVs, 0.5-0.75% required an HREVC to complete the required journey. The main difference in the demand, arising from simulating different HREVC locations, is the difference in magnitude. There is more traffic flow on the M25, which results in higher HREVC demand.

3.4 Discussion

The method to predict EV charge demand uses existing travel data sources in the UK and adds to them through the information gathered in the Open Street Map GPS track dump. When comparing the HREVC use patterns derived in this thesis to those in the literature, some differences are evident. The HREVC demand patterns derived here exhibit a greater tendency to have high demand levels in the early afternoon than other methods used in the literature. This effect is partly due to the nature of the data extracted from the open street map and partly due to the novel methods presented. This

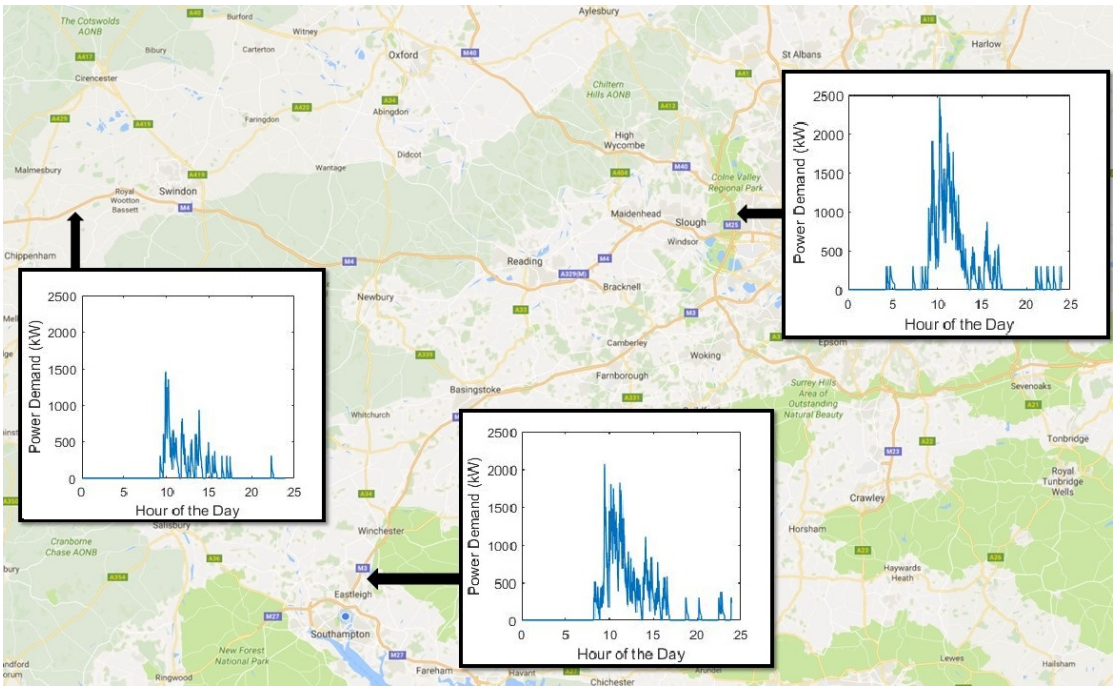

FIGURE 3.17: HREVC demand stochastically generated for three locations in the UK from traffic flow data available for that location, assuming an EV penetration of 10%.

method does not rely solely on traffic flow measurements which gives a tendency to produce an HREVC demand pattern with two peaks, each aligned with the times of high road use. A single peak in HREVC demand is predicted here which aligns with other methods which also do not assume proportionality with traffic flow, such as the work in ref [147]. Contrasting the previous methods which do not assume proportionality to traffic flow ([147] [148] and [149]) to this work, an earlier peak in demand is predicted here. This is due to the travel patterns observed in the Open Street Map GPS trace dump. A tendency for long journeys to begin in the morning was observed. As this data has not been previously used for similar work it is not surprising that there are differences in the outcomes. The journey information extracted from the open street map relates solely to main roads in the UK, it is therefore an important consideration for future planning decisions that demand on these roads may be different to that generally seen in literature from around the world. Additionally, it should be noted that the method presented here avoids the need for expensive and time consuming vehicle tracking. It also provides a more general, locationally dependant result.

This method also allows for locationally dependant predictions of HREVC demand. This will enable informed planning of HREVCs on the SRN. Whilst a general increase in HREVC demand can be expected with roads with higher traffic flow, the characteristics of that

traffic flow are also important in predicting HREVC demand. A higher than average traffic flow in the morning will result in a more distinct peak in HREVC demand, whilst HREVC demand which is more consistent through the day is seen on roads which have lower than average demand in the morning. Understanding this effect and its dependence on location is important in HREVC design as a demand with a distinct peak will need greater power availability and a larger number of charge points than one with a sustained demand pattern through the day (assuming the same overall charger usage).

The assumption that EV SOCs are equal to 1 at the start of the day will not hold for all cases. Specifically, the low power levels available in a domestic setting may not be capable of returning an EV with large battery capacity to full SOC within the duration of overnight parking. Therefore there may be additional uses of an HREVC, by owners of EVs with high battery capacities, to compensate for this which are not predicted in this thesis. Additionally, there may be usage of the HREVC which is not related to long journeys in the way presented, such as charging in preparation for a journey at a later time. There are inevitably many factors such as these which may, or may not, affect the use of HREVCs which a predictive tool such as that proposed in this work is unlikely to sufficiently represent, however it is important to be aware of them and of the potential effect on the charging pattern they may have.

The choice of the Weibull distribution may lead to an under-reporting of the overall number of charges per journey due to over estimation of short journeys ($<$ 1 mile) which do not lead to an HREVC charge. This has been addressed in this work by the removal of these $<$ 1 mile journeys. However, the improved fit with longer distance journeys which is enabled by use of the weibull distribution leads to greater accuracy of the prediction. For this reason, over estimation of short journeys is likely equalled by under estimation of medium length journeys, leaving long journeys accurately represented. This is enabled through varying the rate at which the probability of journey finish varies with respect to the journey distance (by varying the shape factor) and a preference for accurate fitting of the tail of the distribution. This effect was important as accurate predictions of long distance journeys are clearly the priority of this work.

It is impossible to state the accuracy of this work as it is studying a future scenario, and so real world validation is impossible. However, the data used for the probability distribution is from a wide range of real journeys conducted on the specific type of road

in question, and the locational element arising from the traffic count can also be verified for accuracy. Therefore, with the combination of these the charge demand arising from traffic flow should be accurately predicted. The method for forecasting EV battery capacities introduces uncertainty as there is clearly no reliable way of predicting future purchasing patterns for EV consumers, or indeed the overall number of EV consumers. However, new data is continuously being published in this area and as the EV market grows and becomes more generally accepted this forecast can be updated.

This method was designed to be practical and easy to use for developers of EV charging stations. This is due to the ready availability of traffic flow data. Developers can download the traffic flow data for their desired location - or a range of potential locations - and use the methods presented here to predict the nature of the HREVC demand. This forms a powerful tool for planning of the HREVC network.

This work enables improved accuracy of HREVC power demand predictions, both at the current time and for the future. It has also opened the possibility of analysis of the role HREVC power demand can potentially play in the wider energy system. For example, an earlier peak in HREVC demand, as is suggested here has the potential to offset grid unbalances caused by increasing solar power generation. So, this work has wider implications than those of just HREVC design.

3.5 Conclusions

In conclusion a novel method for predicting EV demand at HREVCs has been presented. Critically, this predicts HREVC demand in the UK, using data arising from the UK, in a locationally dependent way. Therefore, HREVC demand can be predicted for varying locations in the UK by using traffic flow measurements from that location.

It has been shown that $\approx 0.5\%$ of SRN journeys undertaken by EVs result in HREVC use. This figure is weakly dependent on the battery capacity factor assumed in the simulation. Additionally, larger EV batteries result in a later peak in HREVC demand

The novel HREVC demand prediction method presented here shows strong potential for pairing with solar power. The demand shapes shown in Figure 3.17 align with the

expected PV generation more strongly than when other methods for predicting HREVC demand have been used in the literature.

This work, therefore, provides a basis for further work to explore the potential for integration between HREVC demand and solar power generation.

Chapter 4

High Rate Electric Vehicle Charger Model

Chapter 4 illustrated the potential correlation between the power demand at HREVCs and solar power generation patterns, and this is further explored in this chapter.

Initially, a statistical analysis of the two aspects (solar energy supply and EV energy demand) of the system is made. This has the aim of qualifying whether a system such as this is viable.

An important aspect of an HREVC system powered by solar power is the associated energy store. The control of the charging and discharging of the energy store must be managed effectively to increase its effectiveness, this is further examined in the second section of this chapter where the model methodology is developed.

Then, the potential use cases of an HREVC with OVES are investigated with particular emphasis on the role an OVES can play in incorporating the HREVC demand with solar power.

4.1 Novel Contributions

Novel analysis of HREVC with OVES and associated solar energy is a key contribution of this chapter. This includes:

1. A unique HREVC model has been produced. This is detailed in Section 4.3.
    - Integration of EV queuing and limited charge points as discussed in Section 4.3.3.1.
    - A novel OVES charging methodology is presented in Section 4.3.6 - charge rate responds to seasonal changes in solar farm production. This is work published in the paper *Dynamic charging algorithm for energy storage devices at high rate EV chargers for integration of solar energy* [217]
2. Analysis of two potential use cases for an HREVC:
    - Solar farm with HREVC - Section 4.4.1
    - HREVC with small solar - Section 4.4.2

4.2 Statistical analysis

The EV demand patterns predicted in Chapter 3 show a peak in demand in the middle of the day and diminishing demand in the afternoon. This is similar to solar power generation patterns. This is advantageous for implementing an HREVC powered by solar PV as a good correlation between electricity generation and demand reduces the need for associated energy storage and the reliance on grid power.

To assess the potential correlation between EV power demand at HREVCs and solar power generation, effective and relevant datasets must be used. I.e. datasets which are dependent on as few factors as possible. For this, an average EV demand profile was generated by finding the mean traffic flow across three locations (same as those used in Figure 3.17) with the intention of removing dependencies on location within the dataset. This data is then used as a representative example of high rate EV power demand in this statistical analysis.

As high resolution solar power generation data for large solar farms ($>$1MW) is difficult to find, only one dataset was used for solar generation data - the power output of a 5MW solar farm in Nottinghamshire UK captured at 5 minute resolution. The mean solar day was found by finding the average generation power for each timestep through the day, which in turn was used for statistical analysis at the day scale.

TABLE 4.1: Correlation between HREVC power demand and solar power for the mean solar day and the year.

EV Factor	Correlation (ρ)	
	Day	Year
30	0.7532	0.2747
40	0.8633	0.2933
50	0.8651	0.2490

By using these datasets it was possible to find a standard representative use case for a HREVC and remove locational and seasonal dependencies from statistical analysis.

4.2.1 Correlation

The most commonly used method for calculating the degree of interrelationship between two variables is the Pearson Correlation (Equation 4.1). This was used to find the correlation between solar power and EV demand. This does not assume that there is any relationship between solar power generation patterns and EV demand, as this is clearly not the case, however, a measure of the strength of the correlation between the two variables provides insight into the requirement for additional sources of energy within the system.

$$\rho(A,B) = \frac{1}{N-1}\sum_{(i=1)}^{(N)}\left(\frac{A_i-\mu_A}{\sigma_A}\right)\left(\frac{B_i-\mu_B}{\sigma_B}\right) \tag{4.1}$$

Where A, B are the variables to calculate the correlation, μ is the mean, σ is the standard deviation and N is the number of points. For this correlation method, a stong correlation is indicated by a ρ value close to 1 and a weak correlation close to 0.

The correlation between these datasets was found for the mean day and the year and shown in Table 4.1. For both of these calculations the solar generation and EV power demand were each normalised by dividing each data point by the sum of that dataset such that their integrals were equal to 1. Thereby the energy generated over the year/-day and had the same sum as the energy used for EV charging in the simulation. This corresponds to a well sized HREVC system.

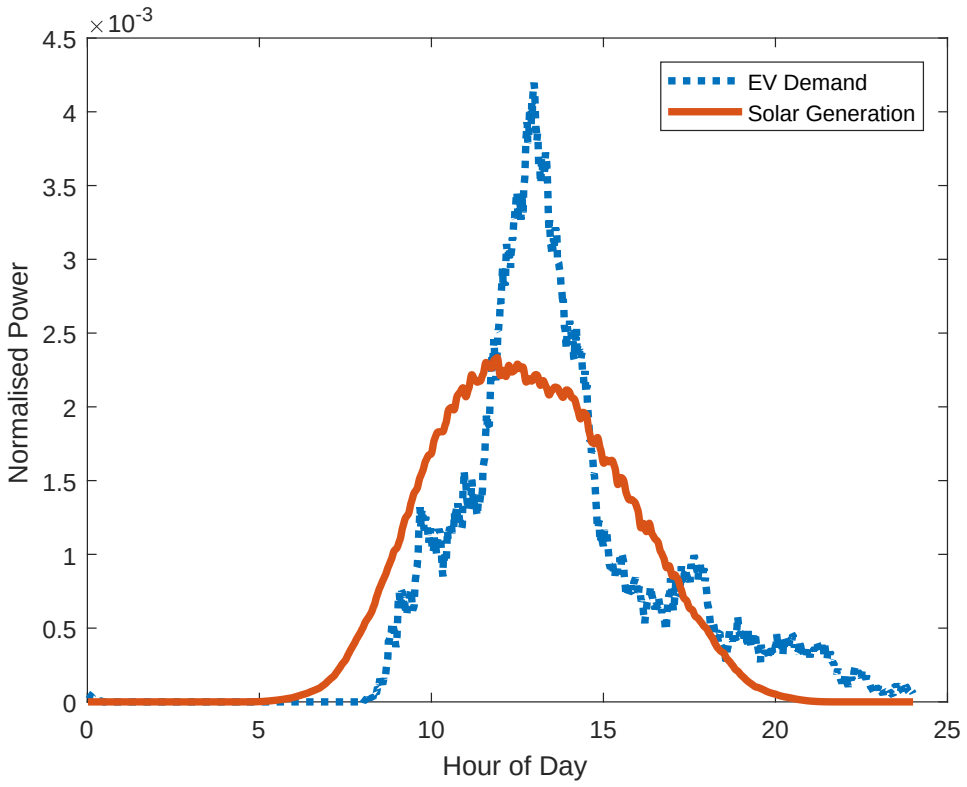

FIGURE 4.1: Normalised power patterns (total energy = 1) for mean solar day (over 1 year) and EV demand at EV factor = 50.

Analysis at the year scale shows correlation values lower than for the single day due to the seasonal variation in solar power generation - a factor of 10 change in power generation is seen between winter and summer. The level of correlation at the day scale however, is high. The energy supply and demand for the day scale analysis is show in Figure 4.1. A high level of correlation is evident, however a small amount of variation between the two variables is also shown. Therefore, a system which enables these to be matched will benefit as additional energy source interventions to enable matching will be minimal in the general case.

Changing the EV battery factor changes the shape of the HREVC demand. At lower EV battery capacities, the journey distance which requires a charge reduces. Therefore the distribution of charge times becomes broader as the journey distance requiring HREVC use are lower thus journeys requiring a HREVC use occur at a wider range of times. This leads to a lower correlation over the mean day for EV Factor of 30. A similar effect can be observed with the correlation between the HREVC power and solar power for an EV factor of 50 over the full year. As the pattern of demand leads to higher peak powers

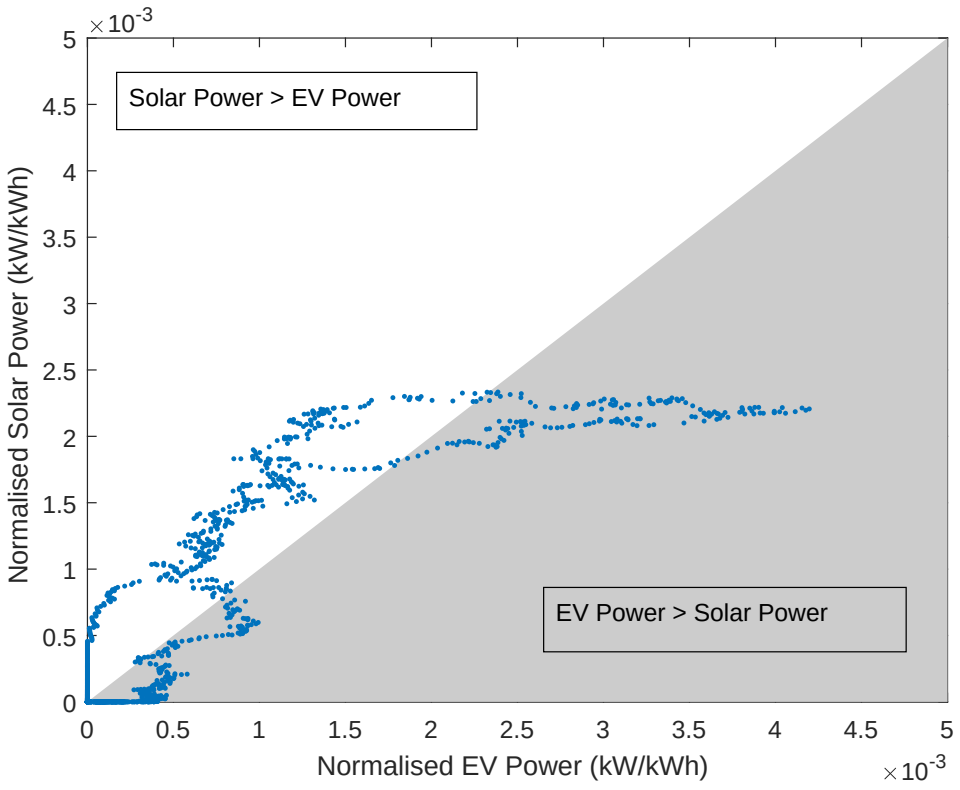

FIGURE 4.2: Scatter plot of normalised mean solar day power and normalised mean EV demand for one day.

over a smaller duration, the correlation is lower.

4.2.2 Energy pattern visualisation

Figure 4.2 is a scatter plot of the supply matched with the demand for the mean day. There is deviation from the centre line caused by unbalance of generation and demand. A general pattern can be seen though, as a consequence of the good correlation at the day scale. The sum of absolute values of this difference is equal to 0.2613 - this deviation accounts for the need for alternate power supply, such as energy storage.

However, this is a representative sample of an average day, whereas a real world system must deal with variations in both demand and supply. Therefore, as many days in the year will see an unbalance in power flows, it is important to assess how this affects the need for energy storage within the system.

To visualise the energy patterns occurring in the HREVC throughout the year the datasets were normalised. This had the aim of modelling a well balanced system where the supply is equal to the demand at the year scale. Each value of solar power or EV demand was divided by the total energy flux throughout the year for each variable. Therefore the sum of both the supply and demand variables over the year are 1.

If it is intended that the OVES is capable of accommodating all of the power deviations then it will have to absorb all the energy from the solar farm for the summer day and provide all the energy for the EV charging for the winter day as the match between solar and EV charging is poor at these times. This highlights the difficulty in designing an off-grid HREVC due to the variability of solar power with the seasons.

This wide variation in weather conditions leads to a non-ideal system. The effect of this is seen in Figure 4.3. There is clearly a range of solar power generation levels, and while there is a smooth distribution over the year, the power level for any one moment has a wide level of uncertainty. The same can be said for the EV demand but to an even greater degree with a 10 times wider range of possible values. Therefore there is no well defined correlation between these variables and clearly a need for an additional element in the system which is capable of balancing the system power for various scenarios throughout the year. Additionally, an OVES will be required to discharge at a significantly higher rate than it will be required to charge since the highest EV demand power is a factor of 10 more than the highest solar power value for a normalised system.

4.2.3 The requirement for energy storage

Imbalances between the solar generation and EV power demand through the duration of the day can be found by examining the sum of the difference between supply and demand up to that point in the day. If all this deviation is accounted for by an energy store, it stands to reason that the capacity of that energy store must be large enough to accommodate the range of cumulative sum values over the given period.

This analysis is shown for the mean solar day and mean EV demand in Figure 4.4 over the day scale using an EV factor of 50. The indicated necessary capacity from this analysis is 0.91kWh/kWp i.e. 0.91 kWh of energy storage is needed for each kWp of

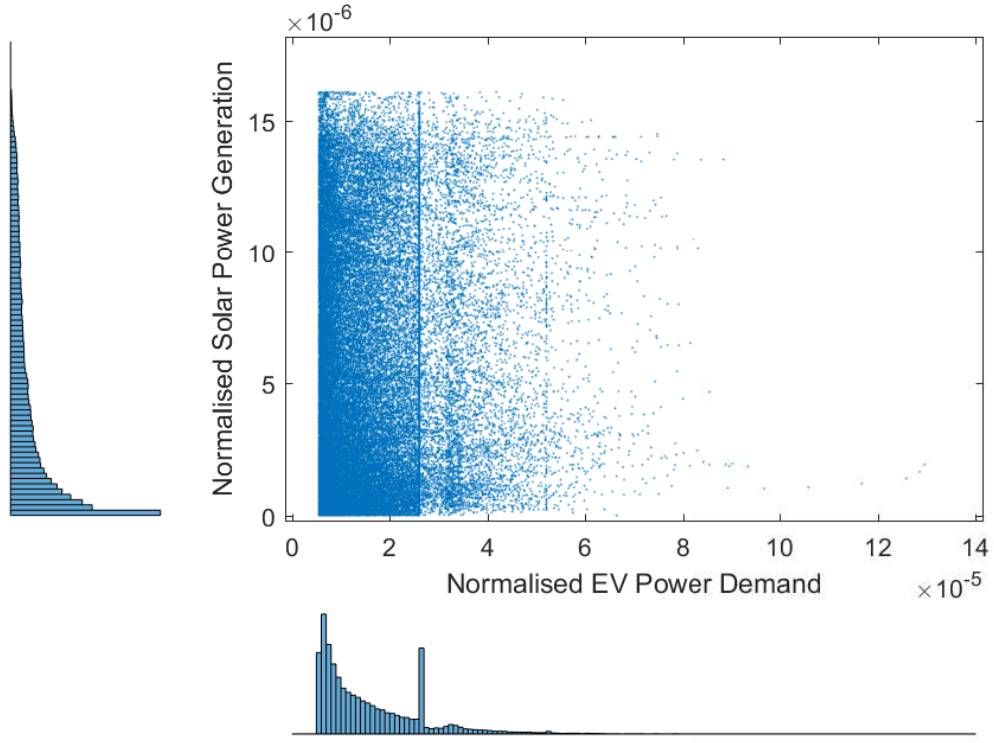

FIGURE 4.3: Scatter plot with histograms showing data point density of normalised solar power and normalised mean EV demand for one year.

solar power. It can also be seen that the OVES will perform 2 cycles a day in this general case.

When the scenario of an energy store balancing the HREVC power deviations for a year is examined the required capacity is far larger than for one day. The requirement for the energy store changes dramatically and it is now required to perform seasonal energy storage; storing solar power generated in the summer to power EV charging in the winter. From Figure 4.5 this leads to a necessary capacity of 248kWh/kWp. The energy store is then required to do just one cycle per year.

Clearly, inter-seasonal storage is not viable for an energy store in an HREVC as a typical solar farm would need an OVES capacity of 50-250MWh. However, at 0.91kWh/kWp, energy storage at the day scale is viable. For the OVES to add value throughout the year, a larger capacity than that may be needed, further analysis is necessary to substantiate this claim through a more detailed model.

If it is not viable for the OVES to balance power deviations over the whole year and a smaller OVES capacity is used for day-scale deviations then an additional power source

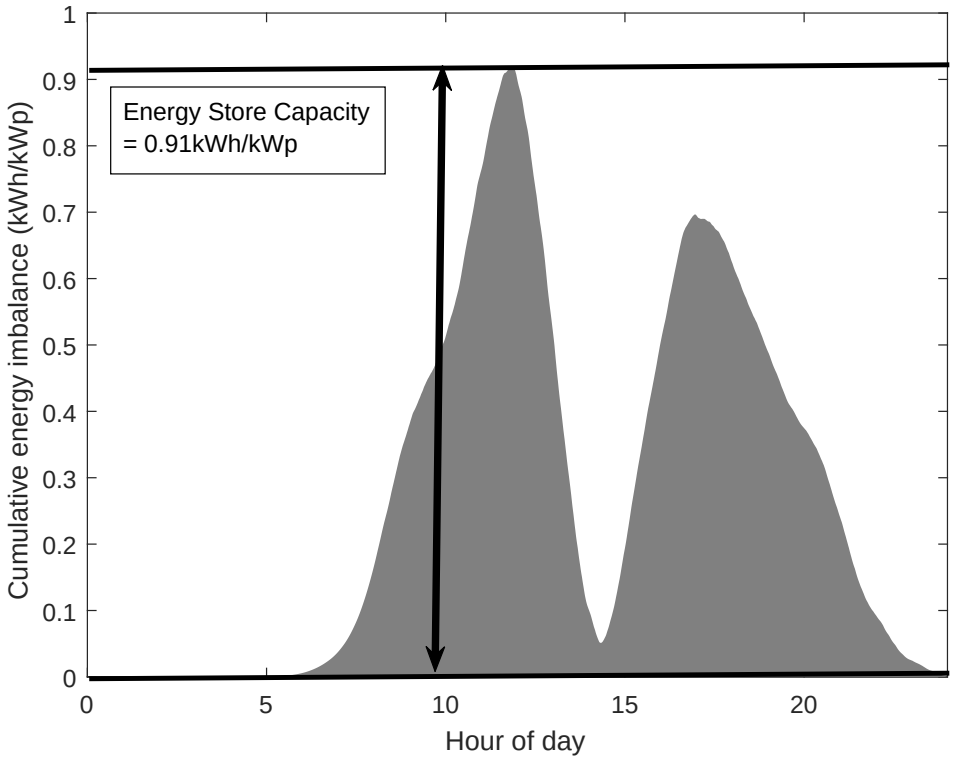

FIGURE 4.4: The requirements of an OVES in balancing supply and demand in an HREVC for the general case of one day.

is required for the HREVC to be functional. This can be provided through a grid connection. To identify the optimum usage of this grid connection to best utilise the solar power, again, a more detailed model is generated. This is the subject of the next sections in this chapter.

4.3 HREVC Model Methodology

To provide a means for calculating the optimal design of an HREVC a model has been developed. As it has been found that energy storage for the day scale is viable, but this is not the case for the year scale, it is important to find a mode of operation of the HREVC which best utilises the OVES throughout the entire year.

The model was written in Matlab and generates a temporal prediction of the grid interface power for a system utilising energy storage to provide high rate charging for EVs from solar energy. A schematic of the HREVC system being modelled is shown in Figure 4.6. The code for this model is included in Appendix B.

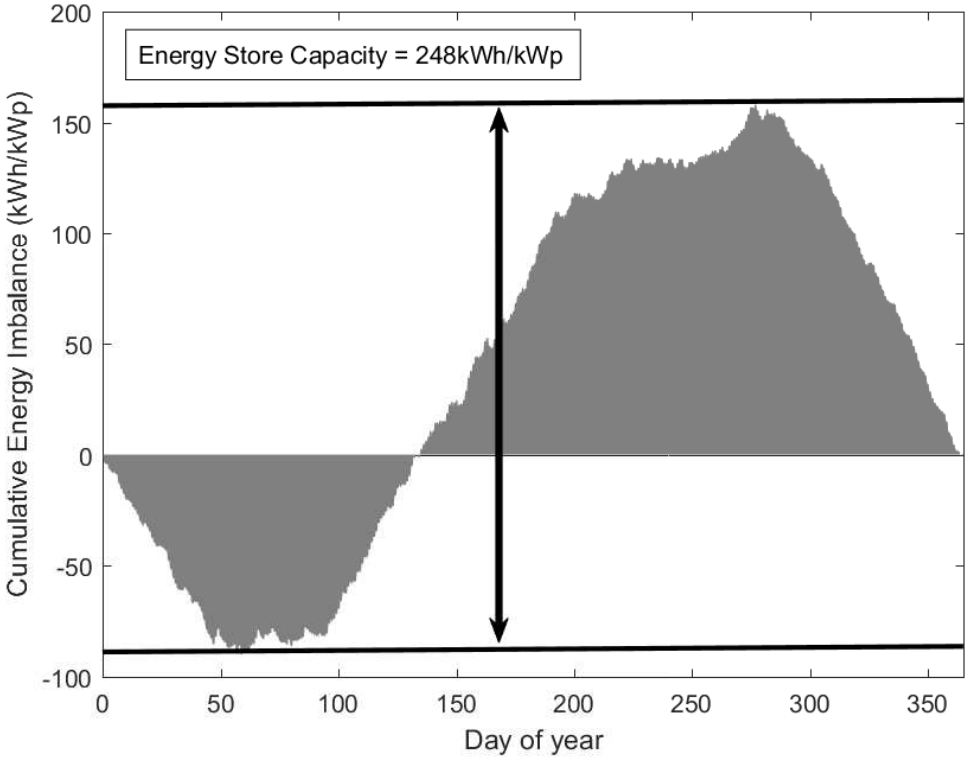

FIGURE 4.5: The requirements of an OVES in balancing supply and demand in an HREVC over one year.

The model uses a temporal iteration loop in order to predict HREVC power flows. There are two time-step durations dependent on the duration of the simulation: A single day simulation uses a timestep of one second and a year simulation uses a timestep of one minute.

4.3.1 Model Inputs

There are 7 key variables which the model takes as inputs which are shown in Figure 4.6. Changing these effects the way the HREVC operates through changing the relative capacities of each component.

Discussed in more detail, they are:

1. **No. Charge Points (N_{CP})** - The number of EVs which can be charging at the station simultaneously.

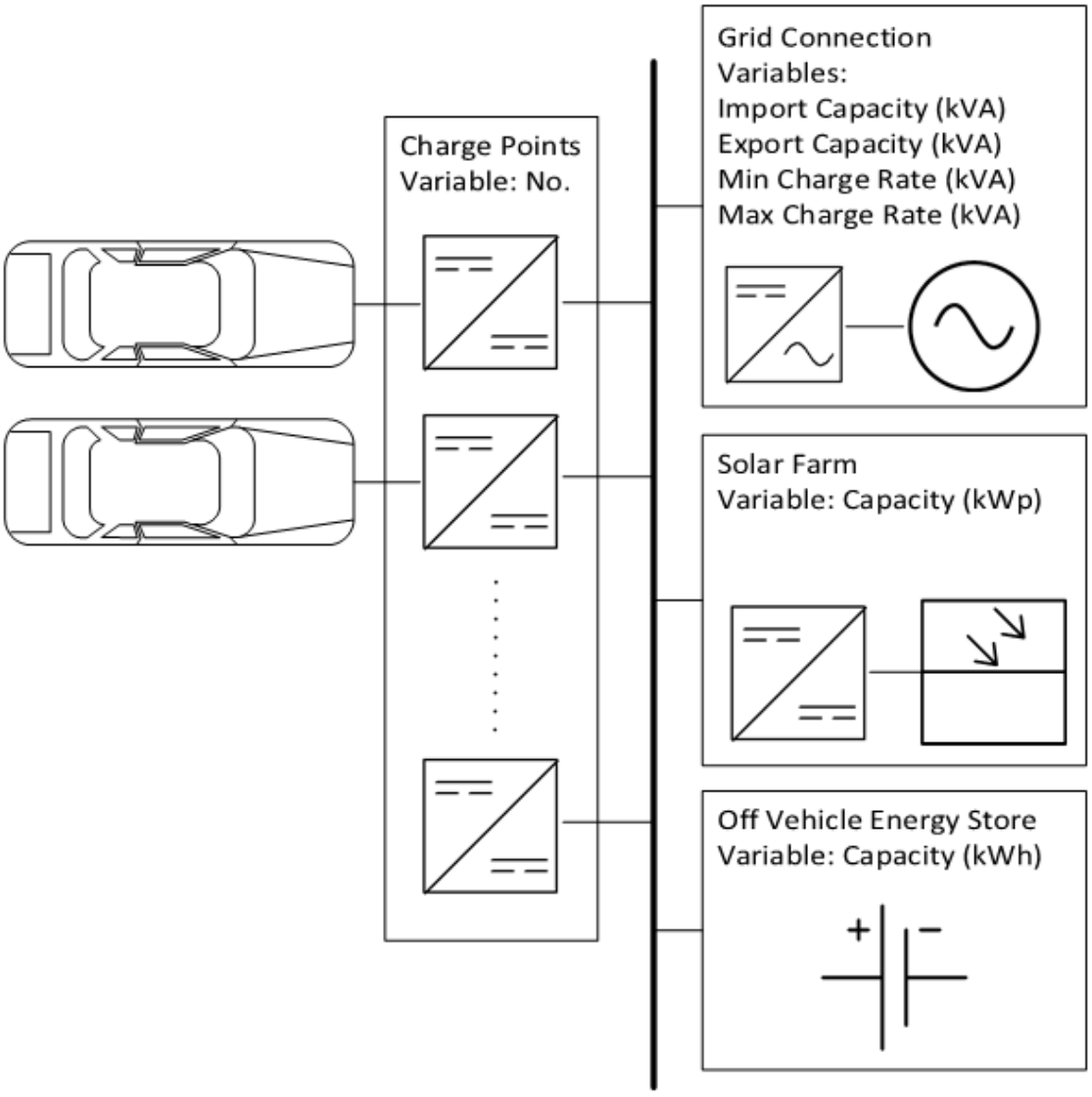

FIGURE 4.6: Schematic overview of the system under consideration in the model, highlighting the 5 key design variables.

2. **Grid Connection Capacity (GC_{min}, GC_{max}) (kVA)** - The maximum available power from the grid connection in import and export.

3. **Grid Charge Rate (P_{GC}) (kW)** - The default charge rate of the OVES. This is the minimum power the OVES will charge at when it has remaining capacity. This power level will either be met by the grid or by the solar farm. A minimum summer value and a maximum winter value are taken for this (discussed in more detail in Section 4.3.6).

4. **Solar Farm Capacity (PV_{cap}) (kWp)** - The rated peak power of the solar farm.

5. **OVES Capacity ($OVES_{cap}$) (kWh)** - The energy storage capacity of the OVES.

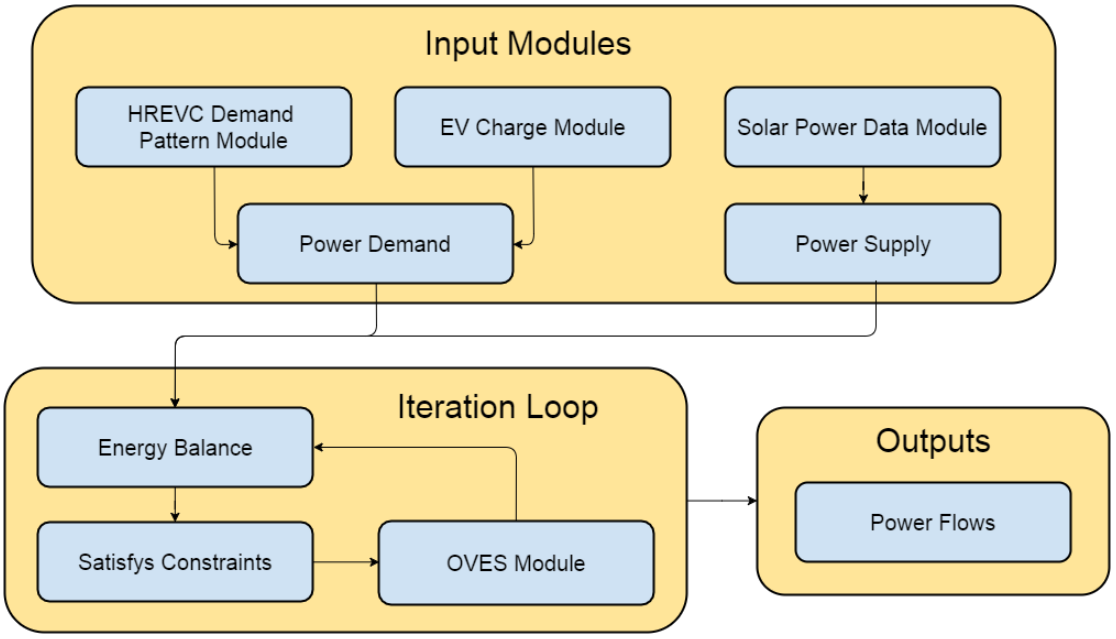

FIGURE 4.7: Schematic work flow of the HREVC Model.

4.3.1.1 Input Modules

There are 3 input modules that feed into the temporal iteration calculation loop. The solar power module uses data from a 5MW solar farm in Nottinghamshire. The method for predicting the power demand was developed in Chapter 3. The EV demand is calculated using two separate modules: the EV Demand module and the off-vehicle energy store module. These are both discussed in Chapter 3. A stochastic prediction for each EV charge session is made with this method and, similarly the EV charge characteristics. A schematic overview of the work flow of the model is shown in Figure 4.7.

4.3.2 Model Overview

4.3.2.1 Off-Vehicle Energy Store Module

An equivalent circuit model of a $LiFePo_4$ battery is used for the OVES. The model calculates the change in the SOC of the OVES along with the energy lost through inefficiency each time step. All loses are assumed to be ohmic and therefore these arise solely from voltage hysteresis (in the form $I\Delta V$). This is achieved by calculating the voltage at a given C-rate and SOC, from the look-up tables generated through curve fitting of voltage and current graphs for varying charging rates. An example of which - the voltage range

during charging of the cell - is shown in Figure 4.8. The maximum allowable power at any SOC is calculated from the 10C charge and discharge profile.

The voltage at C-rates not falling on a specific curve are found through linear interpolation. The difference between this calculated voltage and the voltage at this SOC accounts for losses through ohmic heating. This model is taken from related work [216].

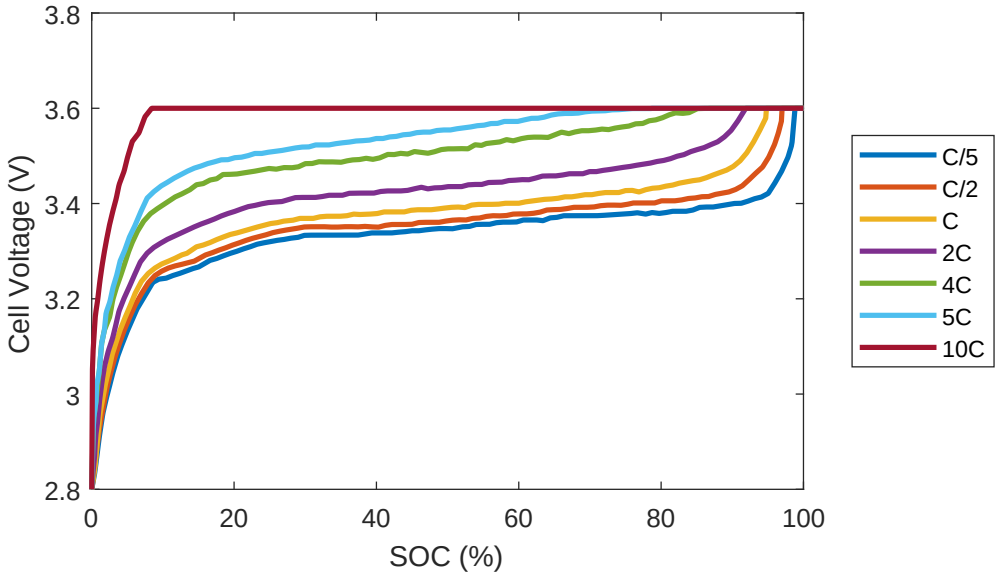

FIGURE 4.8: Data used for look-up tables for the OVES Module charge voltage (8.25Wh cell) [218].

The lifespan of the OVES is assumed to be 10 years.

4.3.2.2 Model Power Flows

It is the aim of the iterative loop section of the model to calculate the power flows within the system for each timestep, thereby performing an energy balance. The power flows are essentially the sum of four individual power values:

- **EV Demand Power (P_{EV})** Ideal power demand from Chapter 3 modified based on the HREVC system constraints of grid connection and number of charge points. This variable can only be demand, i.e. energy cannot be transferred from charging EVs to the HREVC.
- **Grid Power (P_{Grid})** The grid power is a result of the OVES SOC, the EV demand and the Solar Power at each timestep. The relationship between these factors

is relatively complex due to the constraints (discussed in Section 4.3.3) and is shown in Figure 4.9

- **OVES Power (P_{OVES})** The off-vehicle energy store is modelled through data look-up tables. It is controlled to always fill the gap between solar power and EV charge demand unless restrained by SOC or maximum power limits (defined by the 10C charge profile in Figure 4.8). This control is achieved by a final energy balance statement within the algorithm.
- **Solar Generation Power (P_{PV})** This variable can only be generation, i.e. energy cannot be transferred from the HREVC to the solar farm. This variable cannot be changed by the algorithm - there is no control of the solar farm within the HREVC.

The detailed work flow of the energy balance algorithm is shown in Figure 4.9.

4.3.3 Model Equations

The energy balance solves Equation 4.2 through the algorithm shown in Figure 4.9. This algorithm balances energy in the system through Equation 4.2 subject to a number of constraints. Equation 4.2 is the constraint that there can no excess or unaccounted energy within the system for each timestep. In practise this requires modification of power flows for the charging EVs, the grid and the OVES to conform to a number of constraints.

$$0 = -P_{OVES} + P_{PV} + P_{EV} + P_{Grid} \tag{4.2}$$

The first constraint considered is the maximum number of charging EVs, shown in Equation 4.3. This cannot exceed the number of charging points specified for the HREVC.

$$N_{EV} \leq N_{CP} \tag{4.3}$$

If the EV demand module has predicted a charge demand which has led to an EV arriving at the HREVC when all charge points are full, then the charge time for this EV will be

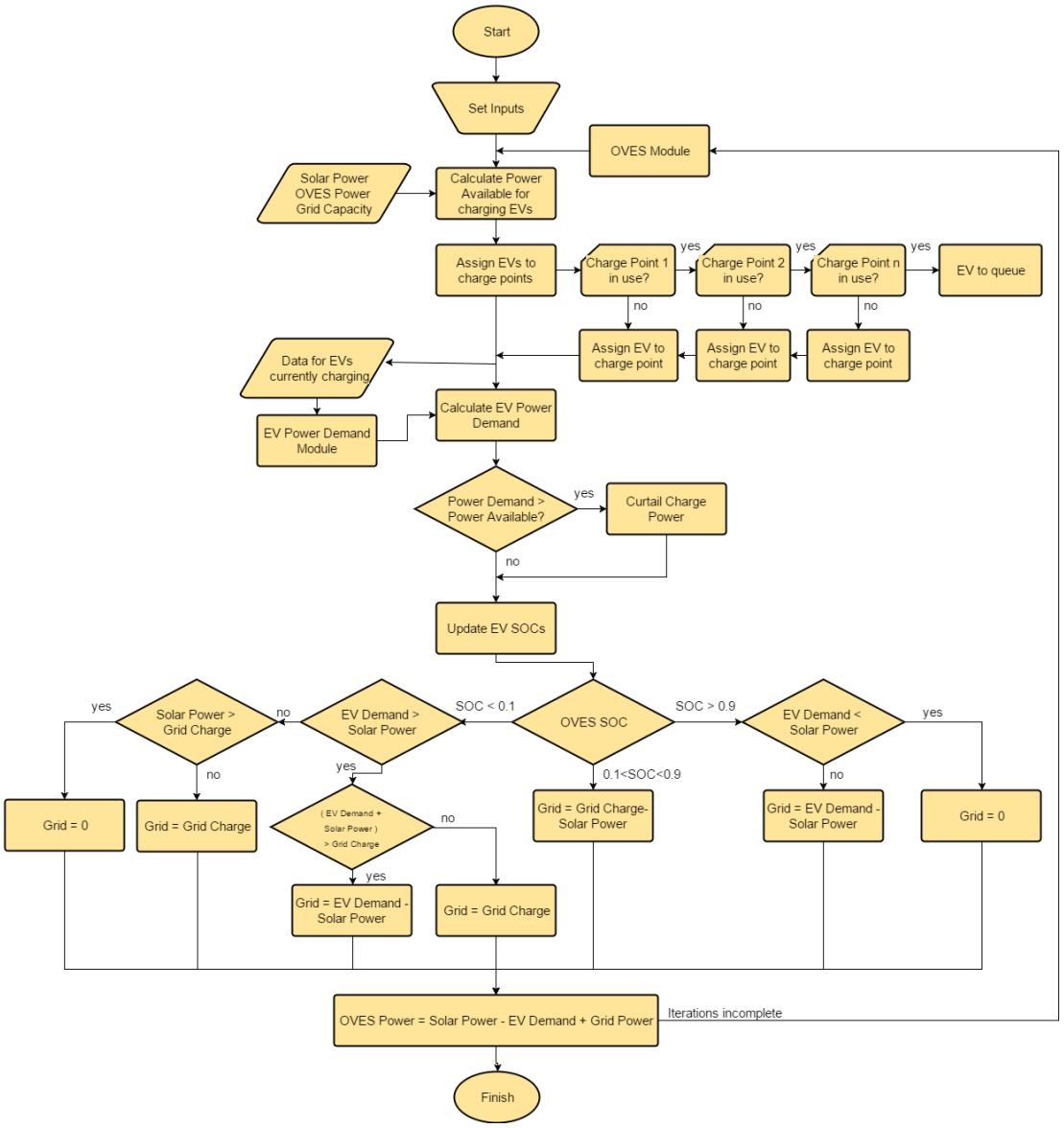

FIGURE 4.9: A detailed flow diagram of the iteration loop containing the HREVC algorithm. The code for this is included in Appendix B

adjusted to be equal to the time at which a charge point becomes available. I.e. a queue will form.

Secondly, the grid power at any moment cannot exceed the capacity of the grid connection. This is shown in Equation 4.4. Different values are given to the grid capacity for import and for export, therefore Equation 4.5 also holds.

$$P_{Grid} \leq GC_{max} \tag{4.4}$$

$$P_{Grid} \geq GC_{min} \tag{4.5}$$

Thirdly, an *available power* figure is calculated for each iteration. This is equal to the maximum power available to charge EVs, and is the sum of the solar generation power in that timestep plus the available power from the OVES plus the grid capacity. This is shown in Equation 4.6.

$$P_{EV} \leq GC_{max} + P_{PV} - P_{OVESmax} \tag{4.6}$$

If P_{EV} for an iteration has been calculated to be higher than the *available power* then the power to each EV is curtailed by the same factor. This step enforces the grid capacity constraint (equation 4.4).

By adjusting P_{EV} such that the grid capacity and charge point constraints will be followed, the algorithm can then calculate P_{Grid}. This requires a decision, based on the OVES SOC and the ratio of P_{PV}, P_{EV} and P_{GC} as is shown in Equation 4.7.

$$P_{Grid} = \begin{cases} P_{GC} - P_{PV} & OVES_{SOC} > 0.9 \\ 0 & OVES_{SOC} > 0.9 \,\&\, P_{EV} > P_{PV} \\ P_{GC} - P_{PV} & 0.1 < OVES_{SOC} < 0.9 \\ 0 & 0.1 > OVES_{SOC} \,\&\, P_{EV} < P_{PV} \,\&\, P_{PV} > P_{GC} \\ P_{GC} & 0.1 > OVES_{SOC} \,\&\, P_{EV} < P_{PV} \,\&\, P_{PV} < P_{GC} \\ P_{EV} - P_{PV} & 0.1 > OVES_{SOC} \,\&\, P_{EV} > P_{PV} \,\&\, P_{PV} + P_{EV} < P_{GC} \\ P_{GC} & 0.1 > OVES_{SOC} \,\&\, P_{EV} > P_{PV} \,\&\, P_{PV} + P_{EV} > P_{GC} \end{cases} \tag{4.7}$$

Equation 4.7 sets P_{Grid} each iteration to fill the gap between P_{PV} and P_{EV} if that lies beyond the capability of the OVES (either through SOC or power limitations). The P_{GC} level allows for OVES charging at a low rate ($P_{Grid} = P_{GC}$) in the absence of P_{PV}. P_{Grid} is then reduced if P_{PV} increases to maintain an OVES charge rate of P_{GC}.

$$P_{OVES} = P_{PV} + P_{EV} + P_{Grid} \tag{4.8}$$

The final stage of the algorithm sets P_{OVES} as the difference between the other three system powers. This ensures the energy conservation constraint in Equation 4.2 is met.

4.3.3.1 Queuing

Due to the implementation of a set number of charge points at the HREVC, the potential for queuing becomes inevitable. The desired time for an EV to begin charging is generated prior to the iteration using the EV Charge Demand Pattern Module. Each time an EV charge session is due to commence, the algorithm looks through the charge stations, if one is free the EV begins charging, otherwise, it is added to the queue. The order in which the EVs enter the charge station remains constant, whether they queue or not.

Clearly, the number of charge points has a significant impact on the likelihood of a queue forming. Figures 4.10 to 4.13 show how increasing the number of charge points both substantially reduces the queue size throughout the day and also affects the EV charge demand at the HREVC.

4.3.3.2 Grid Charge

P_{GC} is set as an input. It describes the power level at which the OVES will be charged in the absence of power flows from the solar farm. This feature allows for a reduction in the peak grid power to be enabled under more situations, allowing the OVES to be of use throughout the year. The grid charge feature allows the OVES to continue to perform energy balancing at the day scale throughout the year despite the shift in solar power generation between seasons.

A higher level of grid charge allows a smaller OVES capacity to be as effective as a higher capacity OVES operating under a lower grid charge due to quicker recharging. However, the OVES would be cycled more rigorously under these circumstances, leading to a trade-off.

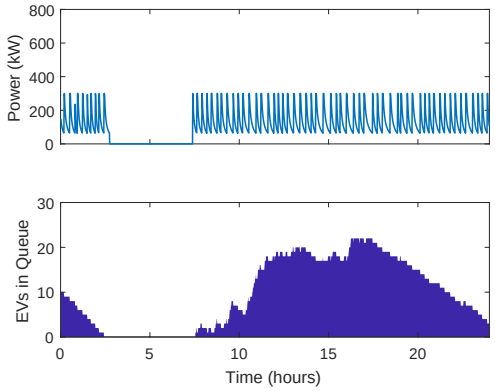

FIGURE 4.10: EV Charge demand power and queue for an HREVC with 1 charge point

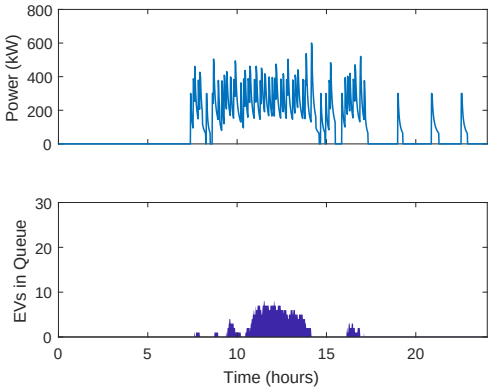

FIGURE 4.11: EV Charge demand power and queue for an HREVC with 2 charge points

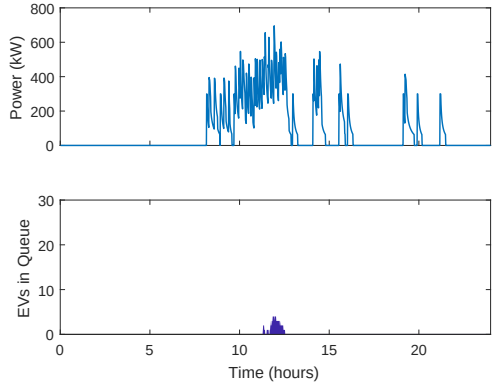

FIGURE 4.12: EV Charge demand power and queue for an HREVC with 3 charge points

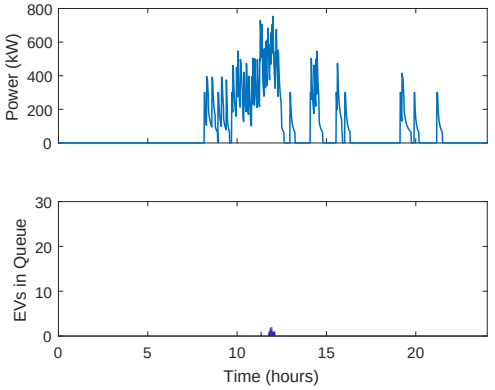

FIGURE 4.13: EV Charge demand power and queue for an HREVC with 4 charge points

The grid charge feature is ineffective, though, when high EV demand leads to energy demand which is continuously at a higher power level than that set by grid charge. In this situation - when EV demand is higher than solar power and grid charge - the OVES cannot charge.

Figure 4.14 shows the operation of the HREVC with a $P_{GC} = 100kW$. The intermittency of P_{EV} is not transfered to P_{Grid} for the majority of the day. The OVES SOC is increased through the night and the reduction in SOC during high periods of demand is less severe due to the additional power from the grid. However, P_{GC} must be selected carefully as if there is not enough power from the grid, the OVES will be ineffective due to diminishing SOC, however, if P_{GC} is too high the OVES will be under-utilised.

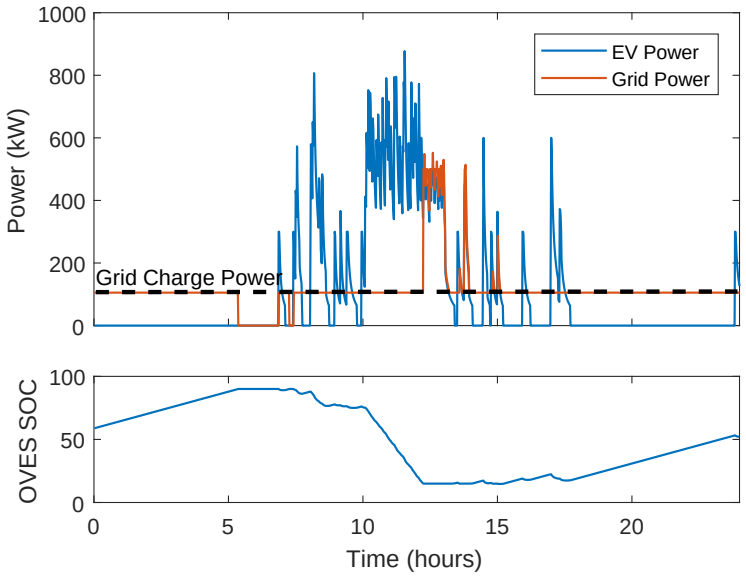

FIGURE 4.14: Power flows within HREVC for one day. Solar farm is removed to highlight the Grid Charge feature.

4.3.3.3 Grid Capacity

The grid capacity is the maximum allowable import/export power that the grid connection is capable of. This reflects engineering practice and network reinforcement works are carried out based on the grid capacity required at each connection. Therefore, by reducing the grid capacity, a lower connection cost will result. This is however, very geographically dependent.

A low grid capacity can lead to longer charge times for each EV due to curtailment of the charging power. This occurs under the situation where there is not enough solar power to provide the required demand and simultaneously the OVES is discharged. Therefore, the OVES is unable to provide the required power. Thus, if the EV demand is higher than the grid capacity, the power level to each EV will be curtailed.

Figure 4.15 shows this happening for one day. The grid capacity is set to 150kW with the solar farm removed. This leads to curtailment of the EV charge power during periods of high demand (between 0900 and 1400 in Figure 4.15). Analysis at the day scale for the HREVC model does not lead to any conclusions as there is much variation in both the HREVC demand and the solar generation. Therefore, analysis of system performance at the year scale is necessary.

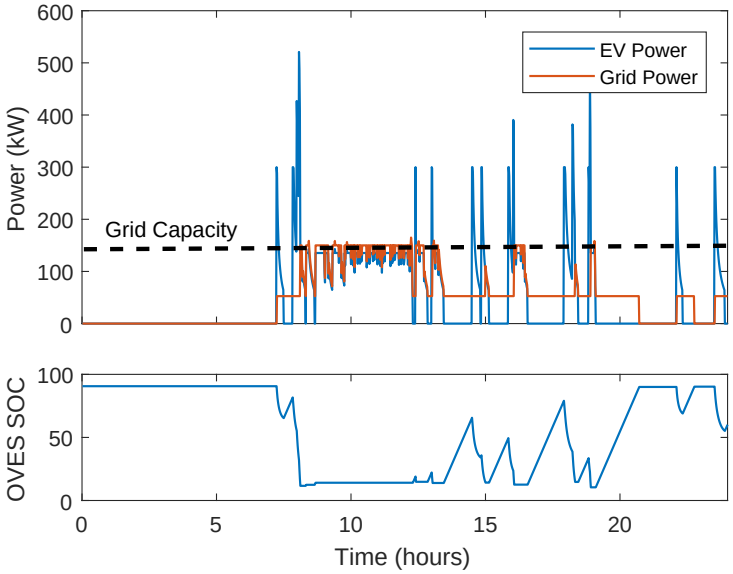

FIGURE 4.15: Power flows within HREVC for one day. Solar farm is removed and grid capacity set to 150kW to highlight the Grid Capacity leading to EV charge curtailment.

4.3.4 Power Flows

In reality, these features of the HREVC algorithm combine in a complex way at many timescales dependent on the values of design variables. The power flows for a typical day are shown in Figure 4.16. The sporadic and peaky nature of P_{EV} leads to the HREVC changing states quickly and often throughout the day. The OVES responds to these changes within the SOC bounds leading to rapid fluctuations in P_{PVES}.

4.3.5 Static grid charge effects

In order to show the effect of changing the OVES capacity on the overall energy flow within the HREVC different graphing methods are used. The important benefit of introducing the OVES is to reduce the total energy exchanged with the grid. Both the exports from the solar farm and imports to power the HREVC should be minimised. Therefore a critical output from the model is the absolute sum of grid energy - as increased exports adds to the total in the same way as increased imports.

The effect of changing the OVES capacity for the HREVC component capacities is shown in Figure 4.17. Clearly a reduction in the absolute sum of grid power is seen, especially

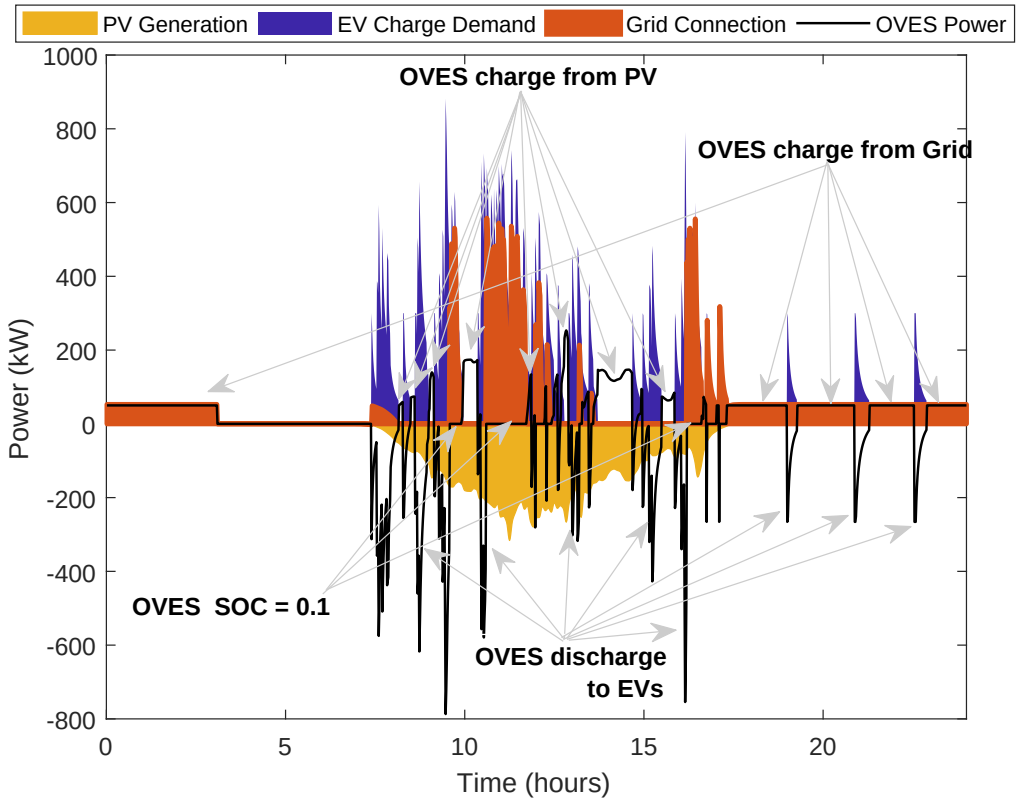

FIGURE 4.16: Power flows within an HREVC for one day.

for OVES capacities of up to 200kWh. However, despite there still being a substantial exchange of energy with the grid, additional OVES capacity is not as effective at reducing this. This effect is further seen in Figure 4.18 (including higher OVES capacities). The effectiveness of the OVES throughout the year can be seen with a cumulative sum. The P_{GC} does not allow for the HREVC to become self sufficient in the Summer, leading to increasing absolute grid power through these months despite increased available solar power.

This is indicative of under-utilisation of the OVES due to it being charged both by the grid (during the night) and the solar farm (during the day) even though this is not necessary with higher solar power availability during summer. This effect additionally leads to reduced utilisation of solar power due to a needless use of the grid to charge the OVES through the night, thereby reducing the capability of the OVES to absorb solar energy. As, the P_{GC} level is needed in the winter, but is deleterious to effective utilisation of the OVES in the summer, a dynamic grid charge algorithm is introduced in Section 4.3.6.

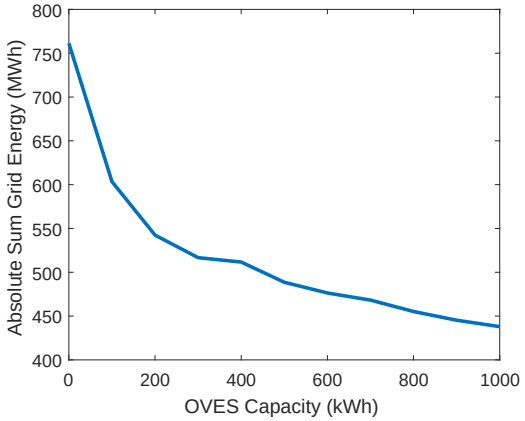

FIGURE 4.17: Absolute sum of grid interconnection energy over one year for varying OVES capacity.

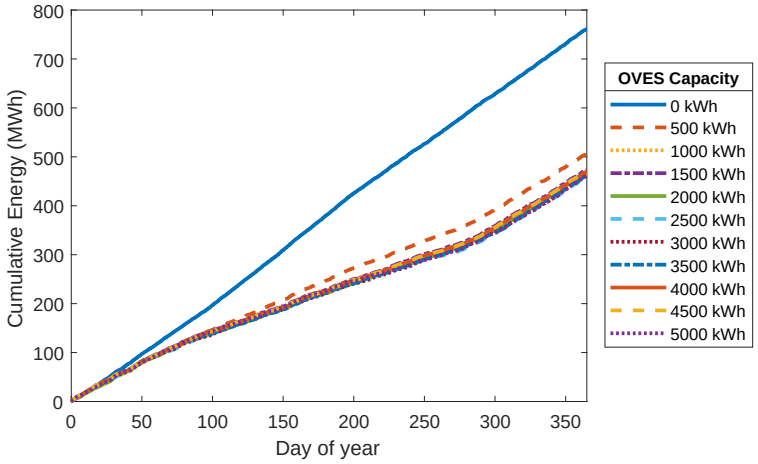

FIGURE 4.18: Cumulative grid interchange energy over one year for varying OVES capacities.

4.3.6 Dynamic Grid Charge

For an effective dynamic grid charge, the power level must respond to the changing generation patterns of the associated solar farm. In this simulation, this is achieved by setting the grid charge power equal to the inverse of the moving mean of the solar power subject to specified maximum and minimum power levels.

Firstly, the normalised moving average of the solar farm energy export data is calculated. Figure 4.19 shows the effect of the number of days over which the mean is calculated. 100 days shows a smooth transition between summer and winter, as such this is the data which was selected to be used as the sample for the dynamic grid charge.

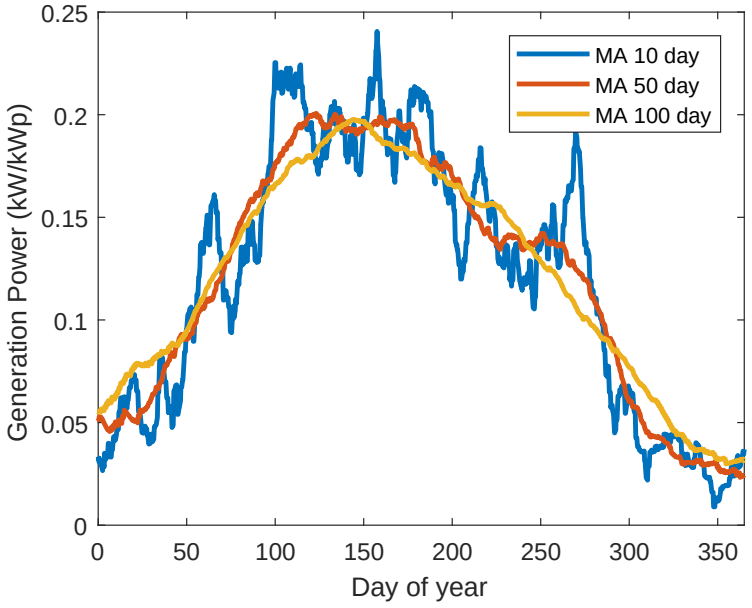

FIGURE 4.19: Solar power generation moving average (MA) for differing MA terms.

To calculate the grid charge power for each time step of the simulation, the solar moving average array is first normalised between the limits of 1 and 0 by dividing by the maximum value, giving $PV_{MovMean}$. Equation 4.9 shows how this array is then used to calculate P_{GC}.

$$P_{GC}(i) = PV_{MovMean}(i)\left(\left(1 + \frac{P_{GCmin}}{PV_{MovMean}(i)}\right) + (P_{GCmax} - P_{GCmin})\right) \tag{4.9}$$

Where:

- $PV_{MovMean}$ is the normalised PV generation power 100 day moving mean array.
- P_{GCmax} and P_{GCmin} are the specified maximum and minimum values for P_{GC}.

Thus, the minimum value of P_{GC} is equal to P_{GCmin} and all values greater than the minimum are multiplied by $(P_{GCmax} - P_{GCmin})$ such that the maximum value is equal to P_{GCmax}. The result of this can be seen in Figure 4.20.

By implementing a dynamic grid charge level with maximum power of 150kW and minimum of zero, a reduction in the absolute sum of grid energy can be seen for a range of OVES capacities. This is shown in Figure 4.21.

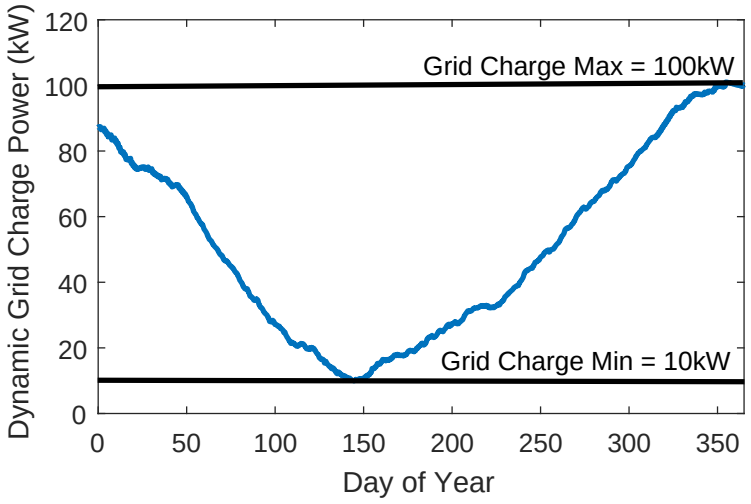

FIGURE 4.20: P_{GC} through the year for $P_{GCmax} = 100kW$ and $P_{GCmin} = 10kW$.

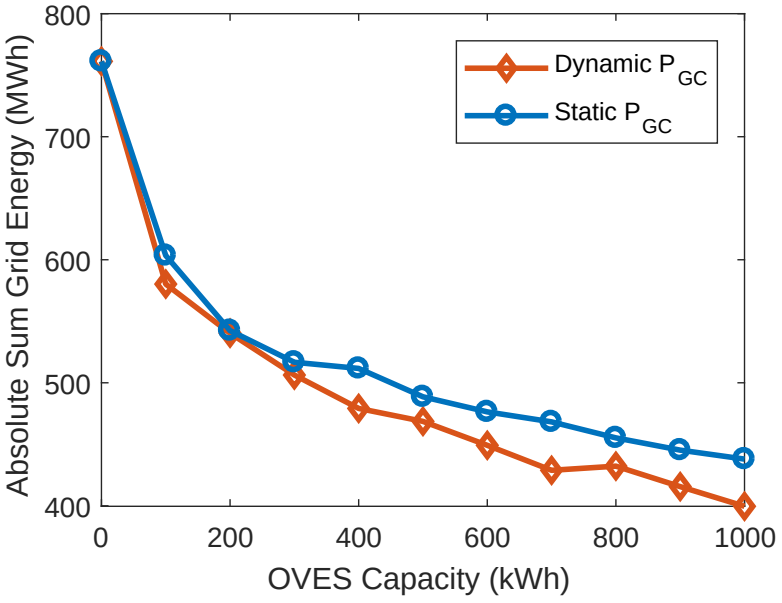

FIGURE 4.21: Absolute sum of grid interchange power for one year with dynamic (0-150kW) and static (100kW) P_{GC} and varying OVES capacities.

The effect of using this technique is shown in Figure 4.22 for varying OVES capacities. Clearly a reduction in the energy exchanged with the grid is enabled over the course of one year. This reduction is through substantially lower grid interchange levels in the summer arising from a lower grid charge level at these times. By comparing this figure to Figure 4.18 a clear benefit can be seen by changing the grid charge level throughout the year, especially at high OVES capacities.

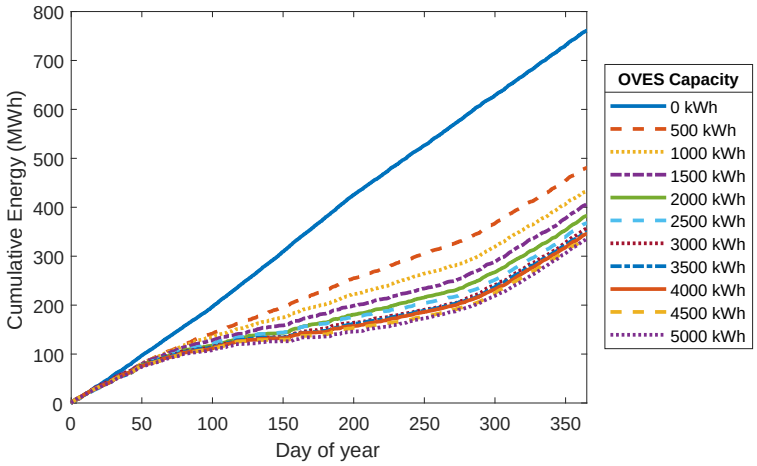

FIGURE 4.22: Cumulative grid interchange energy over one year for varying OVES capacities and a dynamic grid charge power.

This effect is broken down to the change enabled, by introducing a dynamic grid charge, in import and exports for each month of the year in Figures 4.23 and 4.24.

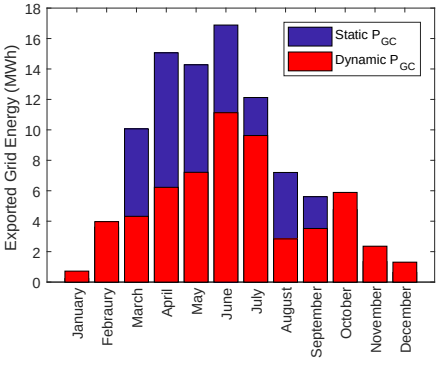

FIGURE 4.23: Exported energy by month for dynamic and static P_{GC}

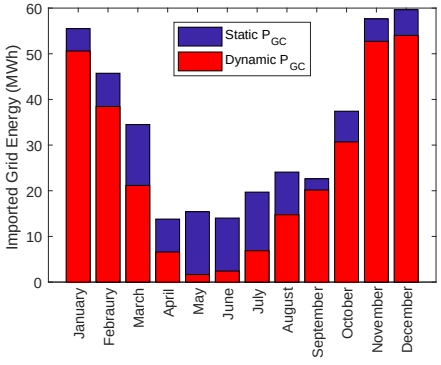

FIGURE 4.24: Imported energy by month for dynamic and static P_{GC}

As the relationship between P_{GC} and OVES capacity needs tuning through optimisation, it is even more crucial for the relationship between P_{GCmin}, P_{GCmax} and the OVES capacity. Especially as the solar farm capacity is now highly relevant to value selection.

4.4 Potential use cases

An HREVC could potentially be installed onto the grid in three ways:

1. **Solar farm with HREVC** An existing, or planned, solar farm chooses to add an HREVC to the system. In this case, it is anticipated that a constrained import connection to the grid will be in place and the HREVC will be powered almost entirely by the substantial solar power resource. This then provides a motivation for the inclusion of an OVES as a way of providing the HREVC demand without needing to import energy from the grid.
2. **HREVC with small solar** An existing, or planned, HREVC chooses to add a small amount of solar power to reduce the net energy demand from the grid. In this case, it is beneficial for all the solar power to be stored such that an export grid connection can be avoided and all the generated electrical energy from the solar can be used for charging EVs (minus conversion losses).
3. **Bespoke installation** A new HREVC installation where a motivation for powering the charger from renewable energy exists. This may arise from financial concerns - where the cost of a grid connection is too large to form a profitable business case for either of the standalone systems. Or from environmental concerns - where policy has been put in place which motivates a direct link between renewable energy and transportation. In this case, a method must be devised to find the optimal design of this system such that it achieves the aims of maximal financial gain or minimum environmental impact.

Therefore, the HREVC model was used to address each of these potential use cases to assess the viability and benefit of including an OVES.

As the statistical analysis in Section 4.2 has shown that a grid connection is needed for a well balanced system, it is of interest to asses whether a non-balanced system could be functional without a grid connection in one direction. By this it is meant, whether a large solar farm could power an HREVC without an import grid connection or whether an HREVC could include a small solar installation without an export grid connection. This is the subject of Sections 4.4.1 and 4.4.2.

4.4.1 Solar farm with HREVC

To asses the feasibility of adding an HREVC to a solar farm, a 1MWp solar farm was simulated. A simulated EV charge demand arising from a 10% EV penetration at J15-16

TABLE 4.2: System design variables for solar farm with HREVC simulation

Design Variable	Value	Unit
N_{CP}	4	-
PV_{cap}	1000 - 5000	kWp
$OVES_{cap}$	0 - 5000	kWh
P_{GCMin}	0	kW
P_{GCMax}	0	kW
GC_{max}	0	kVA
GC_{min}	5000	kVA

on the M25 was then used. The system design variable values used for this simulation are shown in Table 4.2.

Firstly, an HREVC is simulated with an import grid connection to ascertain how the inclusion of an OVES reduces the useage of that grid connection. In this configuration the grid charge maximum and minimum values are each set to zero.

A key advantage of having the HREVC located at a solar farm is that the import grid connection can be limited and the major source of power for the HREVC is that generated at the solar farm. It is important then that this idea is verified; Figure 4.25 shows the substantial reduction in imported energy enabled by the inclusion of an OVES at an HREVC configured as such. This reduction is enabled through charging of the OVES from the solar farm, thereby displacing the need for grid energy.

The overall energy demand of the HREVC is 850MWh/year (as can be seen in Table 4.3). A 1MWp solar farm reduces this demand by 49.8% when no OVES is included, this reduction arises solely from the direct interference between generated solar power and HREVC demand. The inclusion of flexibility in the system from the OVES allows for further reductions in the imported energy. A 73.6% reduction is evident when a 1MWh battery is included. Even a modest OVES capacity of 50kWh can make a substantial reduction in imports of a further 8.3% over the zero OVES capacity case.

To take the HREVC largely off-grid, i.e. have little need for an import grid connection, a larger solar farm is needed. With a solar capacity of 5MWp, and OVES capacity of $>$1MWh the imported energy can be reduced by $>$90%.

Furthermore, there are two other important factors which can be used to analyse the effectiveness of the OVES in this situation. These are the standard deviation of the

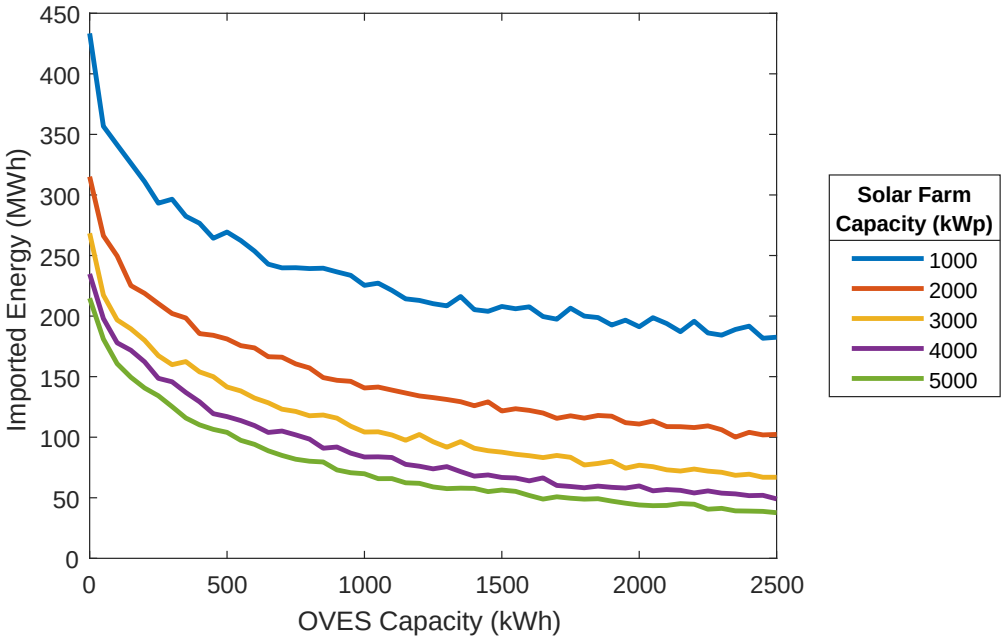

FIGURE 4.25: Energy imported for one year of operation of an HREVC with Solar Farm capacity 1-5MWp on the M25 J15-16 plotted against OVES capacity.

TABLE 4.3: Annual Imported Energy for HREVC located at a solar farm.

OVES Capacity (kWh)	Solar Farm Capacity (kWp)	Imported Energy (MWh)	Import reduction (%)
0	0	850	-
0	1000	427	49.8
50	1000	356	58.1
1000	1000	224	73.6
0	2000	315	62.9
50	2000	266	68.7
1000	2000	140	83.5
2000	2000	110	87.0
0	5000	214	74.8
50	5000	181	78.7
1000	5000	69	91.8
5000	5000	23	97.2

imported power and the mean imported power. It is important for both of these factors to be as small as possible as this indicates that the power demand at the grid connection is low and is not prone to large spikes.

High rate EV charging is likely to lead to spikes in demand due to the EV charging power profile. Therefore the ability of the OVES to mitigate these spikes can be equated to the

reduction in the standard deviation of the imported energy profile. Equally, in this situation, a small mean imported power shows that the majority of the OVES is successfully transferring the solar energy to the EVs without requiring high levels of power from the grid.

Figures 4.26 and 4.27 show that both these metrics fall with larger OVES capacities. However, there are clearly diminishing returns in both cases beyond 1MWh.

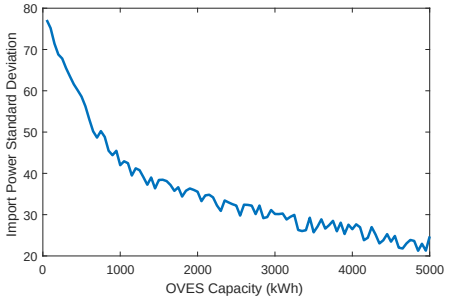

FIGURE 4.26: Import power standard deviation for OVES capacity. PV = 1MWp

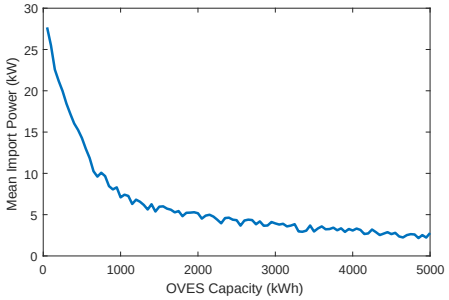

FIGURE 4.27: Import power mean plotted against OVES capacity. PV = 1MWp

It is anticipated though, that in this use cases many installers would prefer to install a HREVC without an import grid connection at all. This may be due to the network constraints in place locally, or simply to avoid the added project complexity and lead time associated with securing a grid connection. In this case, the reliability of the HREVC would be reduced. However, this is mitigated by the inclusion of the OVES as shown in Figure 4.28. This shows the percentage of time the EV charge power is curtailed i.e. the power to the EV is less than requested due to power availability constraints. If there is no import grid connection, and no OVES these constraints would arise whenever an EV requests more power than is currently being generated by the solar farm. Figure 4.28 shows that this is very common in this situation - with EV charging power being curtailed 99.5% of the time with no OVES. Substantial reductions in the curtailed power are available with only a very small OVES (68.9% for 50kWh). With further increases in OVES capacity yielding further reductions.

It should be noted that the curtailed charge power cannot be reduced to zero for reasonable OVES capacities. Therefore, installers of grid free HREVCs should be aware that there will inevitably be a usability penalty.

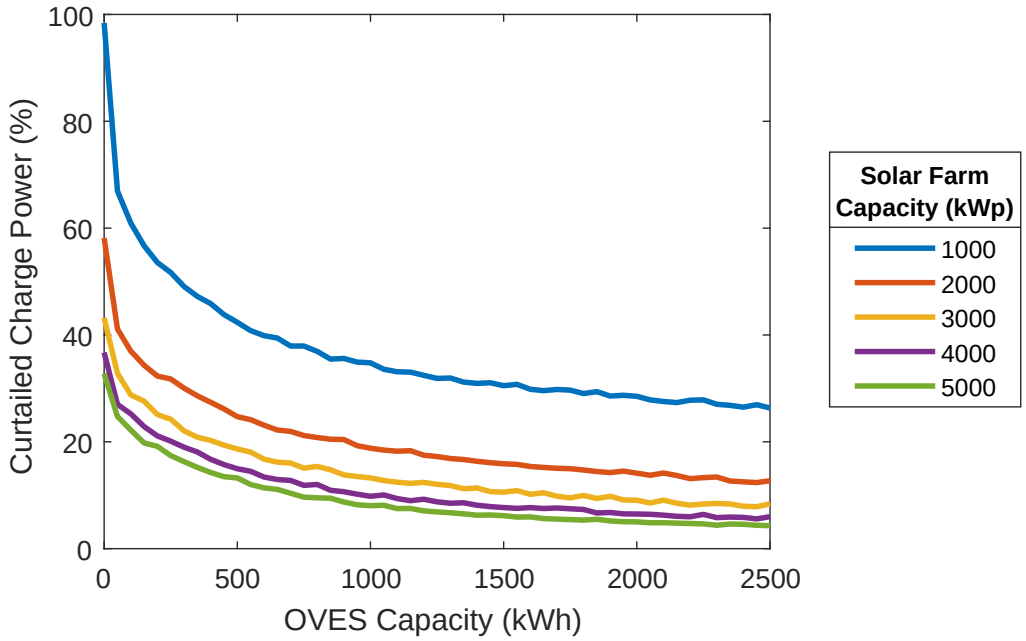

FIGURE 4.28: Percentage of EV charge power curtailed plotted against OVES capacity for HREVC with solar farm capacity 1-5MWp.

The demand used in this simulation is quite high - an HREVC on the M25. It is anticipated that HREVCs in this configuration would mainly be suited for low demand locations. However, as a worst case scenario it is beneficial to see the potential for import reduction and HREVC reliability improvements available from an OVES.

For each potential installation a survey and model of EV demand should be created such that the required OVES capacity can be calculated to avoid energy import for the required percentage of EV charge interruption. In this way the curtailed charge power percentage can be used to inform the design of the HREVC.

4.4.2 HREVC with small solar

The second potential use case for an HREVC with an associated OVES is to enable the installation of a small amount of solar generation without, or with only a small export grid connection.

For this configuration the system specification used for simulation was as shown in Table 4.4.

TABLE 4.4: System design variables for HREVC with small solar simulation

Design Variable	Value	Unit
N_{CP}	4	-
PV_{cap}	100-500	kWp
$OVES_{cap}$	0 - 2500	kWh
P_{GCMin}	50	kW
P_{GCMax}	150	kW
GC_{max}	1000	kVA
GC_{min}	0	kVA

In this case an export grid connection may not be possible or may be expensive. It is the main motivation when installing the additional solar power to reduce energy import costs for the HREVC. Therefore, it is advantageous to utilise as much solar power as possible by storing excess energy in the OVES.

In the case where an export grid connection is utilised it is useful to design a system where the necessary grid connection is minimised. This is achieved through both minimising the energy exported and the power at which that energy is exported. Figure 4.29 shows how the capacity of the solar farm and OVES affects the energy exported. Clearly there is more energy exported for higher solar farm capacities, however this can be reduced substantially through the inclusion of storage. This is advantageous for the HREVC as a reduction in exported energy leads to higher utilisation of the solar farm for EV charging.

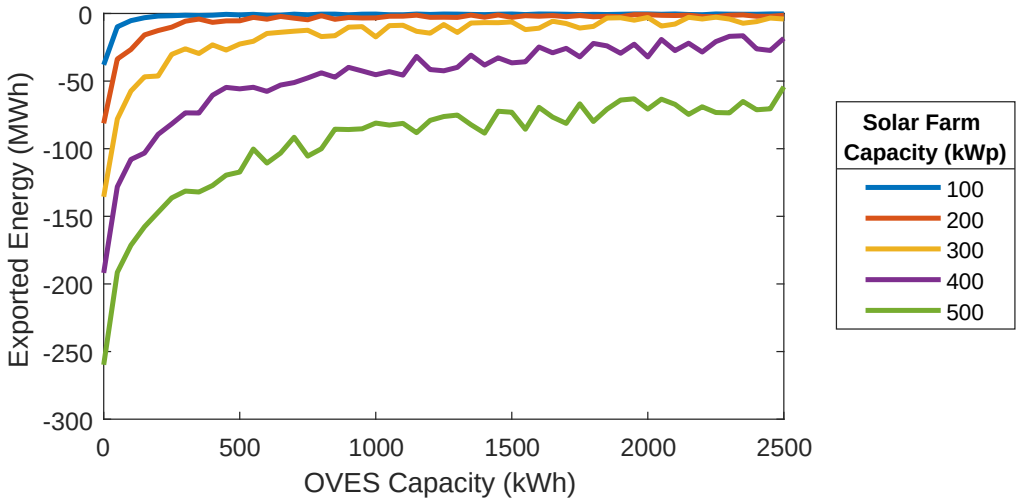

FIGURE 4.29: Exported energy for HREVC with small solar (100-500kWp) for varying OVES capacity over one year.

TABLE 4.5: Annual exported energy reduction for HREVC with small solar.

Solar Capacity (kWp)	Export (MWh)	Export reduction OVES (kWh = kWp)	Difference (%)
100	38.0	5.30	86
200	81.2	12.6	85
300	135	26.1	81
400	192	60.4	69
500	260	117	55

TABLE 4.6: Annual imported energy reduction for HREVC with small solar.

Solar Capacity (kWp)	Import reduction (MWh)	Import reduction OVES (kWh = kWp)	Difference (%)
100	86	96	11.6
200	130	192	47.7
300	204	283	38.7
400	232	358	54.3
500	272	408	50.0

With $OVES_{cap} = PV_{cap}/2$, the average export power can be reduced substantially. This reduction in mean exported power is key as it shows that the OVES is capable of absorbing the majority of the high power fluctuations from the solar farm.

However, for installations without an export grid connection it is critical to assess the import reduction capability of the solar farm and OVES as this would lead to a direct reduction int he energy cost for the installation. Figure 4.30 shows this affect for varying OVES and solar farm capacities. When the solar capacity is small (<100kW) there is little effect arising from the OVES. This is because the HREVC is directly using the majority of the power generated from the solar (as shown when exported energy falls to zero in Figure 4.29). In this case though, the available reduction in imported energy is 100MWh over the year, which would represent a substantial saving.

If further savings are desired, then additional solar capacity can be installed. However, this becomes ineffective without an associated OVES beyond 100kWp. For solar installations of >100kWp an OVES ($OVES_{cap} = PV_{cap}$) enables a significant further reduction in exports of an additional 47.7% (average). When $OVES_{cap} > PV_{cap}$ diminishing returns in import reduction were seen.

The OVES can therefore be seen to be more effective at reducing the mean exported power than reducing imports as a steady state import reduction increase of 50% seems

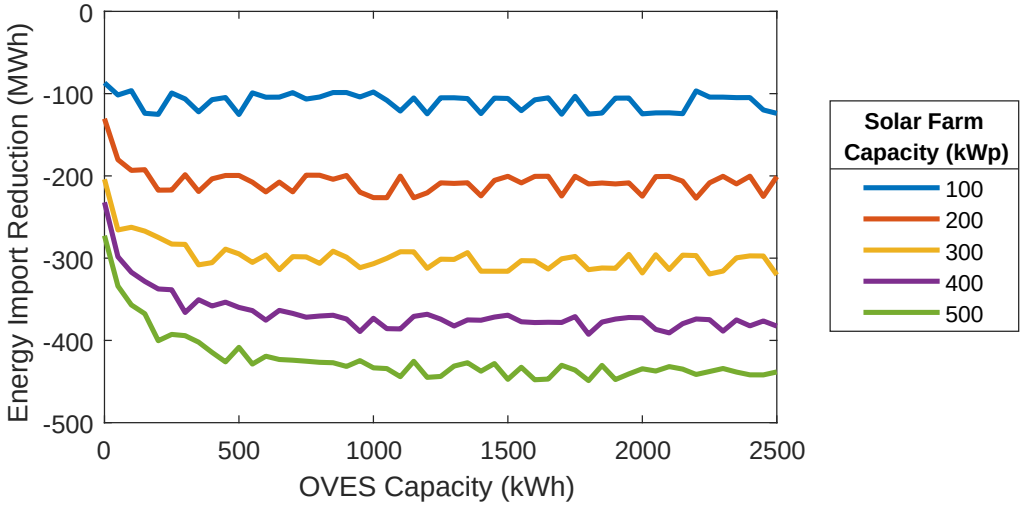

FIGURE 4.30: Reduction in imported energy for HREVC with small solar (100-500kWp) for varying OVES capacity over one year.

to be reached, beyond which the additional OVES capacity does not yield further reduction.

A limit seems to arise of 200kW of installed solar capacity whereby, beyond that an export grid connection is needed to avoid a large amount of wastage. However, this figure is related to the expected demand at the selected HREVC location and would also be a decision when designing the system. For example, additional reductions in imported energy can be made by installing a larger solar capacity, however, this extra installed capacity will be less effective due to the higher quantity of wasted energy if an export grid connection is not installed. Therefore there is a trade-off between reducing imports and over-specifying the solar installation capacity.

4.5 Conclusions

Initial statistical analysis was an important tool to assess the viability of an HREVC powered by solar energy with an OVES. It was shown that an OVES is able to match the supply with demand for a well balanced system over the day scale. However, at the year scale, due to seasonal changes in the solar power generation profile a grid connection is needed for a well balanced system.

To further investigate the control process for the OVES and the potential use cases of an HREVC a model was then made of the system. This highlighted the need for a dynamic OVES charging regime powered by the grid. A queuing system and variable number of charge points was included in this model for added realism. It was found that the relationship between P_{GC} (including P_{GCmin} and P_{GCmax}) and P_{PV} was critical for effective design of the HREVC and therefore optimisation is necessary to tune these design variables.

Two use cases were then investigated in this chapter: Solar farm with HREVC and HREVC with small solar. The aim of each of these was to asses whether a one way grid connection could be used to install an unbalanced system. It was found that:

- An HREVC with a large solar farm can be taken mostly off grid with a large PV farm and $PV_{cap}/2 < OVES_{cap} < PV_{cap}$ but 10-20% of charging power will be curtailed.
- The OVES is more effective at reducing exports than imports when included with an HREVC and small solar installation. This leads to a trade-off between import reduction and over-specifying the OVES.

For many HREVCs, installation onto an existing system, such as those discussed in this chapter may not be the case. In the case where an HREVC is designed from the ground up, further thought must be given to the specific values of the design variables in question. To achieve optimal benefit from the inclusion of an OVES and to finding the best design for an HREVC system, an optimisation procedure is needed. This is the subject of Chapter 6.

Chapter 5

Bespoke Installation Design

Due to the grid constraint concerns associated with HREVCs and renewable energy in the UK highlighted in Chapter 2 a clear objective of the inclusion of solar PV and an OVES within an HREVC should be to alleviate these concerns. However, for an installation to be successful and to be installed, in the real world it must be financially viable. Therefore, these two considerations and the effects they have on the design of an HREVC are studied in parallel in this Chapter.

A financial model is included to enable an assessment of the profitability of an HREVC. Using this, the design of an HREVC which leads to maximum profit for the owner is calculated and presented. Additionally, the design permutations which lead to minimal grid connection usage are found. This enables a contrast to be drawn between the two motivations. Additionally, sensitivity analysis is used to measure the importance of each design variable in the system.

5.1 Novel Contributions

This chapter presents the results of optimisation for maximum profit and minimum grid connection usage and analysis of how sensitive the profit and grid connection usage are to the design variables of the system. This leads to a number of specific claims for novelty:

1. Optimisation provides author's results which use the novel models developed in Chapters 4 and 5.
    - Optimisation for maximum profit. Results shown in Section 5.4.1 supported by the financial model presented in Section 5.2. These results compare favourably with other business cases in which energy storage has been installed in the UK.
    - Optimisation for minimum use of grid connection. Results shown in Section 5.4.2.
2. Sensitivity analysis revealing the order of importance of design variables for correctly achieving design aims. This is included in Section 5.5

5.2 Financial model

A financial model has been integrated into the HREVC model. This calculates the profit over a given time period with inputs of component costs (CAPEX), ongoing costs made up of electricity cost and operation and maintenance (O&M) cost (OPEX) and price of electricity sold to EVs and to the grid (Revenue). The values used for this are shown in Table 5.1. The method of calculating cash flow from these inputs is shown in Equation 5.4.

Firstly, the CAPEX is calculated as shown in Equation 5.1.

$$CAPEX = N_{CP} * c_{N_{CP}} + PV_{cap} * c_{PV_{cap}} + 2 * OVES_{cap} * c_{OVES_{cap}} \tag{5.1}$$

Where c denotes the unit cost of the variable in question (given in Table 5.1) and cap denotes the selected capacity for the variable in question. The OVES cost is doubled due to the 10 year assumed lifespan.

Then the model described in Section 4.3.3 is run to calculate the revenue and OPEX each year, through Equations 5.2 and 5.3.

$$Revenue(y) = \left(c_{P_{EV}} \sum_{i=1}^{8760} P_{EV}(i) \right) + \left(c_{P_{grid}} \sum_{i=1}^{8760} P_{grid}(P_{grid} < 0) \right) \tag{5.2}$$

TABLE 5.1: CAPEX, OPEX and revenue values for HREVC. Values selected corresponding to internal information at Wood PLC.

	Unit	Cost per unit (£)
CAPEX		
Charge point	-	50,000
Battery	kWh	400
Solar Farm	kWp	800
OPEX		
Electricity purchase	kWh	0.12
Solar O&M	kWp/year	25
Battery O&M	kWh/year	5
Revenue		
Electricity sold to EVs	kWh	0.50
Electricity exported to grid	kWh	0.05

$$OPEX(y) = PV_{cap} * c_{PV_{OM}} + OVES_{cap} * c_{OVES_{OM}} + (GC_{max} - GC_{min}) * c_{GC} \quad (5.3)$$

Where OM denotes the annual operation and maintenance cost. Then the cash flow for each year can be calculated through Equation 5.4.

$$C(y) = Revenue(y) - OPEX(y) \quad (5.4)$$

Where: C is the net cash inflow and y is the financial year.

The cash flow for each year of the simulation is then summed for the project over its lifetime to calculate profit.

5.3 Optimisation procedure

The genetic algorithm was chosen for this problem for two reasons:

1. **Stochastic nature of the problem** - As the EV demand is generated randomly there is inevitably a variation from simulation to simulation. Global search algorithms are ideal for dealing with this variation as they do not follow a deterministic path

to the optimal solution, or indeed, claim to find an optimal solution. The algorithm can be terminated once a satisfactory state has been reached, and this state can be specified to allow for inter-iteration variation.

2. **Integer specification of variables** - The implementation of genetic algorithm optimisation in Matlab enables the specification of integer variables. This is advantageous for 2 reasons: some of the design variables (N_{CP}) are discrete and as such need to be specified as an integer; and secondly specification of other variables as integers reduces the amount of time needed to find an acceptable solution.

It was computationally too expensive to run the full EV prediction model included with the HREVC model. 10 sets of EV demand patterns were made for each of the 20 years and each EV growth scenario and one of these was stochastically chosen for use in each iteration of the optimisation algorithm.

5.3.1 EV growth scenarios

As an HREVC will have a projected lifespan of 20 years the fleet share of EVs is likely to change substantially over that time. This will inevitably have an effect on the profitability and design of the HREVC. Therefore, reliable predictions of the changes in fleet share of EVs were sought.

Bloomberg New Energy Finance, in their annual EV Outlook report [219], predict that EV sales will rise to 55% of all vehicles by 2040. This prediction forms the high EV growth scenario used for this optimisation. The medium EV growth scenario was found in the World Oil Outlook from OPEC [220] and the low EV growth scenario was found in the Outlook for Energy published by Exxon Mobil [221]. These are each shown in terms of fleet share in Figure 5.1.

5.3.2 Grid connection cost

It was difficult to find specific values of the cost of grid connection per kVA as this is often private information for the party who bought the grid connection. Moreover, this charge is subject to a large degree of variability since it is calculated on a case by case

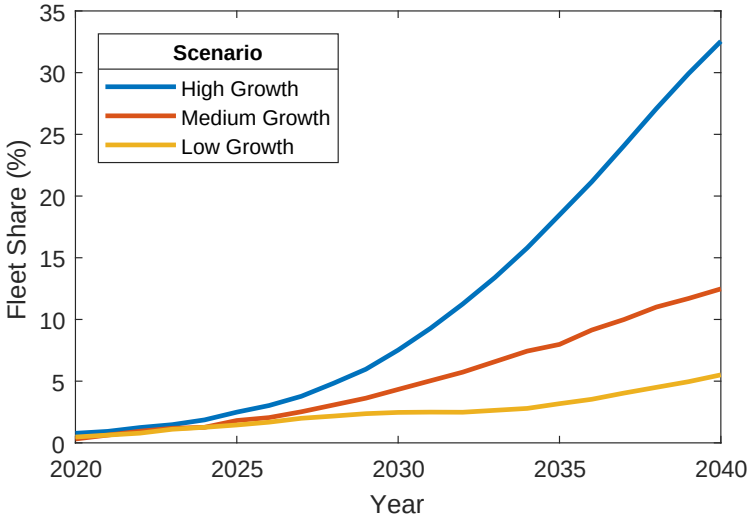

FIGURE 5.1: EV growth scenarios 2020-2040. [219] [220] [221]

TABLE 5.2: Grid connection cost for the 3 scenarios considered.

Scenario	Price (£ kVA year)
Low	-1.89
Medium	16.03
High	94.97

basis, taking into consideration the location of the nearest available connection point and the constraints which already exist on the grid.

Nevertheless, a representative range of prices was found from a letter published by National Grid [222]. In it, customers responded to a request for information - giving annualised costs of the grid connection. National Grid were then able to calculate the ranges shown in Table 5.2. These values were taken as the low, medium and high annualised cost and included within the OPEX of the project (Equation 5.3).

5.3.3 Fitness functions

The entire model (Equations 4.2 to 4.8) presented in Chapter 5 are used within the fitness functions, along with the financial model (Equations 5.1 to 5.4). Thus the actual fitness functions examined in this chapter are as follows:

$$\min_{\forall X \in \Psi} -NPV(X) \tag{5.5}$$

TABLE 5.3: Options for use in the optimisation of fitness functions.

Option	Description	Value
Parallel	Start a parallel session and optimise within a parallel cluster	True
Function Tolerance	End optimisation when results from all workers fall within the specified range of the fitness function	100,000
Population size	Number of workers	16
Generations	Maximum number of generations	75
Crossover	The fraction of the population changed by cross over procedure	0.8
Crossover function	The method for calculating values of the next generation when parents are subject to crossover	Random
Elite children	The fraction of the population guaranteed to survive to the next generation	0.05

$$\min_{\forall X \in \Psi} \sum_{y=1}^{y} \sum_{i=1}^{i=8760} |P_{Grid}(X)| \tag{5.6}$$

Where Ψ is the constraint set (Defined in Section 5.3.4). These fitness functions are subject to a number of options as detailed in Table 5.3.

As a result of the three different scenarios considered for both grid cost and EV fleet growth, nine separate profit based optimisations (Fitness Function 5.5) were completed (one for each combination) and three optimisations for minimal grid impact (Fitness Function 5.6). Thereby, the maximum profit of this system was found for high, medium and low grid costs and high, medium and low EV fleet growth scenarios for each grid cost.

5.3.4 Constraints

5.3.4.1 Bound constraints

Each design variable was assigned bound constraints. These relate to maximum and minimum values which these variables can take. These are detailed in Table 5.4. Wide values were chosen to enable a solution to be reliably found for each of the scenarios despite the wide range of use cases.

TABLE 5.4: Optimisation bounds for each input variable

Variable	Lower Bound	Upper Bound
N_{CP}	0	100
PV_{cap}	0	1,000
$OVES_{cap}$	100	10,000
P_{GCMmin}	0	1,000
P_{GCMax}	0	1,000
GC_{max}	0	10,000
GC_{min}	0	10,000

5.3.4.2 Linear constraints

In addition to the bound constraints, further linear constraints were included within the optimisation problem.

Firstly, the maximum grid charge power (P_{GCMax}) must be lower than the import grid connection capacity (GC_{max}), as shown in Equation 5.7. Clearly, this is a necessary step as it would not be possible to charge the OVES at a higher power than is available from the grid connection when there is no solar power.

$$GC_{max} > P_{GCMax} \tag{5.7}$$

Secondly, the maximum grid charge power (P_{GCMax}) must be greater than or equal to the minimum grid charge power (P_{GCMin}). Again, it stands to reason that this must be the case for correct operation of the HREVC model.

$$P_{GCMax} \geq P_{GCMin} \tag{5.8}$$

5.3.4.3 Non-linear constraints

In addition to the linear constraints and bounds which place direct constraints on the values which can be assigned to the design variables, non-linear constraints are included. These pertain to the overall functioning of the simulated HREVC.

Firstly, the HREVC must be adequate for the number of EVs that wish to charge there. I.e. the overall EV waiting time must not be more than 10 minutes per EV on average. This is shown in Equation 5.9.

$$0 > -\sum_{(y=1)}^{Y} t_{EV_{wait}} + 10N_{EV} \tag{5.9}$$

Where $t_{EV_{wait}}$ is the total wait time at the HREVC for one year (arising from the constrain in Equation 4.3).

Secondly, the HREVC must be capable of providing adequate power to those EVs which wish to charge there. This leads to the constraint in Equation 5.10 which ensures that no more than 5% of the power used to charge the EVs is curtailed (i.e. the EV receives the power it requests for 95% of the time on average).

$$0 > -0.05 + \frac{1}{Y}\sum_{(y=1)}^{Y} 1 - \sum_{i=1}^{i=8760} \frac{GC_{max} + P_{PV}(i) - P_{OVESmax}(i)}{P^*_{EV}(i)} \tag{5.10}$$

Where P^*_{EV} is the requested EV charge power prior to curtailment due to the inequality in Equation 4.6.

5.4 Results

5.4.1 Optimisation for financial gain

The optimum values of design variables for each of the 9 scenarios for which an optimum design have been found are shown in Figures 5.2 to 5.4. Additionally, the numerical results are shown in Appendix C.

It can be seen that for the most part, the design of the HREVC changes substantially through varying operating conditions. However, an $OVES_{cap}$ of between 100-300kWh is seen for all but one scenario and a PV capacity of below 200kWp is seen for all scenarios. The grid charge power levels change more dramatically though, low values are seen for the low EV growth scenario, a high range of values for the medium growth scenario and high values for high growth (Figure 5.3).

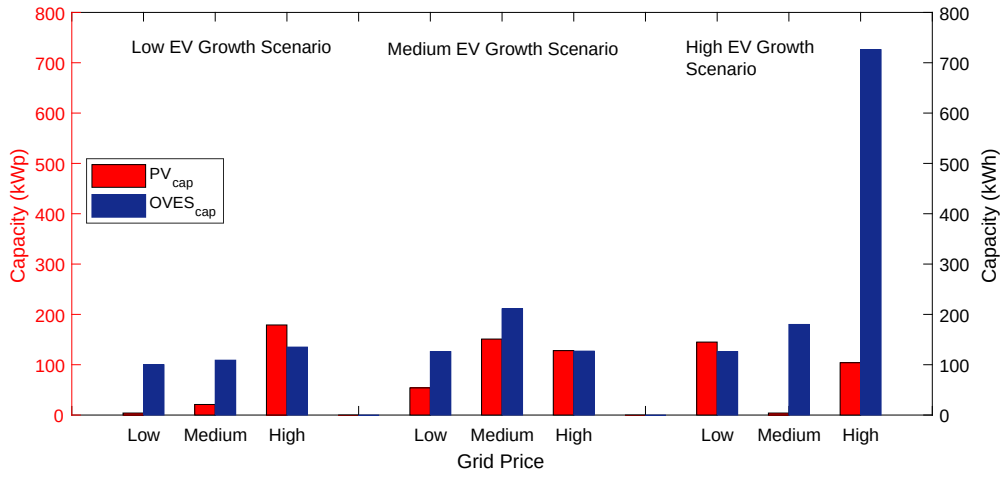

FIGURE 5.2: Optimum capacities of the solar farm and OVES.

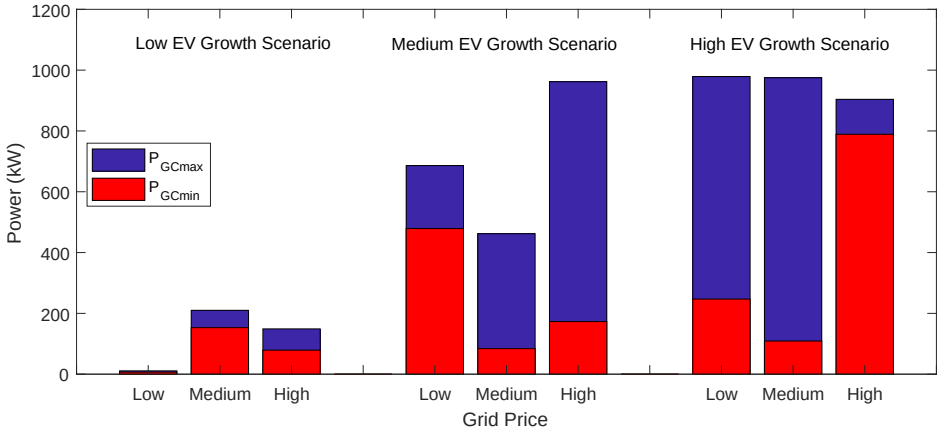

FIGURE 5.3: Optimum values of minimum and maximum grid charge powers.

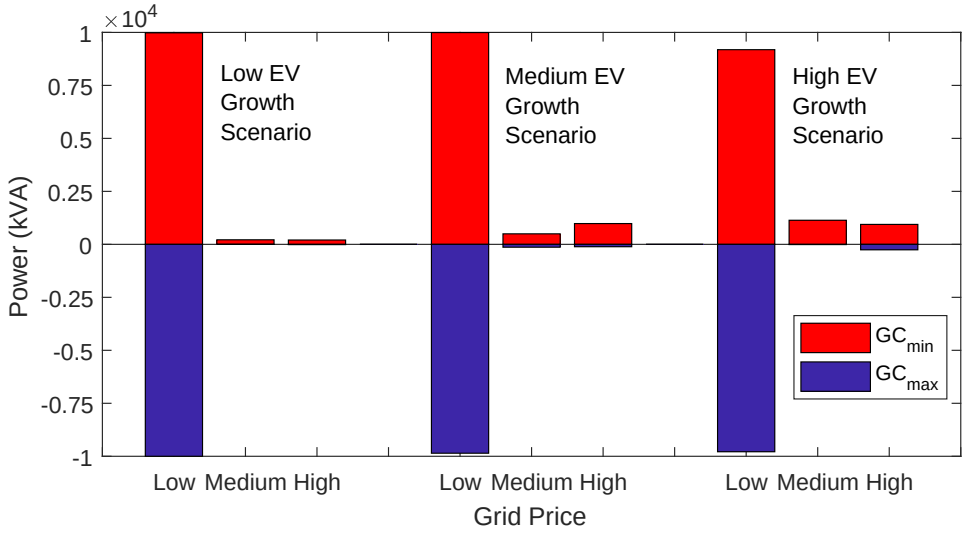

FIGURE 5.4: Optimum values for the import and export grid connections.

The grid capacity is highly dependent on the grid connection cost, as shown in Figure 5.4. For negative connection prices, the export and import values both take the

maximum allowable value as this is financially more efficient. In the other scenarios the capacity responds to the level of demand seen at the charger. GC_{max} remains close to P_{GCmax} for each of these positive grid price scenarios. This shows that the peak power demands which lie above the GC_{max} power level are met adequately by the OVES such that the curtailed power constraint (Equation 5.10) is satisfied.

The design of the charger in the high EV fleet growth and high grid price scenario. In this case the $OVES_{cap}$ is much higher than the other scenarios, additionally both P_{GCmin} and P_{GCmax} take high values. The combination of high grid price and high EV demand leads to a driver for the inclusion of energy storage. This enables the HREVC to meet the high EV demand whilst avoiding the need to have a large grid connection.

The effect of this is seen when the expected profit of the HREVC is compared between scenarios, with and without an OVES and solar power. The results of this comparison can be seen in Figure 5.5. The profits for each system remain largely similar except for the high EV growth scenario. In this scenario, the inclusion of an OVES leads to higher profits than would otherwise be available for the medium and high grid connection prices. On the other hand, including an OVES can reduce profits if done incorrectly, as the battery is expensive, hence unnecessary inclusion will reduce profitability. This can be seen for the low EV growth scenario and high grid connection price (which is the only scenario where a HREVC is not seen to be profitable).

It is useful then, to benchmark the profitability of the OVES against other business cases in which energy stores have proven to be successful. In Section 2.1 it was seen that energy stores generated a revenue of 120 - 210 £k/MWh/year performing frequency response and 55 - 68 £k/MWh/year for energy arbitrage in the UK market. Table 5.5 shows that the results of this simulation compare favourably with these figures. In this table, the change in revenue (Δ Profit) of the HREVC is quoted with and without solar and an OVES. Then the profit which would have arisen from the solar farm alone is subtracted from this value (at 5p/kWh) to give the revenue increase enabled through the inclusion of an OVES. This is then divided by the capacity of the OVES in that scenario to give a value for £m/MWh/year.

As the availability of an export grid connection lead to an increase in the profitability of the system for the negative grid connection price scenario, the values for these were omitted.

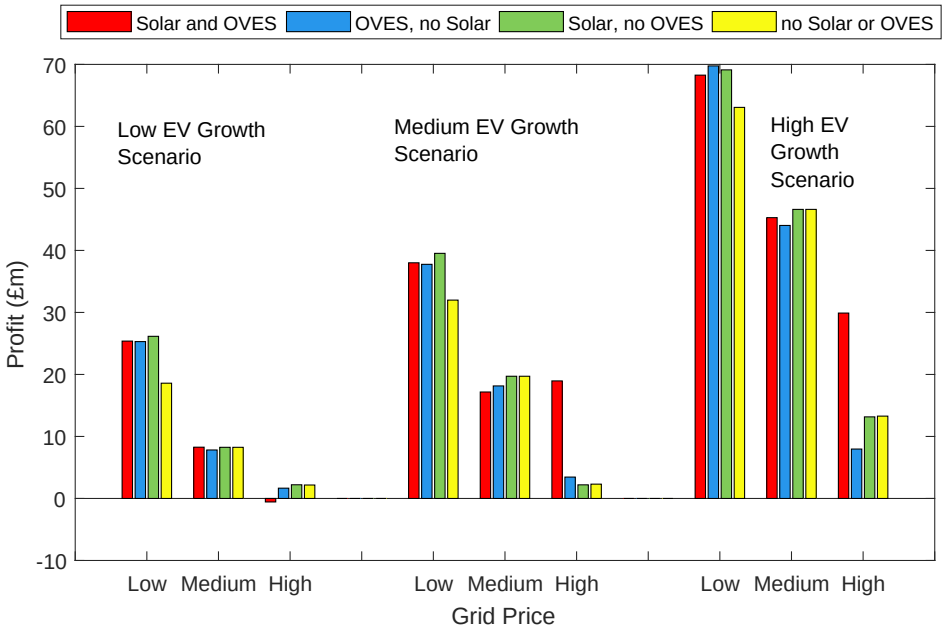

FIGURE 5.5: 20 year Profit for the optimal solutions found for each scenario.

TABLE 5.5: Change in profitability of an HREVC through including and optimised OVES and solar farm.

EV Fleet Growth	Low		Medium		High	
Grid Connection Price (£/ kVA)	16.03	94.97	16.03	94.97	16.03	94.97
Δ Profit (£m)	0.02	-2.73	-2.54	16.65	-1.33	16.62
$OVES_{cap}$	109	135	211	127	180	726
PV_{cap}	21	179	151	128	4	104
Δ Profit (£k) (PV)	1.10	9.50	8.00	6.80	0.21	5.50
£m/MWh/year	0.0046	-0.51	-0.30	3.28	-0.18	0.57

Clearly, in the right scenario, the inclusion of an OVES leads to a more profitable system, indeed this profit when calculated per MWh is well above that seen for other energy storage projects. This is due to the combined benefit of enabling a smaller grid connection and selling renewable energy at a higher price to EVs.

5.4.2 Optimisation for network gain

The minimum grid impact fitness function (Equation 5.6) optimisation leads to a different system design than that for maximum profit. This is shown in Table 5.6. The key differences are that, instead of a measured PV farm capacity seen for optimum profit,

TABLE 5.6: System design for minimum absolute grid energy exchange (Grid Energy figures are cumulative absolute sum over 20 years)

EV Fleet Growth	High	Medium	Low
N_{CP}	12	4	94
PV_{cap} (kWp)	992	946	999
$OVES_{cap}$ (kWh)	848	968	1000
P_{GCMin} (kW)	17	0	0
P_{GCMax} (kW)	129	169	1
GC_{max} (kVA)	5455	313	9952
GC_{min} (kVA)	0	-3	0
Grid Energy (MWh)	8123	2650	314

the maximum value is taken for each scenario. Additionally, without consideration of the cost of the OVES, the maximum capacity of this is taken in each scenario.

The P_{GCmin} is kept low, however it is preferential to prevent it falling to zero in the high EV growth scenario. To counteract the seasonal changes in PV generation, a modest P_{GCMax} is optimal for high and medium EV growth scenarios.

The GC_{max} value does not make any difference to the overall grid energy for the system, so a wide range is seen. Conversely, the GC_{min} is kept low to prevent solar energy export onto the grid. As the financial model is not considered here, there is no penalty for this.

The ideal design then, for minimising grid energy exchange is to have high solar power and OVES capacity, with no export grid connection. This will inevitably lead to curtailment of solar generation power which would otherwise have been financially unfavourable. The increased availability of locally generated electrical energy though, makes this worthwhile for reducing exchanged grid energy.

Table 5.7 shows that there is a substantial penalty in terms of grid energy exchange to take the most profitable solution for each scenario. In particular, the negative grid connection cost leads to very high levels of energy exchanged with the grid. Reduced levels are seen when the price of the grid connection increases.

5.5 Global sensitivity analysis

Sensitivity analysis was used in this section to ascertain which elements of the design of the HREVC have the most effect on the two design drivers studied in this chapter:

TABLE 5.7: Cumulative absolute sum of grid Energy for maximum profit system designs.

EV Scenario	Grid Price (£ kVA year)	Grid Energy (MWh)
Low	-1.89	1,751,800
	16.03	7,238
	94.97	4,474
Medium	-1.89	1,726,800
	16.03	27,007
	94.97	22,158
High	-1.89	1,714,500
	16.03	9,767
	94.97	47,653

Profit and grid exchange energy.

The SAFE toolbox (discussed in Section 2.8.3) was used in this work. Within the SAFE toolbox, the Morris Method was selected to estimate the elementary effects associated with each variable. This allowed for rapid ranking of the sensitivities to variables with a relatively small number of model iterations. This is a key consideration as the HREVC model is computationally expensive. The many iterations associated with variance based methods would have led to excessive computational time.

For these analyses, the EV demand pattern is kept constant. Clearly this has a large effect on both the profitability and the energy exchanged with the grid, it is not however, a design variable and therefore cannot be controlled. The simulation time period used for this was one year.

5.5.1 Profitability sensitivity analysis

As the Morris Method is useful for ranking the sensitivity for each variable, it can be seen that the profit of the HREVC has sensitivity to the design variables in the following order, from most to least sensitive:

1. No. Charge Stations
2. Solar Farm Capacity
3. OVES capacity
4. Grid charge minimum

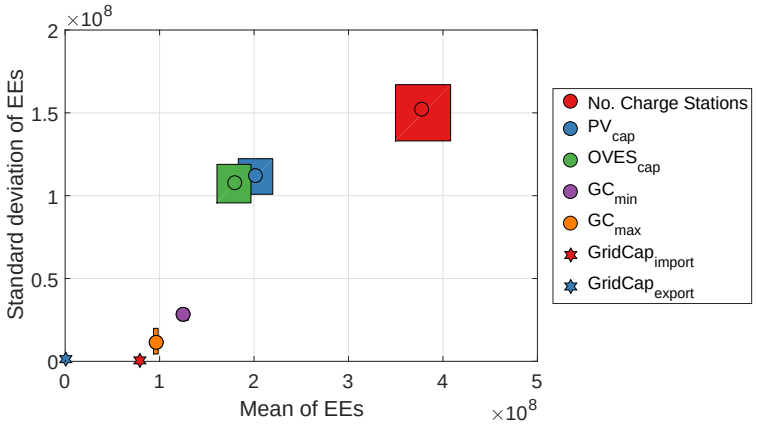

FIGURE 5.6: Elementary effect means plotted against standard deviation for the HREVC profit. The circle represents the final achieved value, with the box representing the standard differentiation of the elementary effect over all generations.

5. Grid charge maximum

6. Grid import connection capacity

7. Grid export connection capacity

As the plot in Figure 5.6 is on a linear scale is clear that the profit is sensitive to all the variables with the exception of the grid export connection capacity. Equally, the sensitivity to the number of charging points is roughly double that of the PV farm capacity and OVES capacity, which in turn are roughly double that of the remaining variables.

5.5.2 Grid interchange energy sensitivity analysis

The elementary effects of the design variables with respect to the grid interchange energy have the same order as the profit elementary effects, however they are distributed over a much larger range. To show this, Figure 5.7 uses a log scale. This has the implication that the grid interchange energy is dependent on the three variables: No. Charge Stations, PV farm capacity and OVES capacity to a much greater degree than the others.

The scatter plots in Figure 5.8 show how the PV farm capacity has a dramatic effect on the sum of the grid interchange energy - there is a direct connection between the two. It is possible, however, to have a large solar farm and low grid interchange energy levels, through effective system design. The other marked connection visible on the scatter plot is the effect of the export grid connection capacity. Reduction of this

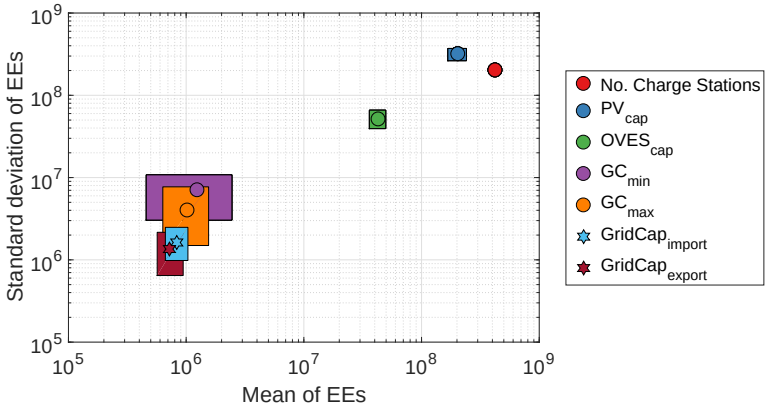

FIGURE 5.7: Elementary effect means plotted against standard deviation for the HREVC grid interchange energy. The circle represents the final achieved value, with the box representing the standard differentiation of the elementary effect over all generations.

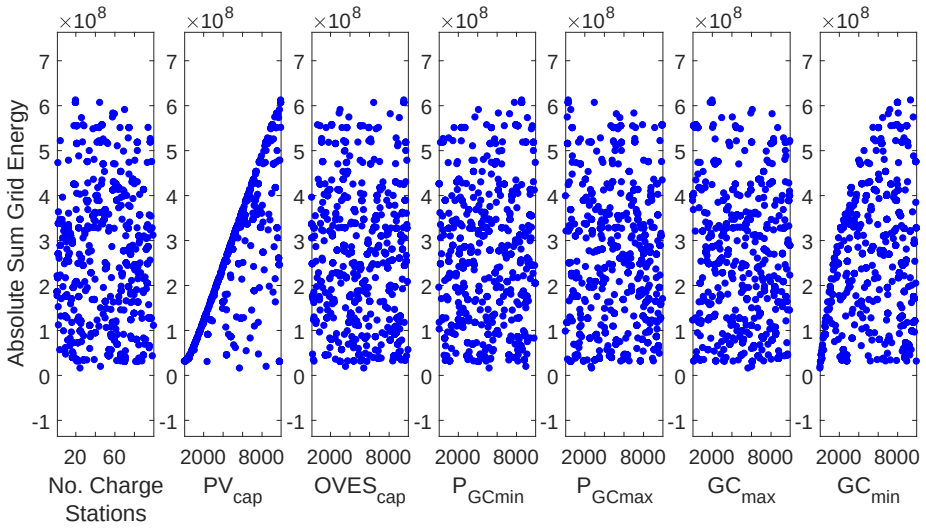

FIGURE 5.8: Scatter plots of absolute sum of grid interchange energy for each design variable of the HREVC.

variable leads to curtailment of the solar farm electricity generation and therefore a substantial reduction in the energy exchanged with the grid. This is not seen for the import grid connection capacity, as restriction of this variable leads only to lower power levels for system imports, not a reduction in the overall amount of energy.

5.6 Discussion

The aim of this work was to discover how the characteristics of the design of HREVCs effect its profitability and the use of the grid connection.

The solutions presented in this chapter are optimal solutions for a specific geographical location (M25 J15-16). The results are thought to be representative of other locations in terms of the general trends, however, the specific numerical results are not transferable.

This work shows that when the grid connection is expensive and the EV demand is high, then there is a key economical driver for the inclusion of renewable energy and an OVES. However, for minimal use of the grid connection a very large OVES and PV farm should be installed. Clearly, these two options are distinct and cannot both be achieved at the same time. However, a modest increase in the size of the PV farm and OVES above that suggested by the financially optimal solution will result in a reduction in grid connection usage. This is at the expense of a higher level of solar energy curtailment, with the benefit of more availability of cheap renewable energy for charging EVs. Therefore, when installing in the real world, it may be beneficial to use a hybrid solution which is a mix of the two solutions presented here.

The system proposed in this work sees most benefit where the grid connection price is high. Enabling solar power installation in these locations is valuable for system wide carbon benefits as these would not be able to take place. Therefore, this system promotes increased renewable energy installations and usage of low carbon energy for transport.

A caveat must be placed on the specific numerical results presented here. The relatively wide range specified for stopping criteria means that, for variables with minimal effect on the output, a range of values could be possible for the same solution. The algorithm must choose one of these values to present as the solution. This is done randomly (the first value being used when the stopping criteria is met) therefore, some unimportant design variables specific results may be subject to error.

A key result of the sensitivity analysis is that both scenarios studied produced the same sensitivity ranking in input variables. When designing an HREVC whether for maximum profit or minimum grid impact, there is a clear ranking of importance of the design variables highlighted by this process.

The sensitivity measure is weighted by the change in value of the input variable, therefore no. of charge points is potentially over represented as a small change in the input

range is smaller for this variable. However, there clearly is a large difference in the operation of the HREVC when going from 1 charge point to 2. The PV_{cap} and $OVES_{cap}$ values, on the other hand, need to change substantially to have a distinguishable change on the output. This means that a higher importance should be given to accurately selecting the no. of charge points, as suggested by the sensitivity analysis.

5.7 Conclusions

The key findings from the work in this chapter are as follows:

- Inclusion of an OVES and solar farm is not beneficial for HREVC profit other than with a high grid connection price where the EV growth scenario is either medium or high.
- The financial benefit arising from the inclusion of an OVES compares favourably with other business cases where energy storage has been installed in the UK. (0.5-3 £m /MWh / year for an HREVC compared to 50 - 200 £k /MWh / year for other revenue streams).
- Optimisation for minimum use of the grid connection leads to a higher OVES and PV farm capacity (independent of the EV growth scenario) when compared to the optimisation for financial gain.
- The number of charging points is the most important variable to correctly specify, followed by PV_{cap} and $OVES_{cap}$, then the grid charge levels and the import and export grid connection capacities. This holds for both designing for profit and minimum grid connection.
- Enabling renewable energy integration where grid cost is high is valuable as these would not otherwise take place.

Chapter 6

Location of energy storage on the low voltage network

A recent concern within the UK has been electric network issues (voltage violations and thermal overload) caused by domestic solar power, creating a demand for energy storage in two areas. Firstly, a homeowner with installed photovoltaic (PV) panels may want to reduce their reliance on supply from the grid and become self-sufficient. In this way the cost of their electricity consumption can be minimised as well as reducing the homeowner's environmental impact. An energy store must be employed to enable this since a typical domestic electrical demand does not match well with solar power generation patterns [223]. Secondly, clustering of PV installations through community organisational effects and passive peer influence [224] leads to a high level of pressure on the grid infrastructure. This, without intervention, can lead to power flows and voltages straying from regulated limits [225]. As such, increased utilisation of energy storage in the distribution system could prevent or defer costly network upgrades needed due to these effects.

In this chapter the effect of the connection location of the energy store is addressed in terms of its influence on the capability of the energy store to combat the network issues of voltage violation (background in Section 2.3.1) and thermal overload (background in Section 2.3.2). To achieve this, two locations are compared: energy storage located on the feeder system, and energy storage located with homes.

6.0.1 Novel contributions

Key novel contributions arising from this chapter are highlighted below:

1. Direct comparison between domestic and feeder connected batteries within the same system and responding to the same load patterns. Section 6.1.
2. Conclusions showing the lower levels of grid stability improvement available from domestic batteries when compared to feeder connected batteries.
    - Domestic batteries exhibit lower peak load export reduction, particularly in periods of high solar irradiance, evidenced in both the specific case in Figure 6.8 compared to Figure 6.12, and the general case between Figures 6.17 and 6.18.
    - Domestic batteries lead to higher energy exports from feeder systems. Figure 6.16.

These novel contributions have been independently peer reviewed in the journal paper reference [14].

6.1 Modelling methodology

This work utilised two key algorithms developed by the author; a domestic battery dispatch strategy presented in Section 6.1.2 and a feeder battery dispatch strategy presented in Section 6.1.2.1. These strategies can be implemented with differing energy storage capacities, PV capacities and dispatch parameters.

6.1.1 Data and software used

The framework data for this work is a dataset of domestic power demand consisting of 96 homes obtained from the Thames Valley Vision project [226]. The PV data was sourced from the Newquay weather station [227]. In order to match the data from the Thames Valley Vision project to the solar data the same dates are used. The household

demand data received from the Thames Valley Vision Project [226] consisted of half hourly demand data for 220 homes located in London.

The simulation of the effects of energy storage on an LV Network are carried out in Matlab and OpenDSS. The matlab model is used to assess real power flows according to aggregated demand and solar generation. A simple battery model is included in the matlab simulations. OpenDSS [228], an open source distribution network modelling tool, is then used to further investigate this modified demand to study the effects associated with three phase supply and line parameters, such as losses and voltage unbalance.

6.1.2 Domestic battery Dispatch Model

The domestic battery model simulates a battery in a home which also has installed solar panels. Domestic demand power and PV generation power data are needed in order to simulate the system in question.

It is assumed that the owner of a domestic battery will aim to achieve minimal grid import (indeed even full independence from the grid) in order to fully utilise their PV and battery investment and minimise their electricity bill. Hence a simple domestic dispatch model is implemented which ensures this through charge and discharge of the battery at the earliest possible opportunity [229]. This also has the benefit of making the algorithm very simple and easy to implement.

Firstly the governing equation of the algorithm is shown in Equation 6.1:

$$P_{bat} = P_{gen} - P_{dem} \tag{6.1}$$

Where P_{bat} is the battery power (positive for charge, negative for discharge), P_{gen} is the generated power from the PV array and P_{dem} is the demand power for the household. All power values are in watts (W). Therefore, the default scenario is that the energy store acts as a buffer between the demand and supply, absorbing excess solar power when required and providing energy to supply the demand when the PV array is incapable of producing the required power. However, this is subject to the constraint of battery capacity as defined in Equation 6.2:

$$0 <= \sum_{0}^{t} P_{bat} dt <= E_{bat} \tag{6.2}$$

Where E_{bat} is the usable battery capacity (10-90% SOC) (kWh) and dt is the computational timestep. In the cases where the system is constrained by Equation 6.2, i.e. the battery is fully charged or fully discharged then the grid must supply the difference between the PV generation power and the domestic demand, Equation 6.3:

$$P_{grid} = P_{gen} - P_{dem} \tag{6.3}$$

Where P_{grid} is the power exchanged with the grid connection.

The matlab code used for the domestic battery dispatch model is shown below. The inputs to this section of code are the usage power profile data (`UW`) and the generated power data (`GW`). Initially, the battery power is set to the difference between the value of generated power and demand power for each iteration and its SOC is set to zero. If the sum of all the values in the battery matrix lies within the allowable values (greater than totally discharged but less than fully charged) then the exchanged power with the grid is zero (`Grid(i)=0`) and the battery absorbs all the excess power or provides the demand. If the battery is fully charged (`sum(B) >= BS`) then the battery power for that iteration is set to zero (`B(i)=0`) and the power exchanged with the grid is set as the difference between generated power and used power. In the case of a fully discharged battery the same holds. This dispatch strategy is shown and discussed in reference [229].

```
for i=1:length(UW)
% Set default operation of the system to allow charge and discharge of the battery
B(i)=GW(i)-UW(i);
% If battery is within SOC limits
if  (BS*0.1 <= sum(B))&&(sum(B) < BS*0.9 )
Grid(i)=0;
% If battery is fully charged
elseif sum(B) >= BS*0.9
% Set battery power to zero
B(i)=0;
```

```
% Use the grid connection
Grid(i)= GW(i)-UW(i);
% If battery is fully discharged
elseif sum(B)< BS*0.1
% Set battery power to zero
B(i)=0;
% Use the grid connection
Grid(i)= GW(i)-UW(i);
end
end
```

Equally, the algorithm is shown graphically in Figure 6.1.

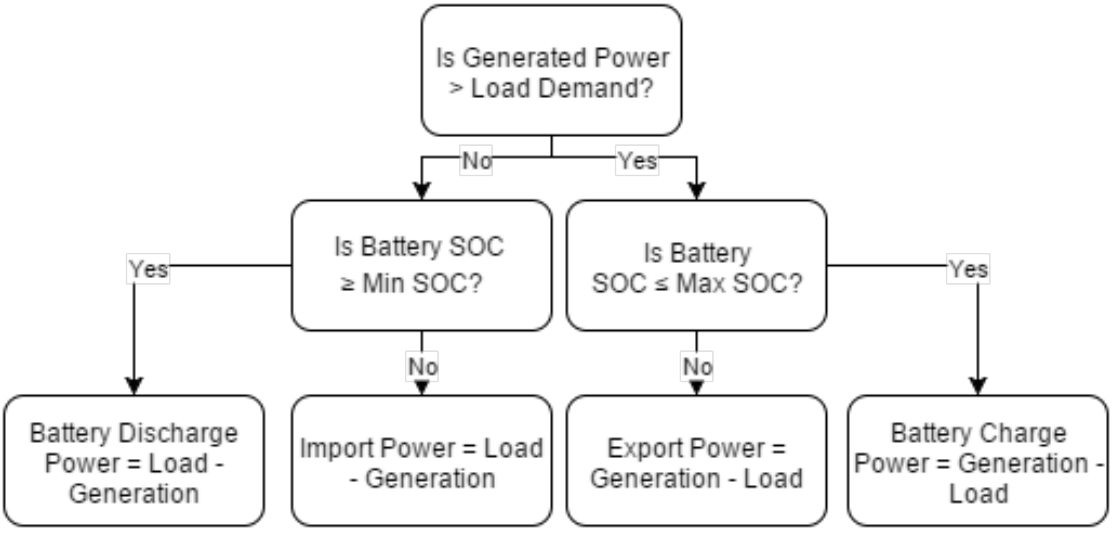

FIGURE 6.1: Dispatch strategy for a domestic battery solely aiming to maximise self-consumption.

6.1.2.1 Feeder connected battery model

The model of a battery connected to the feeder responds to the aggregated load of the sum of each of the domestic dwellings fed by the feeder. In this way it can act to balance the aggregated load.

The first part of this simulation requires the determination of charging and discharging power levels of the aggregated demand, this cannot be set as a single value due to the seasonal changes in feeder demand and solar power generation.

To achieve this, both the moving average (MA) (kW) and moving standard deviation (MSTD) are calculated for the demand over the preceding 24 hours, and dispatch in either charge or discharge mode is controlled with Equation 6.4:

$$Dispatch = MA \pm (MSTD \times n) \tag{6.4}$$

n is the dispatch factor (in per unit standard deviation). A high dispatch factor will lead to lower utilisation of the battery and higher exports but increased likelihood of peak reduction. The dispatch factor should be optimised for the load shape in order to achieve full charge or discharge without feeder power levels straying above or below $MA \pm MSTD \times n$. The feeder connected battery provides the power difference between the charge/discharge level and the feeder power demand given it can do so without exceeding SOC limits. The available power from the battery is assumed to be infinite, however, the dispatch factor is set such that this power does not exceed what a similar capacity Lithium-Ion battery would be capable of (i.e. approximately 5C in extreme cases).

6.1.3 OpenDSS Simulation

For a simulation of the effects of the solar power and energy storage on the real and reactive power flows, and voltage levels the IEEE European Low Voltage Test Case, which is available with the OpenDSS package [163], was utilised. This comprises 55 homes, each with a one phase connection in a generic distribution pattern to a 416V/11kV transformer, shown in Figure 6.4. In an OpenDSS model buses are points of electrical connection and lines are modelled as resistive and inductive elements between buses. There are 906 buses and 905 lines in this model giving a realistic representation of a generic LV Network.

The three-phase transformer is rated at 0.8 MVA with resistance and reactance of the windings is equal to 0.4% and 4% respectively.

These are modelled as having constant power factor - set to 0.95pu for non-solar homes, as the homes are users of energy, and 1 for solar homes, as when the homes are exporting, it is through the inverter and therefore no reactive power is generated. A kW load is then used to model the transient effects of the homes.

Lines and buses are defined by their impedances and admittances as shown in Figure 6.2. This data is populated as part of the IEEE European LV Test Case model.

Line definitions

Name	Bus1	Bus2	Phases	Length	Units	LineCode
LINE1	1	2	ABC	1.098	m	4c_70

Line Codes defined by matrix values

Name	nphases	R1	X1	R0	X0	C1	C0	Units
2c_.007	3	3.97	0.099	3.97	0.099	0	0	km
2c_.0225	3	1.257	0.085	1.257	0.085	0	0	km
2c_16	3	1.15	0.088	1.2	0.088	0	0	km

Ohms, Series Impedance form

nF, Nodal Admittance

FIGURE 6.2: An example of the specification of the buses in the IEEE European LV Test Case [163].

These are build into a model of an LV network as shown in Figure 6.3.

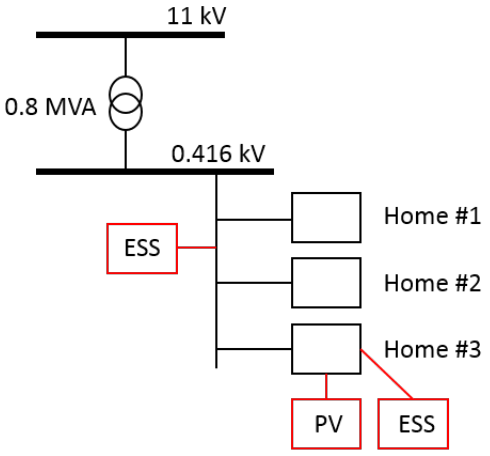

FIGURE 6.3: Schematic diagram of the LV network simulation model. Red parts of the model are simulated for the feeder connected and domestic battery cases.

The actual model used has a higher level of complexity, with the buses set out spatially to reflect a typical European feeder shown in Figure 6.4. Homes in this model are set as loads at the end of each small branch.

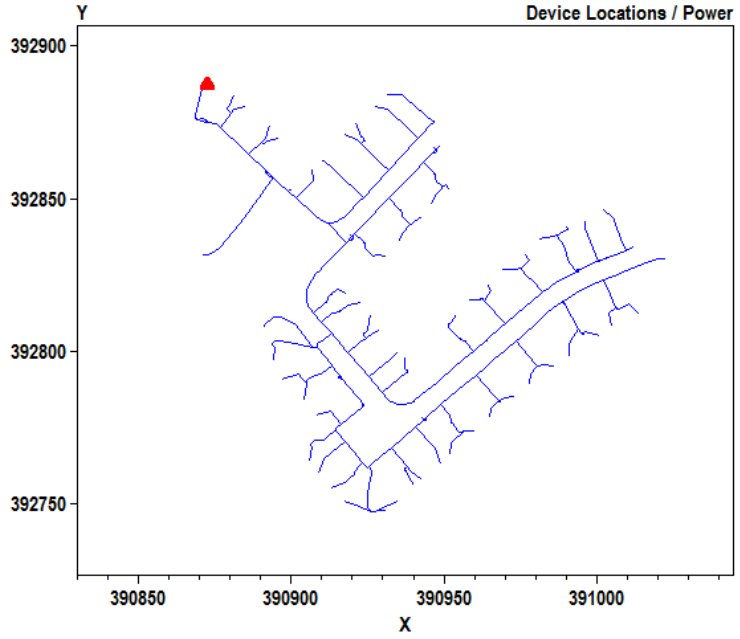

FIGURE 6.4: The topological view of bus orientation in the IEEE European LV Test Case supplied with the OpenDSS package. X and Y axes are length coordinate system with units of meters. The red dot shows the position of the substation.

Data from the Matlab simulation was used to form the load shapes within the OpenDSS model. Three simulations were undertaken as follows:

- 55 homes taken from the Thames Valley Vision data and simulated on the OpenDSS LV Network without the addition of solar power or energy storage.
- 11 homes (20%), from the same 55, randomly assigned with 4kWp solar PV and 7kWh domestic batteries. This data was produced in Matlab following the model shown in Section 6.1.2.
- The same 11 homes (20%) are assigned with 4kWp solar PV, but without batteries. A 77kWh battery is introduced at the substation. The dispatch of the battery is controlled in Matlab as shown in Section 6.1.2.1 and is simply set as a load with positive and negative power flows at 1pu connected to the bus at the substation.

7kWh batteries are chosen for the domestic case as batteries of this size have seen success commercially (Tesla powerwall [48]). For a like for like comparison, the feeder connected battery is given the capacity of the sum of all the domestic batteries.

6.1.4 Limitations and Assumptions

A limitation exists through using existing data and adding energy storage and solar power to the demand profile since the behaviour of the home inhabitants may be changed due to these additions. For example it is common for a homeowner to shift some loads to the day time in order to improve domestic utilisation of solar power. This effect is not expressed here due to the nature of the data.

Only 4kWp solar arrays are studied here. Smaller arrays will lead to a more balanced load profile in the summer where solar panel energy equals load energy rather than exceeding it during summer months. A 4kWp panel was chosen since this size is the most popular due to the tariff structure in the UK [230], however there are many installations with a smaller power capacity.

Since the dispatch factor for the feeder connected battery does not change through the length of the simulation, optimal results are not achieved for feeder connected battery performance. The dispatch factor must be dynamic to respond to changes in load shape for optimal results. This was not the focus of this work and as such static dispatch factors were used. It should be emphasised that, in most cases, the performance of the feeder connected battery will be better than presented here due to this issue.

6.2 Results

The feeder demand “base case” can be seen in Figure **??**. This is the demand on the entire feeder, with the domestic demand profiles from the Thames Valley Vision included for each of the simulated households. The aim of this was to set a standard base case which is representative of many feeder networks across the country.

Figure 6.5 shows the “base case” voltage profile for the feeder system without any embedded solar generation or energy storage. Voltage are shown in red. There is some phase unbalance evident, this is normal and caused by small differences in load patterns between the phases.

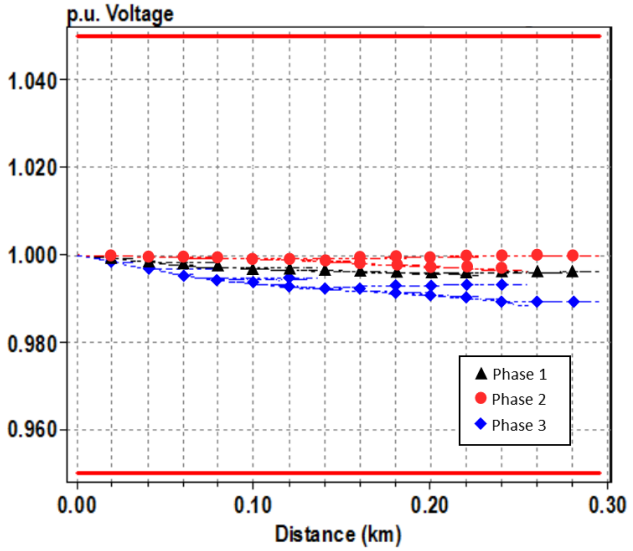

FIGURE 6.5: The three phase per unit voltage plotted against distance from the substation for the feeder. This is the base case voltage profile.

6.2.1 20% PV penetration without storage - Case 1

At 20% PV penetration the peak export power has exceeded the peak demand and as such, unless grid reinforcement has occurred, the likelihood of transformer failure or power line overheating is significantly increased.

Figure 6.6 shows the voltage variation in the feeder system for a period of high solar irradiance where solar panels were operating at very close to maximum power. A 3% voltage rise can be seen at a distance of 300m from the substation on phase 1, with a 1% voltage drop on phase 2. This is due to differing number of PV installations on each phase. A maximum voltage unbalance ratio of 0.577% is observed in this scenario, which is quite low due to the unity power factor of the modelled PV panels. However, as the average feeder length in the UK is 1.5km a higher level of voltage unbalance would be expected for a normal feeder under the same conditions due to the lower overall cable impedance simulated in this example.

The effect of exporting PV panels can be seen in the power flow analysis shown in Figure 6.7 where thicker lines indicate higher power flows. This is a simplified example with only 5 homes with installed solar power to more clearly show their effect in the power flow diagram. The export power can clearly be seen for each of the solar PV installations. It is also clear that too much power is being generated, leading to export

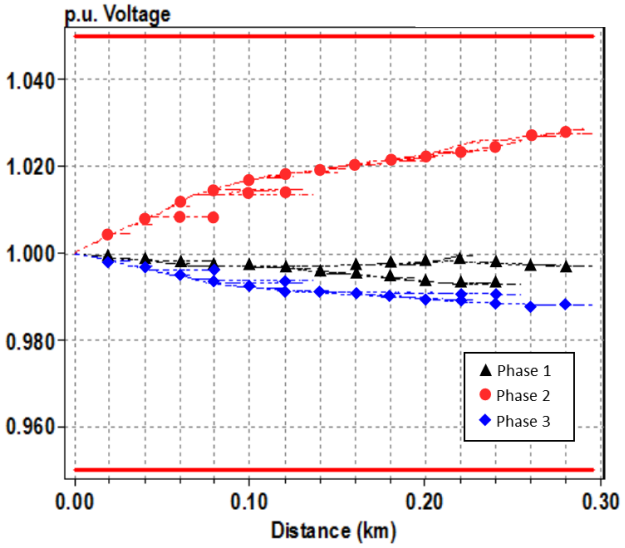

FIGURE 6.6: The three phase per unit voltage plotted against distance from the substation for the feeder with 20% PV penetration and either no storage or a feeder connected battery.

from the feeder system. Clearly there is a role for energy storage within this system with the aim of preventing the export seen here.

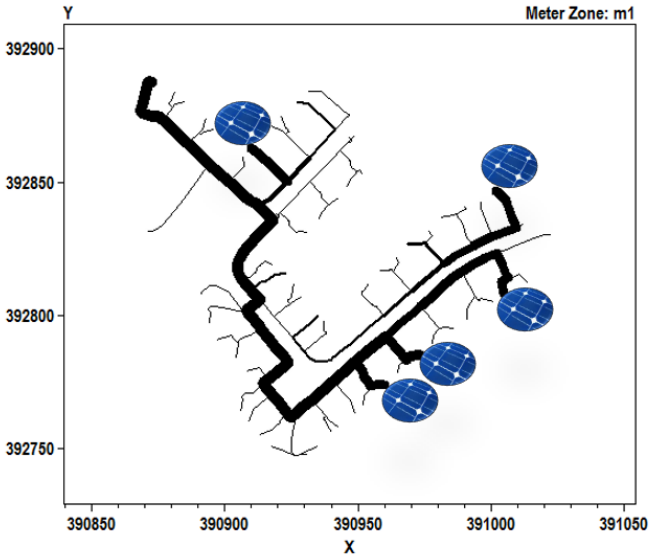

FIGURE 6.7: Feeder without Battery and 5 homes each with 4kWp solar PV.

6.2.2 20% PV Penetration with Domestic Energy Storage - Case 2

In the case of installed domestic batteries, the battery charges whilst the domestic generation exceeds demand and discharges while demand exceeds generation. This dispatch strategy leads to an unpredictable grid connection power profile, where the energy imported or exported depends entirely on the power balance within the home at any moment, regardless of the state of the wider grid at the time.

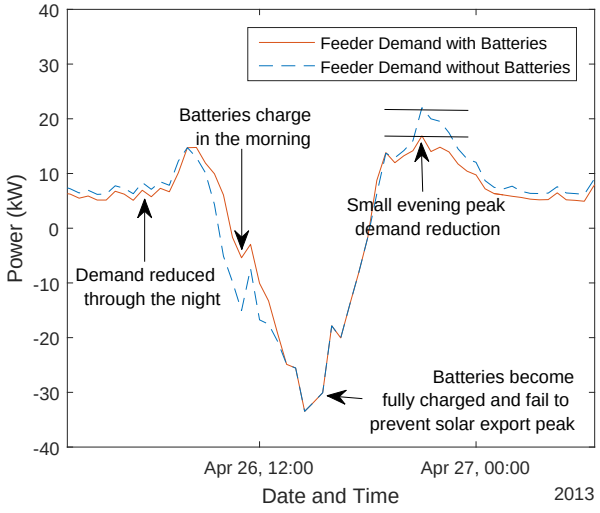

FIGURE 6.8: Typical feeder load profile with 11x7kWh domestic batteries for a day having high solar irradiation levels.

During periods of high solar irradiance the model shows that the domestic battery does not fully discharge between days, this is due to higher levels of electricity generation from the solar panels than the homes' demand. As such, even with very large capacity batteries, the home will need to export solar power at some point in the day when the battery becomes fully charged. Almost no feeder demand peak reduction is therefore enabled by the inclusion of domestic batteries during times when the mean domestic load is lower than the mean solar production over a number of days.

Such domestic batteries can only remove load from the home they are connected to and as such, the percentage of peak load which can be shed is dependent on the PV penetration. This is seen by the modest reduction in peak load in Figure 6.8. In addition, demand reduction occurs through the night, i.e. during very low load conditions.

When solar irradiance levels are low, during winter, the domestic battery utilisation levels fall. It can be shown that low solar irradiance levels lead to a small difference between

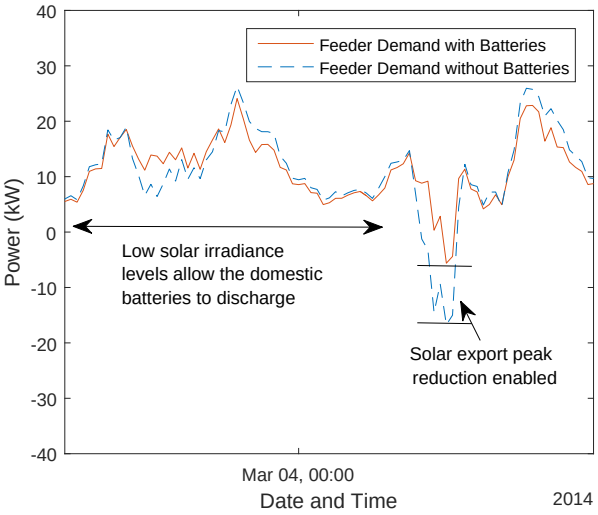

FIGURE 6.9: Typical feeder load profile with 11x7kWh domestic batteries for a day with low solar irradiation levels.

the power profile with and without PV power. As such, there is very little energy available to charge the domestic batteries. Hence, although there is still a high level of energy storage capacity on the feeder system, it cannot be utilised (with this control method) to reduce the high peak powers which occur through the winter. However, since the SOC of the domestic batteries is generally lower during periods of low solar irradiance, the batteries are available to absorb more solar power when it becomes available and as such, the export peaks during periods of low solar irradiance are more effectively reduced. This is shown in Figure 6.9.

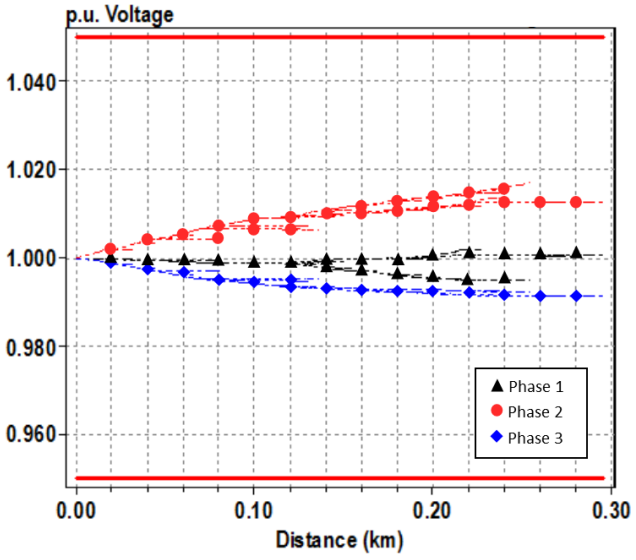

FIGURE 6.10: The three phase per unit voltage plotted against distance from the sub-station for the feeder with 20% PV penetration and 11x7kWh domestic batteries.

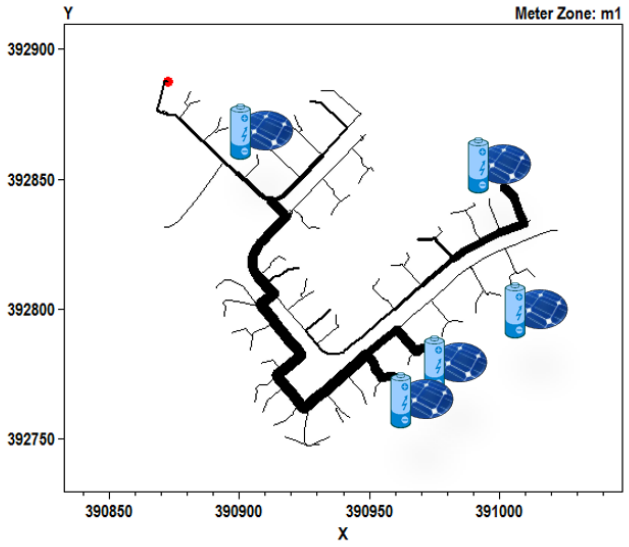

FIGURE 6.11: Line thickness view of power flows on the feeder lines for high solar irradiance levels with Domestic Batteries.

The voltage variation along the feeder system, as shown in Figure 6.10, is more balanced than without the domestic batteries (Figure 6.6) for the instance shown and corresponds to a maximum voltage unbalance of 0.401%. Since the domestic batteries are directly charged by the solar panels they are very effective at mitigating LV network voltage unbalance whilst they are charging. However, as discussed previously, during periods of high solar irradiance, the batteries will become fully charged early in the day. Due to the wide levels of acceptable voltage unbalance (+10%, -6%) on LV networks, voltage balancing effects on these are not of critical importance. Lower losses are seen on the LV network for the domestic battery case due to lower average power flows.

Power flow analysis was carried out on the domestic battery case with 5 solar homes, each with 7kWh domestic batteries. The result is shown in Figure 6.11. When comparing this to Figure 6.7 which shows the same scenario, at the same time step of the simulation, a clear reduction in exported power is observed. Whilst this is clearly positive, 3 of the homes are continuing to export power due to the energy stores in these homes being fully charged and no longer able to absorb the solar PV generation. Much of this generated power is then utilised by other houses on the feeder, however this is a common scenario for the domestic batteries in this simulation.

6.2.3 20% PV penetration with feeder connected storage - Case 3

A feeder connected battery is able to respond directly to the aggregate feeder power flow data. In this way it is able to provide useful services such as valley filling and peak shaving. It can be very effective in doing this due to the relevance of the data available to the feeder energy storage dispatch algorithm; the control strategy can be based on the demand level for the whole feeder at any moment and can therefore target interventions for when they have most impact.

The effectiveness of the feeder connected battery is heavily dependent on charge and discharge levels relative to the moving average of the feeder demand. If the energy store is set to charge at a power level which is too high, the battery will quickly become fully charged and then must allow a large export peak. Conversely if the battery is set to charge at a relatively low feeder demand, it will not be fully utilised and will not fully charge, reducing later peak demand reduction potential.

The choice of charge and discharge levels can be driven by either a desire to minimise exports from the feeder system or to minimise peak feeder demand. For the purposes of this study equal charge and discharge factors were set at the moving average for the past day $\pm$ 0.75 $\times MSTD$ for the past day. For optimal results the shape of the demand profile must be considered such that an equal charge and discharge energy is selected for each day, in this way battery saturation can be prevented.

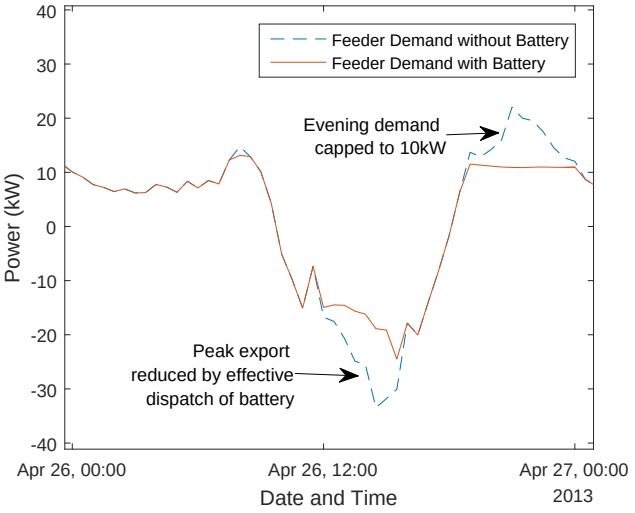

FIGURE 6.12: Typical feeder load profile with a 77kWh feeder connected battery for a day with high solar irradiation levels. Charge command for the battery is at dispatch factor 1.2.

For days of high solar irradiance the feeder battery is able to smooth the peaks of the feeder load and reduce the exports, as shown in Figure 6.12, in this example the peak export power is reduced by 15kW due to the battery. With a PV penetration of 20% the mean power is negative for days of high solar irradiance, i.e. the solar panels are generating more electrical energy than the feeder inhabitants are using. In this case there must be an export of electrical energy unless very high capacity seasonal storage is implemented. As such, the charge level for the battery moves to -15kW, in this way the battery does not become fully charged before the peak export power.

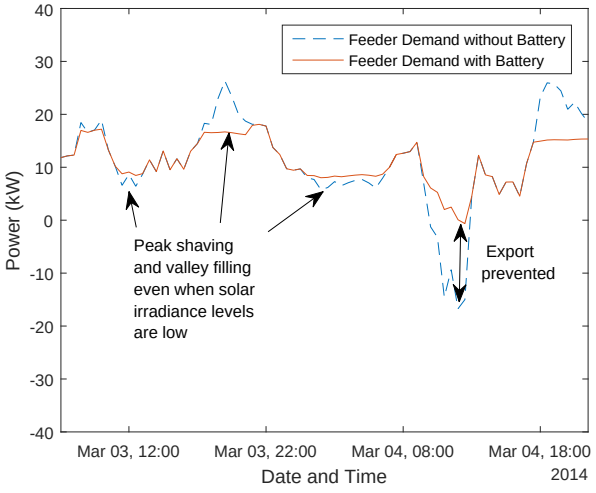

FIGURE 6.13: Typical feeder load profile with 77kWh feeder connected battery for a day low high solar irradiation levels. Charge command for the battery is at dispatch factor 0.75.

When solar irradiance levels are low the feeder connected battery can still act to fill the valleys and shave the peaks. Figure 6.13 shows a preferential feeder demand compared to the domestic battery case since the export was completely prevented and greater reductions were made to the evening demand on both days in this figure. This shows that the dispatch strategy of the feeder connected battery allows for grid services at many states of weather and feeder demand and can reliably reduce the feeder export peak. In contrast, for domestic batteries to be effective with simple dispatch strategies, there must be a low average state of charge and high solar irradiance.

The voltage profile of the feeder system presented from the OpenDSS simulation is shown in Figure 6.14. It is exactly the same for the feeder connected battery as the no storage case since there is no energy storage on the feeder system, as it is located at the substation. There is very little difference between the LV network line losses

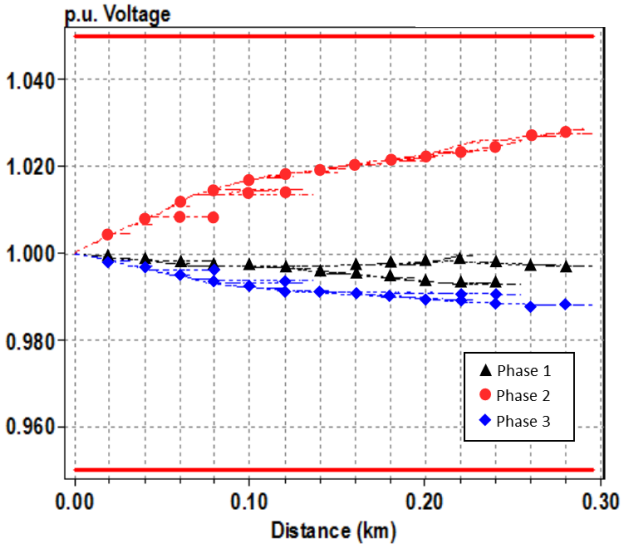

FIGURE 6.14: The three phase per unit voltage plotted against distance from the substation for the feeder with 20% PV penetration and either no storage or a feeder connected battery (subject to it being located at the sub-station).

calculated for the feeder connected battery case and the no storage case, again due to the battery location. If the battery were located centrally within the feeder, the cable length between the battery and the PV panels would be decreased and as such lower losses would be seen.

The power flow for the feeder connected battery case is shown in Figure 6.15. The battery, in this example case, is not connected at the substation in order to show the power

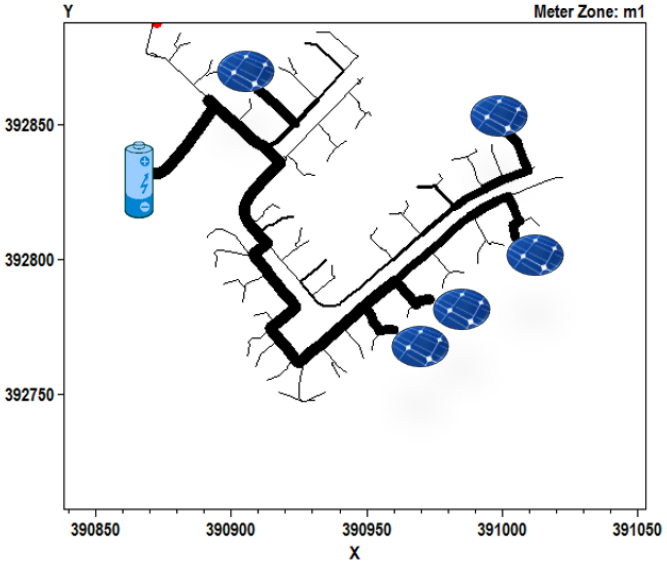

FIGURE 6.15: Line thickness view of power flows on the feeder lines for high solar irradiance levels with Feeder connected battery.

flows to the battery clearly and has a capacity equal to the sum of each of the domestic batteries in case 2 ($5 \times 7kWh = 35kWh$). Each of the homes with installed solar export power in the same way as shown in Figure 6.7, however, the feeder connected battery is able to absorb the excess power and prevent export from the substation.

6.2.4 Export characteristics

For both cases of battery installation, i.e. domestic versus feeder connected, a reduction in the total of the sum of energy exports from the feeder is evident. The reduction in exports is consistently higher for the feeder connected battery case and the benefit of feeder-connected batteries over domestic batteries grows for capacities over 70kWh. This is shown in Figure 6.16 where the sum of all energy exported from the feeder is calculated for a range of battery capacities. In this calculation the domestic batteries continue to be installed in 11 homes, the reduction in energy storage capacity is distributed evenly through the simulated batteries.

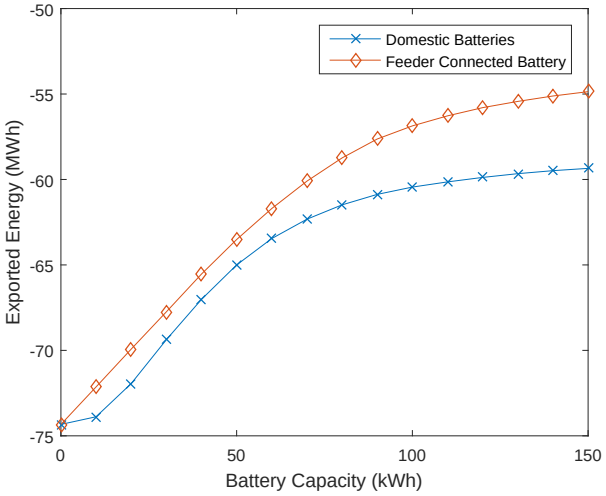

FIGURE 6.16: Export characteristics of domestic and feeder batteries plotted against battery size for the feeder with 20% PV penetration, i.e. 11 x 4kWp PV arrays. Dispatch of the feeder connected battery occurs at dispatch factor 0.75.

The domestic battery case shows a plateau in exports where further increases above a battery capacity of 7kWh per home have a diminished ability to reduce exports. This is largely due to battery saturation, i.e. the home is producing more power than it is using and therefore the battery becomes fully charged and export must occur.

The export characteristics of the feeder-connected battery case are dependent on the charge and discharge levels set for the battery. In order to optimally reduce the peak export power the charge point must be further away from the moving average. However, for optimal export reduction over the course of the year it must be ensured that the full capacity of the battery is utilised for each solar peak. This is best achieved by setting the charge level close to the moving average. However, this leads to a much higher likelihood that the battery will be fully charged before the peak of solar irradiance occurs and as such, peak export reduction capability is reduced. The plateau seen in the exports for the feeder-connected case in Figure 6.16 shows this point, where the charging point of the battery increases in order to ensure effective peak reduction, through control by Equation 6.4, however, the lack of inter-seasonal control due to the static nature of the dispatch factor in this simulation leads to some under-utilisation at high battery capacities. This is a result of the changing shape of the load leading to much a larger export peak than import peaks during the summer due to the high solar power penetration levels. If the dispatch factor was dynamic and changed value effectively to account for this changing load shape, the export reduction would become directly proportional to battery capacity for a feeder connected battery.

For optimal control of the feeder-connected battery, the charging level should be set at the lowest possible power which will fully discharge the battery. Thus, both the export peak and the total exported energy are reduced by the maximum possible amount. These levels change throughout the year due to changing load shapes and as such a dynamic battery control algorithm is needed which is beyond the scope of this work.

Figure 6.17 shows the variation in the mean of the daily moving minimum values for the domestic and feeder-connected battery cases plotted against the battery capacity. A sharp reduction is caused by introducing domestic batteries up to 50kWh ($\approx$4.5kWh per home), but only small further reductions are seen as the battery size increases further. The feeder-connected battery does not reduce the peaks to the same extent as the domestic batteries at low capacities in this simulation. At higher capacities the feeder connected battery becomes much more effective with a 3.5kW reduction in the average peak demand. The charge and discharge levels of the feeder connected battery does not change through this simulation and as such a low-capacity feeder connected battery is not optimised for peak reduction since it will become fully charged or discharged before the peak occurs, as such the battery is under-performing when measured using

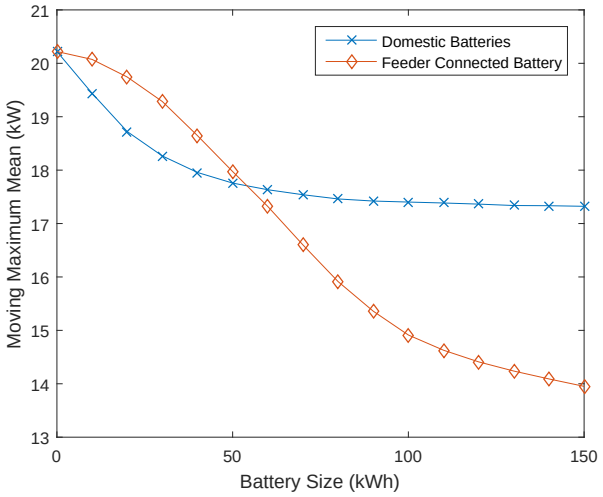

FIGURE 6.17: Moving minimum mean characteristics of domestic and feeder batteries plotted against battery size for the feeder with 20% PV penetration, i.e. 11 x 4kWp PV arrays. Dispatch of the feeder connected battery occurs at dispatch factor 0.75.

this metric. Since the domestic batteries can only mitigate the demand from the home in which they are situated there is an upper limit to demand reduction when the entire demand for that home is met by the combination of solar and batteries. This causes the plateau seen for domestic batteries above 50kWh (4.5kWh x 11 homes) where the peaks from the other homes without solar PV and battery installations drive peak demands.

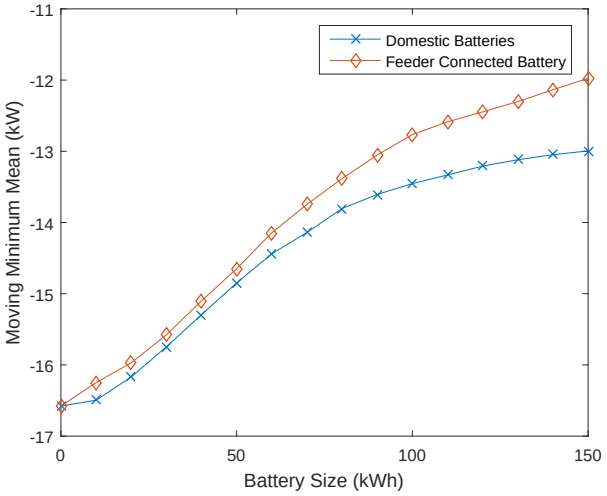

FIGURE 6.18: Moving minimum mean characteristics of domestic and feeder batteries plotted against battery size for the feeder with 20% PV penetration, i.e. 11 x 4kWp PV arrays. Dispatch of the feeder connected battery occurs at dispatch factor 0.75.

The daily moving minimum of the feeder demand for varying battery capacities is shown in Figure 6.18. This clearly shows that in both cases, the addition of energy storage leads

to a decrease of the maximum export power. It can be seen that as the battery size increases for both the domestic and feeder connected cases the moving minimum mean follows an 'S' shape, with most increases coming for battery sizes between 30-100kWh. However, as the size of the batteries increases beyond 100kWh there are diminishing returns in both cases. The feeder connected battery reduces the maximum export power more than the domestic batteries at all points in this simulation. There is no scope for the domestic batteries to further reduce export power if they only react to the domestic load profile. However, the dispatch of the feeder connected battery is not optimal in this case, since the same dispatch parameter was used for the entire simulation. Thus, further reductions could be made to the moving minimum mean of the feeder connected battery case presented here.

6.3 Discussion

6.3.1 Domestic Batteries

The effect of installing a domestic battery paired to a solar panel array can be seen in Figure **??**. The battery charges whilst generation exceeds demand and discharges while demand exceeds generation. This dispatch strategy lead to an unpredictable grid connection power profile. The energy imported or exported depends entirely on the power balance within the home at any moment regardless of the state of the wider grid at the time.

The inclusion of domestic batteries leads to high power transience levels on the feeder system. This is explained by the charging process of the battery; when the battery is not yet fully charged, all the solar power will be utilised in its charging or in meeting the domestic demand. As such, at this point the grid interconnection power levels for the domestic property are zero. When the battery becomes fully charged, the solar power at the time instantly starts being exported to the grid. There is no gradual rise in exportation power as could be seen from the PV panels without an interconnected battery. This process generally takes place in the afternoon, as such the PV generation quickly falls to zero before the peak evening demand. As such the household's energy demand is either "all or nothing" dependent on the SOC of the domestic battery. Overall feeder

demand levels go from minimum to maximum within two-three hours due to this effect. This effect was predicted in reference [229] and was seen throughout the results presented in this chapter.

An issue associated with domestic batteries is that demand reduction can occur through the night, i.e. during very low load conditions. A discharging energy store is adding negligible benefit at these times since the system demand is very low and the infrastructure is under little or no stress. At these times the feeder-connected battery is generally charging. This factor contributes to the poor utilisation of the energy storage capacity introduced with domestic batteries with relation to alleviating distribution system power flow issues due to the none-ideal dispatch times caused by reacting solely to the domestic load.

Additionally, during winter the control algorithm allows only solar charging of domestic batteries. This leads to inherently low charging power levels. Thus, although there is still a high level of energy storage capacity on the feeder system it cannot be utilised to reduce the high peak powers which occur through the winter. The feeder-connected battery, conversely, is still being highly utilised during this period and reductions in the peak load are seen.

6.3.2 Feeder Connected Battery

A feeder connected battery is able to respond directly to feeder power flow data. In this way it is able to provide useful services such as valley filling and peak shaving. It can be very effective at doing this due to the data available to the dispatch algorithm.

There are many factors which affect the benefit of utilising a feeder-connected battery. One such important factor is the duration of the peaks and troughs; a broader peak in the feeder demand requires much more energy to flatten than a narrow one. Thus a feeder-connected battery will be much more effective with narrow peaks. Thankfully, this is promoted with the inclusion of solar PV since there is a shortening of the evening demand peak duration due to PV generation continuing until 17:00-18:00 in the summer months. As such a feeder-connected battery mitigates the transient power flow conditions seen through high PV penetrations levels to a far greater extent than the domestic battery.

The duration of the expected peaks and troughs may be a design driver for the power-capacity ratio for the feeder-connected battery. Wider peaks and troughs require more energy and as such the battery must have a higher energy capacity in order to provide equal peak shaving and valley filling capabilities. However, the power needed to achieve these capabilities remains unchanged, thus the power capacity may also remain unchanged. The width of peaks and troughs is not constant throughout the year, during the winter, even a feeder system with a high PV penetration will not be greatly affected by the PV and as such the evening peak can be much wider.

In contrast to the domestic batteries the feeder-connected battery provides services throughout the year. The dispatch strategy still allows grid services to be carried out. There may be a reduction in the utilisation levels of the battery due to the reduction in PV irradiance leading to fewer opportunities for battery charging. This leads to difficulty in battery sizing since during the winter there are fewer charging opportunities, but higher and wider peaks requiring peak shaving. If the main driver for the battery inclusion is to reduce exportation then these effects can be largely ignored, however, for optimal peak reduction throughout the year, a larger battery than that required purely for prevention of export would be required.

By each of the metrics used to measure effectiveness shown in Section 6.2.4 the feeder-connected battery is preferable with much higher reductions in exportation and reductions in peak loads. However, in this simulation, the battery dispatch occurs when the power level on the feeder goes above or below the daily moving mean plus or minus the daily $MSTD$ multiplied by a factor (n). Thus, the charge and discharge levels are equidistant from the mean. When the battery capacity is very large, it's SOC stays very high since the morning and evening peaks are not enough for a full discharge and as such the export peak is not reduced by a full charge of the battery. An improved algorithm would change the charge-discharge levels dynamically in response to the spread of the feeder power demand - the dispatch factor should be dynamic such that full battery utilisation is enabled i.e. during high solar PV generation the discharge power level should be reduced relative to the charge power level in order to enable a full discharge before the charge cycle. This strategy would maximise battery effectiveness and enable much higher levels of export reduction. This was beyond the scope of this project.

6.4 Conclusions

For the purposes of preventing overload of the substation and keeping feeder power flows within acceptable levels, feeder connected batteries were seen to be superior to domestic batteries. Domestic batteries though, through their dispersed locations on the low voltage feeder led to fewer voltage violations. This effect is only relevant for the low voltage network in question and it is concluded that feeder connected batteries will offer superior support for voltages in the wider network.

As long as domestic generation exceeds supply for a number of days domestic homes will always have to export no matter the capacity of the battery. Feeder connected batteries can effectively prevent exports from the LV network to the MV network.

Feeder connected battery peak shifting is very successful since peaks at this level of the grid are pronounced, easily predicted and easily mitigated. Increased energy storage capacity showed a plateau behaviour for reducing peaks, however, this was due to the simplicity of the dispatch algorithm. Charge and discharge points must be dynamically controlled in order to achieve preferential results. Peak shaving was not as successful with domestic batteries, only the demand of the home with the battery can be removed and load reduction goes through the night, when it is least needed. Domestic batteries can be more effective at valley filling due to the exposure to larger energy flows of the PV array. However, higher levels of energy transience can be seen due to a shift of the minimum demand to later in the day.

Voltage violations on the LV network are more likely with feeder connected batteries. This was seen to depend on the battery connection, however, specific phase control would lead to much improved voltage performance. A mixed effect of the domestic batteries on voltage violation was seen, when the battery is charging the positive effect on the LV network is profound due to complete absorption of the solar energy. However, during the summer months the battery would become fully charged in the afternoon, leaving no protection from voltage violations.

Domestic batteries may be easier to implement, and customers may be more willing to install them than the network operators. As such their effects are likely to become a reality, the only question is at what scale. In this case a hybrid energy storage approach should be implemented with energy storage at both levels.

Chapter 7

Conclusions

This thesis presents a body of work focused on the potential use cases for energy storage in the UK. It is clear this technology will have a role in the future energy landscape and potential installation types have been investigated on low voltage networks and at high rate EV chargers.

In order to understand the effect of location on energy storage installations, domestic and feeder connected batteries were directly compared in Chapter 3. This analysis showed that feeder connected batteries are more capable solutions for preventing voltage violations and feeder overload. This was due to their ability to respond directly to power flows on the network. Domestic batteries always became fully charged for large periods of time, leading to large power flows on the feeder in the summer - due to excessive solar power generation.

To understand the benefits which energy storage may give at high rate electric vehicle chargers (HREVC) a model was developed to predict the demand at these chargers. This model used freely available data from the open street map to estimate travel patterns of EVs. This was then be used with traffic flow patterns for any location on the strategic road network in the UK to give the model locational dependence. A predictive model of future EV battery capacities was also developed by the author to enable a prediction of EV charger power demand. An earlier peak in the EV demand was found, that the literature does not predict, as a tendency for long journeys to begin in the morning was observed. Additionally, approximately 0.5% of EV journeys on the strategic road network, past a HREVC will result in the use of that charger.

It was then found, through combining this predictive demand model with solar power generation patterns that an energy store could be used to balance the supply and demand at the HREVC on the day scale, but not the year scale. This is due to the seasonal changes in solar power generation. Therefore, a grid connection is necessary for these installations.

A model of a HREVC was then produced which includes capabilities for EV queueing, an associated energy store and grid connection capacities. It was found that correct specification of the grid charge power (the power level at which the off vehicle energy store (OVES) charges when there is no solar power) is critical for effective operation of the HREVC. To this end, dynamic (where the grid charge power responds to changes in the average solar generation power) and static (where the grid charge power does not change) algorithms were compared. It was found that the dynamic algorithm led to increased usage of the OVES and therefore reduced overall grid connection usage through higher utilisation of the solar PV.

Two potential use cases for the HREVC with OVES were then addressed: the addition of an EV charger to an existing solar farm, and the addition of a small amount of solar to an existing HREVC. The aim of these studies was to ascertain whether this was possible without additional grid connectivity. It was found that an HREVC with a large solar farm can be taken mostly off grid with a large PV farm and $PV_{cap}/2 < OVES_{cap} < PV_{cap}$ but 10-20% of charging power will be curtailed. For an HREVC with small solar, the OVES is more effective at reducing exports than imports. This leads to a trade-off between import reduction and over-specifying the OVES. In both cases though, the installations could be made without an additional grid connection if the caveats were acceptable.

In the final chapter of this thesis the optimal design of an HREVC was studied. This included optimising for maximum profit and for minimum grid connection usage. Various scenarios were used giving multiple optimal solutions. It was found that the OVES was capable of increasing the profit of the HREVC for installations which had high grid connection costs and medium to high EV growth predictions. In these scenarios the financial benefit arising from the inclusion of an OVES compared favourably with other business cases where energy storage has been installed in the UK. (0.5-3 £m /MWh / year for an HREVC compared to 0.05 - 0.20 £m /MWh / year for other revenue streams). For minimal grid connection usage, large OVES and solar farm capacities were seen in

the optimal results. However, this led to significant curtailment of solar energy. Therefore, it is recommended that designers seek a balance between optimum profit and reduced grid connection usage to facilitate renewable energy powered HREVC proliferation.

7.1 Future Work

The renewable energy and electric vehicle space is evolving rapidly, with many researchers currently working on this subject area. However, to progress the work presented in this thesis, a focus should be made on the following subject areas:

- **Grid connection cost assessment** - The cost of the grid connection is a very hard subject to model as it varies both by power capacity requirement and by geographical location. Further research is needed to more clearly understand these dependencies in order to improve the accuracy of future modelling.
- **Integration of auxiliary services** - With a large battery capacity at the HREVC, there is a possibility to use this to generate alternate income for the HREVC operator through using this battery to perform auxiliary services for the national grid or an aggregator. However, as the OVES would not be usable for the HREVC whilst performing these tasks, an optimisation problem can be formed to balance these two requirements. This would be an interesting problem to solve through further work.

References

[1] Committee on Climate Change. (2016). Uk emissions by sector. Available online at https://www.theccc.org.uk/charts-data/ukemissions-by-sector/.

[2] Department for Environment, Food and Rural Affairs; Department for Transport, "Uk plan for tackling roadside nitrogen dioxide concentrations,"

[3] G. Strbac, M. Aunedi, D. Pudjianto, P. Djapic, F. Teng, A. Sturt, D. Jackravut, R. Sansom, V. Yufit, and N. Brandon, "Strategic assessment of the role and value of energy storage systems in the uk low carbon energy future," *Report for Carbon Trust*, 2012.

[4] L. Bird, M Milligan, and D. Lew, "Integrating variable renewable energy: Challenges and solutions," *National Renewable Energy Laboratory*, 2013.

[5] R. Kemp, P. Blythe, C. Brace, P. James, R. Parry-Jones, D. Thielens, M. Thomas, R. Wenham, and J. Urry, "Electric vehicles: Charged with potential," 2010.

[6] M. Haklay and P. Weber, "Openstreetmap user generated street maps," *Ieee Pervas Comput*, vol. 7, no. 4, pp. 12–18, 2008.

[7] H. Chen, T. N. Cong, W. Yang, C. Tan, Y. Li, and Y. Ding, "Progress in electrical energy storage system: A critical review," *Progress in Natural Science*, vol. 19, no. 3, pp. 291–312, 2009.

[8] National Grid, *Ancillary services national grid uk*, https://www.nationalgrid.com/uk/electricity/balancing-services Last Accessed 20-11-2017.

[9] ——, *Enhanced frequency response national grid uk*. [Online]. Available: https://www.nationalgrid.com/uk/electricity/balancing-services/frequency-response-services/enhanced-frequency-response-efr?overview.

[10] J. Bushnell and K. Novan, “Setting with the sun: The impacts of renewable energy on wholesale power markets,” *Davis Energy Economics Program*, 2018. [Online]. Available: http://deep.ucdavis.edu/uploads/5/6/8/7/56877229/deep_wp020.pdf.

[11] J. Seel, A. D. Mills, and R. H. Wiser, “Impacts of high variable renewable energy futures on wholesale electricity prices, and on electric-sector decision making,” 2018. [Online]. Available: https://emp.lbl.gov/publications/impacts-high-variable-renewable.

[12] P. Bruce, C. Grey, R. Speth, N. Brandon, and R. Bayliss, *Energy storage: Automotive and grids conference report*. [Online]. Available: https://royalsociety.org/~/media/events/2018/01/tof-energy-storage/ToF-Energy-Storage-Conference-Report.pdf?la=en-GB.

[13] B. Irons. (2017). Aurora Battery Conference. Available online at https://www.auroraer.com/wp-content/uploads/2017/11/Aurora-Battery-Conference-31-Oct-2017.pdf.

[14] G. Hilton, A. Cruden, and J. Kent, “Comparative analysis of domestic and feeder connected batteries for low voltage networks with high photovoltaic penetration,” *Journal of Energy Storage*, vol. 13, pp. 334 –343, 2017, ISSN: 2352-152X. DOI: https://doi.org/10.1016/j.est.2017.07.019. [Online]. Available: http://www.sciencedirect.com/science/article/pii/S2352152X17300889.

[15] A. J. Pimm, T. T. Cockerill, and P. G. Taylor, “Time-of-use and time-of-export tariffs for home batteries: Effects on low voltage distribution networks,” *Journal of Energy Storage*, vol. 18, pp. 447–458, 2018.

[16] H. Ding, Z. Hu, and Y. Song, “Value of the energy storage system in an electric bus fast charging station,” *Applied Energy*, vol. 157, pp. 630–639, 2015.

[17] A. S. Hassan, L. Cipcigan, and N. Jenkins, “Optimal battery storage operation for pv systems with tariff incentives,” *Applied Energy*, vol. 203, pp. 422–441, 2017.

[18] *A good practice guide on electrical energy storage*, 2014. [Online]. Available: https://www.eatechnology.com/engineering-projects/electrical-energy-storage/.

[19] G. Huff, "Doe global energy storage database.," Sandia National Laboratories (SNL-NM), Albuquerque, NM (United States), Tech. Rep., 2015. [Online]. Available: http://www.energystorageexchange.org/.

[20] B. Dunn, H. Kamath, and J.-M. Tarascon, "Electrical energy storage for the grid: A battery of choices," *Science*, vol. 334, no. 6058, pp. 928–935, 2011.

[21] N. Nitta, F. Wu, J. T. Lee, and G. Yushin, "Li-ion battery materials: Present and future," *Materials today*, vol. 18, no. 5, pp. 252–264, 2015.

[22] *Our guide to batteries*. [Online]. Available: http://www.jmbatterysystems.com/JMBS/media/JMBS/Documents/JMBS-23946-Battery-Guide-Update-August-2015-Web.pdf.

[23] F. Leng, C. M. Tan, and M. Pecht, "Effect of temperature on the aging rate of li ion battery operating above room temperature," *Scientific reports*, vol. 5, p. 12 967, 2015.

[24] S. Ahn, H.-M. Lee, S.-J. Lee, Y. Park, C.-H. Ku, J. Y. Kim, J.-H. Lee, S. K. Kim, and J. Y. Cho, "The impact of cell geometries and battery designs on safety and performance of lithium ion polymer batteries," in *Electrochemical Society*, 2001.

[25] S. Schindler and M. A. Danzer, "Influence of cell design on impedance characteristics of cylindrical lithium-ion cells: A model-based assessment from electrode to cell level," *Journal of Energy Storage*, vol. 12, pp. 157–166, 2017.

[26] R. E. Ciez and J. Whitacre, "Comparison between cylindrical and prismatic lithium-ion cell costs using a process based cost model," *Journal of Power Sources*, vol. 340, pp. 273 –281, 2017, ISSN: 0378-7753. DOI: https://doi.org/10.1016/j.jpowsour.2016.11.054. [Online]. Available: http://www.sciencedirect.com/science/article/pii/S0378775316315981.

[27] H. Luo, Y. Xia, and Q. Zhou, "Mechanical damage in a lithium-ion pouch cell under indentation loads," *Journal of Power Sources*, vol. 357, pp. 61–70, 2017.

[28] H. C. Hesse, M. Schimpe, D. Kucevic, and A. Jossen, "Lithium-ion battery storage for the grid review of stationary battery storage system design tailored for applications in modern power grids," *Energies*, vol. 10, no. 12, p. 2107, 2017.

[29] J. T. Warner, *The handbook of lithium-ion battery pack design: Chemistry, components, types and terminology*. Elsevier, 2015.

[30] S. Al Hallaj, H. Maleki, J.-S. Hong, and J. R. Selman, "Thermal modeling and design considerations of lithium-ion batteries," *Journal of Power Sources*, vol. 83, no. 1-2, pp. 1–8, 1999.

[31] G. J. Offer, V. Yufit, D. A. Howey, B. Wu, and N. P. Brandon, "Module design and fault diagnosis in electric vehicle batteries," *Journal of Power Sources*, vol. 206, pp. 383–392, 2012.

[32] B. Nykvist and M. Nilsson, "Rapidly falling costs of battery packs for electric vehicles," *Nature Climate Change*, vol. 5, no. 4, pp. 329–332, 2015.

[33] C. Curry, *Batteries and their impact on the energy sector*. [Online]. Available: `https://bnef.turtl.co/story/neo2018?teaser=true`.

[34] F. Lambert. (2016). Tesla slashes price of the powerpack system by another 10with new generation. Available online at `https://electrek.co/2016/11/14/tesla-powerpack-2-price/`.

[35] M Perrin, H Döring, K Ihmels, A Weiss, E Vogel, and R Wagner, "Extending cycle life of lead-acid batteries: A new separation system allows the application of pressure on the plate group," *Journal of power sources*, vol. 105, no. 2, pp. 114–119, 2002.

[36] R. M. Dell and D. A. J. Rand, *Understanding batteries*. Royal Society of Chemistry, 2001.

[37] C. P. De Leon, A Frías-Ferrer, J. González-García, D. Szánto, and F. C. Walsh, "Redox flow cells for energy conversion," *Journal of Power Sources*, vol. 160, no. 1, pp. 716–732, 2006.

[38] A. Z. Weber, M. M. Mench, J. P. Meyers, P. N. Ross, J. T. Gostick, and Q. Liu, "Redox flow batteries: A review," *Journal of Applied Electrochemistry*, vol. 41, no. 10, p. 1137, 2011.

[39] M. Skyllas-Kazacos, G. Kazacos, G. Poon, and H. Verseema, "Recent advances with unsw vanadium-based redox flow batteries," *International Journal of Energy Research*, vol. 34, no. 2, pp. 182–189, 2010.

[40] I. Kougias and S. Szabó, "Pumped hydroelectric storage utilization assessment: Forerunner of renewable energy integration or trojan horse?" *Energy*, vol. 140, pp. 318–329, 2017.

[41] S. Succar and R. Williams, "Compressed air energy storage," *Theory, Resources, and Applications for Wind Power*, 2011.

[42] H. Chen, X. Zhang, J. Liu, and C. Tan, "Compressed air energy storage," in *Energy Storage-Technologies and Applications*, InTech, 2013.

[43] M. Raju and S. K. Khaitan, "Modeling and simulation of compressed air storage in caverns: A case study of the huntorf plant," *Applied Energy*, vol. 89, no. 1, pp. 474–481, 2012.

[44] International Electrotechnical Commission and others, "Iec releases final draft standards for ev charging," *URl: http://www. iec. ch/newslog*, no. 1511, 2011.

[45] CHAdeMO. (2016). Chademo - fast charging stations, [Online]. Available: `http://www.chademo.com/wp/` (visited on 07/03/2016).

[46] Tokyo Electric Power Company. (2010). Press release - establishment of chademo association, [Online]. Available: `http://www.tepco.co.jp/en/press/corp-com/release/10031501-e.html` (visited on 07/03/2016).

[47] *Electric vehicle conductive charging system - part 23: Dc electric vehicle charging station*, International Electrotechnical Commission, 2014. [Online]. Available: `https://webstore.iec.ch/publication/6032`.

[48] Tesla Motors Inc. (2017). Tesla Motors Inc., [Online]. Available: `http://www.teslamotors.com/en` (visited on 08/10/2015). Available online at `http://www.teslamotors.com/en`.

[49] W. W. Tang, Y. M. Wu, and J. Qin, "Comparative study on electric vehicle charging standards at home and abroad," in *Advanced Materials Research*, Trans Tech Publ, vol. 608, 2012, pp. 1553–1559.

[50] *ABB Electric Vehicle Charging Infrastructure - Terra 53 Z*. [Online]. Available: `http://new.abb.com/ev-charging/single-standard/terra-53-z` (visited on 08/03/2016).

[51] *Philong - 2016 EV Chargers*. [Online]. Available: `http://www.phihong.com.tw/newcatalog/2016%20EV%20Chargers%20Catalog_20160107_EN.pdf` (visited on 08/03/2016).

[52] R. C. Cope and Y. Podrazhansky, "The art of battery charging," in *Battery Conference on Applications and Advances, 1999. The Fourteenth Annual*, IEEE, 1999, pp. 233–235.

[53] S. S. Zhang, K. Xu, and T. Jow, "Study of the charging process of a licoo2-based li-ion battery," *Journal of power sources*, vol. 160, no. 2, pp. 1349–1354, 2006.

[54] J. Li, E. Murphy, J. Winnick, and P. A. Kohl, "The effects of pulse charging on cycling characteristics of commercial lithium-ion batteries," *Journal of Power Sources*, vol. 102, no. 1âĂŞ2, pp. 302 –309, 2001, ISSN: 0378-7753. DOI: http://dx.doi.org/10.1016/S0378-7753(01)00820-5. [Online]. Available: http://www.sciencedirect.com/science/article/pii/S0378775301008205.

[55] Ecotricity. (2018). Charging faqs, [Online]. Available: https://www.ecotricity.co.uk/for-the-road/ev-faqs/charging-faqs.

[56] Engenie. (2018). Help with charging, [Online]. Available: http://engenie.co.uk/help-with-charging/.

[57] Genie Point. (2018). Geniepoint pricing, [Online]. Available: https://www.chargepointservices.co.uk/drivers/geniepoint-pricing/.

[58] INSTAVOLT. (2018). Frequently asked questions - how much does it cost? [Online]. Available: https://instavolt.co.uk/driver-faqs/.

[59] Polar. (2018). What a polar plus membership gives you, [Online]. Available: http://polar.chargevision5.com/#info.

[60] Shell Recharge. (2018). Welcome to shell recharge, [Online]. Available: http://polar.chargevision5.com/#info.

[61] N Sujitha and S Krithiga, "Res based ev battery charging system: A review," *Renewable and Sustainable Energy Reviews*, vol. 75, pp. 978–988, 2017.

[62] J. Agenbroad and B. Holland. (2014). What's the true cost of ev charging stations? [Online]. Available: https://www.greenbiz.com/blog/2014/05/07/rmi-whats-true-cost-ev-charging-stations.

[63] C. Dharmakeerthi, N. Mithulananthan, and T. Saha, "Impact of electric vehicle fast charging on power system voltage stability," *International Journal of Electrical Power and Energy Systems*, vol. 57, pp. 241 –249, 2014, ISSN: 0142-0615. DOI: http://dx.doi.org/10.1016/j.ijepes.2013.12.005. [Online]. Available: http://www.sciencedirect.com/science/article/pii/S0142061513005218.

[64] E. Association *et al.*, *Engineering recommendation g81: Framework for design and planning, materials specification, installation and record for greenfield low voltage housing estate underground network installations and associated, new, hv/lv distribution substations*, 2004.

[65] Audi. (2018). Audi e-tron quattro unveiled at frankfurt motor show, [Online]. Available: https://beta.audi.co.uk/electric-car/e-tron.html (visited on 09/01/2018).

[66] Porsche. (2018). Porsche concept study mission e. tribute to tomorrow., [Online]. Available: https://www.porsche.com/microsite/mission-e/international.aspx#/reveal (visited on 09/01/2018).

[67] BMW. (2014). I3 - introduction, [Online]. Available: http://www.bmw.co.uk/en_GB/new-vehicles/bmw-i/i3/2015/introduction.html.

[68] Kia. (2014). All new soul ev, [Online]. Available: http://www.kia.co.uk/new-cars/range/compact-cars/soul-ev.aspx.

[69] Citroen. (2014). Citroen c-zero, [Online]. Available: http://www.citroen.co.uk/new-cars-and-vans/citroen-range/citroen-c-zero.

[70] Mitsubishi. (2014). Mitsubishi i-miev a green, sustainable lifestyle is on the horizon., [Online]. Available: http://www.mitsubishi-cars.co.uk/imiev/.

[71] Peugeot. (2014). Peugeot ion - electric car, [Online]. Available: http://www.peugeot.co.uk/showroom/ion/5-door/.

[72] Jaguar. (2018). New all electric jaguar i-pace. Available online at https://www.jaguar.co.uk/jaguar-range/i-pace/index.html.

[73] Mitsubishi. (2014). The new outlander phev, [Online]. Available: http://www.mitsubishi-cars.co.uk/outlander/.

[74] Nissan. (2013). Nissan leaf - drive further with extended battery range, [Online]. Available: http://www.nissan.co.uk/GB/en/vehicle/electric-vehicles/leaf.html.

[75] ——, (2013). Nissan e-nv200 van - the 100% electric, 100% flexible nissan e-nv200 commercial vehicle, [Online]. Available: http://www.nissan.co.uk/GB/en/vehicle/electric-vehicles/e-nv200.html.

[76] Tesla. (2013). Model s, [Online]. Available: https://www.teslamotors.com/en_GB/models.

[77] ——, (2015). Model x, [Online]. Available: https://www.teslamotors.com/en_GB/modelx.

[78] Volkswagen. (2015). E-up! the future is electric, [Online]. Available: http://www.volkswagen.co.uk/new/e-up-nf/home.

[79] ——, (2015). E-golf! the classic is now electric, [Online]. Available: http://www.volkswagen.co.uk/new/e-golf-vii/home.

[80] T Trigg, P Telleen, R Boyd, and F Cuenot, "Global EV Outlook: Understanding the Electric Vehicle Landscape to 2020," *Iea*, no. April, pp. 1–41, 2013. [Online]. Available: http://www.iea.org/publications/freepublications/publication/name-37024-en.html$\backslash$nhttp://scholar.google.com/scholar?hl=en{\&}btnG=Search{\&}q=intitle:Global+EV+Outlook:+Understanding+the+Electric+Vehicle+Landscape+to+2020{\#}0.

[81] S. Carley, R. M. Krause, B. W. Lane, and J. D. Graham, "Intent to purchase a plug-in electric vehicle: A survey of early impressions in large {us} cites," *Transportation Research Part D: Transport and Environment*, vol. 18, pp. 39 –45, 2013, ISSN: 1361-9209. DOI: http://dx.doi.org/10.1016/j.trd.2012.09.007. [Online]. Available: http://www.sciencedirect.com/science/article/pii/S136192091200-1095.

[82] Element Energy Limited, "Pathways to high penetration of electric vehicles," The committee on climate change, Tech. Rep., 2013.

[83] C. Morton, G. Schuitema, and J. Anable, "Electric vehicles: Will consumers get charged up," in *Universities Transport Study Group Conference January*, 2011.

[84] R. Hanifah, S. Toha, and S. Ahmad, "Electric vehicle battery modelling and performance comparison in relation to range anxiety," *Procedia Computer Science*, vol. 76, pp. 250 –256, 2015, ISSN: 1877-0509. DOI: http://dx.doi.org/10.1016/j.procs.2015.12.350. [Online]. Available: http://www.sciencedirect.com/science/article/pii/S187705091503851X, 2015 {IEEE} International Symposium on Robotics and Intelligent Sensors (IEEE IRIS2015).

[85] T. Stevens, "Non-cost barriers to consumer adoption of new light-duty vehicle technologies," Tech. Rep., 2013.

[86] S. Speidel and T. Braunl, "Driving and charging patterns of electric vehicles for energy usage," *Renewable and Sustainable Energy Reviews*, vol. 40, pp. 97 –110, 2014, ISSN: 1364-0321. DOI: http://dx.doi.org/10.1016/j.rser.2014.07.177. [Online]. Available: http://www.sciencedirect.com/science/article/pii/S13640321-14006297.

[87] P. Morrissey, P. Weldon, and M. Mahony, "Future standard and fast charging infrastructure planning: An analysis of electric vehicle charging behaviour," *Energy Policy*, vol. 89, pp. 257 –270, 2016, ISSN: 0301-4215. DOI: http://dx.doi.org/10.1016/j.enpol.2015.12.001. [Online]. Available: http://www.sciencedirect.com/science/article/pii/S0301421515302159.

[88] National Statistics, "English housing survey," *Department for Communities and Local Government*, 2010. [Online]. Available: https://www.gov.uk/government/uploads/system/uploads/attachment_data/file/6748/2173483.pdf.

[89] FastNed. (2018). Superfast charging - everywhere along the highway, [Online]. Available: http://fastned.nl/en/.

[90] J. Smart and S. Schey, "Battery electric vehicle driving and charging behavior observed early in the ev project," *SAE Int. J. Altern. Powertrains*, vol. 1, no. 1, pp. 27–33, 2012.

[91] L. Liu, F. Kong, X. Liu, Y. Peng, and Q. Wang, "A review on electric vehicles interacting with renewable energy in smart grid," *Renewable and Sustainable Energy Reviews*, vol. 51, pp. 648 –661, 2015, ISSN: 1364-0321. DOI: http://dx.doi.org/10.1016/j.rser.2015.06.036. [Online]. Available: http://www.sciencedirect.com/science/article/pii/S1364032115006085.

[92] B. Yagcitekin and M. Uzunoglu, "A double-layer smart charging strategy of electric vehicles taking routing and charge scheduling into account," *Applied Energy*, vol. 167, pp. 407 –419, 2016, ISSN: 0306-2619. DOI: http://dx.doi.org/10.1016/j.apenergy.2015.09.040. [Online]. Available: http://www.sciencedirect.com/science/article/pii/S0306261915011101.

[93] F. Mwasilu, J. J. Justo, E.-K. Kim, T. D. Do, and J.-W. Jung, "Electric vehicles and smart grid interaction: A review on vehicle to grid and renewable energy sources integration," *Renewable and Sustainable Energy Reviews*, vol. 34, pp. 501 –516, 2014, ISSN: 1364-0321. DOI: http://dx.doi.org/10.1016/j.rser.2014.03.031.

[Online]. Available: http://www.sciencedirect.com/science/article/pii/S1364032114001920.

[94] A. S. Masoum, S. Deilami, P. S. Moses, and A. Abu-Siada, "Impacts of battery charging rates of plug-in electric vehicle on smart grid distribution systems," in *2010 IEEE PES Innovative Smart Grid Technologies Conference Europe (ISGT Europe)*, 2010, pp. 1–6. DOI: 10.1109/ISGTEUROPE.2010.5638981.

[95] K. Yunus, H. Z.D. L. Parra, and M. Reza, "Distribution grid impact of plug-in electric vehicles charging at fast charging stations using stochastic charging model," in *Power Electronics and Applications (EPE 2011), Proceedings of the 2011-14th European Conference on*, 2011, pp. 1–11.

[96] T. Gonen, *Electric power distribution system engineering, second edition*. Taylor & Francis, 2007, ISBN: 9781420062007. [Online]. Available: https://books.google.co.uk/books?id=vX1bbwAACAAJ.

[97] "Ieee recommended practice and requirements for harmonic control in electric power systems," *IEEE Std 519-2014 (Revision of IEEE Std 519-1992)*, pp. 1–29, 2014. DOI: 10.1109/IEEESTD.2014.6826459.

[98] L. Yanxia and J. Jiuchun, "Harmonic-study of electric vehicle chargers," in *Electrical Machines and Systems, 2005. ICEMS 2005. Proceedings of the Eighth International Conference on*, vol. 3, 2005, 2404–2407 Vol. 3. DOI: 10.1109/ICEMS.2005.203002.

[99] Q. Li, S. Tao, X. Xiao, and J. Wen, "Monitoring and analysis of power quality in electric vehicle charging stations," in *Future Energy Electronics Conference (IFEEC), 2013 1st International*, 2013, pp. 277–282. DOI: 10.1109/IFEEC.2013.6687516.

[100] *Distribution and connection use of system agreement (dcusa)*. 2016, Avaliable Online at https://www.dcusa.co.uk/SitePages/Documents/DCUSA-Document.aspx.

[101] E. Acha, *Power electronic control in electrical systems*, ser. Electronics & Electrical. Newnes, 2002, ISBN: 9780750651264. [Online]. Available: https://books.google.co.uk/books?id=O_T81gC-GzcC.

[102] M. Diez-Mediavilla, M. Dieste-Velasco, M. Rodriguez-Amigo, T. Garcia-Calderon, and C. Alonso-Tristan, "Performance of grid-tied pv facilities based on real data in spain: Central inverter versus string system," *Energy Conversion and Management*, vol. 86, pp. 1128 –1133, 2014, ISSN: 0196-8904. DOI: http://dx.doi.org/10.1016/j.enconman.2014.06.087. [Online]. Available: http://www.sciencedirect.com/science/article/pii/S0196890414006128.

[103] A. M. Pavan, S. Castellan, S. Quaia, S. Roitti, and G. Sulligoi, "Power electronic conditioning systems for industrial photovoltaic fields: Centralized or string inverters?" In *2007 International Conference on Clean Electrical Power*, 2007, pp. 208–214. DOI: 10.1109/ICCEP.2007.384213.

[104] J. J. Bzura, "The ac module: An overview and update on self-contained modular pv systems," in *Power and Energy Society General Meeting, 2010 IEEE*, IEEE, 2010, pp. 1–3.

[105] *Quality of Service Guaranteed Standards - Ofgem*. (visited on 09/02/2015), Available online at https://www.ofgem.gov.uk/licences-codes-and-standards/standards/quality-service-guaranteed-standards.

[106] Energy Network Association, "The Distribution Code of Licensed Distribution Network Operators," no. 25, 2014.

[107] S Conti, S Raiti, and G Tina, "Small-scale embedded generation effect on voltage profile: An analytical method," *IEE Proceedings-Generation, Transmission and Distribution*, vol. 150, no. 1, pp. 78–86, 2003.

[108] J. Schlabbach, "Harmonic current emission of photovoltaic installations under system conditions," in *2008 5th International Conference on the European Electricity Market*, 2008, pp. 1–5. DOI: 10.1109/EEM.2008.4579000.

[109] A. Chidurala, T. K. Saha, N Mithulananthan, and R. C. Bansal, "Harmonic emissions in grid connected pv systems: A case study on a large scale rooftop pv site," in *PES General Meeting| Conference & Exposition, 2014 IEEE*, IEEE, 2014, pp. 1–5.

[110] F. Shahnia, R. Majumder, A. Ghosh, G. Ledwich, and F. Zare, "Voltage imbalance analysis in residential low voltage distribution networks with rooftop pvs," *Electric Power Systems Research*, vol. 81, no. 9, pp. 1805 –1814, 2011, ISSN: 0378-7796.

DOI: http://dx.doi.org/10.1016/j.epsr.2011.05.001. [Online]. Available: http://www.sciencedirect.com/science/article/pii/S0378779611001040.

[111] The Electricity Council, "Planning limits for voltage unbalance in the united kingdom," *Engineering Reccomendation P29*, 1990.

[112] K. Lee, G. Venkataramanan, and T. M. Jahns, "Source current harmonic analysis of adjustable speed drives under input voltage unbalance and sag conditions," *IEEE Transactions on Power Delivery*, vol. 21, no. 2, pp. 567–576, 2006, ISSN: 08858977. DOI: 10.1109/TPWRD.2006.871022.

[113] I. Metwally, "Failures, monitoring and new trends of power transformers," *Potentials, IEEE*, vol. 30, no. 3, pp. 36–43, 2011, ISSN: 0278-6648. DOI: 10.1109/MPOT.2011.940233.

[114] R. Murugan and R. Ramasamy, "Failure analysis of power transformer for effective maintenance planning in electric utilities," *Engineering Failure Analysis*, vol. 55, pp. 182 –192, 2015, ISSN: 1350-6307. DOI: http://dx.doi.org/10.1016/j.engfailanal.2015.06.002. [Online]. Available: http://www.sciencedirect.com/science/article/pii/S1350630715001843.

[115] P. Trichakis, P. Taylor, P. Lyons, and R. Hair, "Predicting the technical impacts of high levels of small-scale embedded generators on low-voltage networks," *Renewable Power Generation, IET*, vol. 2, no. 4, pp. 249–262, 2008, ISSN: 1752-1416. DOI: 10.1049/iet-rpg:20080012.

[116] J. Keller, B. Kroposki, R. Bravo, and S. Robles, "Fault current contribution from single-phase pv inverters," in *Photovoltaic Specialists Conference (PVSC), 2011 37th IEEE*, IEEE, 2011, pp. 001 822–001 826.

[117] Scottish and Southern Electricity Power Distribution. (2016). Generation availability map. Available online at https://www.ssepd.co.uk/GenerationAvailabilityMap/?mapareaid=1.

[118] S. Mallett. (2016). Renewable energy map. Available online at http://www.renewables-map.co.uk/Solar.asp?Status=1&mycompid=0.

[119] Western Power Distribution. (2018). Distributed generation ehv constraint maps. Available online at https://www.westernpower.co.uk/connections/generation/distributed-generation-ehv-constraint-maps.aspx.

[120] ——, (2016). Wpd south west 132kv network capacity restriction update march 2016. Available online at `http://www.westernpower.co.uk/docs/connections/Generation/Generation-capacity-map/Distributed-Generation-EHV-Constraint-Maps/WPD-South-West-F-Route-Constraint-Information-Marc.aspx`.

[121] D. P. Birnie III, "Solar-to-vehicle (s2v) systems for powering commuters of the future," *Journal of Power Sources*, vol. 186, no. 2, pp. 539–542, 2009.

[122] H.-M. Neumann, D. Schär, and F. Baumgartner, "The potential of photovoltaic carports to cover the energy demand of road passenger transport," *Progress in Photovoltaics: Research and Applications*, vol. 20, no. 6, pp. 639–649, 2012.

[123] P. J. Tulpule, V. Marano, S. Yurkovich, and G. Rizzoni, "Economic and environmental impacts of a pv powered workplace parking garage charging station," *Applied Energy*, vol. 108, pp. 323–332, 2013.

[124] P. Nunes, T. Farias, and M. C. Brito, "Day charging electric vehicles with excess solar electricity for a sustainable energy system," *Energy*, vol. 80, pp. 263–274, 2015.

[125] ——, "Enabling solar electricity with electric vehicles smart charging," *Energy*, vol. 87, pp. 10–20, 2015.

[126] M. ElNozahy and M. Salama, "Studying the feasibility of charging plug-in hybrid electric vehicles using photovoltaic electricity in residential distribution systems," *Electric Power Systems Research*, vol. 110, pp. 133–143, 2014.

[127] N. S. Pearre and L. G. Swan, "Electric vehicle charging to support renewable energy integration in a capacity constrained electricity grid," *Energy Conversion and Management*, vol. 109, pp. 130–139, 2016.

[128] K. E. Forrest, B. Tarroja, L. Zhang, B. Shaffer, and S. Samuelsen, "Charging a renewable future: The impact of electric vehicle charging intelligence on energy storage requirements to meet renewable portfolio standards," *Journal of Power Sources*, vol. 336, pp. 63–74, 2016.

[129] M. S. Alam, "Conceptual framework of a solar pv based high voltage battery charging strategyfor phevs and evs," *American Journal of Electrical Power and Energy Systems*, vol. 2, no. 6, pp. 137–143, 2013.

[130] D. Sbordone, I Bertini, B Di Pietra, M. Falvo, A Genovese, and L Martirano, "Ev fast charging stations and energy storage technologies: A real implementation in the smart micro grid paradigm," *Electric Power Systems Research*, vol. 120, pp. 96–108, 2015.

[131] C. Capasso, D. Iannuzzi, and O. Veneri, "Dc charging station for electric and plug-in vehicles," *Energy Procedia*, vol. 61, pp. 1126–1129, 2014.

[132] C. Capasso, S. Riviera, S. Kouro, and O. Veneri, "Charging architectures integrated with distributed energy resources for sustainable mobility," *Energy Procedia*, vol. 105, pp. 2317–2322, 2017.

[133] J. P. Torreglosa, P. García-Triviño, L. M. Fernández-Ramirez, and F. Jurado, "Decentralized energy management strategy based on predictive controllers for a medium voltage direct current photovoltaic electric vehicle charging station," *Energy Conversion and Management*, vol. 108, pp. 1–13, 2016.

[134] J. Ugirumurera and Z. J. Haas, "Optimal capacity sizing for completely green charging systems for electric vehicles," *IEEE Transactions on Transportation Electrification*, vol. 3, no. 3, pp. 565–577, 2017.

[135] M. O. Badawy and Y. Sozer, "Power flow management of a grid tied pv-battery system for electric vehicles charging," *IEEE Transactions on Industry Applications*, vol. 53, no. 2, pp. 1347–1357, 2017.

[136] E. Beimborn and R. Kennedy, "Inside the blackbox: Making transportation models work for livable communities," 1996.

[137] R. Abousleiman and R. Scholer, "Smart charging: System design and implementation for interaction between plug-in electric vehicles and the power grid," *IEEE Transactions on Transportation Electrification*, vol. 1, no. 1, pp. 18–25, 2015.

[138] Y.-T. Liao and C.-N. Lu, "Dispatch of ev charging station energy resources for sustainable mobility," *IEEE Transactions on Transportation Electrification*, vol. 1, no. 1, pp. 86–93, 2015.

[139] C. Le Floch, F. Belletti, and S. Moura, "Optimal charging of electric vehicles for load shaping: A dual-splitting framework with explicit convergence bounds," *IEEE Transactions on Transportation Electrification*, vol. 2, no. 2, pp. 190–199, 2016.

[140] Y. Ma, T. Houghton, A. Cruden, and D. Infield, "Modeling the benefits of vehicle-to-grid technology to a power system," *Power Systems, IEEE Transactions on*, vol. 27, no. 2, pp. 1012–1020, 2012.

[141] Department for Transport. (2016). National travel survey. Available online at `https://www.gov.uk/government/statistics/national-travel-survey-2016`.

[142] H Höimoja, M. Vasiladiotis, and A. Rufer, "Power interfaces and storage selection for an ultrafast ev charging station," in *Power Electronics, Machines and Drives (PEMD 2012), 6th IET International Conference on*, IET, 2012, pp. 1–6.

[143] M Tsirinomeny, H Hõimoja, A Rufer, G Dziechciaruk, and A Vezzini, "Optimizing ev driving-recharge time ratio a under limited grid connection," in *Power Electronics, Machines and Drives (PEMD 2014), 7th IET International Conference on*, IET, 2014, pp. 1–6.

[144] G. Mauri and A. Valsecchi, "Fast charging stations for electric vehicle: The impact on the mv distribution grids of the milan metropolitan area," in *Energy Conference and Exhibition (ENERGYCON), 2012 IEEE International*, IEEE, 2012, pp. 1055–1059.

[145] K. Yunus, H. Z. De La Parra, and M. Reza, "Distribution grid impact of plug-in electric vehicles charging at fast charging stations using stochastic charging model," in *Power Electronics and Applications (EPE 2011), Proceedings of the 2011-14th European Conference on*, IEEE, 2011, pp. 1–11.

[146] National Renewable Energy Laboratory. (2017). Transportation secure data center. Available online at `https://www.nrel.gov/transportation/secure-transportation-data.html`.

[147] M Simpson and T Markel, "Plug-in electric vehicle fast charge station operational analysis with integrated renewables," in *International Battery, Hybrid and Fuel Cell Electric Vehicle Symposium*, vol. 26, 2012.

[148] N. S. Pearre, W. Kempton, R. L. Guensler, and V. V. Elango, "Electric vehicles: How much range is required for a days driving?" *Transportation Research Part C: Emerging Technologies*, vol. 19, no. 6, pp. 1171–1184, 2011.

[149] M. Khan and K. M. Kockelman, "Predicting the market potential of plug-in electric vehicles using multiday gps data," *Energy Policy*, vol. 46, pp. 225–233, 2012.

[150] A. Dinger, R. Martin, X. Mosquet, M. Rabl, D. Rizoulis, M. Russo, and G. Sticher, "Batteries for electric cars: Challenges, opportunities, and the outlook to 2020," *The Boston Consulting Group*, p. 18, 2010.

[151] McKinsey and Company, "Electric vehicles in europe: Gearing up for a new phase?," 2014. [Online]. Available: https://www.mckinsey.com/~/media/McKinsey/Locations/Europe%20and%20Middle%20East/Netherlands/Our%20Insights/Electric%20vehicles%20in%20Europe%20Gearing%20up%20for%20a%20new%20phase/Electric%20vehicles%20in%20Europe%20Gearing%20up%20for%20a%20new%20phase.ashx.

[152] A. Sakti, I. M. Azevedo, E. R. Fuchs, J. J. Michalek, K. G. Gallagher, and J. F. Whitacre, "Consistency and robustness of forecasting for emerging technologies: The case of li-ion batteries for electric vehicles," *Energy Policy*, vol. 106, pp. 415–426, 2017.

[153] M. Catenacci, E. Verdolini, V. Bosetti, and G. Fiorese, "Going electric: Expert survey on the future of battery technologies for electric vehicles," *Energy Policy*, vol. 61, pp. 403–413, 2013.

[154] E. Gibson, K. van Blommestein, J. Kim, T. Daim, and E. Garces, "Forecasting the electric transformation in transportation: The role of battery technology performance," *Technology Analysis & Strategic Management*, vol. 29, no. 10, pp. 1103–1120, 2017. DOI: 10.1080/09537325.2016.1269886.

[155] J. Speirs, M. Contestabile, Y. Houari, and R. Gross, "The future of lithium availability for electric vehicle batteries," *Renewable and Sustainable Energy Reviews*, vol. 35, pp. 183–193, 2014.

[156] M. Contestabile, G. Offer, R. Slade, F Jaeger, and M Thoennes, "Battery electric vehicles, hydrogen fuel cells and biofuels. which will be the winner?" *Energy & Environmental Science*, vol. 4, no. 10, pp. 3754–3772, 2011.

[157] M.-A. Moffet, F. Sirois, and D. Beauvais, "Review of open-source code power grid simulation tools for long-term parametic simulation," *CanmetENERGY, Tech. Rep.*, vol. 137, 2011.

[158] CYME International. (2018). CYME Power Engineering Software. Available online at http://www.cyme.com/software/.

[159] etap. (2018). ETAP PS Power System Modelling, Analysis and Optimization Software. Available online at https://etap.com/software/product-overview-main.

[160] Siemens. (2018). PSSE âĂŞ high-performance transmission planning and analysis software. Available online at https://www.siemens.com/global/en/home/products/energy/services/transmission-distribution-smart-grid/consulting-and-planning/pss-software/pss-e.html.

[161] D. P. Chassin, K Schneider, and C Gerkensmeyer, "Gridlab-d: An open-source power systems modeling and simulation environment," in *Transmission and distribution conference and exposition, 2008. t&d. IEEE/PES*, IEEE, 2008, pp. 1–5.

[162] M. A. Al Faruque and F. Ahourai, "Gridmat: Matlab toolbox for gridlab-d to analyze grid impact and validate residential microgrid level energy management algorithms," in *Innovative Smart Grid Technologies Conference (ISGT), 2014 IEEE PES*, IEEE, 2014, pp. 1–5.

[163] R. C. Dugan, "Reference guide: The open distribution system simulator (opendss)," *Electric Power Research Institute, Inc*, vol. 7, 2012.

[164] A. S. Bozin, "Electrical power systems modeling and simulation using simulink," in *IEE Colloquium on The Use of Systems Analysis and Modelling Tools: Experiences and Applications (Ref. No. 1998/413)*, 1998, pp. 10/1–10/8. DOI: 10.1049/ic:19980594.

[165] S. P. Evans, "A relationship between the gravity model for trip distribution and the transportation problem in linear programming," *Transportation Research*, vol. 7, no. 1, pp. 39–61, 1973.

[166] K Kusakana, H. Vermaak, and B. Numbi, "Optimal sizing of a hybrid renewable energy plant using linear programming," in *Power Engineering Society Conference and Exposition in Africa (PowerAfrica), 2012 IEEE*, IEEE, 2012, pp. 1–5.

[167] G. Privitera, A. R. Day, G. Dhesi, and D. Long, "Optimising the installation costs of renewable energy technologies in buildings: A linear programming approach," *Energy and Buildings*, vol. 43, no. 4, pp. 838–843, 2011.

[168] F. Babonneau, M. Caramanis, and A. Haurie, "A linear programming model for power distribution with demand response and variable renewable energy," *Applied Energy*, vol. 181, pp. 83–95, 2016.

[169] E. A. Silver, R Victor, V Vidal, and D. de Werra, "A tutorial on heuristic methods," *European Journal of Operational Research*, vol. 5, no. 3, pp. 153–162, 1980.

[170] J. H. Holland, *Adaptation in natural and artificial systems: An introductory analysis with applications to biology, control, and artificial intelligence*. MIT press, 1992.

[171] A. E. Eiben, P.-E. Raue, and Z. Ruttkay, "Genetic algorithms with multi-parent recombination," in *International Conference on Parallel Problem Solving from Nature*, Springer, 1994, pp. 78–87.

[172] O. Hasançebi and F. Erbatur, "Evaluation of crossover techniques in genetic algorithm based optimum structural design," *Computers & Structures*, vol. 78, no. 1-3, pp. 435–448, 2000.

[173] J. Kennedy and R. Eberhart, "Particle swarm optimization," in *Neural Networks, 1995. Proceedings., IEEE International Conference on*, vol. 4, 1995, 1942–1948 vol.4. DOI: 10.1109/ICNN.1995.488968.

[174] D. Bratton and J. Kennedy, "Defining a standard for particle swarm optimization," in *Swarm Intelligence Symposium, 2007. SIS 2007. IEEE*, IEEE, 2007, pp. 120–127.

[175] F. Van Den Bergh and A. P. Engelbrecht, "A study of particle swarm optimization particle trajectories," *Information sciences*, vol. 176, no. 8, pp. 937–971, 2006.

[176] Y. Del Valle, G. K. Venayagamoorthy, S. Mohagheghi, J.-C. Hernandez, and R. G. Harley, "Particle swarm optimization: Basic concepts, variants and applications in power systems," *IEEE Transactions on evolutionary computation*, vol. 12, no. 2, pp. 171–195, 2008.

[177] A. Saltelli, S. Tarantola, F. Campolongo, *et al.*, "Sensitivity anaysis as an ingredient of modeling," *Statistical Science*, vol. 15, no. 4, pp. 377–395, 2000.

[178] E. Borgonovo and E. Plischke, "Sensitivity analysis: A review of recent advances," *European Journal of Operational Research*, vol. 248, no. 3, pp. 869–887, 2016.

[179] E. Borgonovo and C. L. Smith, "A study of interactions in the risk assessment of complex engineering systems: An application to space psa," *Operations Research*, vol. 59, no. 6, pp. 1461–1476, 2011.

[180] J. C. Helton, "Uncertainty and sensitivity analysis techniques for use in performance assessment for radioactive waste disposal," *Reliability Engineering & System Safety*, vol. 42, no. 2-3, pp. 327–367, 1993.

[181] M. D. Morris, "Factorial sampling plans for preliminary computational experiments," *Technometrics*, vol. 33, no. 2, pp. 161–174, 1991.

[182] W. F. Morris, D. F. Doak, *et al.*, "Quantitative conservation biology," *Sinauer, Sunderland, Massachusetts, USA*, 2002.

[183] F. Campolongo, A. Saltelli, and J. Cariboni, "From screening to quantitative sensitivity analysis. a unified approach," *Computer Physics Communications*, vol. 182, no. 4, pp. 978–988, 2011.

[184] P. Heiselberg, H. Brohus, A. Hesselholt, H. Rasmussen, E. Seinre, and S. Thomas, "Application of sensitivity analysis in design of sustainable buildings," *Renewable Energy*, vol. 34, no. 9, pp. 2030–2036, 2009.

[185] M. Ruano, J Ribes, A. Seco, and J. Ferrer, "An improved sampling strategy based on trajectory design for application of the morris method to systems with many input factors," *Environmental Modelling & Software*, vol. 37, pp. 103–109, 2012.

[186] I. M. Sobol, "Sensitivity estimates for nonlinear mathematical models," *Mathematical modelling and computational experiments*, vol. 1, no. 4, pp. 407–414, 1993.

[187] A. Saltelli, "Making best use of model evaluations to compute sensitivity indices," *Computer physics communications*, vol. 145, no. 2, pp. 280–297, 2002.

[188] F. Pianosi and T. Wagener, "A simple and efficient method for global sensitivity analysis based on cumulative distribution functions," *Environmental Modelling & Software*, vol. 67, pp. 1–11, 2015.

[189] R. Cukier, H. Levine, and K. Shuler, "Nonlinear sensitivity analysis of multiparameter model systems," *Journal of Computational Physics*, vol. 26, no. 1, pp. 1 –42, 1978, ISSN: 0021-9991. DOI: https://doi.org/10.1016/0021-9991(78)90097-9. [Online]. Available: http://www.sciencedirect.com/science/article/pii/0021999178900979.

[190] A. Saltelli and R. Bolado, "An alternative way to compute fourier amplitude sensitivity test (fast)," *Computational Statistics & Data Analysis*, vol. 26, no. 4, pp. 445–460, 1998.

[191] Y. Gan, Q. Duan, W. Gong, C. Tong, Y. Sun, W. Chu, A. Ye, C. Miao, and Z. Di, "A comprehensive evaluation of various sensitivity analysis methods: A case study with a hydrological model," *Environmental Modelling & Software*, vol. 51, pp. 269–285, 2014.

[192] R. Cukier, J. Schaibly, and K. E. Shuler, "Study of the sensitivity of coupled reaction systems to uncertainties in rate coefficients. iii. analysis of the approximations," *The Journal of Chemical Physics*, vol. 63, no. 3, pp. 1140–1149, 1975.

[193] F. Pianosi, F. Sarrazin, and T. Wagener, "A matlab toolbox for global sensitivity analysis," *Environmental Modelling & Software*, vol. 70, pp. 80–85, 2015.

[194] F Sarrazin, F Pianosi, and T Wagener, "An introduction to the safe matlab toolbox with practical examples and guidelines," in *Sensitivity Analysis in Earth Observation Modelling*, Elsevier, 2017, pp. 363–378.

[195] *Sensitivity analysis*. [Online]. Available: `https://www.vanguardsw.com/`.

[196] G. Pujol, B. Iooss, A. Janon, K. Boumhaout, S. D. Veiga, T. Delage, J. Fruth, L. Gilquin, J. Guillaume, L. L. Gratiet, P. Lemaitre, B. L. Nelson, F. Monari, R. Oomen, B. Ramos, O. Roustant, E. Song, J. Staum, T. Touati, and F. Weber, *Package sensitivity - global sensitivity analysis of model outputs*, 2017.

[197] M. G. McNally, "The four-step model," in *Handbook of Transport Modelling: 2nd Edition*, Emerald Group Publishing Limited, 2007, pp. 35–53.

[198] T. F. Golob and J. Gould, "Projecting use of electric vehicles from household vehicle trials," *Transportation Research Part B: Methodological*, vol. 32, no. 7, pp. 441–454, 1998.

[199] A. Lojowska, D. Kurowicka, G. Papaefthymiou, and L. van der Sluis, "Stochastic modeling of power demand due to evs using copula," *IEEE Transactions on Power Systems*, vol. 27, no. 4, pp. 1960–1968, 2012.

[200] J. D. Kim and M. Rahimi, "Future energy loads for a large-scale adoption of electric vehicles in the city of los angeles: Impacts on greenhouse gas (ghg) emissions," *Energy Policy*, vol. 73, pp. 620–630, 2014.

[201] M. De Gennaro, E. Paffumi, G. Martini, and H. Scholz, "A pilot study to address the travel behaviour and the usability of electric vehicles in two italian provinces," *Case studies on transport policy*, vol. 2, no. 3, pp. 116–141, 2014.

[202] M. Muratori, M. J. Moran, E. Serra, and G. Rizzoni, "Highly-resolved modeling of personal transportation energy consumption in the united states," *Energy*, vol. 58, pp. 168–177, 2013.

[203] S. A. Khan and M. Kushler, "Plug-in electric vehicles: Challenges and opportunities," American Council for an Energy-Efficient Economy, 2013.

[204] M. A. Tamor and M. Milačić, "Electric vehicles in multi-vehicle households," *Transportation Research Part C: Emerging Technologies*, vol. 56, pp. 52–60, 2015.

[205] Department for Transport. (2018). Traffic counts. Available online at `http://www.dft.gov.uk/traffic-counts/`.

[206] Open Street Map. (2017). Available online at `https://www.openstreetmap.org/`.

[207] *Data.gov.uk find open data*. [Online]. Available: `https://data.gov.uk/`.

[208] Highways England. (2017). Traffic flow data. Available online at `http://tris.highwaysengland.co.uk/detail/trafficflowdata`.

[209] C. Thiel, J. Schmidt, A. Van Zyl, and E. Schmid, "Cost and well-to-wheel implications of the vehicle fleet co 2 emission regulation in the european union," *Transportation Research Part A: policy and practice*, vol. 63, pp. 25–42, 2014.

[210] The Society of Motor Manufacturers and Traders. (2017). Smmt vehicle data. Available online at `https://www.smmt.co.uk/vehicle-data/` Date Accessed 15-09-2017.

[211] J. Axsen, S. Goldberg, and J. Bailey, "How might potential future plug-in electric vehicle buyers differ from current pioneer owners?" *Transportation Research Part D: Transport and Environment*, vol. 47, pp. 357–370, 2016.

[212] M. K. Hidrue, G. R. Parsons, W. Kempton, and M. P. Gardner, "Willingness to pay for electric vehicles and their attributes," *Resource and Energy Economics*, vol. 33, no. 3, pp. 686–705, 2011.

[213] Department for Transport. (2015). Free flow vehicle speed statistics: Great britain. Last accessed 15-09-2017. Available online at `https://www.gov.uk/government/uploads/system/uploads/attachment_data/file/533244/free-flow-vehicle-speeds-great-britain-2015.pdf`.

[214] ——, *Policy on service areas and other roadside facilities on motorways and all purpose trunk roads in england*, 2008, Available online at https://www.whatdotheyknow.com/request/1679/response/3572/attach/3/DfT20circ20010820web.pdf.

[215] X. Wu, D. Freese, A. Cabrera, and W. A. Kitch, "Electric vehicles energy consumption measurement and estimation," *Transportation Research Part D: Transport and Environment*, vol. 34, pp. 52–67, 2015.

[216] T. S. Bryden, A. J. Cruden, G. Hilton, B. H. Dimitrov, C. P. de Leon, and A. Mortimer, "Off-vehicle energy store selection for high rate ev charging station," in *6th Hybrid and Electric Vehicles Conference (HEVC 2016)*, 2016, pp. 1–9. DOI: 10.1049/cp.2016.0986.

[217] G. Hilton, T. Bryden, C. P. de Leon, and A. Cruden, "Dynamic charging algorithm for energy storage devices at high rate ev chargers for integration of solar energy," *Energy Procedia*, vol. 151, pp. 2–6, 2018.

[218] C. Reid, "Lithium iron phosphate cell performance evaluations for lunar extravehicular activities," 2007, Available online at http://ntrs.nasa.gov/archive/nasa/casi.ntrs.nasa.gov/20070032058.pdf.

[219] C. McKerracher, S. Morsy, N. Kou, L. Goldie-Scot, A. ODonovan, and D. Doherty, "Electric vehicle outlook 2017," *Bloomberg New Energy Finance*, 2017, Available online at https://about.bnef.com/electric-vehicle-outlook/toc-download.

[220] Organization of the Petroleum Exporting Countries, "World oil outlook, 2017," 2017, Available online at http://www.opec.org/opecweb/en/publications/340.htm.

[221] Exxon Mobil, "2017 outlook for energy: A view to 2040," 2017, Available online at http://corporate.exxonmobil.com/en/energy/energy-outlook.

[222] National Grid, *Embedded benefit review open letter*, Available online at http://www2.nationalgrid.com/WorkArea/DownloadAsset.aspx?id=32765 Last Accessed 20-11-2017, 2014.

[223] I. Richardson, M. Thomson, D. Infield, and C. Clifford, "Domestic electricity use: A high-resolution energy demand model," *Energy and Buildings*, vol. 42, no. 10, pp. 1878–1887, Oct. 2010, ISSN: 03787788. DOI: 10.1016/j.enbuild.2010.05.

023, Available online at http://www.sciencedirect.com/science/article/pii/S0378778810001854.

[224] D. Noll, C. Dawes, and V. Rai, "Solar Community Organizations and active peer effects in the adoption of residential PV," *Energy Policy*, vol. 67, pp. 330–343, Apr. 2014, ISSN: 03014215. DOI: 10.1016/j.enpol.2013.12.050, Available online at http://www.sciencedirect.com/science/article/pii/S0301421513013141.

[225] M. Bortolini, M. Gamberi, and A. Graziani, "Technical and economic design of photovoltaic and battery energy storage system," *Energy Conversion and Management*, vol. 86, pp. 81 –92, 2014, ISSN: 0196-8904. DOI: http://dx.doi.org/10.1016/j.enconman.2014.04.089. [Online]. Available: http://www.sciencedirect.com/science/article/pii/S0196890414004014.

[226] *Thames Valley Vision*. (visited on 08/18/2015), Available online at http://www.thamesvalleyvision.co.uk/.

[227] *Newquay Weather Station*. (visited on 08/18/2015), Available online at http://www.newquayweather.com/index.php.

[228] R. C. Dugan, "The Open Distribution System Simulator (OpenDSS)," *Electric Power Research Institute, Inc.*, no. November, pp. 1–177, 2012.

[229] A. Zeh and R. Witzmann, "Operational strategies for battery storage systems in low-voltage distribution grids to limit the feed-in power of roof-mounted solar power systems," *Energy Procedia*, vol. 46, pp. 114 –123, 2014, ISSN: 1876-6102. DOI: http://dx.doi.org/10.1016/j.egypro.2014.01.164. [Online]. Available: http://www.sciencedirect.com/science/article/pii/S1876610214001805, 8th International Renewable Energy Storage Conference and Exhibition (IRES 2013).

[230] Ofgem, "Feed-in tariff generation and export payment rate table for photovoltaic installations - feed in tariff year 7 (2016/17)," 2016, Available online at https://www.ofgem.gov.uk/system/files/docs/2016/02/feed_in_tariff_scheme_tariff_table_1_april_2016_31_march_2017_pv_only.pdf.

Appendices

Appendix A

EV demand prediction code

The code used to implement the work in Chapter 4 is included here. Each script is used in turn to extract, sort and filter the GPX files from the Open Street Map dump.

```
% TracksInShapefile
% Separated those OSM tracks which use the SRN, i.e. are long trips in
% cars.
% Author: George Hilton Email: g.hilton@soton.ac.uk
% Date 20/01/2017

% Load shapefile of road network
load('C:\Local\Traffic Data\Highways Shape File\HighwaysLatLon.mat')

Tracks = dir('C:\Local\Traffic Data\Matlab OSM tracks');

% Remove current and parent directory markers to prevent infinite loop
yg = ismember({Tracks.name},{'.','..'});
Tracks(yg) = [];

itr = 0
Number = 1

% Iterate through all tracks
for i1 = 1 : length(Tracks)

    ThisTrack = Tracks(i1).name;
    load(ThisTrack)

    flag = 0;

```

```
    TrackBox = [min(data.Latitude(1),data.Latitude(length(data))) , min(data.
    Longitude(1),data.Longitude(length(data))) , max(data.Latitude(1),data.
    Latitude(length(data))) , max(data.Longitude(1),data.Longitude(length(data)))
    ];

    % Iterate through all highway polygons
    for i2 = 1 : length(Highways)

            % Check Latitudes
            if TrackBox(1) < Highways(i2).BoundingBox(1) && TrackBox(3) >
    Highways(i2).BoundingBox(2)
                % Check Longitudes
                if TrackBox(2) < Highways(i2).BoundingBox(3) && TrackBox(4) >
    Highways(i2).BoundingBox(4)

                    Number = Number + 1

                    % Save track in subfolder
                    str = sprintf('SuccessTrack_%d',Number);
                    save(str,'data')

                    break
                end
            end
    end
    clear data
    clear TrackBox
    itr = itr + 1
 end
```

```

Highways = shaperead('HE_HighwayBoundary_v3_3_1');

prof = geotiffinfo('GBOverview');

HighwaysLat = cell(length(Highways),1);
HighwaysLon = cell(length(Highways),1);

for i = 1 : length(Highways)
    highwaysX = Highways(i).X;
    highwaysY = Highways(i).Y;

    [HighwaysLat_temp, HighwaysLon_temp] = projinv(prof, highwaysX, highwaysY);

    Highways(i).X = HighwaysLat_temp;
    Highways(i).Y = HighwaysLon_temp;

    Highways(i).BoundingBox(1) = min(Highways(i).X);
```

```
    Highways(i).BoundingBox(2) = min(Highways(i).Y);
    Highways(i).BoundingBox(3) = max(Highways(i).X);
    Highways(i).BoundingBox(4) = max(Highways(i).Y);
end

save('HighwaysLatLon', 'Highways')
```

```
% GPX to Matlab
% Processes the .gpx files from the OSM dump to matlab geopoint format.
% Author George Hilton email: g.hilton@soton.ac.uk
% Date: 17/01/2017

clear all

cd ('C:\Local\Traffic Data\Open Stret Map tracks\great_britain.tar\gpx-planet
    -2013-04-09\identifiable\001')

% Assess top level directory
folders = dir('C:\Local\Traffic Data\Open Stret Map tracks\great_britain.tar\gpx-
    planet-2013-04-09\identifiable\001');

% Remove current and parent directory markers to prevent infinite loop
yg = ismember({folders.name},{'.','..'});
folders(yg) = [];

% Create empty cell ready to populate with all files
files = cell(length(folders));

% Iterate through folders in top level directory. Run dir() on each folder
% in top level directory and assign to files array.
for K = 1 : length(folders)
  thisdir = folders(K).name;
  files{K} = dir(thisdir);
end

% Iterate through all files within OSM dump
for i = 10:length(files)

    % Prevent infinite loop
    yg = ismember({files{i,1}.name},{'.','..'});
    files{i,1}(yg) = [];

    % Add path for each folder to enable gpxread function use.
    addpath(files{i,1}.folder)

    % Iterate throughall files in each folder
    for p = 1:length(files{i,1})

```

```
        % Convert to matlab format and save
        fileName = files{i,1}(p).name;
        %A = gpxread(fileName);
        data = gpxread(fileName);
        str = sprintf('A_%d_%d',i,p);
        save(str,'data')
    end

end
```

```
% ResultsSort
% Sort journey lengths by time of day to create energy used per time of day
% distribution. Uses mid-time of the journey for time stamp.
%
% Author George Hilton. email: g.hilton@soton.ac.uk
% Date 2/2/2017

load('Results.mat')

% Order journeys into time of day.

TimeofDayStart = regexp([Results{:,2}],'T','split');
TimeofDayStart = TimeofDayStart.';
TimeofDayEnd = regexp([Results{:,3}],'T','split');
TimeofDayEnd = TimeofDayEnd.';

TimeofDay = zeros(2287,2);

for i1 = 1:length(TimeofDay)

    hour_start = str2double(TimeofDayStart{i1,1}{2}(1:2));
    minute_start = str2double(TimeofDayStart{i1,1}{2}(4:5));

    hour_end = str2double(TimeofDayEnd{i1,1}{2}(1:2));
    minute_end = str2double(TimeofDayEnd{i1,1}{2}(4:5));

    minutes_start = hour_start*60 + minute_start;
    minutes_end = hour_end*60 + minute_end;

    minutes_middle(i1) = (minutes_end + minutes_start)/2;

    hour = floor(minutes_middle(i1)/60);
    minute = minutes_middle(i1) - hour*60;

    TimeofDay(i1,1) = hour;
    TimeofDay(i1,2) = minute;
end

```

```
% B is time figures, I is order
[B,I] = sort(minutes_middle);

for i2 = 1:length(Results)
    SortedDistanceResults(i2) = Results(I(i2),1);
end

SortedDistanceResultsMat = cell2mat(SortedDistanceResults);

for i3 = 1:length(I)
TimeofDaySorted(i3) = TimeofDay(I(i3));
end

% ts = timeseries(SortedDistanceResultsMat,TimeofDaySorted);
% plot(ts)
% hold
%
% ts1 = resample(ts,[0:0.025:1]);
%
% plot(ts1)

% times = datetime(TimeofDaySorted);

for i4 = 1:24

    i0 = i4 - 1;

    data = [];

    for i5 = 1 : length(TimeofDay)

        if TimeofDaySorted(i5) < i4 && TimeofDaySorted(i5) >= i0
            if SortedDistanceResultsMat(i5)>1
                data = vertcat(data,SortedDistanceResultsMat(i5));
            end
        end
    end

    str = sprintf('hourmidlong%d',i4);
    save(str,'data')

end
```

```
% LengthTime
% Filter trips of length greater than 50 miles.
% Author: George Hilton Email: g.hilton@soton.ac.uk
% Date 26/01/2017

```

```
Tracks = dir('C:\Local\Traffic Data\Matlab OSM tracks\Uses SRN');

% Remove current and parent directory markers to prevent infinite loop
yg = ismember({Tracks.name},{'.','..','LengthTime.m'});
Tracks(yg) = [];

Results = cell(length(Tracks),3);

% Iterate through all tracks
for i1 = 1 : length(Tracks)

    ThisTrack = Tracks(i1).name;
    load(ThisTrack)

    for i2 = 1 : length(ThisTrack)

        % Record length and time of track
        lat = data.Latitude;
        lon = data.Longitude;

        d = distance(lat(1:end-1), lon(1:end-1), lat(2:end), lon(2:end));
        dist = sum(d)*69.047;
        start = data.Time(1);
        finish = data.Time(end);

        Results{i1,1} = dist;
        Results{i1,2} = start;
        Results{i1,3} = finish;
    end
end
```

Appendix B

HREVC Model code

```
1
2  % HREVC Model function for use in optimisation for profit. Takes
3  % pre-calculated datasets for EV demand to reduce computational time.
4  % Particle Swarm method expected.
5  %
6  % Author: George Hilton - email: g.hilton@soton.ac.uk
7  % Date: 31/05/2017
8
9  % Efficiencies
10
11 Sol_Eff = 0.95;              % Solar Power Electronic efficiencies
12 Grid_Eff = 0.95;             % Grid connection Power Electronic efficiencies
13 Charger_Eff = 0.95;          % Charger Power Electronic efficiencies
14
15 % Max EV Power
16
17 P_Max = 300000;                                    % Maximum power available
       from charge station
18
19 %%
20 %%%%%%%%%%%%%%%%%%%%%%%%%%%%%%%%%%%%%%%%%%%%%%%%%%%%%%%%%%%%
21 % ---- ENERGY BALANCE PREREQUISITES ----
22 %%%%%%%%%%%%%%%%%%%%%%%%%%%%%%%%%%%%%%%%%%%%%%%%%%%%%%%%%%%%
23
24 % ---- Load Data ----
25
26     % Load solar and wind data arrays
27     load('SgurrWindSolar')
28     % Load Battery Data
29     load('DataManipulationResults.mat')
30
31 %% Calculate Grid Charge
```

```
32
33 SolarMA100 = movmean(ACp,100*1440);
34 SolarMA100 = max(SolarMA100)-SolarMA100;
35 SolarMA100 = SolarMA100/0.1679;
36
37 SolarMAShape(:) = SolarMA100 + Grid_Charge_min;
38 Grid_Charge(:) = SolarMAShape + SolarMA100*(Grid_Charge_max-Grid_Charge_min);
39
40 % --- Load EV Charge times ---
41
42 % Load randomly selected dataset
43 str = sprintf('EV_DataSet_M25Factor30_y%d_scen%d',year,scen);
44 load(str);
45
46 % --- Create EV Charge Station Arrays ---
47
48 % A zero array for each charging station, will be set to one when the
49 % charge station is in use.
50
51 % Number of created arrays is given by variable Charge_Stations
52 % To index Charge_Station (b can be ommitted):
53 % Charge_Station{a,b}(c,d)
54 % a - 1-Number_Charge_Stations, describes number of the charge station
55 % b - Three cells, 1 contains time vector for charge station, 2 contains use
56 % stamp, 1 if in use 0 if not, 3 contains number of EV to be charged at charging
       station.
57 % c - 1-2, 1 is power to EV 2 is SOC of EV
58 % d - 1-length(DCp), time vector
59
60 Charge_Station=cell(Number_Charge_Stations,3);
61
62 for f=1:Number_Charge_Stations
63     Charge_Station{f,1}=zeros(2,length(ACp));
64     Charge_Station{f,2}=0;
65     Charge_Station{f,3}=0;
66 end
67
68 % --- Set Zeros ---
69 Grid = zeros(1, length(ACp));
70 ESM_SoC_day_vec = zeros(1,length(ACp));
71 Day_Power = zeros(1,length(ACp));
72
73 % Calculate initial max charge and discharge powers. Set as 5C for first
74 % second to allow Model.m to be called.
75 ESM_P_max_charge = ESM_ES_cap_kWh*5;
76 ESM_P_max_discharge = ESM_ES_cap_kWh*-5;
77
78 %%
```

```
%%%%%%%%%%%%%%%%%%%%%%%%%%%%%%%%%%%%%%%%%%%%%%%%%%%%%%%%%%%%%
% ---- Energy balance section ----
%%%%%%%%%%%%%%%%%%%%%%%%%%%%%%%%%%%%%%%%%%%%%%%%%%%%%%%%%%%%%

EV_Number_run=1;

% For loop for length of day
for i=1:length(ACp)

% Set time given to model script to integer value of i
ESM_time=round(i);

% Run battery model every second other than the first, this is because
% previous SOC values are needed for effective running
if i > 1
%%
%%%%%%%%%%%%%%%%%%%%%%%%%%%%%%%%%%%%%%%%%%%%%%%%%%%%%%%%%%%%%%%%%%%%%%%%%%%
% INITIAL CALCULATIONS
%%%%%%%%%%%%%%%%%%%%%%%%%%%%%%%%%%%%%%%%%%%%%%%%%%%%%%%%%%%%%%%%%%%%%%%%%%%

% Define the initial value of the SoC vector as 0.11
ESM_SoC_day_vec(1) = 0.11;

% Calculate the C rate of the charge or discharge, put this value in a
% vector of C rates, with each point in the vector being a new time
ESM_C_rate(ESM_time) = abs(ESM_P_to_from_energystore/ESM_ES_cap_kWh);

%%%%%%%%%%%%%%%%%%%%%%%%%%%%%%%%%%%%%%%%%%%%%%%%%%%%%%%%%%%%%%%%%%%%%%%%%%%
% DETERMINE THE CURVES THAT THE C RATE CALCULATED IS BETWEEN
%%%%%%%%%%%%%%%%%%%%%%%%%%%%%%%%%%%%%%%%%%%%%%%%%%%%%%%%%%%%%%%%%%%%%%%%%%%

%%%%%%%%%%%%%%%%%%%%%%%%%%%%%%%%%%%%%%%%%%%%%%%%%%%%%%%%%%%%%%%%%%%%%%%%%%%
% If loop for charging case
if ESM_P_to_from_energystore > 0

    % Cycle for the number of curves
    for ESM_i = 1 : ESM_N_Charge_Curves-1

        % If the C-rate is less than the lowest value from the battery
        % tests the ESM_curve_ref is set at 0
        if ESM_C_rate(ESM_time) <= ESM_C_Rate_Charge_Curves(1)
            ESM_curve_ref = 0;
            break

        % If the C-rate is between the two values in
        % ESM_C_Rate_Charge_Curves then use ESM_i as the ESM_curve_ref
        elseif (ESM_C_Rate_Charge_Curves(ESM_i) < ESM_C_rate(ESM_time))...
```

```
127                 &&(ESM_C_rate(ESM_time)<=ESM_C_Rate_Charge_Curves(ESM_i+1))
128             ESM_curve_ref = ESM_i;
129             break
130
131         % If the C-rate is higher than the largest C-rate measured, this
132         % should not happen
133         elseif ESM_C_rate(ESM_time) > ESM_C_Rate_Charge_Curves(
    ESM_N_Charge_Curves)
134             warning('Too high power to off-vehicle energy store')
135         end
136
137     end
138
139 %%%%%%%%%%%%%%%%%%%%%%%%%%%%%%%%%%%%%%%%%%%%%%%%%%%%%%%%%%%%%%%%%%%%%%%%
140 % If for discharging case
141 elseif ESM_P_to_from_energystore < 0
142
143     % Cycle for the number of curves
144     for ESM_i = 1 : ESM_N_Discharge_Curves-1
145
146         % If the C-rate is less than the lowest value from the battery
147         % tests the ESM_curve_ref is set at 0
148         if ESM_C_rate(ESM_time) <= ESM_C_Rate_Discharge_Curves(1)
149             ESM_curve_ref = 0;
150             break
151
152         % If the C-rate is between the two values in
153         % ESM_C_Rate_Charge_Curves then use ESM_i as the ESM_curve_ref
154         elseif (ESM_C_Rate_Discharge_Curves(ESM_i)<ESM_C_rate(ESM_time))...
155                 &&(ESM_C_rate(ESM_time)<=ESM_C_Rate_Discharge_Curves(ESM_i+1))
156             ESM_curve_ref = ESM_i;
157             break
158
159         % If the C-rate is higher than the largest C-rate measured, this
160         % should not happen
161         elseif ESM_C_rate(ESM_time) > ESM_C_Rate_Discharge_Curves(
    ESM_N_Charge_Curves)
162             warning('Too high power to off-vehicle energy store')
163
164         end
165
166     end
167
168 end
169
170 %clear ESM_i
171
172 %%%%%%%%%%%%%%%%%%%%%%%%%%%%%%%%%%%%%%%%%%%%%%%%%%%%%%%%%%%%%%%%%%%%%%%%
```

```
% CALCULATE THE CELL VOLTAGE AND THEN THE EFFICIENCY AND NEW SOC
%%%%%%%%%%%%%%%%%%%%%%%%%%%%%%%%%%%%%%%%%%%%%%%%%%%%%%%%%%%%%%%%%%%%%%%%%%%%

% Determine the vector location of the previous SoC
% ESM_SoC_day_vec(ESM_time-1) reads the previous SoC value, as the SoC
% varies between 0 and 100 and the vector varies from 1 to 1001, the SoC
% value is multiplied by 10 and 1 is added to determine the vector
% location. The round function is used to ensure this value is an integer.

ESM_NVec_SoC_prev = round((ESM_SoC_day_vec(ESM_time-1))*1000+1);

%%%%%%%%%%%%%%%%%%%%%%%%%%%%%%%%%%%%%%%%%%%%%%%%%%%%%%%%%%%%%%%%%%%%%%%%%%%%
% If loop for charging case
if ESM_P_to_from_energystore > 0

    % If for case where ESM_curve_ref is 0. For this case the cell voltage
    % is taken as the same as for the lowest C rate
    if ESM_curve_ref < 0.5
        ESM_Volt_cell(ESM_time) = ESM_Charge_V((ESM_NVec_SoC_prev),1);

    % Else to interpolate between the curves
    else
        % Vector of 2 x values, which are the two C rates
        ESM_x_temp = [ESM_C_Rate_Charge_Curves(ESM_curve_ref)
    ESM_C_Rate_Charge_Curves(ESM_curve_ref+1)];

        % Vector of 2 y values, which lookup the voltages in the charging
        % voltage matrix
        ESM_y_temp = [ESM_Charge_V(ESM_NVec_SoC_prev,ESM_curve_ref) ESM_Charge_V(
    ESM_NVec_SoC_prev,ESM_curve_ref+1)];

        % Interpolate between these values at the value
        % ESM_C_rate(ESM_time) to find the cell voltage
        ESM_Volt_cell(ESM_time) = interp1(ESM_x_temp,ESM_y_temp,ESM_C_rate(
    ESM_time));

        %clear ESM_x_temp ESM_y_temp
    end

    % Calculate the new SoC, this is equal to the previous SoC + the
    % standard charge/discharge efficiency * the charge efficiency at the
    % charge rate * energy transferred/off-vehicle energy store capacity
    ESM_SoC_day_vec(ESM_time) = ESM_SoC_day_vec(ESM_time-1) + ...
        ESM_Eff_cd * ...
        (ESM_Charge_V(ESM_NVec_SoC_prev,1)/ESM_Volt_cell(ESM_time))* ...
        ESM_P_to_from_energystore*(1/60)/ESM_ES_cap_kWh;

%%%%%%%%%%%%%%%%%%%%%%%%%%%%%%%%%%%%%%%%%%%%%%%%%%%%%%%%%%%%%%%%%%%%%%%%%%%%
```

```
218 % Elseif loop for discharging case
219 elseif ESM_P_to_from_energystore < 0
220     if ESM_curve_ref < 0.5
221         ESM_Volt_cell(ESM_time) = ESM_Discharge_V(ESM_NVec_SoC_prev,1);
222 
223     % Else to interpolate between the curves
224     else
225         % Vector of 2 x values, which are the two C rates
226         ESM_x_temp = [ESM_C_Rate_Discharge_Curves(ESM_curve_ref)
    ESM_C_Rate_Discharge_Curves(ESM_curve_ref+1)];
227 
228         % Vector of 2 y values, which lookup the voltages in the
229         % discharging voltage matrix
230         ESM_y_temp = [ESM_Discharge_V(ESM_NVec_SoC_prev,ESM_curve_ref)
    ESM_Discharge_V(ESM_NVec_SoC_prev,ESM_curve_ref+1)];
231 
232         % Interpolate between these values at the value
233         % ESM_C_rate(ESM_time) to find the cell voltage
234         ESM_Volt_cell(ESM_time) = interp1(ESM_x_temp,ESM_y_temp,ESM_C_rate(
    ESM_time));
235 
236     end
237 
238     % Calculate the new SoC, this is equal to the previous SoC + the
239     % standard charge/discharge efficiency * the discharge efficiency at
240     % the discharge rate * energy transferred/off-vehicle energy store
241     % capacity
242     ESM_SoC_day_vec(ESM_time) = ESM_SoC_day_vec(ESM_time-1) + ....
243         ESM_Eff_cd*...
244         (ESM_Volt_cell(ESM_time)/ESM_Discharge_V(ESM_NVec_SoC_prev,1))*...
245         ESM_P_to_from_energystore*(1/60)/ESM_ES_cap_kWh;
246 
247 %%%%%%%%%%%%%%%%%%%%%%%%%%%%%%%%%%%%%%%%%%%%%%%%%%%%%%%%%%%%%%%%%%%%%%%%
248 % Else for case when energy store is neither charging nor discharging. In
249 % this case the new SoC simply equals the previous SoC
250 else
251     ESM_SoC_day_vec(ESM_time) = ESM_SoC_day_vec(ESM_time-1);
252 end
253 
254 %%%%%%%%%%%%%%%%%%%%%%%%%%%%%%%%%%%%%%%%%%%%%%%%%%%%%%%%%%%%%%%%%%%%%%%%
255 % CALCULATE THE MAXIMUM POWER TO AND FROM THE ENERGY STORE
256 %%%%%%%%%%%%%%%%%%%%%%%%%%%%%%%%%%%%%%%%%%%%%%%%%%%%%%%%%%%%%%%%%%%%%%%%
257 
258 % Determine the vector location of the SoC
259 % ESM_SoC_day_vec(ESM_time-1) reads the previous SoC value, as the SoC
260 % varies between 0 and 100 and the vector varies from 1 to 1001, the SoC
261 % value is multiplied by 10 and 1 is added to determine the vector
262 % location. The round function is used to ensure this value is an integer.
```

```
263 ESM_NVec_SoC = round((ESM_SoC_day_vec(ESM_time))*1000+1);
264
265 ESM_P_max_charge = ESM_ES_cap_kWh*ESM_Max_C_Charge(ESM_NVec_SoC);
266 ESM_P_max_discharge = ESM_ES_cap_kWh * ESM_Max_C_Discharge(1001-ESM_NVec_SoC) *
        -1;
267
268 %%
269     if ESM_SoC_day_vec(i) < 0.15
270         ESM_P_max_discharge = 0;
271     end
272 end
273
274 % Calculate max available power for EV charging
275 Max_charge_available(i) = Grid_Capacity*Grid_Eff + DCp(i)*Wind_Factor*Sol_Eff +
        ACp(i)*Solar_Factor*Sol_Eff - ESM_P_max_discharge;
276
277 % --- Asign EVs to charging stations ---
278
279 % Every time there is a new EV arriving or one waiting. EV_Charge_Time
280 % signifies a waiting EV. Its value relates to how many EVs there are
281 % waiting to charge.
282 if EV_Charge_Time(i) >= 1
283
284     % Iterate through all the charging stations
285     for q=1:Number_Charge_Stations
286
287         % Assign the EV to a charging stations which is not in use, if
288         % staion is not in use
289         if Charge_Station{q,2} == 0
290
291             % Set charging station to in use.
292             Charge_Station{q,2} = 1;
293
294             % Assign current EV to the charging station and increase
295             % EV_Number_Run such that the next EV to be charged is not the
296             % same.
297             Charge_Station{q,3} = EV_Number_run;
298             EV_Number_run = EV_Number_run+1;
299
300             % EV_Charge_Time to -1 to signify that one EV has begun
301             % charging
302             EV_Charge_Time(i) = EV_Charge_Time(i) - 1;
303
304             % If there are no EVs waiting to be charged leave the for loop
305             % and continue onto charging code.
306             if EV_Charge_Time(i)==0
307                 break
308             end
```

```
309
310         end
311
312         % If we have iterated through all the charging stations and didnt
313         % break out of the for loop this means there is an EV waiting and
314         % all charging stations are full.
315         if q == Number_Charge_Stations
316
317             % To prevent error on the last iteration.
318             if i < length(ACp)-1
319
320                 % Hold the Current EVs waiting over to the next iteration
321                 EV_Charge_Time(i+1) = EV_Charge_Time(i) + EV_Charge_Time(i+1);
322             end
323             break
324         end
325     end
326 end
327
328 % --- EV charge power and SOC calculation for each charging station ---
329
330 % Charge at max power for 1 EV at a charging station
331 % If charge is in use
332 for f=1:Number_Charge_Stations
333
334     if Charge_Station{f,2} == 1
335
336         % Run power demand function to calculate power to EV and change in
337         % SOC of EV. EV_Stats{EV_Number_run} is current EV being charged by
338         % this charge station. Results from Power_demand_v2 are assigned to
339         % Charge_Station for this iteration.
340         [Charge_Station{f,1}(1,i),Charge_Station{f,1}(2,i)]=Power_demand_v2(
    EV_Stats{Charge_Station{f,3}});
341
342         %Update the SOC of the EV with new SOC returned from
343         %Power_demand_v2
344         EV_Stats{Charge_Station{f,3}}(1)=Charge_Station{f,1}(2,i);
345
346         % if loop to end charge when the SOC exceeds SOC_fin
347         if EV_Stats{Charge_Station{f,3}}(1) > EV_Stats{Charge_Station{f,3}}(3)
348
349             %Show charge station no longer in use
350             Charge_Station{f,2}=0;
351         end
352     end
353
354     % Sum all charging station powers into Day_Power variable
355     Day_Power(i) = Day_Power(i) + Charge_Station{f,1}(1,i);
```

```
356
357 end
358
359 Day_Power(i)=Day_Power(i)/1000;          % Power W -> kW
360
361
362 % --- Power Limit Section ---
363
364 % If power to EVs will lead to exceeding the grid capacity, i.e. is over
365 % the max charge available variable then the power to each EV is brought
366 % down to acceptable levels
367
368
369 if Day_Power(i)*Charger_Eff > Max_charge_available(i);
370
371     % calculate multiplicative factor to return Day_Power to acceptable
372     % levels
373     factor = Max_charge_available(i) / Day_Power(i)*Charger_Eff;
374     Day_Power(i)=0;
375
376     % Iterate through charging stations to adjust the power and SOC for
377     % each EV
378     for f=1:Number_Charge_Stations
379
380         if Charge_Station{f,2} == 1
381
382             % Ammend SOC by subtracting the energy associated with the
383             % power reduction caused by the multiplicative factor
384             EV_Stats{Charge_Station{f,3}}(1) = EV_Stats{Charge_Station{f,3}}(1) -
     (Charge_Station{f,1}(1,i)*(1-factor))/(EV_Stats{Charge_Station{f,3}}(4)*3.6e
    +6);
385
386             % Ammend power to EV
387             Charge_Station{f,1}(1,i)=Charge_Station{f,1}(1,i)*factor;
388
389             % Sum all charging station powers into Day_Power variable
390             Day_Power(i) = Day_Power(i) + Charge_Station{f,1}(1,i)/1000 ;
391
392         end
393     end
394 end
395
396
397
398
399   %If loop for battery in a useable state i.e. SOC between allowable
400     %values
401     if  (0.1 <= ESM_SoC_day_vec(i)) && (ESM_SoC_day_vec(i) < 0.9 )
```

```
402
403         %If battery is useable call script to calculate grid power value
404         % When solar plus wind power does not provide full charge capability use
    grid to 'top
405         % up'
406         if (Wind_Factor*DCp(i) + Solar_Factor*ACp(i)) >= 0 && (Wind_Factor*DCp(i)
    *Sol_Eff + Solar_Factor*ACp(i)*Sol_Eff) < Grid_Charge(i)
407             Grid(i) = (Grid_Charge(i) - (Wind_Factor*DCp(i)*Sol_Eff +
    Solar_Factor*ACp(i)*Sol_Eff))/Grid_Eff;
408
409         %If solar power is providing adequate charging power set grid power to
410         %zero.
411         elseif (Wind_Factor*DCp(i)*Sol_Eff + Solar_Factor*ACp(i)*Sol_Eff) >=
    Grid_Charge(i);
412             Grid(i) = 0;
413
414         % Else, ie when there is no solar, set grid to grid charge.
415         else
416             Grid(i) = Grid_Charge(i)/Grid_Eff;
417         end
418
419     % If Battery is fully charged
420     elseif ESM_SoC_day_vec(i) > 0.9
421
422         % If the power in the system is positive, i.e. default is to
423         % further charge the battery then intervene and set grid power
424         % to export. Else, battery discharge begins and grid power = 0.
425         if (Wind_Factor*DCp(i)*Sol_Eff + Solar_Factor*ACp(i)*Sol_Eff) - Day_Power
    (i)/Charger_Eff > 0
426             Grid(i) = (Day_Power(i)/Charger_Eff - (Wind_Factor*DCp(i)*Sol_Eff +
    Solar_Factor*ACp(i)*Sol_Eff))/Grid_Eff;
427         else
428             Grid(i)=0;
429         end
430
431     % If battery is fully discharged
432     elseif ESM_SoC_day_vec(i) < 0.1
433
434         % If the power in the system is negative, i.e. default is to
435         % further discharge the battery then intervene and set grid power
436         % to import. Else calculate grid levels
437         if (Wind_Factor*DCp(i)*Sol_Eff + Solar_Factor*ACp(i)*Sol_Eff) - Day_Power
    (i)/Charger_Eff < 0
438
439             % If power demand and solar power go below grid charge level,
440             % hold grid power to grid charge. Else allow full import.
441             if (Day_Power(i)/Charger_Eff + (Wind_Factor*DCp(i)*Sol_Eff) +
    Solar_Factor*ACp(i)*Sol_Eff) < Grid_Charge(i)
```

```
442                 Grid(i) = Grid_Charge(i)/Grid_Eff;
443             else
444                 Grid(i) = (Day_Power(i)/Charger_Eff - (Wind_Factor*DCp(i)*Sol_Eff
     + Solar_Factor*ACp(i)*Sol_Eff))/Grid_Eff;
445             end
446
447         else
448             % When solar power does not provide full charge capability use grid
    to 'top
449             % up'
450             if (Wind_Factor*DCp(i) + Solar_Factor*ACp(i)) >= 0 && (Wind_Factor*
    DCp(i)*Sol_Eff + Solar_Factor*ACp(i)*Sol_Eff) < Grid_Charge(i)
451                 Grid(i) = (Grid_Charge(i) - (Wind_Factor*DCp(i)*Sol_Eff +
    Solar_Factor*ACp(i)*Sol_Eff))/Grid_Eff;
452
453             %If solar power is providing adequate charging power set grid power
    to
454             %zero.
455             elseif (Wind_Factor*DCp(i)*Sol_Eff + Solar_Factor*ACp(i)*Sol_Eff) >=
    Grid_Charge(i);
456                 Grid(i) = 0;
457
458             % Else, ie when there is no solar, set grid to grid charge.
459             else
460                 Grid(i) = Grid_Charge(i)/Grid_Eff;
461             end
462
463         end
464
465     end
466
467     % Power balance statement: Battery power equals solar power minus
468     % charge demand plus grid power levels
469     ESM_P_to_from_energystore = (Wind_Factor*DCp(i)*Sol_Eff + Solar_Factor*ACp(i)
    *Sol_Eff) - Day_Power(i)/Charger_Eff + Grid(i)*Grid_Eff;
470
471 %%
472
473 % Section to prevent very high charge and discharge levels
474
475     % If battery power is higher than maximum allowable calculate allowable
476     % power and set grid to balance power flows.
477     if ESM_P_to_from_energystore >= ESM_P_max_charge
478
479         % If battery is fully charged, set battery power to zero.
480         if ESM_SoC_day_vec(i) > 0.9
481              ESM_P_to_from_energystore = 0;
482
```

```
483         % Else, set battery power to maximum allowable.
484         else
485              ESM_P_to_from_energystore = ESM_P_max_charge;
486         end
487
488         % Energy balance statement for new battery power levels.
489         Grid(i) = (Day_Power(i)/Charger_Eff - (Wind_Factor*DCp(i)*Sol_Eff +
    Solar_Factor*ACp(i)*Sol_Eff) + ESM_P_to_from_energystore)/Grid_Eff;
490
491     % If battery power is lower than maximum discharge power calculate
492     % allowable power and set grid to balance powers.
493     elseif ESM_P_to_from_energystore <= ESM_P_max_discharge
494
495         % If battery is fully discharged, do not allow further discharge
496         if ESM_SoC_day_vec(i) < 0.1
497             ESM_P_to_from_energystore = 0;
498
499         % Else, allow discharge to maximum allowable
500         else
501             ESM_P_to_from_energystore = ESM_P_max_discharge;
502         end
503
504         % Modify grid power to balance power flows.
505         Grid(i) = (Day_Power(i)/Charger_Eff - (Wind_Factor*DCp(i)*Sol_Eff +
    Solar_Factor*ACp(i)*Sol_Eff) + ESM_P_to_from_energystore)/Grid_Eff;
506     end
507     Energy_Store_Power(i) = ESM_P_to_from_energystore;
508
509     %Curtail excess solar power exports
510     if Grid(i) < -1 * Grid_Capacity_export
511         Grid(i) = -1 * Grid_Capacity_export;
512     end
513
514 end
```

Appendix C

Optimisation Results

TABLE C.1: Optimisation Results: Full HREVC System

EV Scenario	Low			Medium			High		
Grid Price	-1.89	16.03	94.97	-1.89	16.03	94.97	-1.89	16.03	94.97
N_{CP}	2	2	2	4	4	4	8	8	8
PV_{cap}	4	21	179	54	151	128	145	4	104
$OVES_{cap}$	100	109	135	126	211	127	126	180	726
P_{GCMmin}	7	153	79	479	84	173	247	109	789
P_{GCMax}	11	210	149	686	462	962	979	975	904
GC_{max}	9981	216	205	9993	497	981	9186	1137	941
GC_{min}	-9999	-2	-13	-9856	-136	-112	-9786	-11	-258
Profit (20y)	25.38	8.27	-0.5633	38.01	17.17	18.96	68.27	45.29	29.90

TABLE C.2: Optimisation Results: HREVC system no solar

EV Scenario	Low			Medium			High		
Grid Price	-1.89	16.03	94.97	-1.89	16.03	94.97	-1.89	16.03	94.97
N_{CP}	2	2	2	4	4	9	8	8	16
$OVES_{cap}$	100	129	139	115	120	223	100	322	157
P_{GCMmin}	53	127	184	868	387	309	154	116	482
P_{GCMax}	988	200	192	952	799	524	248	239	839
GC_{max}	10000	224	196	9838	799	529	9797	1157	1137
Profit (20y)	25.30	7.82	1.66	37.76	18.15	3.45	69.76	44.03	7.97

TABLE C.3: Optimisation Results: HREVC system no OVES

EV Scenario	Low			Medium			High		
Grid Price	-1.89	16.03	94.97	-1.89	16.03	94.97	-1.89	16.03	94.97
N_{CP}	2	2	2	4	4	4	8	8	8
PV_{cap}	0	0	0	0	0	0	0	0	0
GC_{max}	10000	372	330	9990	616	546	7945	1237	1038
GC_{min}	-10000	0	-1	-9988	0	-3	9963	0	-2
Profit (20y)	26.15	8.25	2.21	39.53	19.71	2.20	69.12	46.62	13.16

TABLE C.4: Optimisation Results: HREVC system no solar or OVES

EV Scenario	Low			Medium			High		
Grid Price	-1.89	16.03	94.97	-1.89	16.03	94.97	-1.89	16.03	94.97
N_{CP}	2	2	2	4	4	4	8	8	8
GC_{max}	10000	372	330	10000	619	546	9913	1234	1036
Profit (20y)	18.59	8.25	2.17	31.99	19.71	2.31	63.07	46.62	13.28